

Dissertation zur Erlangung des Doktorgrades
der Fakultät für Chemie und Pharmazie
der Ludwig-Maximilians-Universität München

Role of Valosin-containing protein (VCP) in tau disaggregation in mammalian cells

Cellular characterization of polymorphic tau aggregates

Itika Saha

aus

Meerut, Indien

2020

Erklärung

Diese Dissertation wurde im Sinne von § 7 der Promotionsordnung vom 28. November 2011 von Herrn Prof. Dr. Franz-Ulrich Hartl betreut.

Eidesstattliche Versicherung

Diese Dissertation wurde eigenständig und ohne unerlaubte Hilfe erarbeitet.

München, 12.03.2020

Itika Saha

Dissertation eingereicht am: 13.03.2020

1. Gutachter: Prof. Dr. Franz-Ulrich Hartl

2. Gutachter: PD Dr. Dietmar E. Martin

Mündliche Prüfung am: 09.06.2020

ACKNOWLEDGEMENTS

I express my profound gratitude to Prof. Dr. F-Ulrich Hartl for providing me the opportunity to work in his scientifically stimulating lab and for his invaluable guidance throughout my thesis work. I thank him for his patience and concern that helped me to deal with both personal and research related problems encountered during the course of this work.

I am immensely thankful to Dr. Mark Hipp for scientific discussions and the mentorship, which not only made this work possible but also nurtured me as a scientist.

I would like to thank my collaborators Dr. Roman Körner, Dr. Patricia Yuste-Checa, Dr. Qiang Guo and Dr. Saurabh Gautam for their important contributions to this work. I am grateful to Ralf Zenke, Dr. Martin Spitaler and Marcus Oster from the core facility of MPI Biochemistry for their technical expertise and support. I also thank Albert Ries, Silvia Gärtner, Nadine Wischnewski and Anastasia Jungclaus for technical help in the Hartl lab. I acknowledge the support from Evelyn Frey-Royston, Burghardt Emmanuel and Darija Pompino for the smooth management of administrative matters.

I sincerely thank Dr. Dietmar Martin for co-evaluating my thesis. I additionally thank Dr. Mark Hipp, Prof. Dr. Christian Behrends, Prof. Dr. Julian Stingele and Prof. Roland Beckmann for participating in my thesis examination board. I also take the opportunity to thank Dr. Ruben Fernandez-Busnadiego and Prof. Dr. Rüdiger Klein for helpful discussions and suggestions during my TAC meetings. I am grateful to Dr. Hans Jörg Schäffer, Dr. Ingrid Wolf and Maximiliane Reif from the IMPRS graduate school for the unending support and for providing great opportunities to develop scientific and soft skills through various workshops and seminars.

I heartily thank Dr. Lavannya Sabharwal, Hauke Holthusen, Dr. Andreas Wörner, Dr. Lisa Vincenz-Donnelly, Dr. Gopal Jayaraj, Dr. Frédéric Frottin, Dr. Débora Broch Trentini, Dr. Rongqin Li and Dr. Young Jun Choe for their friendship and enlightening discussions that made science enjoyable.

Lastly, I am deeply indebted to my parents, Mrs. Aparna and Mr. Ajoy Kumar Saha, and my brother, Mr. Srijan Kumar Saha, for their unconditional love and encouragement that made it possible for me successfully conclude this journey.

CONTENTS

1. Summary	1
2. Introduction	3
2.1 Protein folding and molecular chaperones	3
2.2 Protein quality control (PQC).....	6
2.3 Protein degradation pathways	7
2.3.1 Ubiquitin proteasome system (UPS).....	7
2.3.2 Autophagy	15
2.4 Protein aggregation	17
2.4.1 Cellular mechanisms to cope with aggregated proteins	18
2.4.2 The amyloid state of proteins	19
2.5 Tau in physiology and pathology	23
2.5.1 Normal function of tau	24
2.5.2 Role of tau in neurodegeneration	25
2.5.3 Tau hyperphosphorylation.....	26
2.5.4 Tau aggregation and polymorphism	27
2.6 Prion-like propagation and spreading.....	29
2.6.1 Prion-like properties of tau	30
2.6.2 Yeast prions.....	30
2.7 Protein unfolding and disaggregation.....	32
2.7.1 Hsp100 disaggregases- Hsp104 and ClpB	33
2.7.2 Disaggregation by Hsp70 system	34
2.7.3 Other putative disaggregases in higher eukaryotes	37
2.8 Valosin-containing protein (VCP)-The Segregase	38
2.8.1 Structure and mechanism of action of VCP	39
2.8.2 Role of VCP in proteostasis	40
2.8.3 Disease association of VCP	42
2.9 Significance & aims of this work	43
2.10 Cellular model of polymorphic prion-like tau aggregates	45
3. Results	47
3.1 Regeneration and characterization of monoclonal cell lines propagating prion-like tau-YFP aggregates	47
3.1.1 Seeding Clone1 with extracts from parental Clone9 and Clone10 cell lines.....	47
3.1.2 Nuclear aggregates in Clone9.....	49
3.1.3 Aggresome-like characteristics of tau-YFP aggregates in Clone10	50
3.1.4 Amyloidogenicity of tau-YFP aggregates in Clone9 and Clone10.....	51

3.1.5	Fate of soluble and aggregated Tau-YFP under proteostatic stress conditions....	54
3.2	Analysis of tau-YFP interactome in Clone9 and Clone10.....	60
3.3	Autophagy perturbation in Clone10.....	64
3.3.1	Steady state levels of LC3-II and p62.....	64
3.3.2	Assessment of autophagic flux.....	66
3.4	Aggregate clearance in Clone10.....	68
3.4.1	Aggregate clearance by limiting tau synthesis with cycloheximide	69
3.4.2	Proteasome dependent turnover of tau-YFP aggregates	70
3.5	Understanding cellular disaggregation in a tet-regulated tau-YFP expression model	74
3.5.1	Tau-YFP mRNA and protein turnover kinetics	76
3.5.2	Proteasomal degradation of tau-YFP and aggregate stabilization	77
3.6	Identification of a cellular disaggregase	81
3.6.1	VCP interacts with tau-YFP aggregates.....	81
3.6.2	VCP is required for tau-YFP aggregate clearance	82
3.6.3	VCP minimally influences turnover or aggregation of non-aggregated tau-YFP...	85
3.7	Role of ubiquitination in VCP dependent tau-YFP disaggregation	87
3.7.1	Ubiquitination status of tau-YFP	87
3.7.2	K48 ubiquitin chains on tau-YFP aggregates and clearance by VCP.....	88
3.7.3	Ubiquitin dependent recruitment of VCP to tau-YFP aggregates	91
3.8	Co-operation of Hsp70 and VCP in protein disaggregation.....	95
3.8.1	Hsp70 in tau-YFP clearance.....	95
3.8.2	Disaggregation of firefly luciferase aggregates	99
3.9	VCP activity and tau-YFP seeding	101
3.10	Disease associated VCP mutations in tau-YFP disaggregation	105
4.	Discussion	108
4.1	Cell culture model of tau strains.....	108
4.2	Cellular characteristics of tau-YFP strains.....	109
4.2.1	Compartmentalization and composition of IBs in tau-YFP strains.....	110
4.2.2	Consequences of polymorphic aggregation	111
4.3	Aggregate clearance in the mammalian system	112
4.3.1	Strain-specific clearance of tau-YFP aggregates	112
4.3.2	Aggregate clearance under amino acid starvation	113
4.3.3	Role of proteasomes in handling protein aggregates	114
4.4	VCP-dependent Disaggregation of aggregated tau-YFP	115
4.4.1	Cellular dynamics of aggregate clearance	116
4.4.2	Role of VCP in aggregate clearance.....	118
4.4.3	VCP as a protein disaggregase	119

4.4.4	Fate of disaggregated material.....	121
4.4.5	Targeting VCP to protein aggregates	122
4.4.6	Regulation of VCP-mediated disaggregation by ubiquitination	123
4.4.7	VCP and Hsp70: Co-operators or competitors	124
4.4.8	Degradation-coupled-disaggregation and protein aggregation disorders	125
5.	Materials.....	128
5.1	Cell culture reagents	128
5.2	Inhibitors	128
5.3	Antibodies.....	129
5.3.1	For western blotting	129
5.3.2	For immunofluorescence.....	129
5.4	siRNAs.....	130
5.5	Kits & accessories.....	130
5.6	Chemicals.....	130
5.7	Softwares.....	131
5.8	Plasmids	132
5.9	Human Cell Lines.....	132
5.10	Media and Buffers	133
5.11	Miscellaneous	134
6.	Methods.....	135
6.1	Regeneration of Clone9 and Clone10 cell lines.....	135
6.1.1	Preparation of cell lysates	135
6.1.2	Seeding Clone1 with aggregate containing lysates.....	135
6.1.3	Propagation and selection of aggregate containing cells.....	135
6.2	Cell culture and maintenance	136
6.3	Chemical treatments	136
6.4	Genomic sequencing of Tau-YFP construct in cell lines	137
6.5	siRNA transfections.....	138
6.6	Western blotting	138
6.6.1	Sample preparation & electrophoresis.....	138
6.6.2	Transfer and imaging	139
6.7	Fluorescent staining	139
6.7.1	Antibody staining	139
6.7.2	Amyloid dye staining	140
6.8	Quantification of aggregates/cell and average size	140
6.9	Biochemical detection of aggregated tau	140
6.9.1	Ultracentrifugation based solubility assay	141

6.9.2 Filter trap assay	141
6.10 Amino acid starvation	141
6.11 Detection of Tau ubiquitination by biochemical assays.....	141
6.11.1 Denaturing ubiquitin pulldown	141
6.11.2 Non-denaturing Tau-YFP pulldown.....	142
6.12 Interactome analysis	142
6.12.1 SILAC labelling of cells and tau-YFP immunoprecipitation.....	142
6.12.2 MS Sample processing	143
6.12.3 LC-MS	144
6.12.4 MS data analysis	144
6.13 Firefly luciferase aggregation and disaggregation analysis.....	144
6.14 HEK293T FRET Biosensor cell line generation.....	145
6.15 Tau-YFP Seeding assay.....	145
6.16 Size exclusion chromatography	146
6.17 Generation of VCP-myc constructs.....	147
6.18 Generation of transformation competent <i>E. coli</i>	147
6.19 Plasmid preparation	147
7. Appendix	149
8. References	163

1. SUMMARY

Protein folding into a correct three-dimensional structure is vital for normal cellular function. Misfolded or unfolded proteins expose hydrophobic patches and become prone to aggregation. Cellular protein quality control (PQC) pathways ensure that such aberrant polypeptides are either refolded or targeted for degradation. However, when PQC capacity is overwhelmed due to ageing, environmental stress or mutations, proteins may aggregate. Protein aggregation could be toxic due to loss-of-function of the aggregating protein or due to gain of toxic function by the aggregates that indulge in abnormal interactions with other essential cellular proteins thereby making them unavailable for their normal function. Protein aggregation is associated with neurodegenerative disorders such as Alzheimer's disease (AD) and several forms of dementias which present with widespread intracellular aggregation of the tau protein.

Recently, tau was shown to form polymorphic aggregates in cultured cells in a manner reminiscent of the prion protein, which also forms and propagates structurally distinct non-native conformations, so-called prion strains. The first part of this study aimed at characterizing the cellular features of tau aggregates in two previously established tau strains, Clone9 and Clone10, in cultured cells (Sanders et al., 2014). We found that the tau aggregates in these strains were located at unique cellular deposition sites and showed distinct structural properties. The aggregates interacted with other cellular proteins to different extents, which in part represented the distinct PQC response to each type of aggregate. Furthermore, we demonstrated that autophagy was impaired in a strain-specific manner, providing proof-of-principle that protein aggregates conforming to different strains have different biological consequences for cells that may underlie the phenotypic diversity observed in tau aggregation disorders.

Further in this work, we uncovered a novel mechanism of protein disaggregation coupled to proteasomal degradation in a mammalian model of amyloid-like tau aggregates. By using a proteomics approach, we identified a PQC component, Valosin-containing protein (VCP), as being critical for tau disaggregation and degradation. VCP, like the canonical disaggregase

chaperones, belongs to a family of AAA+ ATPases and uses the energy from ATP hydrolysis to structurally remodel and segregate its client proteins from complexes. We used a Tet-regulated model for tau expression to show that amyloid-like tau aggregates can be disaggregated and degraded in cells in a proteasome and VCP dependent manner. VCP co-localized with tau aggregates and disaggregation was abrogated when VCP was downregulated by siRNA or inhibited with chemical inhibitors. Ubiquitination of aggregated tau was necessary for VCP recruitment and subsequent disaggregation. Similar to the action of the known yeast disaggregase, Hsp104, availability of seeding competent tau species was dependent on VCP. This is particularly interesting as inhibition of aggregate seeding is a much sought-after strategy for limiting the spread of tau pathology in patient brains. Other components of the PQC network such as Hsp70 assist aggregate clearance seemingly downstream of VCP without affecting the seeding process.

Overall, this work demonstrates the potential of VCP to act as a disaggregase for amyloid-like tau aggregates. While canonical disaggregases of the Hsp100 family exist in prokaryotes (ClpB) and in yeast (Hsp104), a homolog has so far not been found in higher metazoans. Our findings significantly advance the field of metazoan protein disaggregation in cells and provide a platform to further understand the inhibition of such an activity to limit the spread of prion-like aggregates in disease states.

2. INTRODUCTION

2.1 PROTEIN FOLDING AND MOLECULAR CHAPERONES

Proteins are fundamental to any life form and contribute up to 60% of the cellular dry weight in bacteria, yeast and mammalian cells (Feijo Delgado et al., 2013). At the molecular level, proteins are polymers of amino acids (aa) covalently linked via peptide bonds. This linear sequence of aa is the primary structure of a protein and is on average ~560 aa long in the human proteome (Balchin et al., 2016). By virtue of their ability to adopt a defined three-dimensional structure in space, proteins in their native or functional state participate in a variety of biological processes including metabolism, signalling, storage, immune defence, and maintenance of structural integrity. With the exception of so-called intrinsically unstructured proteins, a correctly folded structure is therefore a prerequisite for functional activity (Balchin et al., 2016). The folding of globular proteins in aqueous solution is thought to be driven via hydrophobic collapse of the polypeptide chain burying nonpolar amino acids in the interior of the folded structure and exposing polar amino acids on the surface (Dinner et al., 2000). Furthermore, depending upon the nature of amino acids present, the polypeptide chain can adopt local secondary structures such as α -helices and β -sheets stabilized by intramolecular hydrogen bonds involving the peptide backbone. Electrostatic interactions, Van-der-Waals forces and disulphide bridges are other dominant forces contributing to protein folding and stability (Dill, 1990). Thus, the native state of a protein in a given environment is a thermo-dynamically stable state determined by the totality of its interatomic interactions (Anfinsen, 1973). Proteins must however maintain conformational flexibility to function, and are therefore only marginally stable in their physiological environment.

The observation of spontaneous folding of denatured proteins *in vitro* established the concept that the primary sequence of amino acids in a protein encodes sufficient information to achieve its native state (Anfinsen, 1973). While this is achievable for small (<100 aa) single domain proteins, folding and assembly of large multimeric proteins, especially in the crowded cellular

environment, is a complex process hindered by thermodynamic and kinetic barriers in the folding landscape (Figure 1).

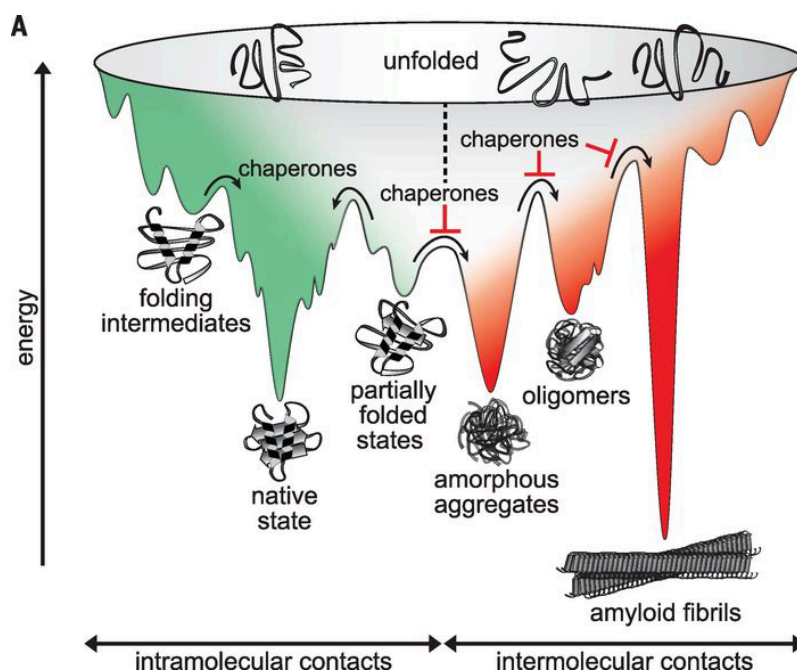


Figure 1. Energy landscape for protein folding

During protein folding, polypeptide chains encounter a rugged energy landscape to reach their thermodynamically stable native state. Chaperones assist protein folding by helping the folding intermediates to overcome free energy barriers. Chaperones also prevent unfolded proteins from forming oligomers or amorphous aggregates or highly stable amyloid fibrils. Figure from (Balchin et al., 2016).

Folding of larger proteins often proceeds via the formation of kinetically trapped intermediates which may lack specific native-like contacts and expose buried hydrophobic regions to the solvent (Dinner et al., 2000). Failure to reach the native conformation in a biologically relevant time frame therefore risks populating partially folded or misfolded off-pathway intermediates that, through the exposed hydrophobic regions, are prone to engage in non-native interactions within the polypeptide as well as with other proteins (Brockwell and Radford, 2007). Such interactions between polypeptides are mostly non-productive and give rise to protein aggregates with higher thermodynamic stability than the native state, and are often associated with diseased states (Jahn and Radford, 2005). Therefore, fast and efficient folding of proteins is necessary to maintain cellular health.

To assist protein folding and assembly *in vivo*, cells have evolved an organised system of ATP-dependent and independent machineries called molecular chaperones. Historically, the term 'molecular chaperone' was first used to describe the aggregation prevention activity of the protein nucleoplasmin which promoted the assembly of DNA and histones into nucleosomes in *Xenopus* egg extracts (Laskey et al., 1978). Later, molecular chaperones were proposed to guide the process of Rubisco (Ribulose-1,5-bisphosphate carboxylase/oxxygenase) assembly from 8 large and 8 small subunits into an active photosynthetic enzyme (Ellis, 1987). The fundamental role of molecular chaperones in protein folding was finally demonstrated by findings that the heat-shock protein- Hsp60 was required for the folding of newly imported mitochondrial proteins (Cheng et al., 1989; Ostermann et al., 1989). These studies revolutionized the perspectives on spontaneous folding of proteins and developed the paradigm of chaperone-assisted protein folding (Hartl, 1996).

A molecular chaperone can be defined as a protein that binds other proteins in their non-native conformation and, through regulated cycles of binding and release, facilitates their correct fate *in vivo*: be it folding, oligomeric assembly or transport to a particular subcellular compartment (Hartl et al., 1994). Chaperone action limits non-native interactions during the folding process and smoothens the folding energy landscape of substrate proteins (Figure 1). In doing so, chaperones prevent the formation of aggregation prone off-pathway intermediates. Chaperones are also vital for the maintenance of protein conformation, as proteins are often only marginally stable in their physiological environment and constantly challenged by denaturing stresses such as high temperature. Consequently, the majority of molecular chaperones are stress-inducible and belong to the heat-shock protein (Hsp) family (Hsp60, Hsp70, Hsp90, Hsp100, Hsp40 and small Hsps). Besides their role in *de novo* protein folding and aggregation prevention, some specialized members of the Hsp100 family act as protein unfoldases and disaggregases (Doyle and Wickner, 2009). Research over the last three decades has unveiled the diversity of chaperone functionality in cell physiology making them an integral component of protein quality control and homeostasis.

2.2 PROTEIN QUALITY CONTROL (PQC)

Cell survival is unequivocally dependent on the integrity of its proteome. Proteins throughout their lifetime are at a risk of confronting destabilizing challenges in the form of mutations, environmental stresses such as perturbations in pH, temperature, pressure and osmotic conditions, or overall physiological alterations as in aging. Therefore, it becomes necessary to constantly monitor the health of the proteome and respond to these changes in a timely manner to maintain protein homeostasis or 'proteostasis'.

Cellular factors responsible for maintaining proteostasis form a complex network of ~2000 proteins referred to as the proteostasis network (PN) (Klaips et al., 2018). The components of the PN attend to protein synthesis at the ribosome (ribosomal PQC), protein sorting and folding in different organelles, and target proteins for degradation as a part of their normal turnover or when they are terminally misfolded or aggregated. Molecular chaperones as the fundamental constituents of the PN, participate in every step from protein synthesis to degradation (Figure 2). In healthy cells, the PN fine-tunes the functionality of its different modules in response to environmental conditions or functional demand. For example, under heat-shock conditions, a number of proteostatic reorganizations take place. Hsps are induced to chaperone misfolded proteins, transcription and translation are downregulated to further minimize protein load, and degradative capacity may be enhanced to eliminate terminally misfolded proteins (Ashburner and Bonner, 1979; Richter et al., 2010). In other systems such as embryonic stem cells, upregulation of protein degradation capacity or accumulation of specific chaperones may occur as an attempt to maintain a pristine proteome prior to differentiation (Jayaraj et al., 2019).

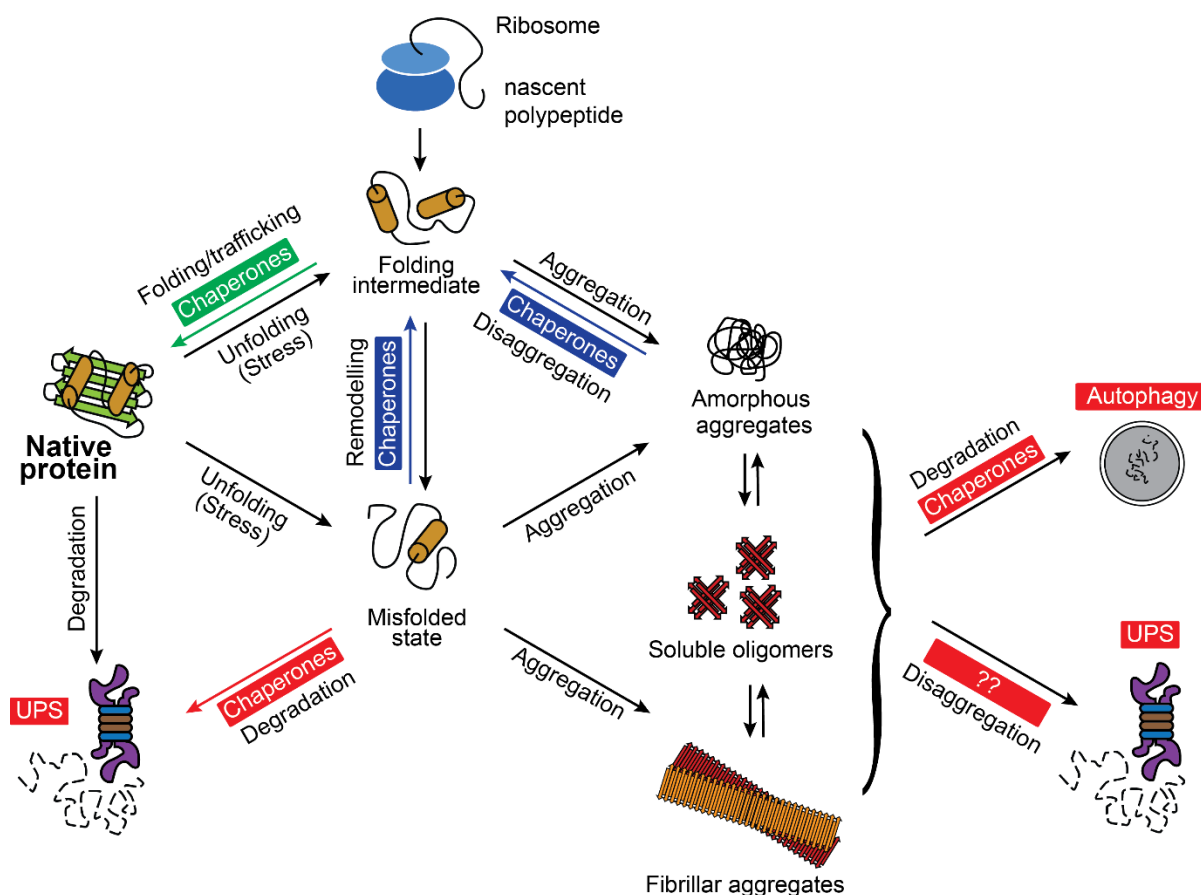


Figure 2. Maintenance of proteostasis by molecular chaperones and protein degradation pathways

Newly synthesized proteins achieve their native state with the help of molecular chaperones. Chaperones can attempt to remodel misfolded or aggregated proteins. If folding or remodelling fails, proteins are targeted for degradation. Persistent stress overwhelms cellular chaperone capacity and results in protein aggregation into structurally diverse aggregates. Aggregates may be further degraded by autophagy or disaggregated followed by targeting to the proteasome. Figure modified from (Hipp et al., 2014).

2.3 PROTEIN DEGRADATION PATHWAYS

Proteins are targeted for degradation- i) as a part of their normal turnover, ii) when they are rendered non-functional by terminal misfolding, aggregation or modifications such as oxidation, and iii) under high catabolic demand such as starvation. Cells have evolved specialized pathways and machineries for degrading proteins in a controlled manner. The two major protein turnover pathways in cells are the ubiquitin proteasome system and autophagy.

2.3.1 Ubiquitin proteasome system (UPS)

The UPS unifies the covalent modification of target proteins by ubiquitin moieties to processing by an ATP dependent protein unfolding and shredding machine, the proteasome. Besides its

role in protein quality control, clearance of proteins by the UPS regulates cell cycle progression, inflammation, apoptosis, signal transduction, antigen presentation and several other essential cellular processes (Finley, 2009). The UPS degrades short-lived regulatory proteins or terminally misfolded proteins in the cytoplasm and nucleus. Proteins from other cellular compartments such as the endoplasmic reticulum (ER) and the mitochondrial outer membrane are also targeted to the UPS via retro-translocation to the cytoplasm prior to degradation (Karbowski and Youle, 2011; Meusser et al., 2005). The UPS therefore contributes to almost 80% of protein degradation in mammalian cells (Collins and Goldberg, 2017).

2.3.1.1 Ubiquitin conjugation cascade

Ubiquitin is a small 76 aa protein and is expressed in all eukaryotic cells. Ubiquitin was initially referred to as 'ubiquitous immunopoietic polypeptide (UBIP)' after its identification in a study that originally aimed to detect factors responsible for inducing differentiation of pro-thymocytes to thymocytes (Goldstein et al., 1975). Later, ubiquitin (ATP-dependent proteolytic factor-1 or APF-1) was recognized as the covalent modifier of proteins critical for their turnover (Ciechanover et al., 1980; Hershko et al., 1980; Wilkinson et al., 1980), and today, is known to direct the fate of proteins in a myriad of cellular processes (Komander and Rape, 2012).

In the majority of ubiquitination reactions, the carboxyl (COOH) group of the C-terminal glycine (G76) in ubiquitin is conjugated to the ϵ -amino (NH₂) group of lysine residues in proteins forming a covalent isopeptide linkage (Hershko et al., 1980; Hershko et al., 1981). However more recently, ubiquitin conjugation to the NH₂ terminal and other amino acids such as cysteine, threonine, and serine, have also been observed (Metzger et al., 2012; Rittinger and Ikeda, 2017). The ubiquitin conjugation reaction is a hierarchical process involving the coordinated action of three enzymes: i) an E1 activating enzyme, ii) an E2 conjugating enzyme, and iii) an E3 ligase (Figure 3). In an ATP dependent process, the C-terminus of ubiquitin is linked to the active-site cysteine of E1 enzyme by a thioester linkage thereby activating ubiquitin for a nucleophilic attack. The activated ubiquitin is then trans-thiolated to the active-site cysteine of an E2 enzyme in a relatively rapid reaction. Finally, the ubiquitin moiety is shuttled to the

by their cognate E1, E2 and E3s in a reaction similar to ubiquitin conjugation (Cappadocia and Lima, 2018). Examples of Ubl proteins include SUMO, NEDD8, LC3, ATG12, URM1, UFM1, FAT10, HUB1, and ISG15, and regulate a growing list of cellular processes including nuclear transport, proteasomal degradation, translation, autophagy and antiviral response (Hipp et al., 2005; van der Veen and Ploegh, 2012).

2.3.1.2 Diverse facets of ubiquitination

The simple three-step ubiquitin conjugation pathway can potentially lead to a multitude of ubiquitination patterns on target proteins. Attachment of one ubiquitin molecule at the ϵ -NH₂ group of a single lysine residue results in monoubiquitination while the same reaction occurring on several lysines gives rise to a multi-monoubiquitinated protein (Figure 4). Ubiquitin can also form polymers by allowing the attachment of the next ubiquitin molecule to one of its own 7 lysine residues (K6, K11, K27, K29, K33, K48, K63) or the α -amino group of the first methionine residue (M1-linear). When the extension always occurs on the same lysine residue, homotypic chains are formed. In addition, the same polymer might also contain other linkages thus forming heterotypic chains. In this manner, a vast array of ubiquitin chain topologies can be generated (Figure 4).

The functional importance of this diversity is only starting to become clear as different ubiquitination patterns confer different fates to the substrates (Yau and Rape, 2016). Monoubiquitination of histone H2A, the first ubiquitin modified protein identified, regulates transcription (Goldknopf et al., 1977; Zhang, 2003). Homotypic UbK63 (ubiquitin molecules linked via K63) chains can mediate innate immune responses, clearance of impaired mitochondria and DNA repair (Yau and Rape, 2016). Moreover, K63 linkages were shown to target proteins and aggregates to autophagy (Ferreira et al., 2015; Tan et al., 2008). Linear ubiquitination is an important regulator of immune response and has also recently been shown to participate in protein quality control (Gerlach et al., 2011; van Well et al., 2019).

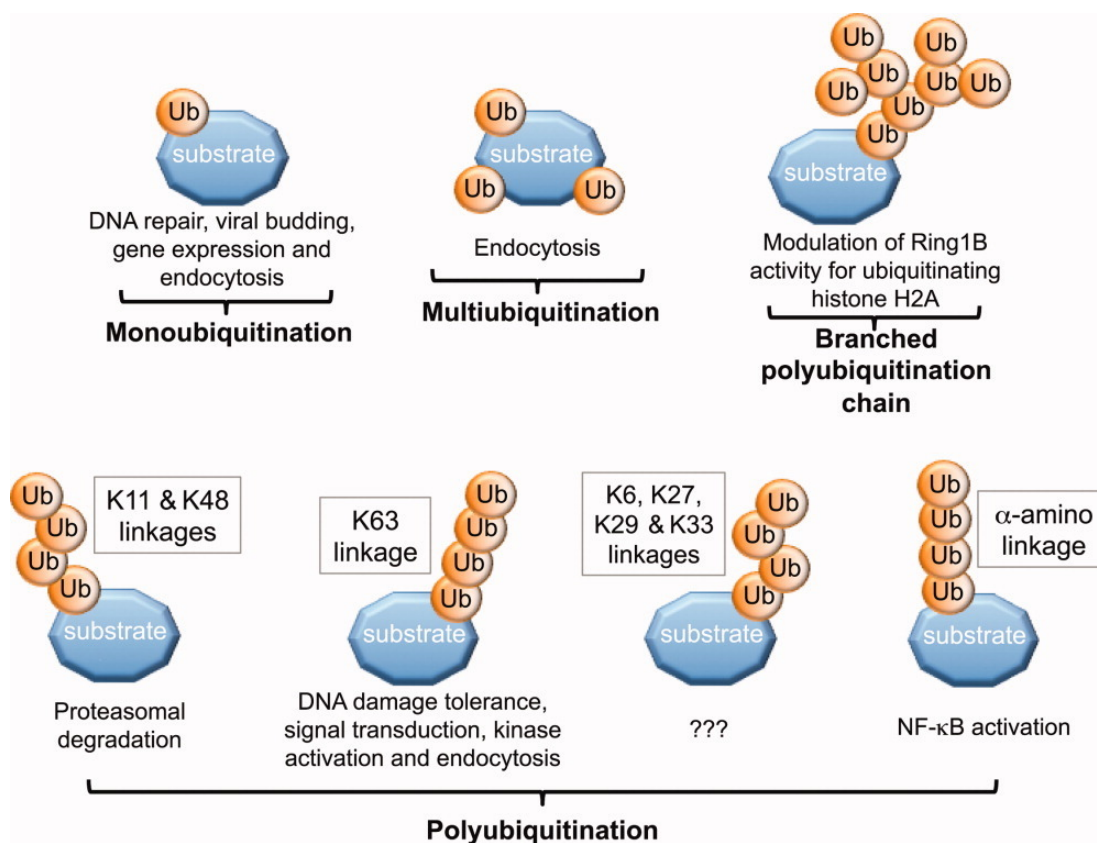


Figure 4. Diversity of ubiquitin linkages and their functions

Target proteins can be modified with ubiquitin in a variety of arrangements. Different ubiquitination patterns direct substrates to different cellular fates. Figure from (Sadowski et al., 2012).

Amongst all other homotypic chains, UbK48 (ubiquitin molecules linked via K48) is the most abundant ubiquitin linkage and directs substrates to the 26S proteasome for degradation (Chau et al., 1989; Finley, 2009; Finley et al., 1994; Xu et al., 2009). This preference of UbK48 over UbK63 chains for proteasomal targeting might be due to better accessibility of the former to the proteasome and limited deubiquitination (Jacobson et al., 2009). In cells, deubiquitination is the process of reversing ubiquitination by the action of deubiquitinating enzymes (DUBs) thereby adding another regulatory step in determining degradation of ubiquitinated substrates. DUBs can trim long ubiquitin chains on substrates prior to proteasomal degradation thus preventing the depletion of cellular ubiquitin pool (Hochstrasser, 1996). This activity might be particularly relevant for efficient ubiquitin recycling since a K48 chain of 4 ubiquitin molecules is sufficient for proteasomal targeting (Thrower et al., 2000).

2.3.1.3 Evolution of compartmentalized protein degradation

Protein degradation in compartmentalized proteases is an ancient mechanism. It is a way to restrain rampant proteolysis in the cell as both protein synthesis and degradation require cellular energy. In bacteria, intracellular proteases like ClpP, HslV, Lon and FtsH represent early prototypes of the eukaryotic proteasome where proteins are degraded in a central hydrolytic chamber. To mark another regulatory layer, proteolysis in the chamber is stimulated only in the presence of Hsp100 proteins of the superfamily of AAA+ ATPases (ATPases Associated with diverse cellular Activities). Two heptameric rings of ClpP protease can associate with different hexameric AAA+ proteins, ClpA or ClpX in Gram-negative and ClpC or ClpX in Gram-positive bacteria forming the functional ClpAP, ClpXP or ClpCP complex (Culp and Wright, 2017). ATP dependent unfolding is an inherent function of AAA+ ATPases (Olivares et al., 2016). The associated AAA+ protein not only allows ClpP to adopt an active conformation but also recruits substrate and unfolds it to facilitate translocation into the proteolytic chamber (Culp and Wright, 2017).

2.3.1.4 The eukaryotic proteasome

The eukaryotic proteasome is a 2.5 MDa structure comprising of a 20S core and a 19S regulatory particle. The 20S particle is a hollow chamber comprising of four stacked heptameric rings of α and β subunits and constitutes the actual site of protein degradation analogous to bacterial ClpP. Two β rings form the proteolytic core with their openings engaged by two α rings resulting in a $\alpha\beta\beta\alpha$ structure (Figure 5). Of the seven β subunits, only $\beta 1$, $\beta 2$ and $\beta 5$ possess proteolytic active sites and perform caspase-like, trypsin-like and chymotrypsin-like activities, respectively (Heinemeyer et al., 1997; Tanaka, 2009). This proteolytic diversity allows the proteasome to digest proteins with a variety of amino acid sequences into 3-22 aa long peptides (Kisselev et al., 1999). The N-terminal tails of the α subunits keep the 20S particle in a proteolytically repressed state by closing the molecular gate of the axial channel thereby guarding substrate entry (Groll et al., 2000). Association of the 19S regulatory particle releases this repression and gives rise to an enzymatically active proteasome.

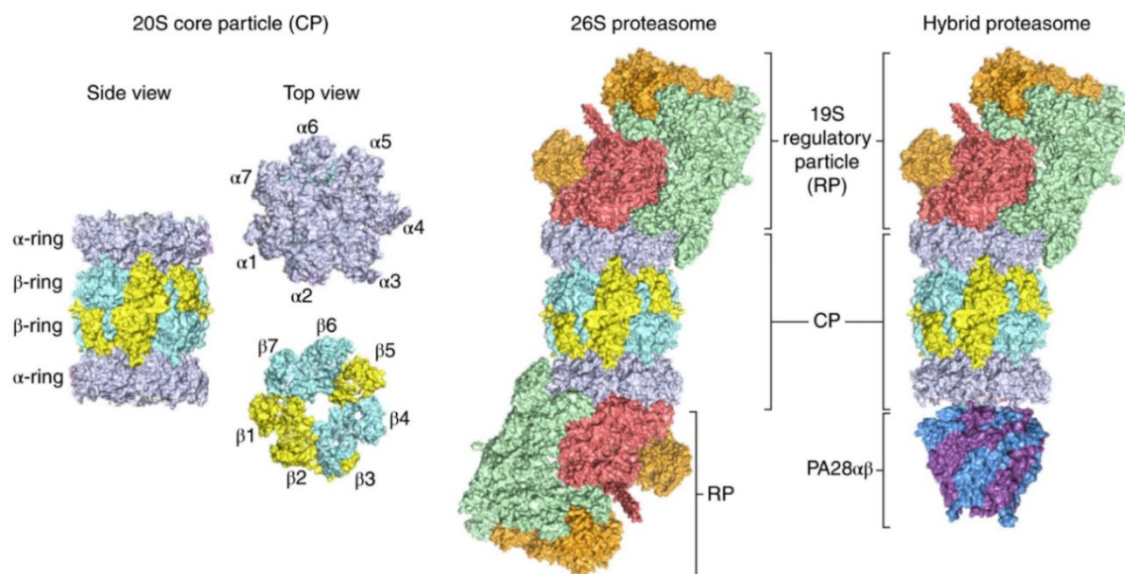


Figure 5. Structure of the eukaryotic proteasome

The 20S peptidase comprises of heptameric α and β rings stacked together to form a barrel like structure. Conventionally, the 20S associates with 19S regulatory particle on one or both ends. Alternatively, an IFN- γ induced PA28 $\alpha\beta$ subunit can replace one 19S particle resulting in highly processive hybrid proteasomes. Figure modified from (Murata et al., 2018).

The 20S core can associate with one or two 19S regulatory particles to form the functional proteolytic proteasome (Figure 5). The 19S cap is further composed of proximal ATPase and distal non-ATPase units. The ‘regulatory particle of triple-ATPase’ (Rpt) subunits form a single hexameric ring of AAA+ ATPases with a central pore which is aligned with the cavity of the 20S particle. Similar to their bacterial counterparts, these AAA+ ATPases are required for unfolding substrates and threading them into the 20S because only unfolded proteins can access the spatially restricted catalytic sites. Despite their sequence similarity and multiplicity, each of the six subunits is functionally unique and essential for degradation (Rubin et al., 1998). In addition to the AAA+ component, the 19S particle comprises of the ‘regulatory particle of non-ATPase’ (Rpn) subunits that perform different functions like scaffolding (Rpn1, Rpn2), ubiquitin recognition (Rpn10, Rpn13) and deubiquitination (Rpn11) of substrates prior to unfolding (Rosenzweig et al., 2008; Tanaka, 2009; Verma et al., 2002). Evolution of ubiquitin modification as a degradation signal for proteasomes might have necessitated the constitution of a more complex regulatory particle in eukaryotes. Intriguingly, the archaeal 20S can associate with a double-ring AAA+ ATPase Cdc48 to form a functional proteasome reminiscent of bacterial proteases (Barthelme et al., 2014; Barthelme and Sauer, 2012). Also, the 19S particle can

perform proteolysis independent functions in stimulating transcription elongation by RNA polymerase II (Ferdous et al., 2001; Ferdous et al., 2002).

Whilst most bacteria lack proteasomes, it is noteworthy that a phylum of gram-positive bacteria called actinobacteria seem to have acquired proteasomal genes via horizontal gene transfer from eukaryotes and in parallel evolved a ubiquitin-like modification of the protein Pup (Pupylation) as substrate recognition signal (Muller and Weber-Ban, 2019). Ubiquitin modification however does not always target substrates to the proteasome. Enzymes like thymidylate synthase and ornithine decarboxylase undergo proteasomal degradation in a ubiquitin-independent manner (Erales and Coffino, 2014; Murakami et al., 1992). Denatured proteins can also be degraded by the proteasome without ubiquitination *in vitro* (Kisselev et al., 1999). Conversely, ubiquitination of a protein alone does not warrant degradation as this modification can direct proteins to other fates. Recent studies highlight the significance of unstructured regions within substrates that are required to engage the proteasome and initiate degradation. The requisite of such an unstructured initiation region also plausibly explains the need for accessory AAA+ unfoldases like Cdc48 for the turnover of certain target proteins (Explained in section 2.8.2) (Tomita and Matouschek, 2019).

As a variant of constitutive proteasomes, immune cells in vertebrates express specialized proteasomes called 'immunoproteasomes' that are conferred with altered cleavage specificity. In immunoproteasomes, the classical proteolytic β subunits are replaced by the corresponding immunosubunits $\beta 1i$, $\beta 2i$ and $\beta 5i$ that are competent generators of MHC class I compatible antigenic peptides to be presented on cell surface for immunosurveillance (Murata et al., 2018). Induction of immunoproteasomes in response to interferon- γ (IFN- γ) stimulation is important to elicit a rapid and controlled immune response (Heink et al., 2005). IFN- γ stimulation also induces the PA28 $\alpha\beta$ subunit which can replace the 19S on one end of 20S to form hybrid proteasomes with enhanced processivity (Figure 5) (Murata et al., 2018; Schwarz et al., 2000). Additionally, cortical epithelial cells in the thymus incorporate a different $\beta 5$ subunit, $\beta 5t$, exclusively expressed in these cells. The 'thymoproteasomes' have an important role in the development of CD8 (+) T cells (Murata et al., 2007).

2.3.2 Autophagy

Autophagy is the process of degradation of cellular material in vacuoles (yeast) or lysosomes (higher eukaryotes). It is a bulk degradation system wherein the material to be degraded is enclosed in a membranous vesicle called autophagosome which further fuses with the vacuole/lysosome resulting in enzymatic degradation of the engulfed material. Historically, autophagy was thought to be specifically induced by starvation to degrade parts of the cytoplasm non-selectively, in order to recycle amino acids, lipids, and carbohydrates. However, autophagy is now known to be constitutively active at basal levels, in addition to being induced by other cellular stresses such as infection, reactive oxygen species (ROS) and hypoxia thereby forming an important regulatory arm of the PN. Moreover, recent research has categorically established substrate selectivity in autophagy which is used to target invading bacteria, organelles (mitochondria, ER, peroxisomes, lysosomes, nucleus and chloroplasts) and aggregated proteins for degradation (Anding and Baehrecke, 2017; Kaushik and Cuervo, 2018).

Components & mechanism of selective autophagy

Initiation- Under nutrient rich conditions, autophagy is repressed by the activity of TORC1 kinase (target of rapamycin complex/ mTORC1 in mammals), a master regulator that senses amino acid availability in cells. Inactivation of TORC1 under starvation results in the dephosphorylation of its clients that trigger downstream steps in autophagy activation. The ULK1 complex along with Class III phosphatidylinositol 3-kinase (PtdIns3K) complex assembles at the pre-autophagosomal structure (PAS) which is the proposed site of autophagosome formation (Yin et al., 2016). This step marks the nucleation of the cup-shaped isolation membrane called phagophore and creates a platform for its further expansion by the action of other autophagy proteins. The entire process of autophagosome formation is coordinated by a repertoire of 31 autophagy-related proteins (ATGs) that work as functional units at different stages of autophagy (Nakatogawa et al., 2009).

Expansion- A crucial step during expansion of the phagophore membrane is the processing of Atg8 (LC3 in mammals). LC3 is a ubiquitin-like protein which is cleaved at its C-terminus by Atg4. The product of this cleavage is LC3-I, a cytosolic form of LC3. In a reaction similar to the

ubiquitin conjugation, LC3-I is attached to a phosphatidylethanolamine (PE) moiety resulting in the formation of lipidated LC3 molecule, LC3-II. This reaction requires the E1-like enzyme Atg7, E2-like enzyme Atg3 and an E3-like activity of the Atg12-Atg5 conjugate (Yang and Klionsky, 2010). LC3-II is then embedded in the inner and outer surface of the phagophore membrane, a process crucial for the closure of mature autophagosomes (Fujita et al., 2008).

Substrate recruitment- Initial substrate recognition in selective autophagy is mediated by receptor proteins such as p62, Optineurin, NBR1, Alfy, etc. (Figure 6). Most autophagy receptors have a ubiquitin associated (UBA) domain through which they recognise ubiquitinated cargo (Deng et al., 2017). However, substrates can also be recognized in a ubiquitin-independent manner by specific types of lipid-, protein- and sugar-based cues (Khaminets et al., 2016). The receptor proteins additionally possess a conserved motif Trp/Phe/Tyr-x-x-Leu/Ile/Val (W/F/YxxL/I/V) called LC3-interacting region (LIR) through which they concomitantly attach the cargo to the growing phagophore via attachment to LC3 (Dikic and Elazar, 2018). The eventual expansion and closure of the phagophore around the cargo gives rise to the double membrane autophagosome. Subsequent fusion of the autophagosome with the lysosome results in the formation of an autolysosome where the sequestered cargo material along with the autophagy receptors and LC3-II is degraded.

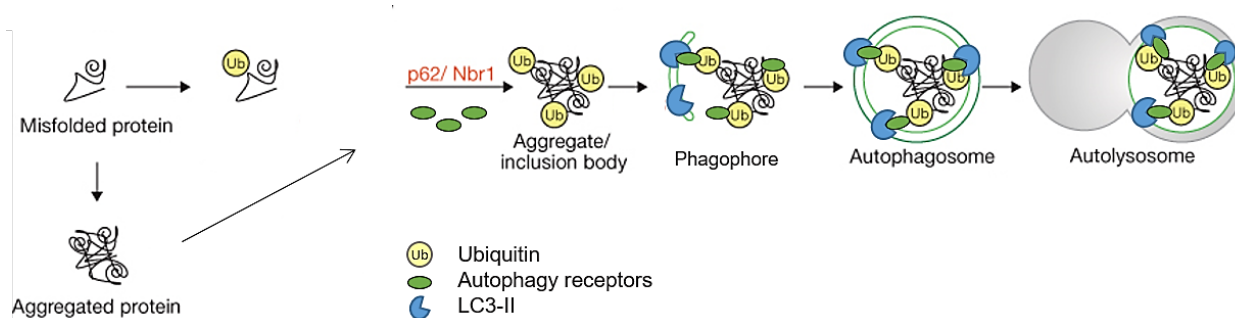


Figure 6. Selective autophagy of protein aggregates

Selective autophagy can degrade bulky substrates such as protein aggregates. Misfolded or aggregated proteins accumulate in ubiquitinated inclusion bodies that are recognized by ubiquitin-binding autophagy receptors. The cargo is then bridged to a growing phagophore by the binding of autophagy receptors to LC3-II on the phagophore membrane. Phagophore closure around the cargo results in the formation of autophagosomes which finally fuse with lysosomes. Figure modified from (Kraft et al., 2010).

In addition to conformational parameters, aggregation is a highly concentration-dependent process driven by the increase in concentration of a protein beyond its critical level of solubility (Ciryam et al., 2015). Such a situation may arise when the protein degradation capacity of the cell is compromised or overwhelmed. Moreover, conformation destabilizing mutations or the presence of intrinsically disordered regions can also predispose polypeptides to aggregation. Consequently, a plethora of human diseases feature protein aggregates in different organs of the body. Protein aggregation not only deprives the cell of functional proteins causing possible loss-of-function effects but the aggregates might also gain a novel toxic function by impeding cellular processes and sequestering essential proteins. Therefore, dealing with aggregated proteins is necessary to conserve proteostasis and general organismal fitness.

2.4.1 Cellular mechanisms to cope with aggregated proteins

When protein aggregation becomes inevitable, the cellular PQC can execute specialized mechanisms as a second line of defence to handle aggregated proteins and minimize their toxicity. Most of these mechanisms utilize the existing cellular resources such as molecular chaperones to various ends, and protein degradation pathways to ultimately eliminate the aggregates. Misfolded proteins and aggregates can be spatially sequestered and stored in a presumably less toxic form in PQC compartments or inclusion bodies (IBs). The formation of IBs is an active process which proceeds via the recognition of misfolded/aggregated proteins by different molecular chaperones of the Hsp70, Hsp90, Hsp110, and small heat shock protein family (Sontag et al., 2017). A number of different IBs have been described in the yeast cytosol such as the juxtannuclear quality control compartment (JUNQ), the insoluble protein deposit (IPOD), and Q-bodies, all of which seem to serve specific proteostasis needs of the cells under physiological and stress conditions. The JUNQ is a dynamic perinuclear compartment and actively exchanges material with the cytosol whereas the IPOD is a deposition site for terminally aggregated proteins (Kaganovich et al., 2008). Q-bodies are punctate structures that also represent dynamic inclusions and sequester misfolded proteins at an early stage to allow re-solubilization or degradation (Escusa-Toret et al., 2013). Similar to the JUNQ, the mammalian aggresome is a juxtannuclear compartment formed in response to the accumulation of

misfolded/aggregated proteins due to proteasome inhibition (Johnston et al., 1998). Aggresome formation requires the microtubule-based retrograde transport of misfolded/aggregated proteins to the pericentriolar region where they can be targeted for degradation by the UPS or autophagy. Consistently, several studies have reported aggresome clearance and autophagy has been implicated as the main pathway behind this clearance (Olzmann et al., 2008). Therefore, disease-associated IBs may not denote a PQC endpoint; rather an orchestrated protective strategy to confine protein aggregates (Arrasate et al., 2004).

2.4.2 The amyloid state of proteins

The term 'amyloid' (starch-like) was introduced by Rudolph Virchow in 1854 to indicate pathological IBs in patient brains that stained violet with iodine, which is used to detect starch. The findings of Friedreich and Kekule later demonstrated the enrichment of proteins and absence of carbohydrates in these deposits. Over the years, amyloids have been identified by their characteristic tinctorial properties and their fibrillar appearance in EM (Sipe and Cohen, 2000). Congo red (CR) and Thioflavin T (ThT) dyes have been conventionally used to selectively detect amyloid structures *in vitro* and *in vivo*. Upon binding to amyloid fibrils, CR emits an apple-green birefringence under cross-polarized light while ThT shows an enhanced red shifted fluorescence (Howie and Brewer, 2009; LeVine, 1993). However, there are now improved tracers such as AmyloGlo that are brighter, have unique emission spectra that allow simultaneous high contrast co-labelling with red and green probes, and preclude the use of harsh reagents which may induce artefacts (Schmued et al., 2012).

Solid state nuclear magnetic resonance (ssNMR) spectroscopy and X-ray diffraction analyses of amyloid fibrils formed from diverse precursor proteins reveal a highly organized β -sheet rich structure represented by the 'cross- β ' pattern. This is a unifying molecular pattern of the core of all amyloid fibrils and corresponds to parallel or anti-parallel β -sheets running perpendicular to the fibrillar axis (Eisenberg and Jucker, 2012). The final amyloid structure is inter-digitated with H-bonds between the β -strands that confer amyloids exceptional stability and tensile strength (Knowles et al., 2007). Therefore, the amyloid structure may represent a thermodynamic endpoint in the folding landscape of proteins unrelated in structure, function, and amino acid

sequence. However, the final stability, structural details, and mechanism of formation of the amyloid can vary for different proteins (Knowles et al., 2014).

2.4.2.1 Mechanism of amyloid biogenesis

Mechanisms governing amyloid formation have been primarily deciphered from *in vitro* aggregation reactions of proteins or synthetic peptides into fibrillar structures. Amyloid formation is a nucleation-dependent process that involves *de novo* formation of an aggregation nucleus or seed from monomers (Chen et al., 2002; Lomakin et al., 1996; Wood et al., 1999). This step, also referred to as primary nucleation, is thermodynamically unfavourable and is therefore rate limiting for amyloid formation (Bhattacharyya et al., 2005). Structural details of the aggregation nucleus have so far remained obscure mainly due to its unstable nature and transient existence. Based upon kinetic parameters of *in vitro* aggregation reactions, some studies have attempted to determine the size of the critical nucleus, which is defined as the number of monomeric units involved in the formation of an energetically unfavourable aggregation nucleus, and suggest that a monomer can act as the critical nucleus to initiate the aggregation cascade (Bhattacharyya et al., 2005; Chen et al., 2002; Kar et al., 2011). Alternatively, aggregation seeds can comprise of several monomers clustered to form oligomers (Poirier et al., 2002; Rochet et al., 2000). Oligomers are metastable species held together by weak intermolecular interactions and mostly lack the long-range order of the final amyloid structure (Chiti and Dobson, 2017). Besides nucleating aggregation, soluble oligomers can also exist as intermediates in equilibrium with the monomer and amyloid fibrils (Figure 8), and are increasingly thought to be the key mediators of amyloid-associated toxicity.

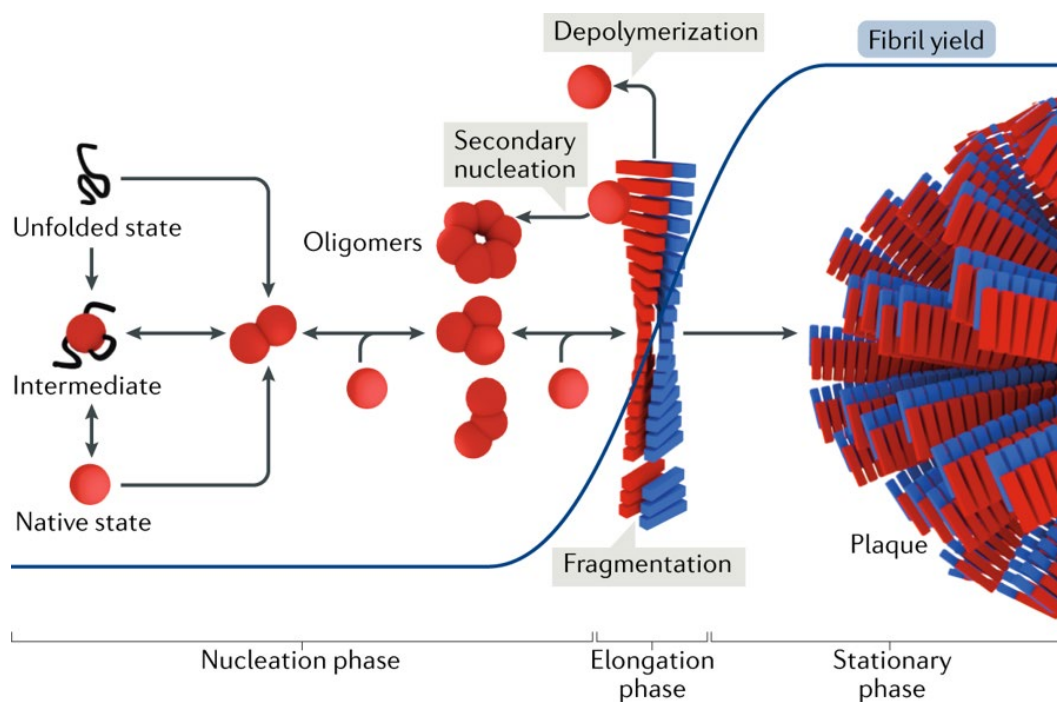


Figure 8. General scheme of amyloid aggregation

Amyloid aggregation begins with a rate limiting nucleation phase. Proteins in native or non-native conformations initiate amyloid formation by forming oligomers which can further develop to form higher-order oligomers. Any of these oligomeric species may act as a fibril nucleus which grows by recruiting monomers or other oligomers. Fibrils can further elongate or self-associate in different topologies giving rise to filamentous structures with different morphologies. Depending upon their stability, fibrils may exhibit dynamic fragmentation or depolymerisation and release oligomers or monomers which may or may not be similar to the ones before incorporation into the fibril. Figure from (Iadanza et al., 2018).

After the primary nucleation, monomers are rapidly recruited to the seed to form mature fibrils in an energetically favourable elongation phase (Figure 8). Pre-formed amyloid fibrils promote further aggregation either by providing a reactive surface for secondary nucleation or by acting as templates for a new round of elongation thereby eliminating the rate limiting nucleation phase (Knowles et al., 2014). Some amyloid fibrils may spontaneously fragment and increase the number of growing ends which further increases their seeding capacity (Kundel et al., 2018). Aggregate growth on a pre-formed template establishes a similar in-register incorporation of monomers to the fibril ends thereby maintaining the structural definition of the seeding amyloid at the molecular level. In the physiological context, such a template-based propagation of structural conformation underlies the concept of ‘prions’ (Continued in section 2.6).

2.4.2.2 Physiological and disease-related amyloids

Although amyloids were discovered in the context of disease, they also exist in healthy cells and perform biological functions. For instance, some endocrine hormones are stored as amyloids in secretory granules of pituitary, hypothalamus and pancreas (Maji et al., 2009). The Pmel17 protein in melanosomes forms amyloid-like filaments which not only catalyse melanin polymerization but also alleviate the toxicity of highly reactive melanin precursors (Fowler et al., 2006). The eggshell of silk moths is rich in proteins containing β -sheet rich amyloidogenic segments that are thought to confer mechanical stability required for protecting the developing embryo (Benaki et al., 1998; Iconomidou et al., 2000). Bacteria produce proteinaceous curli fibres with amyloid-like characteristics that mediate attachment to biofilms (Barnhart and Chapman, 2006). Thus, the occurrence of amyloids is not an obvious threat to organismal fitness as long as specific amyloids have evolved to fulfil a biological function.

In contrast, disease-related amyloid aggregates, despite being structurally similar to physiological amyloids, form in an uncontrolled manner and can overwhelm the cellular proteostasis capacity. Amongst others, amyloid deposition is characteristic of polyglutamine (polyQ) expansion disorders such as Huntington's disease (HD) and some hereditary forms of amyotrophic lateral sclerosis (ALS). In these diseases, an aberrant expansion in a repetitive sequence harboured in the protein coding region of the huntingtin gene and the non-coding region of the C9orf72 gene results in the expression of the amyloidogenic protein (Iadanza et al., 2018). The polyQ expansion mutation has a high penetrance and the severity of disease directly correlates with the length of the expansion, which in turn determines the aggregation potential thereby strongly indicating that aggregation is critical component of the disease. Consequently, polyQ aggregation and toxicity is reproducibly observed by exogenous expression of the protein in a variety of model systems such as cultured mammalian cells, nematodes, drosophila and mice (Bates, 2003; Faber et al., 1999; Jackson et al., 1998; Li and Li, 1998; Rubinsztein, 2002). Other debilitating amyloid deposition diseases such as Alzheimer's disease (AD) and Parkinson's disease (PD) mainly manifest in an age-dependent manner and are characterized by widespread aggregation of amyloid β (A β) and tau, and α -synuclein,

respectively. Proteostasis decline during aging is thought to play a critical role in the onset of these diseases (Hipp et al., 2019).

2.5 TAU IN PHYSIOLOGY AND PATHOLOGY

The microtubule associated protein tau (MAPT) is the major component of intracellular amyloid deposits or neurofibrillary tangles (NFTs) observed in human patient brains with progressive neurodegenerative conditions such as AD. Tau aggregation is a compelling hallmark of more than two dozen clinically distinct disorders collectively referred to as tauopathies (Table 1). Tauopathies can be classified as primary or secondary based on the expression of mutant or wild-type tau respectively (Simic et al., 2016). Frontotemporal dementia and parkinsonism linked to chromosome 17 (FTDP-17) is an example of a primary tauopathy, whereas AD is the most prevalent secondary tauopathy. Tau aggregation may also be observed at low levels in the brains of normally aged individuals (Baner et al., 1989; Ulrich, 1985).

Table 1: Tauopathies. Modified from (Goedert et al., 2017b).

Alzheimer's disease
Amyotrophic lateral sclerosis/parkinsonism-dementia complex
Argyrophilic grain disease
Chronic traumatic encephalopathy
Corticobasal degeneration
Diffuse neurofibrillary tangles with calcification
Down's syndrome
Familial British dementia
Familial Danish dementia
Familial frontotemporal dementia and parkinsonism
Gerstmann-Sträussler-Scheinker disease
Guadeloupean parkinsonism
Huntington's disease
Meningio-angiomasia
Myotonic dystrophy
Neurodegeneration with brain iron accumulation
Niemann-Pick disease, type C
Nodding syndrome
Non-Guamanian motor neuron disease with neurofibrillary tangles

Pick's disease
 Postencephalitic parkinsonism
 Progressive supranuclear palsy
 SLC9A6-related mental retardation
 Subacute sclerosing panencephalitis
 Tangle-only dementia
 White matter tauopathy with globular glial inclusions

2.5.1 Normal function of tau

Tau was first identified in 1975 as a heat stable assembly factor necessary to induce the polymerization of α - β tubulin dimers into microtubules *in vitro* (Bryan et al., 1975; Keates and Hall, 1975; Weingarten et al., 1975). In the adult human central nervous system (CNS), tau is expressed as six isoforms resulting from alternative splicing of its pre-mRNA (Goedert et al., 1989). The longest tau isoform is 441 aa long and is composed of an acidic N-terminal projection domain (containing 2 inserts N1 and N2 of 29 amino acids each), a proline-rich domain, a microtubule binding repeat domain (RD; 4 inserts R1-R4 of 31-32 amino acids each) and a basic C-terminal tail (Figure 9). The products of alternative splicing differ in terms of having no, one or both N1 inserts in addition to 3R or 4R repeats (Kolarova et al., 2012). The different tau isoforms are developmentally regulated and differ in their affinities for microtubule binding (Kosik et al., 1989; Wang and Mandelkow, 2016).

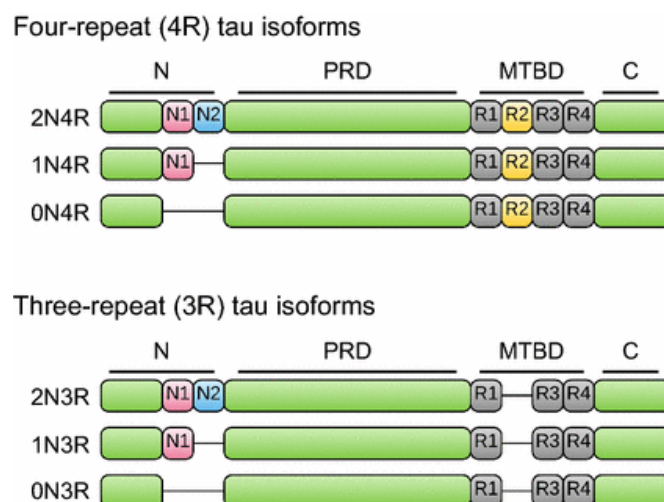


Figure 9. Tau domain architecture and isoforms

Full length tau (2N4R) is divided into four domains; The N-terminal projection domain (N), a proline-rich domain (PRD), a microtubule binding repeat domain (MTBD) and a C-terminal domain (C). Tau is processed into six isoforms by alternative splicing of the MAPT mRNA. One set of spliced products

contains all four repeats of the MTBD (4R) and the other set contains three repeats (3R) depending upon the inclusion or exclusion of the repeat region 2 (R2) respectively. These splice variants can further have either (2N), one (1N) or no (0N) N-domain. The C-terminal domain is present in all isoforms. Figure adapted from (Guo et al., 2017)

Tau is highly expressed in the CNS but also occurs in small amounts in kidney, lung, and testis (Morris et al., 2011). Tau, via its repeat domain, binds the interface between tubulin dimers to promote their polymerization and stabilizes them against depolymerisation (Drubin and Kirschner, 1986; Kellogg et al., 2018). In cultured neurons, tau is required for proper axonal and neurite development (Caceres and Kosik, 1990; Dawson et al., 2001). Despite the role of tau in neuronal cell morphogenesis, tau knockout (KO) mice are viable, do not display any physical abnormalities and develop normally (Dawson et al., 2001; Harada et al., 1994; Tucker et al., 2001). This lack of phenotype in tau KO mice is attributed to the compensatory upregulation of other functionally redundant microtubule associated proteins (MAPs) during development, which are later restored to normal levels in adult mice (Dawson et al., 2001; Harada et al., 1994). Consistently, mice carrying double deletions of tau and MAP1B suffer postnatal lethality pointing towards a critical function of overall cytoskeletal development for organismal growth and survival (Takei et al., 2000).

2.5.2 Role of tau in neurodegeneration

AD is the most prevalent tauopathy and characterized by the deposition of intracellular tau aggregates in addition to extracellular deposits of the A β protein in insoluble plaques. According to the amyloid cascade hypothesis, tau pathology (or aggregation) follows A β deposition, which is considered as the primary trigger for disease progression in AD (Hardy and Selkoe, 2002). However, reducing endogenous tau levels is protective against A β induced behavioural deficits and mortality in mice showing that tau mediates part of the pathological features in an AD mouse model (Roberson et al., 2007). Moreover, in most other tauopathies, tau pathology is observed independent of A β deposition, indicating that tau dysfunction or aggregation *per se* can lead to neurodegeneration (Nisbet et al., 2015).

While no tau mutations have been identified in AD so far, dominant tau mutations (e.g. P301L, V337M) are found to segregate with familial forms of FTDP-17 or related disorders. So far, 49 such mutations have been found in the coding region of tau and 10 in introns (Dumanchin et al., 1998; Goedert et al., 2017a; Poorkaj et al., 1998). The majority of the mutations in the coding regions are localized in and around the microtubule binding RD of tau and affect its ability to promote tubulin polymerization (Goedert and Spillantini, 2000). Other mutations alter the splicing pattern of tau mRNA resulting in a higher proportion of the more pathogenic 4R tau isoform (Hutton et al., 1998; Spillantini et al., 1997). Contrary to what is observed in tau KO mice, mouse models that over express mutant human tau show disease relevant pathological phenotypes (Denk and Wade-Martins, 2009). Specifically, a mouse model that expresses a double mutant of tau (P301L, R406W) at low levels in the forebrain in addition to endogenous murine tau displays frontotemporal dementia-like behavioural deficits accompanied by progressive tau phosphorylation (Koss et al., 2016). A rat model expressing human P301S tau exhibits age-dependent tau aggregation and global neurodegeneration, closely recapitulating human tauopathy-like features (Malcolm et al., 2019). These studies indicate that mutant tau gains a toxic function and is capable of driving neurodegeneration.

2.5.3 Tau hyperphosphorylation

In disease conditions, tau fails to perform its normal function and deposits in abnormally phosphorylated NFTs in the neuronal cell body (Grundke-Iqbal et al., 1986; Iqbal et al., 1986). Phosphorylation is a physiological modification of tau which negatively regulates its microtubule polymerization activity *in vitro* (Cleveland et al., 1977; Lindwall and Cole, 1984). While the normal phosphate content of tau is ~2 mol phosphate/mol protein, tau in PHF is hyperphosphorylated and contains as much as 8 mol phosphate/mol protein (Ksiezak-Reding et al., 1992). Hyperphosphorylation of tau is believed to be an early event in disease progression that precedes its aggregation into PHFs, and correlates with the appearance behavioural deficits in animal models (Baner et al., 1989; Kopke et al., 1993; Koss et al., 2016). Although what triggers tau hyperphosphorylation is not clearly understood, this modification can, directly or indirectly, result in tau dysfunction by a variety of mechanisms such as missorting of tau from

axons to the somatodendritic compartment, altered cleavage pattern, reduced turnover, enhanced aggregation propensity and engagement in aberrant cellular interactions (Wang and Mandelkow, 2016). Hyperphosphorylation may shield the repulsive positive charges on tau and promote intramolecular tau interactions leading to its aggregation (Alonso Adel et al., 2004).

Intriguingly, while tau aggregates in human brain are hyperphosphorylated, not all hyperphosphorylated tau is found in aggregates or is associated with disease. For instance, during development, human fetal brain expresses a tau isoform which is as heavily phosphorylated as PHFs in AD (Kenessey and Yen, 1993). A similar increase of tau phosphorylation is observed in fetal tau in rats (Watanabe et al., 1993). PHF-like hyperphosphorylated tau in squirrels may even regulate neuronal plasticity switches between hibernation and arousal (Arendt et al., 2003). Moreover, non-phosphorylated recombinant tau assembles into PHF-like aggregates *in vitro* (Crowther et al., 1994; Goedert et al., 1996). Thus, hyperphosphorylation may not be the most critical factor mediating tau aggregation in disease conditions. Hitherto, the mechanisms and cellular factors involved in initiating tau aggregation *in vivo* are not well understood.

2.5.4 Tau aggregation and polymorphism

Tau is a highly soluble hydrophilic protein and exhibits marked resistance to aggregation *in vitro* and in cultured cells even at high concentrations. However, FTDP-17 associated mutations predispose tau to aggregation, mainly by introducing aggregation-promoting signatures in its otherwise intrinsically disordered structure (von Bergen et al., 2006; von Bergen et al., 2001). The tau RD plays a critical role in aggregation because it is the only region of tau with hydrophobic residues. Particularly, two hexapeptide motifs in the tau RD, VQIINK in R2 and VQIVYK in R3, undergo a conformational change from random coil to β -sheet (von Bergen et al., 2005), thereby setting off the transition from a soluble to amyloid-like fibrillar state. In fully assembled AD PHFs, RD forms the β -sheet rich core of tau fibrils while the rest of the protein appears as a 'fuzzy coat' around the core (Barghorn et al., 2004; Crowther et al., 1989; Wischik et al., 1988). Consistent with its presence in the amyloid core, the RD fragment itself assembles into AD-like filamentous aggregates more readily than full length tau (Crowther et al., 1992; von

Bergen et al., 2000; Wille et al., 1992). Consequently, tau RD expressing models have been extensively used to study various aspects of tau aggregation (Kaufman et al., 2016; Khlistunova et al., 2006; Sanders et al., 2014).

The *in vitro* aggregation propensity of tau can be significantly enhanced in the presence of sulphated glycosaminoglycans like heparin (Goedert et al., 1996; Perez et al., 1996). Heparin induces pro-aggregation structural alterations in tau which involve loss of long range order and a concomitant compaction of the RD into a β -sheet structure (Elbaum-Garfinkle and Rhoades, 2012). Heparin may also integrate into the amyloid core and stabilize it by neutralizing the positive charges in the regions around RD (Sibille et al., 2006). However, despite their amyloid-like fibrillar appearance in low-resolution negative stain micrographs, tau assemblies formed in the presence of heparin are not homogenous and exhibit structural polymorphism (Fichou et al., 2018). Structural polymorphism in amyloids is a result of the precursor protein adopting more than one conformation in the β -sheet arrangement. As a result, the 2N4R tau isoform gives rise to four different conformations of filaments- snake (~45%), twister (~30%), hose (~20%) and jagged (~5%), with a variety of widths and periodicities (Zhang et al., 2019). Interestingly, tau fibrils obtained from patient brains also manifest such a structural heterogeneity (Figure 10). While NFTs in AD are predominantly rich in PHFs, they also contain a different fibrillar conformer called straight filament (SF) (Crowther, 1991). Interestingly, cryo-EM based 3-D reconstruction of the fibrillar cores in both PHFs and SFs reveals two identical protofilaments folded into a compact C-shaped structure from residues 306-378 of tau (Fitzpatrick et al., 2017). The point of difference, however, lies in the lateral contact sites between the two protofilaments (Figure 10). Moreover, the fibrillar core in Pick's disease adopts an extended conformation markedly different than the C-shaped fold in AD and comprises of a single protofilament formed out of residues 254-378 of tau (Figure 10) (Falcon et al., 2018). Similar to tau, amyloids of A β peptide and α -synuclein have also been shown to exhibit structural polymorphism (Tycko, 2015). Notably, these structural polymorphs may define unique *strains* which self-propagate and amplify their molecular arrangement by seeded fibril growth akin to prions and are increasingly studied for

their relevance in the phenomenon of pathological spreading observed in neurodegenerative diseases (Jucker and Walker, 2018; Soto and Pritzkow, 2018).

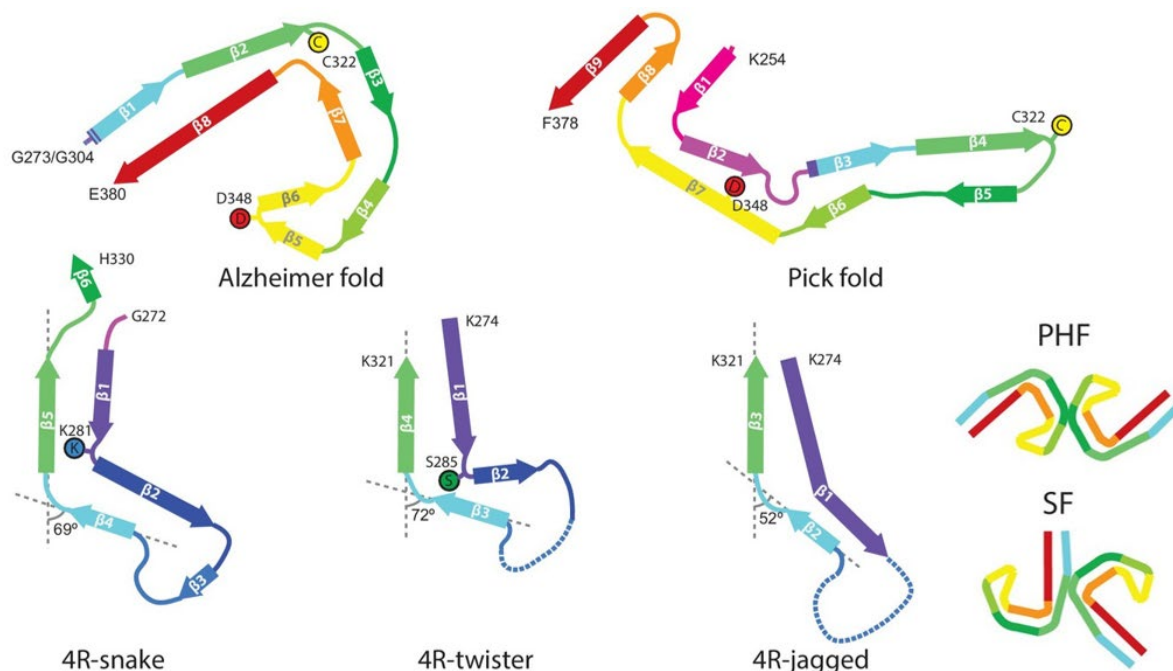


Figure 10. Cryo-EM structures of tau filament cores

Schematic representation of the different tau folds from disease-related and *in vitro* formed tau fibrils highlighting polymorphic aggregation. Yellow and red circles in disease folds indicate residue Cys322 and Asp384 respectively, and show reversed solvent-exposure in the two folds. Figure adapted from (Zhang et al., 2019).

2.6 PRION-LIKE PROPAGATION AND SPREADING

The archetypical prion or 'proteinaceous infectious particle' is an abnormal self-propagating conformation (PrP^{Sc}) of the cellular prion protein (PrP^{C}). Prions are responsible for causing neurodegenerative diseases like Creutzfeldt–Jakob disease, kuru and Gerstmann–Sträussler–Scheinker disease in humans, scrapie in goats and sheep, transmissible spongiform encephalopathy in cattle and mink, and chronic wasting disease in deer and elk (Prusiner, 2013). The origin of PrP^{Sc} in an organism can be sporadic, genetic or transmitted. Once acquired, PrP^{Sc} corrupts the normal PrP^{C} through a templated conformational change to form transmission-competent oligomers and/or amyloids (Meyer et al., 1986; Prusiner et al., 1983). Synthetic PrP^{Sc} aggregates or brain homogenates from diseased animals when inoculated in healthy animals induce neurodegeneration and retain their infectivity even after serial transmission of brain

material (Hsiao et al., 1994; Tremblay et al., 2004). Structurally polymorphic PrP^{Sc} conformers or strains elicit distinct biological consequences and determine disease characteristics like incubation period, histopathological profiles, and spreading to targeted brain areas (Aguzzi et al., 2007).

2.6.1 Prion-like properties of tau

Studies in the last decade have demonstrated prion-like features of tau aggregates in animal models under laboratory conditions. These features include horizontal transmission of tau pathology, spreading via inter-cellular contact and propagation of unique strains by self-replication. Tau fibrils obtained from AD brains are capable of inducing tau aggregation in mice brains expressing mutant human tau (Iba et al., 2013). A similar seeding effect is observed if, instead, the brain extract is obtained from a mouse model of tauopathy (Clavaguera et al., 2009). Additionally, aggregates in a transgenic mouse expressing human tau, spread from their site of origin across neuroanatomically connected brain regions, co-aggregate with endogenous mouse tau and trigger neuronal loss (de Calignon et al., 2012). In agreement with the model that different tauopathies propagate different tau strains, aggregated tau from AD and corticobasal degeneration induce spreading of tau aggregates in distinct cell types in injected mouse brains (Boluda et al., 2015). Moreover, cultured cells exposed to recombinant tau fibrils can propagate morphologically distinct tau aggregate strains which differ in their seeding competency and *in vivo* pathological phenotypes (Kaufman et al., 2016; Sanders et al., 2014). Mechanistically, it has been shown that extracellular tau aggregates can enter cells and propagate their aberrant conformation to intracellular tau resulting in aggregation (Frost et al., 2009; Kfoury et al., 2012). Therefore, like prions, exogenous tau aggregates can infect cells, induce aggregation of endogenous tau and form distinct strains.

2.6.2 Yeast prions

Yeast prions have unveiled important aspects of prion biology which may be directly relevant for understanding the behaviour of their mammalian counterparts. Prions in yeast are protein-based

genetic elements which confer biologically relevant phenotypes without any concomitant changes at the level of nucleic acid (Uptain and Lindquist, 2002). The most studied yeast prions are formed by the Sup35, Ure2 and Rnq1 proteins. Under normal conditions, Sup35 is a subunit of the yeast translation termination factor. In the prion state [PSI⁺], Sup35 loses its functional conformation and aggregates into β -sheet rich amyloid fibrils (Glover et al., 1997; Patino et al., 1996; Paushkin et al., 1996). As a result, the fidelity of translation termination is reduced and ribosomes read through stop codons leading to a nonsense-suppression phenotype (Cox et al., 1988). In the Ure2 prion state [URE3], yeasts overcome nitrogen catabolite repression and metabolise nitrogen-poor sources like ureidosuccinate even in the presence of nitrogen-rich compounds like ammonium (Wickner, 1994).

Over-expression or mutation of the prion-precursor protein increases the probability of prion formation which otherwise occurs at low frequency in nature (Chernoff et al., 1993; Wickner, 1994). However, once established, the prion propagates via direct cytoplasmic transfer from mother to daughter cells. Like mammalian prions, yeast prions rely on conformational conversion for propagation, which is achieved by continued synthesis of the prion-precursor protein and segregation of the prion seed in daughter cells post-mitosis and meiosis (Uptain and Lindquist, 2002). Prion seeds are fragments of the parental amyloid fibres which act as self-perpetuating templates to initiate prion formation (Figure 11). On the molecular level, Hsp104, a chaperone that disintegrates protein aggregates, fragments Sup35 amyloid fibrils to generate prion seeds (Shorter and Lindquist, 2004). Consequently, the prion propagation terminates and prion state is irreversibly cured when Hsp104 is deleted. Paradoxically, the prion state is also cured when Hsp104 is over-expressed. This curing effect is due to over-fragmentation of the fibrils resulting in their complete elimination from cells (Chernoff et al., 1995). If mammalian prions are also fragmented by disaggregase activity is not yet known.

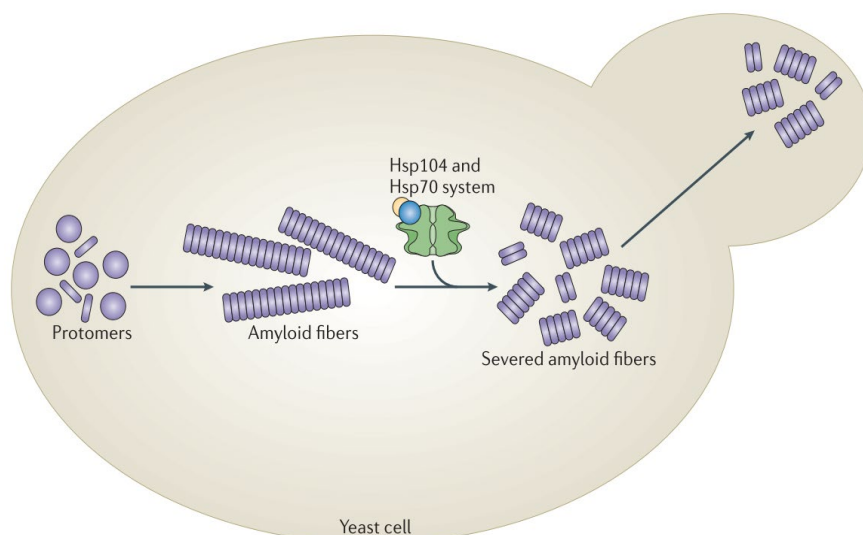


Figure 11. Role of Hsp104 in amyloid seeding

Hsp104, in cooperation with the Hsp70 system, fragments amyloid fibrils of yeast endogenous prions. Fragmented fibres are relatively smaller and can be easily transmitted from mother to daughter cells where they act as seeds to initiate amyloid fibril formation and propagation of the prion phenotype. Figure adapted from (Doyle et al., 2013).

2.7 PROTEIN UNFOLDING AND DISAGGREGATION

A functional PN limits protein aggregation that may result from unsuccessful folding, environmental stress, or mutations. However, under certain conditions like ageing or chronic stress, the load of faulty proteins can overwhelm the capacity of the PN, resulting in aggregation. Subsequently, in order to maintain proteostasis, PQC pathways can recognize protein aggregates and handle them in a number of ways, one of which is disaggregation. Rescuing proteins via disaggregation can be beneficial for cells recovering from stress, because post-stress cells might be in an energy-deficient state and degrading existing proteins and synthesizing them new requires cellular energy. Therefore, cells deploy molecular chaperones that, alone or in combination with other chaperones, perform protein unfolding and disaggregation. These specialized chaperones belong to the Hsp100 family and are found in bacteria (ClpB), yeast (Hsp104), plants (Hsp101) and mitochondria of eukaryotes (Hsp78).

2.7.1 Hsp100 disaggregases- Hsp104 and ClpB

The *Saccharomyces cerevisiae* Hsp104 and its homolog in *Escherichia coli* ClpB are canonical disaggregases that solubilize both amorphous and amyloidic protein aggregates *in vitro* and *in vivo* (Doyle et al., 2013). Consequently, cells lacking Hsp104/ClpB fail to dissolve protein aggregates formed by exposure to high temperature and become highly vulnerable to heat stress (Mogk et al., 1999; Parsell et al., 1994b; Sanchez and Lindquist, 1990; Squires et al., 1991). Thus, despite not being essential under normal growth conditions, Hsp104/ClpB is obligatory for survival under stress. Unlike other Hsp100 proteins ClpA, ClpC, and ClpX, Hsp104/ClpB is not associated with a proteolytic compartment and therefore not directly involved in the degradation of substrate proteins. In fact, an engineered ClpB-ClpP protease fusion which degrades proteins post-disaggregation abolishes stress tolerance highlighting the importance of solubilisation and re-activation of aggregated proteins (Weibezahn et al., 2004).

Similar to other members of Hsp100 family, Hsp104/ClpB belongs to the superfamily of AAA+ proteins that act as ATP-driven protein remodelling machines in a wide range of cellular activities. In its functional form, Hsp104/ClpB forms a hexameric ring with a central pore. The individual subunits comprise of two AAA modules or nucleotide binding domains (NBD1 and NBD2), an N-terminal domain and a unique middle (M) domain which differentiates Hsp104/ClpB from other Hsp100 proteins (ClpA, ClpX). The AAA modules are highly conserved among all Hsp100 proteins and utilize the Walker A and Walker B motifs as active sites for ATP binding and hydrolysis (Wendler et al., 2012). The AAA modules are critical for Hsp104/ClpB activity as mutations in this domain impair the chaperone function and compromise thermotolerance, and arrest prion propagation (Hattendorf and Lindquist, 2002; Parsell et al., 1991; Wegrzyn et al., 2001). While ATP binding in the NBDs contributes to the stabilization of the hexameric state and the interaction with substrates (Bosl et al., 2005; Parsell et al., 1994a; Weibezahn et al., 2003; Zolkiewski et al., 1999), ATP hydrolysis powers the molecular movements required to exert a mechanical force to unfold substrates. Specifically, the allosteric regulation of ATP binding and hydrolysis in the AAA domains drives synchronous conformational changes within the hexamer to generate a pulling force (Mogk et al., 2018). Substrate unfolding is achieved via translocation

through the central pore of Hsp104/ClpB and is a common mechanism of action of many AAA+ proteins (Tessarz et al., 2008; Weibezahn et al., 2004). Initiation of unfolding is not solely dependent on accessible N- and C-termini as exposed internal segments like loops can also be engaged, thereby increasing the probability and efficiency of substrate processing (Haslberger et al., 2008).

2.7.2 Disaggregation by Hsp70 system

Members of the Hsp70 family (Ssa in *S.cerevisiae*; DnaK in *E.coli*) are structurally and functionally conserved chaperones that support cell survival under normal and stress conditions. Humans express 13 homologs of Hsp70 that differ in amino acid sequence, expression pattern in tissues and organs, expression level, and sub-cellular localization (cytosol, nucleus, ER, and mitochondria) (Daugaard et al., 2007; Rosenzweig et al., 2019). While some forms of Hsp70 are stress-inducible, others are constitutively expressed and perform housekeeping functions such as folding newly synthesized proteins, protein translocation across membranes, assembly and disassembly of protein complexes, preventing aggregation and targeting terminally misfolded proteins for degradation.

2.7.2.1 Hsp70 chaperone cycle

The chaperone activity of Hsp70 is regulated by cycles of ATP binding and hydrolysis which is further assisted by co-chaperones of the Hsp40 (DNAJ; DnaJ in *E.coli*) family and nucleotide exchange factors (NEFs- Hsp110 in mammals, GrpE in *E.coli*). Hsp70 in its ATP bound state has high on and off rates for its substrates as the lid segment of the substrate binding domain (SBD) adopts an open conformation (Hartl et al., 2011). The β -sandwich pocket in the SBD is responsible for recognising exposed hydrophobic stretches which are characteristic of unfolded proteins (Rudiger et al., 1997). An incoming Hsp40 accelerates hydrolysis of ATP to ADP in the nucleotide binding domain (NBD) resulting in an allosteric closure of the SBD lid segment and a stably associated substrate that is prevented from having unfavourable interactions in its exposed hydrophobic regions (Mayer, 2010). In addition, Hsp40 via its SBD directly interacts with a variety of clients and targets them to Hsp70, thereby expanding the substrate and functional diversity of Hsp70 (Acebron et al., 2008; Kampinga and Craig, 2010). To release the

Hsp70 bound substrates, NEFs catalyse ADP dissociation followed by ATP re-binding which triggers another round of conformational changes resulting in lid opening and resetting Hsp70 to accept a new substrate (Rosenzweig et al., 2019).

2.7.2.2 Synergistic role of the Hsp70 system and Hsp100 proteins in disaggregation

Although Hsp100 proteins are thought to be the main force generators in dissolving protein aggregates, disaggregation requires synergistic activity of the Hsp70 system (Glover and Lindquist, 1998; Mogk et al., 1999). The synergy between these two ATP-driven systems exists at different stages of the disaggregation process (Figure 12).

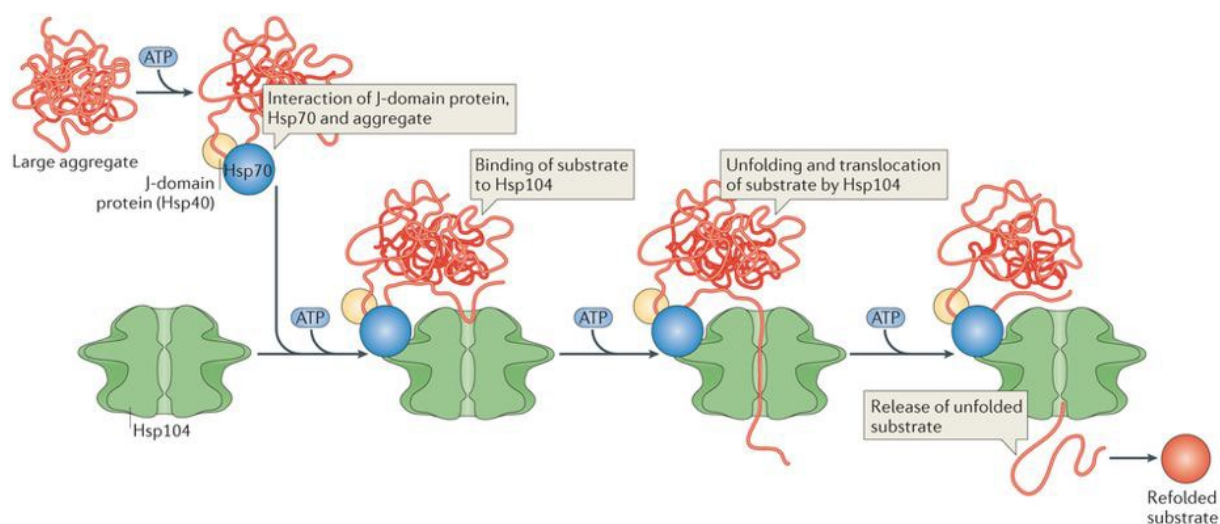


Figure 12. Proposed model of disaggregation involving Hsp104 and the Hsp70 system

Hsp40 recognises aggregated proteins and recruits Hsp70 to the aggregates. Hsp70 may partly disentangle the aggregate and present it to Hsp104. Hsp70 binding additionally stimulates the ATPase activity of Hsp104 which initiates substrate threading through the central pore of Hsp104 resulting in an unfolded substrate. The released substrate can enter the re-folding cycle or be targeted for degradation. Figure from (Doyle et al., 2013).

In the initial stage, Hsp70 binds to the aggregates in an Hsp40 dependent manner and executes the initial untangling of the aggregates (Acebron et al., 2009; Winkler et al., 2012b; Zietkiewicz et al., 2006). Hsp70 further recruits Hsp104/ClpB to the surface of the aggregates and triggers the ATPase and threading activity by physically interacting with the M-domain (Mogk et al., 2015). The M-domain in each subunit of Hsp104/ClpB is embedded on the exterior of the upper AAA+ module. Normally, the horizontal head-to-tail positioning of the M-domains in the hexamer results in its tight binding to the AAA ring and repressing its ATPase activity (Carroni et al., 2014;

Heuck et al., 2016; Oguchi et al., 2012). Interaction of Hsp70 with Hsp104/ClpB displaces the M-domains and stabilizes it in this conformation resulting in a de-repressed state (Mogk et al., 2018). Thereby, Hsp70 binding stimulates ATP hydrolysis in Hsp104/ClpB and initiates the substrate threading movement necessary for disaggregation (Rosenzweig et al., 2013; Seyffer et al., 2012). Due to the repression from the M-domains, the intrinsic disaggregation activity of Hsp104/ClpB is lower than that of other Hsp100 proteins like ClpA (Seyffer et al., 2012). Engineered variants of Hsp104 that are constitutively active have an augmented unfolding capacity and are partially independent of Hsp70 activation (Lipinska et al., 2013; Oguchi et al., 2012). Although these hyperactive Hsp104 variants in yeast can mitigate the toxicity of pathological aggregates such as TAR DNA-binding protein 43 (TDP-43), FUS and α -synuclein (Jackrel et al., 2014; Ryan et al., 2019), under normal conditions the expression of these variants is toxic to cells, presumably due to the uncontrolled unfolding of functional cellular proteins (Lipinska et al., 2013). Hence, Hsp70 acts as a regulator of the unfolding capacity of Hsp104/ClpB (Chamera et al., 2019).

2.7.2.3 Hsp70 based disaggregation

Besides assisting Hsp104/ClpB mediated disaggregation, the Hsp70 system alone is also able to exert mechanical force to unfold and rescue proteins from misfolded states (Sharma et al., 2010). The unfolding potential of bacterial DnaK-DnaJ-GrpE (KJE) complex has been shown to effectively resolve heat-denatured aggregates of RNA polymerase and more stable glucose-6-phosphate dehydrogenase (G6PDH) aggregates *in vitro* (Diamant et al., 2000; Skowyra et al., 1990). Notably, the KJE system also initiates early unfolding events on the surface of aggregates prior to disaggregation by the Hsp100 disaggregases (Zietkiewicz et al., 2004; Zietkiewicz et al., 2006). However, the capacity of Hsp70 for disaggregation may be limited to disordered aggregates, as aggregates with higher β -sheet content seem to require the strong pulling forces of the Hsp100s chaperones (Lewandowska et al., 2007).

Surprisingly, higher eukaryotes lack a cytosolic and/or nuclear homolog of the Hsp100 disaggregases. Yet, various higher eukaryotic models (mice, nematodes, and mammalian cells in culture) exhibit an inherent ability to eliminate amorphous and amyloid-like protein aggregates

hinting at the presence of an active disaggregation or aggregate clearance mechanism (Cohen et al., 2006; Pinto et al., 1991; Yamamoto et al., 2000). Recent investigations of the Hsp70 system from humans and *C.elegans* have revealed aggregate re-solubilizing activity similar to the bacterial and yeast disaggregases. This disaggregation complex is also ATP-driven and is composed of the constitutively expressed cognate human Hsc70, the DNAJ protein DNAJB1 and the Hsp110 class of NEFs (Rampelt et al., 2012; Shorter, 2011). Despite being a close relative of Hsp70 with similar refolding activity *in vitro* (Tutar et al., 2006), Hsc70 is remarkably more potent at disaggregation and suppressing aggregation suggesting mechanistic differences between the action of these two proteins (Kirstein et al., 2017; Scior et al., 2018; Shorter, 2011). The disaggregation efficiency is further enhanced by the simultaneous presence of different classes of DNAJ proteins, namely class A and class B (Nillegoda et al., 2015). Both class A and class B proteins contain an N-terminal J-domain (JD) which binds to Hsp70 and stimulates its ATPase activity. However, class A proteins have an additional zinc-finger motif extruding from their C-terminal domain (CTD), which is mostly not found in the CTD of class B proteins (Kampinga and Craig, 2010). Class A and B J-proteins can oligomerize via charged interactions between JD and CTD of the opposite class and form mixed complexes that confer Hsc70 higher disaggregation capacity compared to when they act alone (Nillegoda et al., 2015; Nillegoda et al., 2017). Such mixed complexes may act *in vivo* to resolve heat induced protein aggregates in addition to promoting thermotolerance and maintaining organismal health (Kirstein et al., 2017). In contrast, disaggregation of amyloid-like fibrils of α -synuclein into shorter fragments and monomers is efficiently achieved by a single J-protein DNAJB1 working in cooperation with Hsc70-Hsp110 (Gao et al., 2015).

2.7.3 Other putative disaggregases in higher eukaryotes

Other than the Hsp70 system, some other proteins in the mammalian cytosol such as RuvBL1/2 and HTRA1 are thought to possess disaggregase activity mainly against amyloid-like aggregates. RuvBL1/2 is a dodecameric complex of two AAA+ ATPase hexamers, RuvBL1 and RuvBL2, which is a component of different protein complexes including the RNA polymerase II and telomerase complex (Qiu et al., 1998; Venteicher et al., 2008). In the presence of ATP, the

RuvBL1/2 complex remodels insulin fibrils into disordered aggregates (Zaarur et al., 2015). HTRA1 belongs to the conserved family of high temperature requirement A (HtrA) serine proteases and has been shown to digest tau fibrils in an ATP-independent manner (Poepsel et al., 2015). This proteolytic activity however is not specific to aggregated tau as soluble tau is similarly degraded by HTRA (Tennstaedt et al., 2012).

2.8 VALOSIN-CONTAINING PROTEIN (VCP)-THE SEGREGASE

Valosin-containing protein (VCP/p97 in vertebrates, Cdc48 in yeast, CDC-48 in nematodes, Ter94 in flies, VAT in archaea) is a highly conserved unfoldase of the AAA+ ATPase family present in archaea and eukaryotes. It was first discovered in a yeast screen for regulators of cell-division-cycle (Cdc) in cold sensitive mutants (Moir et al., 1982). Since then, this essential chaperone has been studied in the context of diverse cellular processes including protein degradation, membrane fusion, chromatin reorganization, DNA replication and damage response, transcriptional regulation, and cell death (Braun and Zischka, 2008; Deichsel et al., 2009; Meyer et al., 2012; Meyer, 2005; Verma et al., 2011; Wilcox and Laney, 2009). In all these processes, substrate ubiquitination serves as a signal for VCP recruitment which can occur directly or via a specific set of substrate recruiting cofactors (Meyer et al., 2012). Once recruited, like other members of the AAA+ family, VCP utilizes energy from ATP hydrolysis to unfold and segregate client proteins from binding partners in protein complexes located at various cellular locations (ribosomes, chromatin, ER or mitochondria) (Stolz et al., 2011). In addition to providing substrate specificity, cofactor interactions can modulate VCP activity and even regulate substrate processing after VCP action (Rumpf and Jentsch, 2006; Zhang et al., 2015). In the majority of cases, extracted proteins are targeted to the proteasome, however, in certain cases they can also be exempted from degradation (Ramadan et al., 2007; Stolz et al., 2011). Owing to the plethora of regulatory and PQC associated activities, functional defects in VCP caused by mutations lead to pathological conditions like multisystem proteinopathy (MSP), frontotemporal dementia (FTD), familial ALS and Charcot-Marie-Tooth disease (Tang and Xia, 2016).

2.8.1 Structure and mechanism of action of VCP

Similar to ClpB and Hsp104, the functional form of VCP is a homo-hexamer with two concentric AAA ATPase rings around a central pore (Figure 13A) (Rouiller et al., 2000; Zhang et al., 2000). Each subunit in the hexamer contains a regulatory N-domain, two tandem ATPase domains, D1 and D2, and an unstructured C-terminal tail (Xia et al., 2016). While the D1 and D2 domains form the upper and lower AAA rings respectively, the N-domain laterally protrudes from the D1 ring. Depending upon the nucleotide present in the D1 domain, the N-domain can exist in an ATP-bound Up- or ADP-bound Down-conformation signifying allosteric inter-subunit communication (Banerjee et al., 2016; Tang et al., 2010a). In the Up-conformation, the N-domain is positioned above the D1 domain. Upon nucleotide exchange, the N-domain assumes the Down-conformation where it becomes co-planar with the D1 domain (Figure 13B) (Ye et al., 2017). VCP engages substrates in its Up-conformation via the interaction of substrate recruiting cofactors with the N-domain (Cooney et al., 2019).

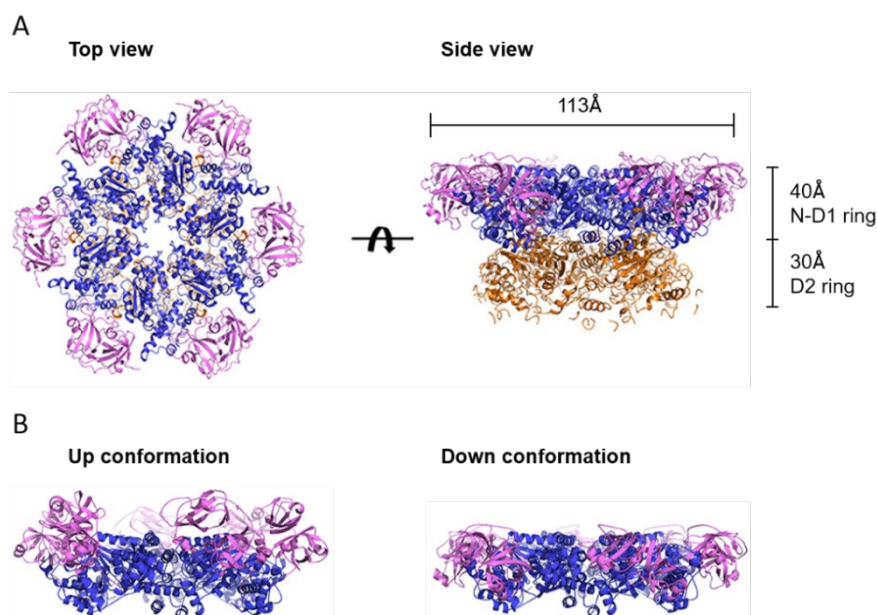


Figure 13. Molecular structure of the VCP hexamer

(A) Ribbon diagrams of top and side views of the mouse VCP hexamer showing the N-domain, D1 and D2 rings with the respective ring dimensions. (B) Ribbon diagram of the D1 ring showing the Up- and Down conformations of the N-domain. N-domains are represented in pink, D1 ring in blue and D2 ring in golden. Figure adapted from (Tang and Xia, 2016).

ATP hydrolysis in the D1 and D2 domains triggers molecular motions that are transmitted to the bound substrate resulting in unfolding. The AAA rings have a total of 12 nucleotide binding sites at the interface between adjacent subunits, all of which may or may not bind ATP at the same time (Ye et al., 2017). In fact, the D1 domain preferentially binds to ADP and has only a weak ATPase activity. Moreover, ATPase deficient D1 mutants preserve unfolding activity at slightly reduced rates (Blythe et al., 2017; Bodnar and Rapoport, 2017). This suggests that the ATPase activity of the D1 domain does not directly generate the required force for protein unfolding. Besides its ATPase function, the D1 domain drives the assembly and confers stability to the VCP hexamer, as the D2 domain in isolation tends to form heptamers (Davies et al., 2008; Wang et al., 2003). In contrast to D1, the D2 domains have a strong ATPase activity which is stimulated by the binding of ubiquitinated substrate close to the opening of the D1 ring highlighting another instance of inter-ring communication (Bodnar and Rapoport, 2017). ATP hydrolysis in the D2 ring is the main driver of substrate unfolding by VCP. Cryo-EM structures of VCP in the act of unfolding a substrate show the D1 and D2 rings in a helical symmetry and propose a hand-over-hand mechanism of substrate translocation through the central pore (Cooney et al., 2019). Specifically, the staircase like pore loops within the D2 ring undergo conformational changes over cycles of ATP hydrolysis and propel the substrate through the pore resulting in a pulling force that unfolds proteins (Twomey et al., 2019).

2.8.2 Role of VCP in proteostasis

The well-studied role of VCP in PQC mainly involves targeting proteins for degradation. Some cytosolic proteins intended for degradation in the proteasome especially depend on VCP activity (Verma et al., 2011; Xu et al., 2016). This dependence is attributed to the proteasomal requirement of unstructured or disordered regions in its substrates, which can be generated by VCP, allowing the engagement and initiation of unfolding at the 19S (Tomita and Matouschek, 2019). The unfolding activity of VCP, however, does not depend on the presence of disordered regions since it can initiate unfolding at the ubiquitin conjugated to the substrate (Twomey et al., 2019). Therefore, VCP-dependent unfolding pre-processes well folded, and possibly insoluble and aggregated proteins for proteasomal degradation (Gallagher et al., 2014; Kobayashi et al.,

2007; Olszewski et al., 2019). Moreover, VCP is also involved in the extraction of proteasomal substrates from organelles and protein complexes.

One of the well understood roles of VCP in this regard is in ER-associated degradation (ERAD), a pathway that results in the removal of terminally misfolded or undesired proteins from the ER lumen followed by their degradation in the cytosolic proteasomes. Protein transport from the ER to the cytosol involves a retrotranslocation step through the ER membrane performed by a sophisticated machinery of protein complexes. As the target protein moves across the ER membrane and emerges at the cytosolic face, it is ubiquitinated by the membrane bound E3 ligase Hrd1. VCP along with its cofactor complex, Ufd1-Npl4, is recruited to the site of retrotranslocation where it is tethered to the ER membrane via Ubx2. The VCP-Ufd1-Npl4-Ubx2 complex then dislocates the ubiquitinated substrate from the ER and releases it in the cytosol. Additional shuttling factors like Rad23 or Dsk2 can act downstream of VCP and guide the substrate to the proteasome for degradation (Stolz et al., 2011; Vembar and Brodsky, 2008; Ye et al., 2017).

Similar to ERAD, VCP is involved in a mitochondrial PQC pathway called MAD (mitochondria-associated degradation) that is important for cellular viability. Upon mitochondrial stress, VCP is recruited to the mitochondria by the action of Vms1 (VCP/Cdc48-associated mitochondrial stress-responsive protein 1) in yeast and Parkin in mammals (Heo et al., 2010). Selective mitochondrial proteins may be retrotranslocated to the outer mitochondrial membrane and can there be ubiquitinated, extracted by VCP and targeted for proteasomal degradation in the cytosol (Taylor and Rutter, 2011). Additionally, VCP-dependent degradation of mitofusins (proteins that accomplish mitochondrial fusion) on damaged mitochondria results in mitochondrial fission thereby facilitating their clearance by mitophagy (Tanaka et al., 2010).

Other crucial roles of VCP in proteostasis include its role in RQC (ribosomal quality control) wherein VCP removes nascent misfolded polypeptides on stalled ribosomes (Defenuillere et al., 2013; Verma et al., 2013). Ribosome stalling during translation may occur as a consequence mRNA truncation, loss of a stop codon and tRNA insufficiency. The E3 ligase, Ltn1, ubiquitinates the aberrant nascent chains which are then extracted from the ribosomes by the VCP-Ufd1-Npl4

complex and are targeted to proteasomes (Brandman and Hegde, 2016). The failure of this quality control pathway results in the aggregation of nascent polypeptides and proteotoxic stress (Choe et al., 2016).

2.8.3 Disease association of VCP

In addition to its role as a segregase, VCP has been proposed to execute PQC activities on aggregated proteins due to its co-localization with expanded polyQ aggregates in HD, ubiquitin-positive intraneuronal inclusions in motor neuron disease with dementia and Lewy bodies in PD patient tissues (Hirabayashi et al., 2001; Mizuno et al., 2003). Dominant negative mutations in VCP itself cause severe diseases-like MSP or inclusion body myopathy with early-onset Paget disease and frontotemporal dementia (IBMPFD) with progressive damage in muscles, bones or brain (Ye et al., 2017). IBMPFD neurons often show the deposition of ubiquitin positive aggregates, reflecting the loss of VCP mediated proteostasis as an underlying element of these diseases. The disease associated mutations mostly occur at the interface between the N and D1 domains and deregulate the ATP cycle of VCP (Niwa et al., 2012). Some mutations reduce the binding affinity of the D1 domain to ADP thereby increasing the ATPase activity in D2 and altering overall inter-subunit communication (Tang et al., 2010b; Tang and Xia, 2013). Other mutations can affect conformation of the N-domain or abolish interaction with cofactors (Bulfer et al., 2016; Zhang et al., 2015). The increased ATPase activity observed in specific VCP mutants also translates to higher unfolding capacity (Blythe et al., 2017), and might reflect a toxicity mechanism reminiscent of Hsp104 hyperactivity in yeast.

2.9 SIGNIFICANCE & AIMS OF THIS WORK

This study was conducted to advance the current understanding of cellular protein aggregation with an emphasis on, i) characterizing morphologically diverse aggregates and, ii) the cellular PQC mechanisms utilized to eliminate them.

- i. Tauopathies are characterized by the deposition of tau aggregates in different brain regions. How the aggregation of one protein leads to distinct disease manifestations is still enigmatic. Recent evidence on tau being able to form unique strains in cell culture raised speculations that, similar to bona fide prion disorders, strain variations may account for the clinical diversity of tauopathies (Kaufman et al., 2016; Sanders et al., 2014). This idea is strongly supported by the revelation of different tau conformations in the core of aggregated material from different tauopathies (Falcon et al., 2018; Falcon et al., 2019; Fitzpatrick et al., 2017; Zhang et al., 2020). Moreover, *in vitro* generated tau strains exhibit strain-specific features such as rate of disease progression, patterns of cell pathology and regional vulnerability in mouse brain (Kaufman et al., 2016; Sanders et al., 2016). While these studies illustrate distinct pathological outcomes of tau strains, it is not clear how strain-specific phenotypes are elicited at the molecular level and define different biological consequences. Since strains are essentially aggregated proteins, it is important to generate a fundamental understanding of how these aggregates affect cell physiology differentially. The information gained may lead to a better understanding of the differences of disease progressions at the cellular level in the various tauopathies and pave the way to target relevant pathways for treatment. In line with these ideas, the initial part of this work specifically aimed at-
 - Systematically characterizing the localization, structure, cellular interactions and consequences of morphologically distinct aggregates using tau as a model protein.
- ii. Protein aggregation can be deleterious for cells due to the loss- and/or gain-of-function of the aggregating protein. Protein aggregates gain a toxic function in cells by engaging essential proteins in aberrant interactions and sequestering them from their normal function (Olzscha et al., 2011; Woerner et al., 2016). In addition, amyloid-like fibrillar aggregates can mediate toxicity by binding and physically disrupting cellular membranes and disturbing

organellar homeostasis (Bauerlein et al., 2017; Milanesi et al., 2012; Pieri et al., 2012). In order to counteract such toxic effects, the cellular PQC system has evolved to recognize aggregated proteins and resolve them via disaggregation and/or degradation. Notably, conditional mouse models of neurodegenerative diseases such as HD and tauopathy show a correlation between reversal of aggregation and amelioration of disease symptoms (Polydoro et al., 2013; Yamamoto et al., 2000). Therefore, understanding cellular mechanisms of aggregate clearance may be beneficial for the treatment of diseases with gain-of-function toxicity. Autophagy is a well-understood cellular pathway for aggregate clearance, however, the contribution of the proteasome to this process is limited by the accessibility of aggregated proteins to the proteolytic sites and requires prior disaggregation. While protein disaggregation machineries in bacteria and yeast are well-defined, it is not clear how this process is executed and regulated in mammalian cells, especially in the context of amyloid-like aggregates. Thus, the second aim of this work was-

- To establish a model of amyloid disaggregation in mammalian cells using tau as a model protein and identify the major molecular players, and to gain insight into the mechanism of disaggregation.

2.10 CELLULAR MODEL OF POLYMORPHIC PRION-LIKE TAU AGGREGATES

In this study, we used a tau aggregation model which was established in human embryonic kidney 293 (HEK293) cells by Marc Diamond and co-workers (Sanders et al., 2014). In this model, the cells express a fragment of full-length tau consisting of the repeat domain (RD) with two prevalent FTDP mutations P301L and V337M fused to YFP (tau-YFP) (Figure 14A). In agreement with published results (Sanders et al., 2014), HEK293 cells that stably express tau-YFP, Clone1, show a diffuse tau-YFP signal throughout the cell and no visually detectable aggregates (Figure 14B).

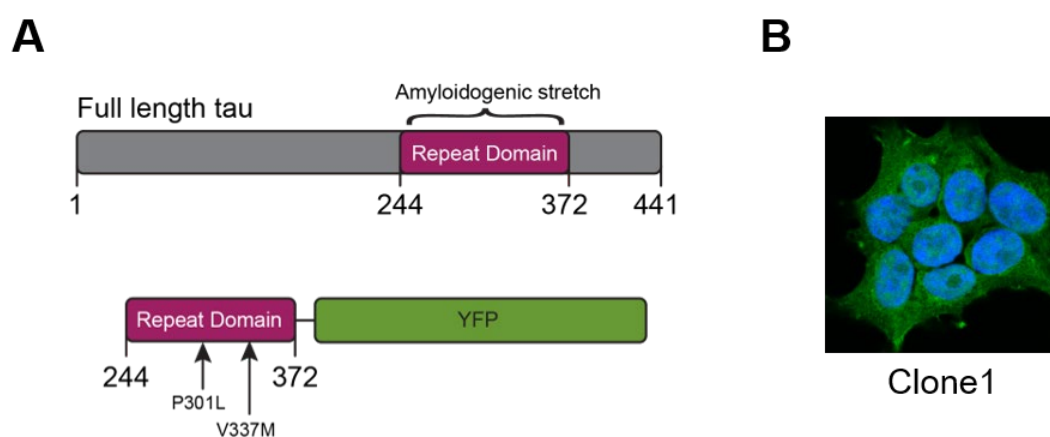


Figure 14. Construct diagram and tau-YFP distribution in Clone1

(A) Full length tau contains an aggregation competent repeat domain (RD). Tau RD with two mutations, P301L and V337M, fused to YFP was stably expressed in HEK293 cells. **(B)** Clone1 expressing tau RD (LM)-YFP shows diffuse signal. Image shows merge of tau-YFP (green) and DAPI (blue).

To induce tau-YFP aggregation, Sanders et al. exposed Clone1 cells to fibrillar aggregates of tau RD, pre-assembled from recombinant tau RD monomers in the presence of heparin. Upon exposure to cells, *in vitro* generated tau RD fibrils enter cells and act as a template to initiate the aggregation of intracellularly expressed tau-YFP. Clone1 cells treated with tau RD fibrils showed a heterogeneous population of cells with different morphologies of tau-YFP aggregates distributed in the nucleus and cytosol (Figure 15A). Some cells with aggregates generated identical aggregate morphologies with cell division indicating the transmission of this morphological information between dividing cells. This feature allowed Sanders et al. to isolate clonal cultures propagating unique aggregate morphologies, which were associated with unique biophysical and pathological characteristics reminiscent of prion strains. Clone9 and Clone10

were two of several homogenous and non-toxic strains with persistent aggregates derived from Clone1. Clone9 contained tau-YFP foci in the cytosol and nucleus while Clone10 mostly showed a peri-nuclear inclusion in the cytosol (Figure 15B). Notably, the prion-like propagation of these tau-YFP aggregates allows the re-introduction of the specific strains in naïve Clone1 cells by the addition of crude cell extracts from parental clones (Sanders et al. 2014).

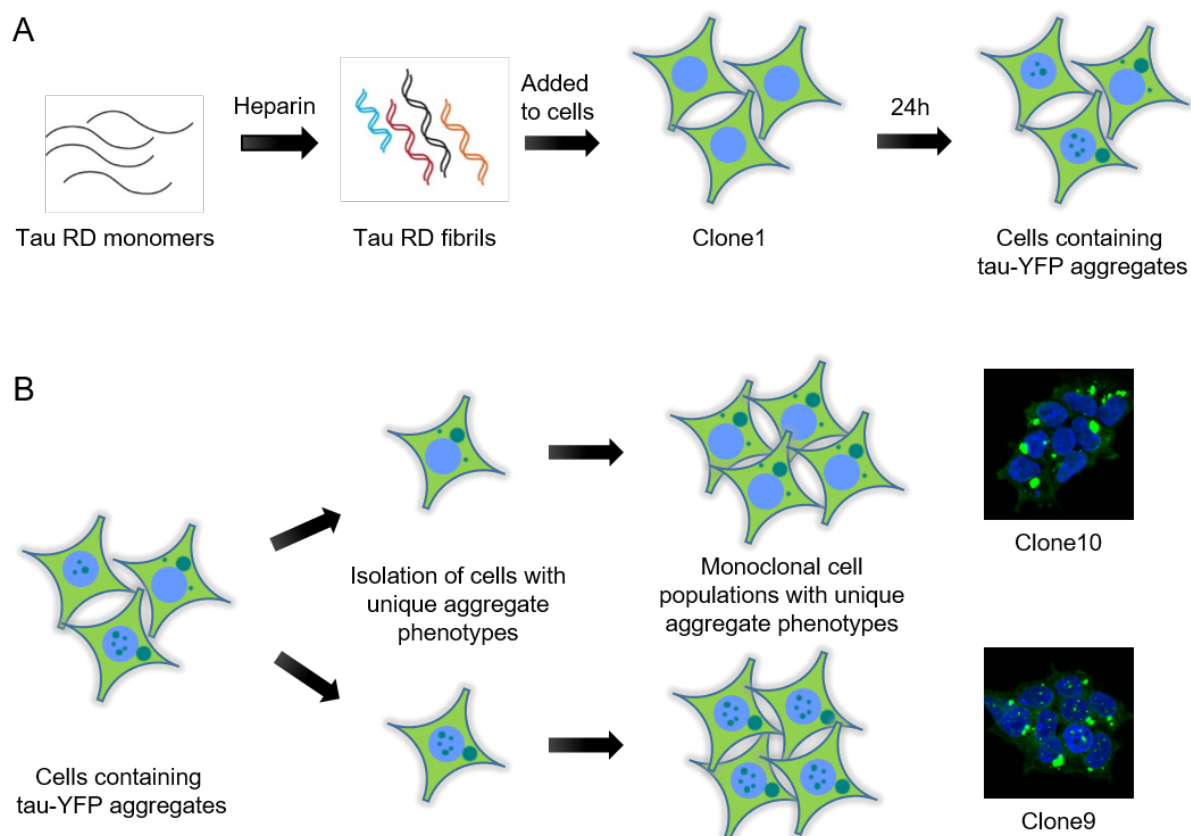


Figure 15. Schematic of (A) Seeding cellular tau-YFP with exogenous tau fibrils and (B) Isolation monoclonal cell lines propagating unique aggregate strains.

See text above for details.

3. RESULTS

3.1 REGENERATION AND CHARACTERIZATION OF MONOCLONAL CELL LINES PROPAGATING PRION-LIKE TAU-YFP AGGREGATES

Sanders et al. suggested that the tau-YFP strains, Clone9 and Clone10, are able to indefinitely propagate distinct aggregate phenotypes in culture. However, we observed that freshly thawed Clone9 and Clone10 cell lines often did not exhibit a homogenous aggregate-containing phenotype and progressively reverted to the Clone1 phenotype (data not shown). It appeared that the persistent propagation of tau-YFP aggregates was interrupted by freeze-thaw cycles necessary for amplification and cryopreservation of mammalian cells. Therefore, to restore aggregate homogeneity in the cell lines, the strains were re-introduced in naive Clone1 cells and new sub-clonal cell lines were isolated as previously described (Sanders et al., 2014).

3.1.1 Seeding Clone1 with extracts from parental Clone9 and Clone10 cell lines

To generate cell lines with homogenous aggregate phenotypes that are comparable to the lines described previously (Sanders et al., 2014), HEK293 cells stably expressing tau-YFP (Clone1) were treated with cell lysates obtained from two cell lines containing tau-YFP aggregates that were kindly provided by Marc Diamond (parental Clone9 and Clone10). The lysates were prepared by lysing the cells in a mild detergent containing buffer to preserve the integrity of tau-YFP aggregates in the lysates. Cell lysis was followed by a gentle centrifugation to clear non-lysed cells, nuclei and cell debris.

Western blot analysis of the soluble extract (S) and the insoluble, pelleted fraction (P) showed a tau-YFP band at the expected molecular weight (~40kDa) in addition to a cleaved fragment at ~35kDa in Clone1, 9 and 10 (Figure 16A). The cleaved fragment was specific to tau-YFP expressing cell lines as it was not present in wild-type HEK293 cells. Notably, a large part of total tau-YFP in Clone9 and Clone10 was found in the detergent insoluble pellet fraction (Figure 16A). The pellet of Clone10 additionally revealed discrete tau-YFP bands at higher molecular weight suggestive of posttranslational modification of tau-YFP, such as ubiquitination. The nuclear marker, histone H3, was also found entirely in the pellet (Figure 16A), suggesting that

nuclei were not solubilised during the lysis. Therefore, it is also likely that the nuclear (Clone9) or juxtannuclear (Clone10) tau-YFP aggregates were eliminated from the final extracts. However, the soluble extract from Clone 9 and Clone10 when applied to Clone1 still resulted in the formation of aggregate morphologies similar to the respective parental clones, hinting at the existence of smaller, seeding competent tau-YFP species in these fractions. 4 different sub-clonal cell lines for each strain were isolated, all of which homogeneously propagated the respective parental aggregate phenotype in a prion-like manner (Figure 16B-C). As expected lysates from Clone1 did not lead to any visible tau-YFP aggregates (data not shown). In addition, an ultracentrifugation-based solubility assay of tau-YFP from the secondary clones (Clone9.1.1 and Clone10.1.2) yielded comparable tau-YFP insolubility patterns as previously reported for the parental Clone9 and Clone10 by Sanders et al. (Figure 16D), indicating that the secondary clones (Clone9.1.1 and Clone10.1.2) were not only morphologically but also biochemically similar to the parental clones. Hence, secondary cell lines homogeneously propagating Clone9 and Clone10 tau-YFP aggregate strains were successfully generated. The secondary cell lines Clone9.1.1 and Clone10.1.2 will be referred to as Clone9 and Clone10, respectively, in the rest of this work.

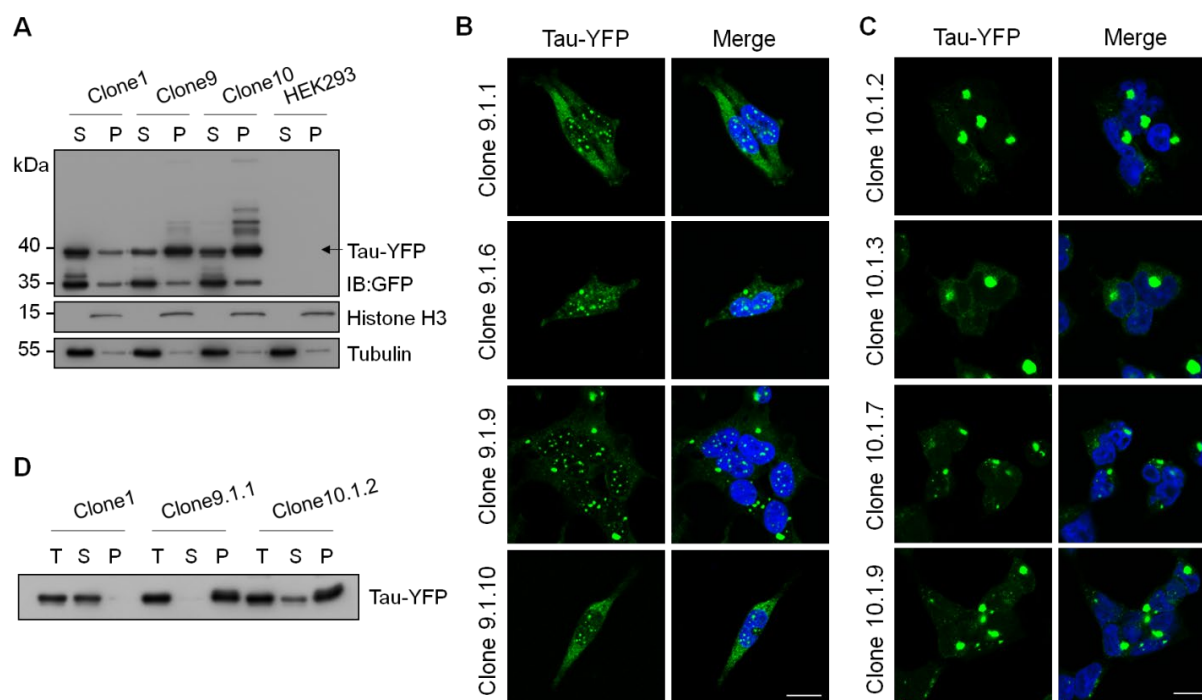


Figure 16. Regeneration of Clone9 and Clone10

(A) Fractionation of cell extracts to generate seeding competent lysates. Clone1, 9, 10 and blank HEK293 cell lysates were centrifuged at 1000xg for 5min and comparable volumes of the soluble (S) and pellet (P) fractions were analysed by western blotting. HistoneH3 and tubulin were used as nuclear and cytosolic markers respectively. (B-C) Different secondary clones of Clone9 and Clone10 obtained by treating Clone1 with lysates from respective parental clones. Tau YFP in green and DAPI in blue. Scale bar: 15 μ m. (D) Ultracentrifugation analysis of Clone1 and secondary clones 9.1.1 and 10.1.2. Lysates were centrifuged at 186,000xg for 1 h. Total (T), soluble (S) and pellet (P) fractions were analysed for tau-YFP by western blotting with an anti-GFP antibody.

3.1.2 Nuclear aggregates in Clone9

In order to further characterize the sub-cellular localization of tau-YFP aggregates in the model cell lines, nuclear boundaries were marked by Nuclear Pore Complex (NPC) immunofluorescence. NPC staining confirmed the occurrence of tau-YFP aggregates inside the nucleus of Clone9 cells in addition to cytosolic aggregates, whereas aggregates in Clone10 were almost exclusively juxtannuclear (Figure 17A). Notably, there were NPC puncta in the cytosol of both Clone9 and 10 which co-localized with tau-YFP aggregates. No such puncta were seen in Clone1 where tau-YFP does not aggregate. This observation suggests that tau-YFP aggregates sequester NPC components which might affect nucleo-cytoplasmic transport events (Eftekharzadeh et al., 2018; Woerner et al., 2016). Further on, staining against Nucleophosmin1

(NPM1) showed that the nuclear aggregates in Clone9 were excluded from nucleoli (Figure 17B).

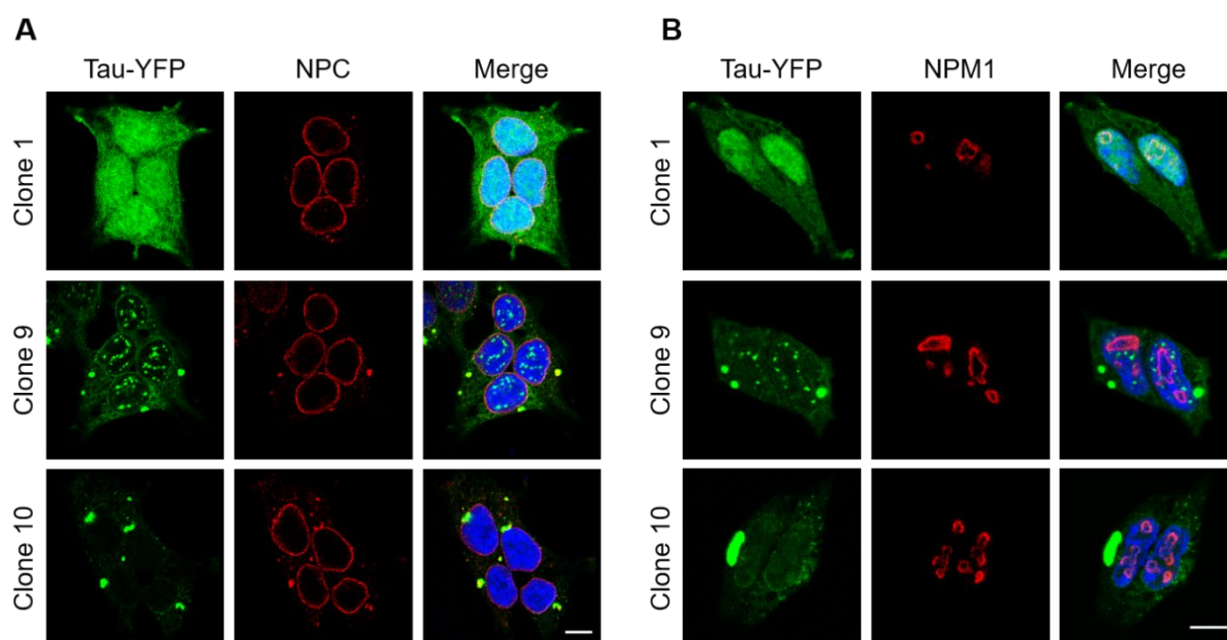


Figure 17. Subcellular localization of tau-YFP aggregates in Clone9 and Clone10

Representative images of Clone1, 9 and 10 at steady state, immuno-labelled with **(A)** anti-nuclear pore complex (NPC), and **(B)** anti-nucleophosmin1 (NPM1) primary and cy3 conjugated secondary antibodies. Merge shows tau-YFP (green), NPC/ NPM (red) and DAPI (blue). Scale bar: 10 μ m.

3.1.3 Aggresome-like characteristics of tau-YFP aggregates in Clone10

The perinuclear nature of the Clone10 aggregates prompted us to ask if this structure might be an aggresome. An aggresome is a depot of misfolded or aggregated proteins at the microtubule-organizing center (MTOC) accompanied by the local rearrangement of the intermediate filament protein vimentin (Johnston et al., 1998). Similar to aggresome structures, the cytosolic aggregates of Clone10, but not Clone9, were encased in vimentin (Figure 18A). Immunostaining against the MTOC marker protein γ -tubulin revealed that only the cytosolic aggregates in Clone10 were localized at MTOC (Figure 18B). Therefore, the cytosolic IBs in Clone10 fulfil the criteria for canonical aggresomes, whereas the IBs observed in Clone9 represent an alternative structure.

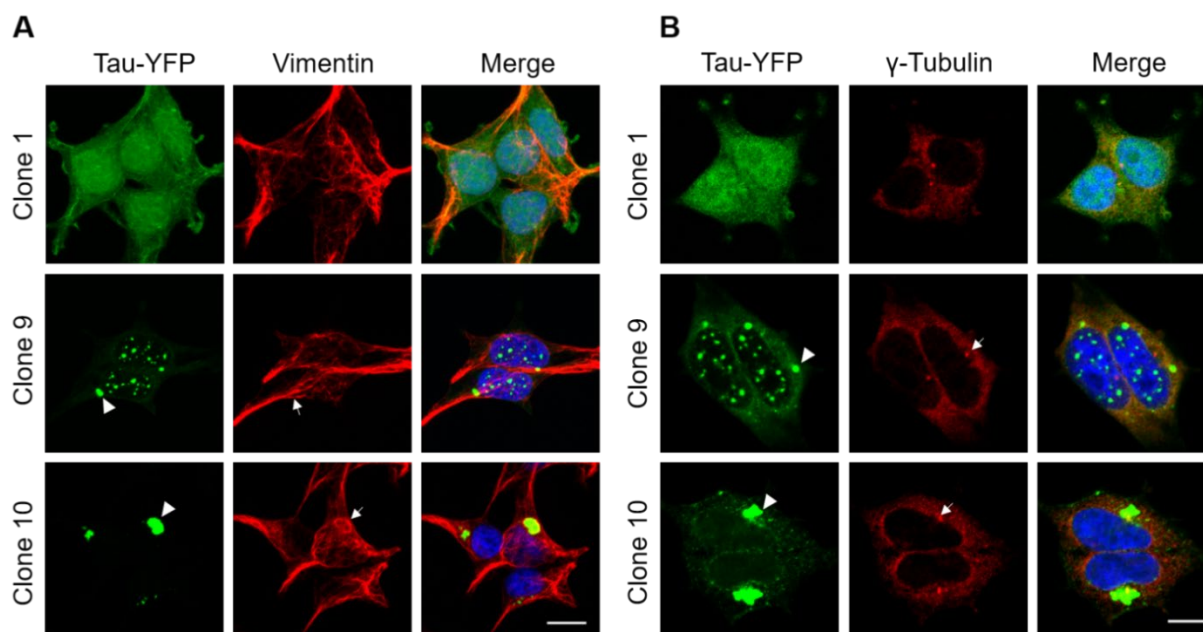


Figure 18. Aggresome structure in Clone10

Representative images of Clone1, 9 and 10 at steady state immuno-labelled with **(A)** anti-vimentin and **(B)** anti- γ -tubulin primary and cy3 conjugated secondary antibodies. Merge shows tau-YFP (green), vimentin/ γ -tubulin (red) and DAPI (blue). Arrows point at vimentin reorganization or γ -tubulin localization and arrow heads indicate tau-YFP aggregates in cells. Scale bar: 10 μ m.

3.1.4 Amyloidogenicity of tau-YFP aggregates in Clone9 and Clone10

Disease associated protein aggregates like those of mutant huntingtin (Htt97Q) and C9orf72 poly-GA have been shown to form amyloid-like fibrils in cells (Bauerlein et al., 2017; Guo et al., 2018). To investigate the structural properties of tau-YFP aggregates, the model cell lines were stained with the amyloid-specific dyes AmyTracker and AmyloGlo (de Waal et al., 2018; Schmued et al., 2012). Tau-YFP aggregates in Clone10 stained brightly with both dyes suggesting the presence of amyloid-like fibrils in the aggresome. In contrast to this Clone9 aggregates were only weakly stained when imaged under similar conditions (Figure 19A-B). To exclude that the low signal intensity in Clone9 aggregates was simply due to the smaller size of tau-YFP aggregates in this cell line, we compared them with aggregates of similar size in Clone10. The difference in amyloid staining was also present in tau-YFP foci with comparable size and YFP fluorescence in both cell lines, suggesting that the tau-YFP aggregates in Clone9 and Clone10 are biophysically distinct.

To independently confirm the structure of the cytosolic aggregates in Clone9 and Clone10, we analyzed them by cryo-electron tomography (Cryo-ET). Vitrified cultures were first imaged by light microscopy to determine the location of the inclusions within the cells, followed by cryo-focussed ion beam milling at these locations to generate 100-200 nm thick lamellas containing parts of the inclusions. Cryo-ET demonstrated the presence of amyloid-like fibrils in the area occupied by tau-YFP inclusions in Clone10 (Figure 19D). However, the Clone10 tau-YFP inclusion architecture differed from the radially arranged fibrils observed for Htt97Q and instead showed a more random organization (Bauerlein et al., 2017). In addition, both tau-YFP and Htt97Q aggregate fibrils were distinct from the ribbon-shaped structures described for poly-GA aggregates (Guo et al., 2018).

In contrast to Clone10, amyloid-like fibrils were not discernible in Clone9 inclusions. Here, short and fragmented filament-like structures were observed (Figure 19C). These structures might not interact with amyloid-binding dyes the way fibrillar tau-YFP in Clone10 did, which would therefore explain the low signal intensity observed for the Clone9 inclusions. Notably, neither of the tau-YFP aggregates, Clone9 or Clone10, markedly associated with cellular organelles such as the endoplasmic reticulum as shown for Htt97Q aggregates. Moreover, ribosomes that are largely excluded from the Htt97Q and poly-GA inclusions appeared interspersed within tau-YFP inclusions in both Clone9 and Clone10. Taken together, we not only observed how tau aggregates were different from other disease relevant aggregates but also detected structural differences between aggregates formed from identical monomeric tau-YFP protein in Clone9 and Clone10. These structural differences might underlie the biological distinctions between these prion-like strains and hint at the structural origin of different tauopathies.

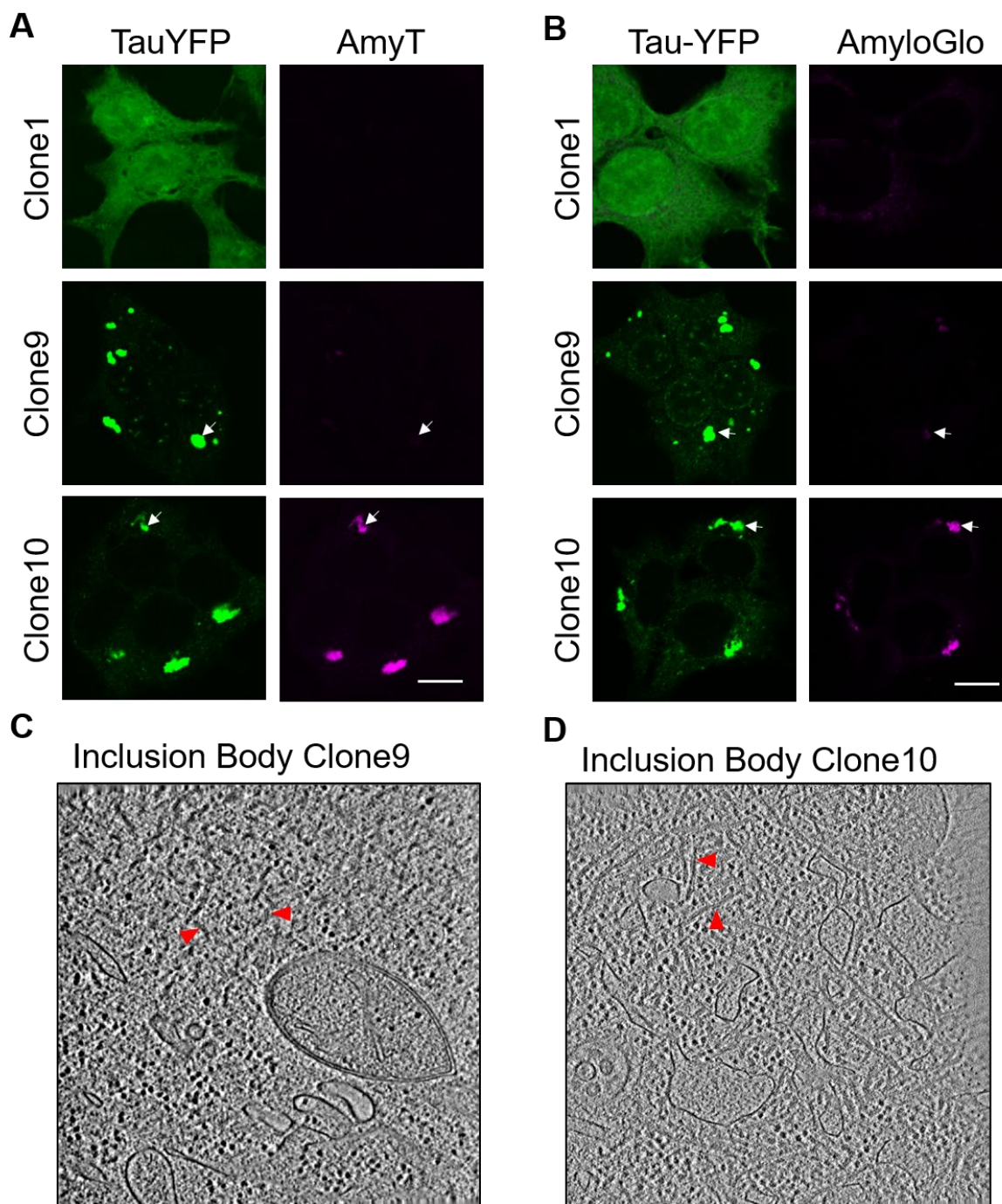


Figure 19. Amyloid structure of tau-YFP aggregates

(A-B) Clone1, 9 and 10 were stained with two amyloid specific dyes (A) AmyTracker (AmyT) and (B) AmyloGlo. Cover slips for each dye were imaged using identical settings to be able to compare intensities between the different clones. Tau-YFP is shown in green and amyloid-dye signal in magenta. Scale bar: 10 μ m. (C-D) Tomographic slice of a tau-YFP inclusion in (C) Clone10 (D) Clone9 cells. Red arrow heads point to fibrillar material. Cryo-ET performed by Dr. Qiang Guo.

3.1.5 Fate of soluble and aggregated Tau-YFP under proteostatic stress conditions

Tau, by virtue of its charged and minimally hydrophobic nature, is highly resilient to spontaneous aggregation *in vitro*. In cells, proteotoxic insults like heat shock or proteasome inhibition trigger the aggregation of metastable model and endogenous cellular proteins (Bennett et al., 2005; Gupta et al., 2011; Wallace et al., 2015). We therefore tested if these forms of stress could induce tau-YFP aggregation in Clone1 or alter existing aggregates. Heat shock at 43°C for 2 h or proteasome inhibition for 20 h did not result in any aggregation of tau-YFP in Clone1 observable by fluorescence microscopy (Figure 20A-B). Tau-YFP aggregates in Clone9 and Clone10 also did not show any altered appearance upon heat shock. However, after proteasome inhibition, enlarged aggregates were observed in Clone10 and to a lesser extent in Clone9 (Figure 20B), suggesting that aggregated material was degraded by the proteasome in these cell lines. Nevertheless, these proteostasis stressors were not sufficient to induce aggregation of soluble tau-YFP *per se* in Clone1.

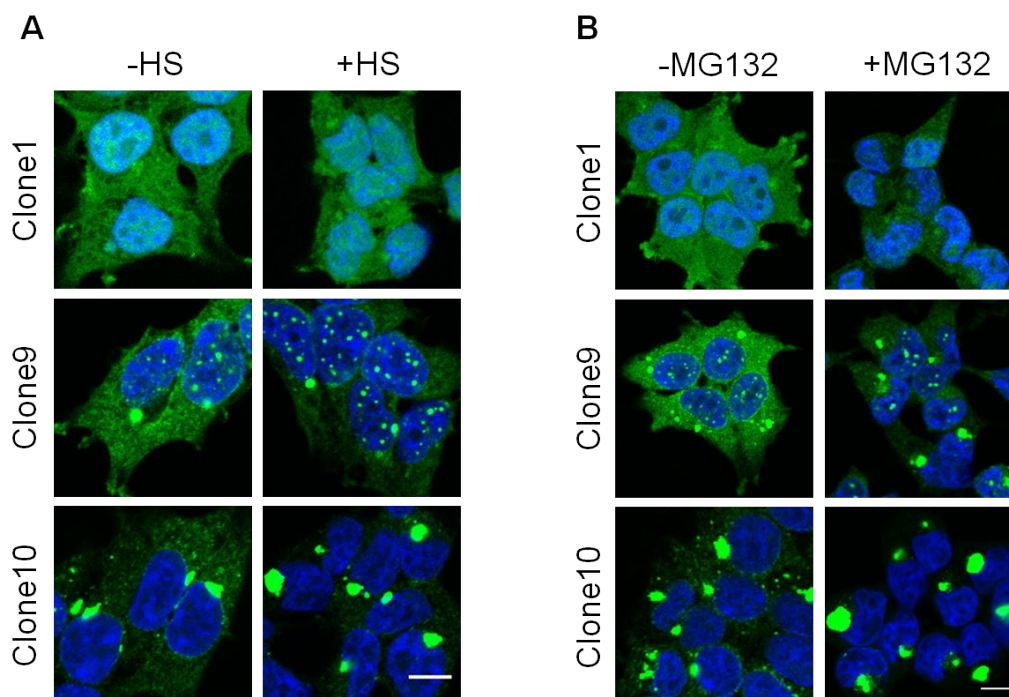


Figure 20. Effect of heat shock and proteasome inhibition on soluble and aggregated tau-YFP

(A) Clone1, 9 and 10 cells were heat shocked (HS) at 43°C for 2 h or (B) treated with 5 μ M proteasome inhibitor (MG132) for 20 h. After the indicated treatments cells were immediately fixed, stained with DAPI and mounted. Images show merge of tau-YFP (green) and DAPI (blue). Scale bar: 10 μ m.

Tau-YFP in Clone1 readily aggregates upon seeding with pre-formed tau aggregates as described earlier (Section 3.1). This is an example of homotypic seeding. Additionally, clinically distinct proteinopathies like PD and HD feature tau aggregates that co-exist either in the same deposits as the primary aggregating protein or independently (Fernandez-Nogales et al., 2014; Sengupta et al., 2015). Therefore, we sought to explore if tau-YFP could undergo heterotypic seeding or aggregation in response to the expression of different amyloid-like protein aggregates.

Towards this aim, we used the de-novo designed amyloid forming β -sheet proteins (West et al., 1999). These proteins do not have any endogenous function in the cell and have successfully served as a model to study gain-of-function toxicity of amyloids (Olzscha et al., 2011; Woerner et al., 2016). Three myc-tagged β -sheet forming proteins in increasing order of aggregation propensity- β 4, β 17, β 23, and a soluble control α -helical α S824 protein were expressed in Clone1 cells. As described for HEK293 cells not expressing tau (Olzscha et al., 2011), α S824 protein was diffusely distributed in Clone 1 cells, while β 4, β 17 and β 23 aggregates were observed in cytosol and nucleus of transfected cells (Figure 21A). Interestingly, tau-YFP co-localized with all three β -sheet protein aggregates in both nuclear and cytosolic compartments (Figure 21A). Clone1 cells expressing the soluble control α S824 protein showed diffuse tau-YFP signal. Due to comparable phenotypes of the three β -sheet protein variants, further experiments were performed with β 23. Tau-YFP co-aggregation with β 23 was confirmed by a solubility assay. Consistent with the microscopic observation of tau-YFP aggregates upon β 23 expression, tau-YFP was found in the pellet fraction only in presence of β 23, and not α S824 (Figure 21B). Next, we tested if tau-YFP co-aggregation was specific to the expression of β -sheet protein aggregates. Notably, Htt97Q aggregates did not cause tau-YFP aggregation in Clone1 cells (Figure 21C). This observation suggests that tau-YFP aggregation is not merely a consequence of the loss of cellular proteostasis capacity due to the occurrence of β -sheet protein aggregates. We speculated that the β -sheet aggregates might engage tau-YFP into specific interactions that result in its aggregation.

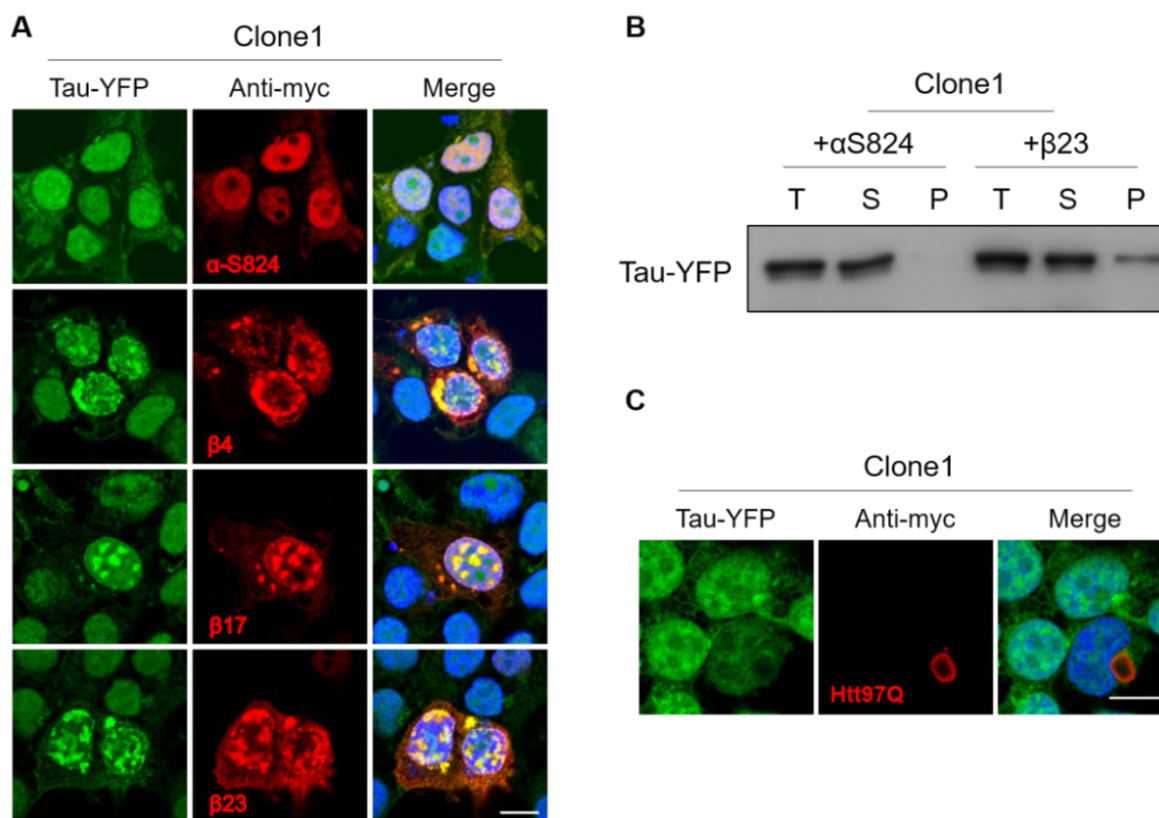


Figure 21. β -sheet protein aggregates lead to tau-YFP aggregation

(A) Clone1 cells were transfected with constructs expressing myc-tagged α -S824, β 4, β 17 and β 23. 24 h after transfection, cells were fixed and stained with an anti-myc primary antibody followed by cy5 conjugated secondary antibody. Merged images show tau-YFP (green), myc (red) and DAPI (blue). (B) Cell lysates from Clone1 expressing α -S824 or β 23 protein were centrifuged at 186,000xg for 1 h. Total (T), soluble (S) and pellet (P) fractions were analysed for tau-YFP by western blotting with an anti-GFP antibody. (C) Clone1 cells were transfected with a myc-tagged Htt97Q construct. Cells were treated as described in (A). Scale bar: 10 μ m.

To further investigate the phenomenon of tau-YFP co-aggregation with β 23, two other variants of the tau-RD were used. The first variant was the wild-type tau repeat domain (RD-WT) which is thought to be less aggregation prone than the double mutant tau repeat domain (RD-LM) in Clone1. The second variant was an anti-aggregation mutant of the tau repeat domain (RD- Δ K280/2P) which lacks the critical proline residues required for adopting an amyloid-like cross β -sheet conformation. The RD- Δ K280/2P tau variant has been previously reported to resist aggregation even after being exposed to pre-formed tau aggregates (Sanders et al., 2014). HEK293 cells stably expressing the tau-RD variants fused to YFP were transfected with β 23 and analysed by microscopy. RD-WT tau-YFP co-aggregated with β 23 similar to RD-LM in Clone1; however, the co-aggregation of RD- Δ K280/2P tau-YFP appeared less robust (Figure 22A).

Further, almost no RD- Δ K280/2P tau-YFP was found in the insoluble fraction compared to RD-LM tau-YFP, despite comparable β 23 aggregation in both cell lines (Figure 22B). This observation indicates that the ability of tau-YFP to adopt the cross β -sheet conformation promotes its co-aggregation with β 23. Next, we analysed if tau-YFP was directly interacting with β 23 and compared the extent of this interaction between the tau-YFP variants. To do this, tau-YFP was immunoprecipitated with anti-GFP beads from cells expressing the tau-YFP variants transfected with β 23. A small fraction of β 23 was non-specifically bound to the anti-GFP beads as observed in the control HEK293 eluate (Figure 22C). In comparison, a higher amount of β 23 was pulled down with RD-LM tau-YFP compared to RD- Δ K280/2P tau-YFP (Figure 22C). These results show that β 23 induces tau-YFP aggregation by directly interacting with it and this co-aggregation is dependent on the ability of tau-YFP to adopt cross β -sheet conformation.

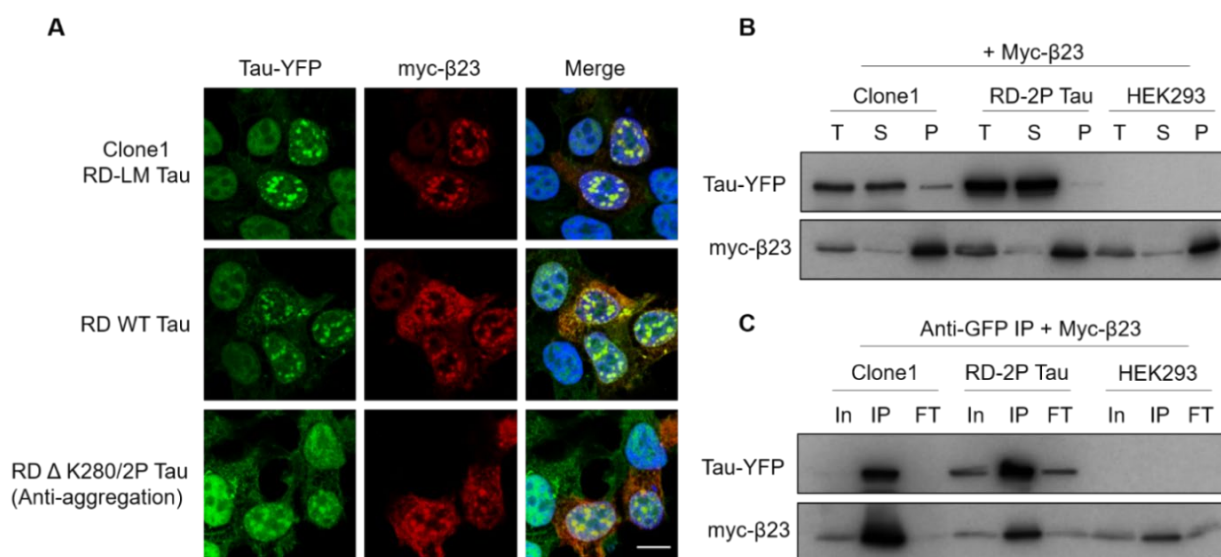


Figure 22. Co-aggregation of different tau-RD variants with β 23

(A) HEK293 cell lines stably expressing tau RD-LM (Clone1), RD-WT and RD- Δ K280/2P were transfected with myc- β 23. 24 h after transfection, cells were fixed and stained with an anti-myc primary antibody followed by cy5 conjugated secondary antibody. Merged images show tau-YFP (green), myc (red) and DAPI (blue). Scale bar: 10 μ m. **(B)** Cell lysates from Clone1, RD- Δ K280/2P and wild type HEK293 cells expressing β 23 were centrifuged at 186,000xg for 1 h. Comparable volumes of total (T), soluble (S) and pellet (P) fractions were analysed for tau-YFP and β 23 by western blotting with an anti-GFP and anti-myc antibody respectively. **(C)** Cell lysates from Clone1, RD- Δ K280/2P and wild type HEK293 cells expressing β 23 were subjected to anti-GFP immunoprecipitation. Input (In), eluate (IP) and flow-through (FT) fractions were analysed by western blotting. Tau-YFP and β 23 were detected as stated in (B).

Furthermore, we investigated if pre-formed tau-YFP aggregates in Clone9 and Clone10 would also co-aggregate with β 23. Interestingly, β 23 aggregates did not co-localize with either cytosolic or nuclear tau-YFP aggregates in Clone9 (Figure 23A). β 23 aggregates were in the vicinity of tau-YFP aggregates, sometimes even excluding them (Figure 23A zoom). While in Clone10, β 23 aggregates were often found to co-localize with tau-YFP aggregates thus displaying a mixed response compared to Clone9 (Figure 23B). We further investigated the interaction of aggregated tau-YFP with Htt97Q aggregates. In Clone9 and Clone10, Htt97Q aggregates were found close to the cytosolic tau-YFP aggregates while spatially excluding each other (Figure 23C).

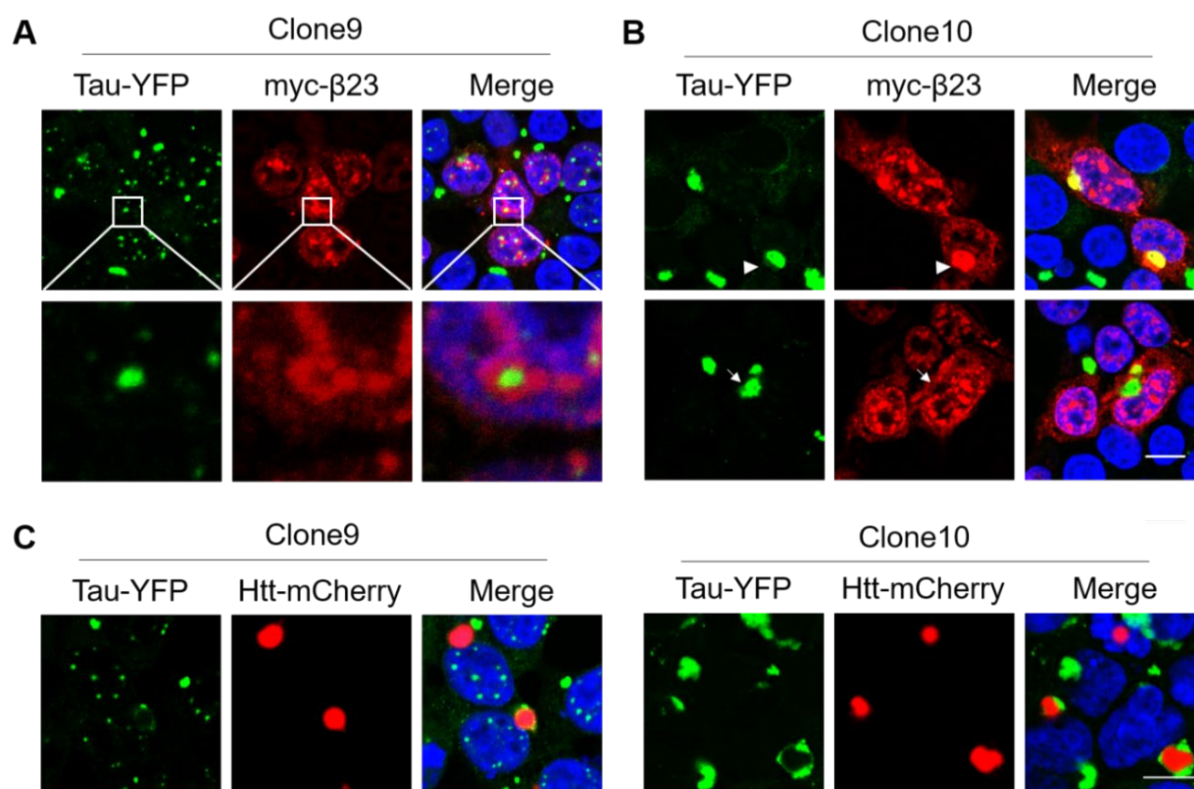


Figure 23. Interaction of tau-YFP aggregates with β 23 and Htt97Q aggregates

(A-B) β 23 was expressed in (A) Clone9 and (B) Clone10 cells. 24 h after transfection, cells were fixed and stained with an anti-myc primary and cy5 conjugated secondary antibody. Merge shows tau YFP (green), myc- β 23 (red) and DAPI (blue). White triangles point at tau-YFP aggregates co-localizing with β 23 and arrows show aggregates with no co-localization. (C) Htt97Q-mCherry aggregates in Clone9 and Clone10. Merge shows tau YFP (green), Htt97Q (red) and DAPI (blue). Scale bar: 10 μ m.

Taken together, these results highlight the ability of soluble tau-YFP to co-aggregate with designed β -sheet protein aggregates. The co-aggregation may result from specific structural interactions between the β -sheet proteins and exposed hydrophobic regions on soluble tau-YFP,

as pre-formed tau-YFP aggregates tend to not efficiently co-deposit. Alternatively, the sub-structural differences between tau-YFP aggregates in Clone9 and Clone10 might further prevent or favour interaction with β 23. Htt97Q excluded soluble and aggregated tau-YFP probably due to its unique biophysical aggregation properties. This is consistent with independent aggregation of expanded polyQ and tau in HD brains (Fernandez-Nogales et al., 2014). Overall, these results highlight the principles that might determine co-deposition of aggregation prone proteins and provide additional insight into the distinct character of tau-YFP aggregates in Clone9 and Clone10.

3.2 ANALYSIS OF TAU-YFP INTERACTOME IN CLONE9 AND CLONE10

To further understand the differences between tau-YFP aggregates in Clone9 and Clone10, we set out to analyse if tau-YFP in these cell lines had distinct interaction partners. For these experiments we employed a stabile isotope labelling by amino acids in cell culture (SILAC) based quantitative proteomics approach (Ong et al., 2002).

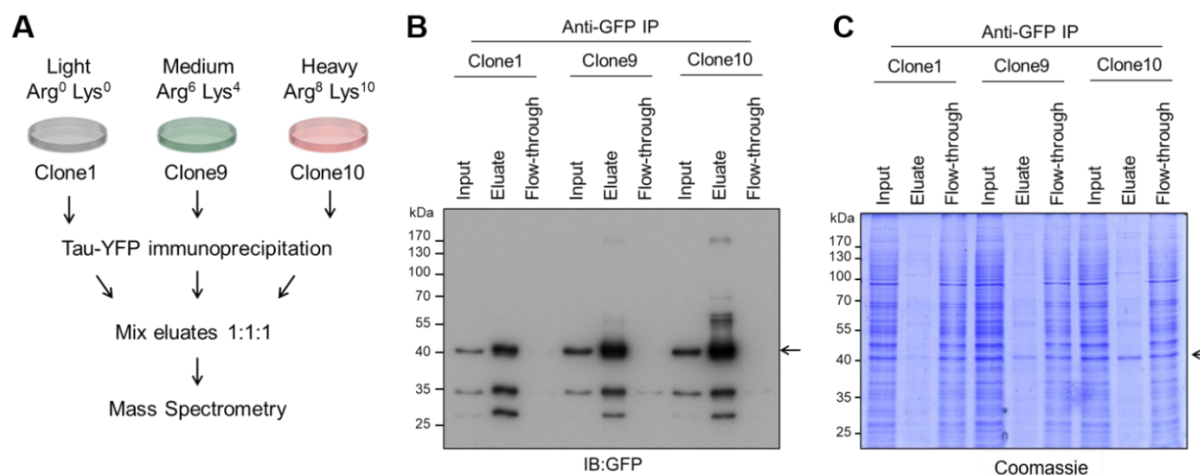


Figure 24. SILAC based interactome analysis of tau-YFP

(A) Experimental scheme for the analysis of tau-YFP interactors in Clone9 and Clone10. **(B)** Tau-YFP was immuno-precipitated from Clone1, 9 and 10 using anti-GFP beads. Equal volumes of input, eluate and flow-through fractions were analysed by western blotting against GFP or **(C)** coomassie staining. Arrow indicates monomeric tau-YFP band.

Clone1, 9 and 10 were grown in media containing light (L), medium (M) and heavy (H) amino acid isotopes, respectively (Figure 24A). Labelled cells were lysed and tau-YFP was immuno-precipitated using anti-GFP magnetic beads. Equal volumes of eluates were then mixed and analysed by mass spectrometry (MS). Tau-YFP immunoprecipitation was highly efficient as no tau-YFP could be detected in the flow-through fractions (Figure 24B). The total amount of tau-YFP in the three cell lines was however not similar, as observed in the input and the corresponding eluate fractions (Figure 24B). Clone10 had the highest tau-YFP level followed by Clone9 and Clone1. This difference in the amount of bait could influence interactor abundance in the eluates and was therefore corrected for during MS data analysis by normalizing against the abundance of total identified proteins in the eluates.

We defined interactors of tau-YFP aggregates as proteins identified by MS in at least two out of three biologically independent experiments with median enrichment ≥ 2 fold in Clone9 or Clone10 over Clone1. 88 proteins in Clone9 (M/L) and 127 proteins in Clone10 (H/L) met these criteria and were therefore designated as specific interactors of aggregated tau-YFP (Figure 25A-B) Supplementary Table 3 and 4). 61 of these proteins were enriched over the threshold in both Clone9 and Clone10. Among these were subunits of the 26S proteasome, particularly the ATPase and the non-ATPase subunits of 19S, were highly represented in the interactome of both forms of tau-YFP aggregates (Figure 25A-D). The relative abundance of proteasomal subunits was higher for the aggresome-like tau-YFP aggregates in Clone10 (Figure 25C-D), which is consistent with the association of proteasomes with aggresomes (Wigley et al., 1999). This observation is in line our previous idea of tau-YFP aggregate clearance by the proteasome (Figure 20). Other proteins involved in UPS mediated degradation were also identified as tau-YFP interactors. For instance, the AAA+ ATPase VCP and its cofactors, NSFL1C/p47 and NPLOC4-UFD1L complex, were highly enriched in Clone10 and to a lesser degree in Clone9 (Figure 25A-B).

SQSTM1/p62 and NBR1, two autophagy receptors associated with protein aggregates in different disease contexts (D'Agostino et al., 2011; Salminen et al., 2012), were present in both Clone9 and Clone10 interactomes, suggesting that there might be other disease relevant interactors in our dataset. Amongst other proteins, members of the endosomal sorting complexes required for transport (ESCRT), CHMP2B and CHMP1A, also showed significant enrichment in Clone10 (See Appendix-II for CHMP2B IF). The interaction of NBR1 and CHMP2B with tau-YFP aggregates was confirmed by immunofluorescence (Supplementary Figure S1).

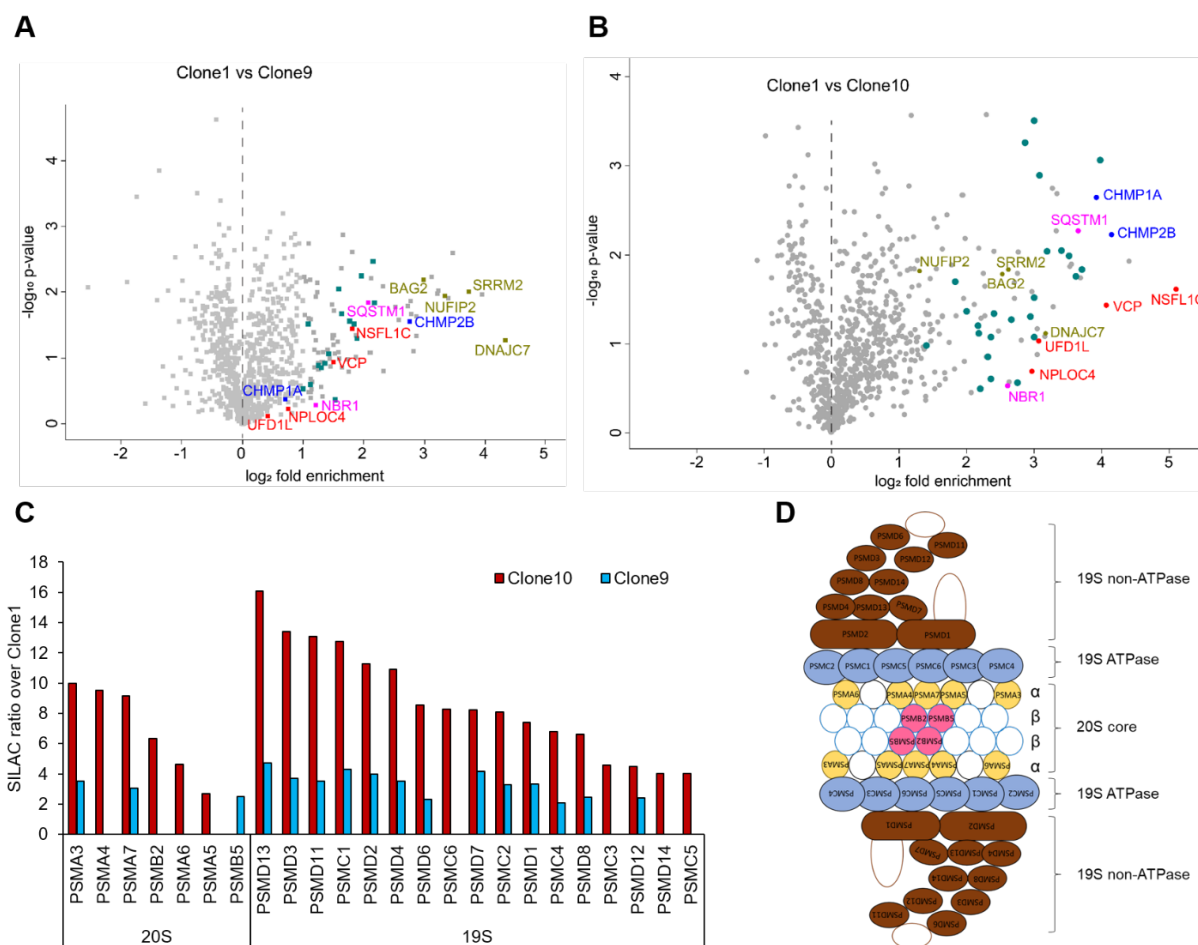


Figure 25. Interactome analysis of tau-YFP in Clone1, 9 and 10

(A-B) Volcano plots of proteins co-immunoprecipitated with tau-YFP from (A) Clone9 (M/L) and (B) Clone10 (H/L) against reference Clone1. $-\log$ of p-value is plotted against \log_2 fold enrichment. Proteins of interest or proteins with the highest fold enrichments are highlighted for both aggregate containing cell lines. Unlabelled green symbols represent proteasome subunits from 19S and 20S. Data analysis was performed in Perseus1.6.2.3. (C) Comparison of median SILAC ratios obtained for proteasome 19S and 20S subunits between Clone9 and Clone10. (D) Schematic of a 30S proteasome highlighting (filled symbols) subunits that were found to interact with tau-YFP aggregates in Clone9 and Clone10.

The direct comparison of SILAC ratios between Clone9 and Clone10 revealed CHMP1A to be a very specific interactor of tau-YFP aggregates in Clone10 (Figure 26) (Supplementary Table 5). Additionally, two other proteins belonging to the endosome-associated recycling protein (EARP) complex, VPS51 and VPS53, also preferentially interacted with tau-YFP in Clone10. Although extracellular tau (monomeric and aggregated) can enter the cell via the endosomal route, endogenous tau also appears to undergo ESCRT dependent sorting to pre-endosomal structures (Evans et al., 2018; Vaz-Silva et al., 2018). However, the nature of the interaction between tau-YFP and endosomal components in this model may not be of functional origin and

these proteins could be non-specifically sequestered in the aggregates resulting in the loss of their normal cellular function.

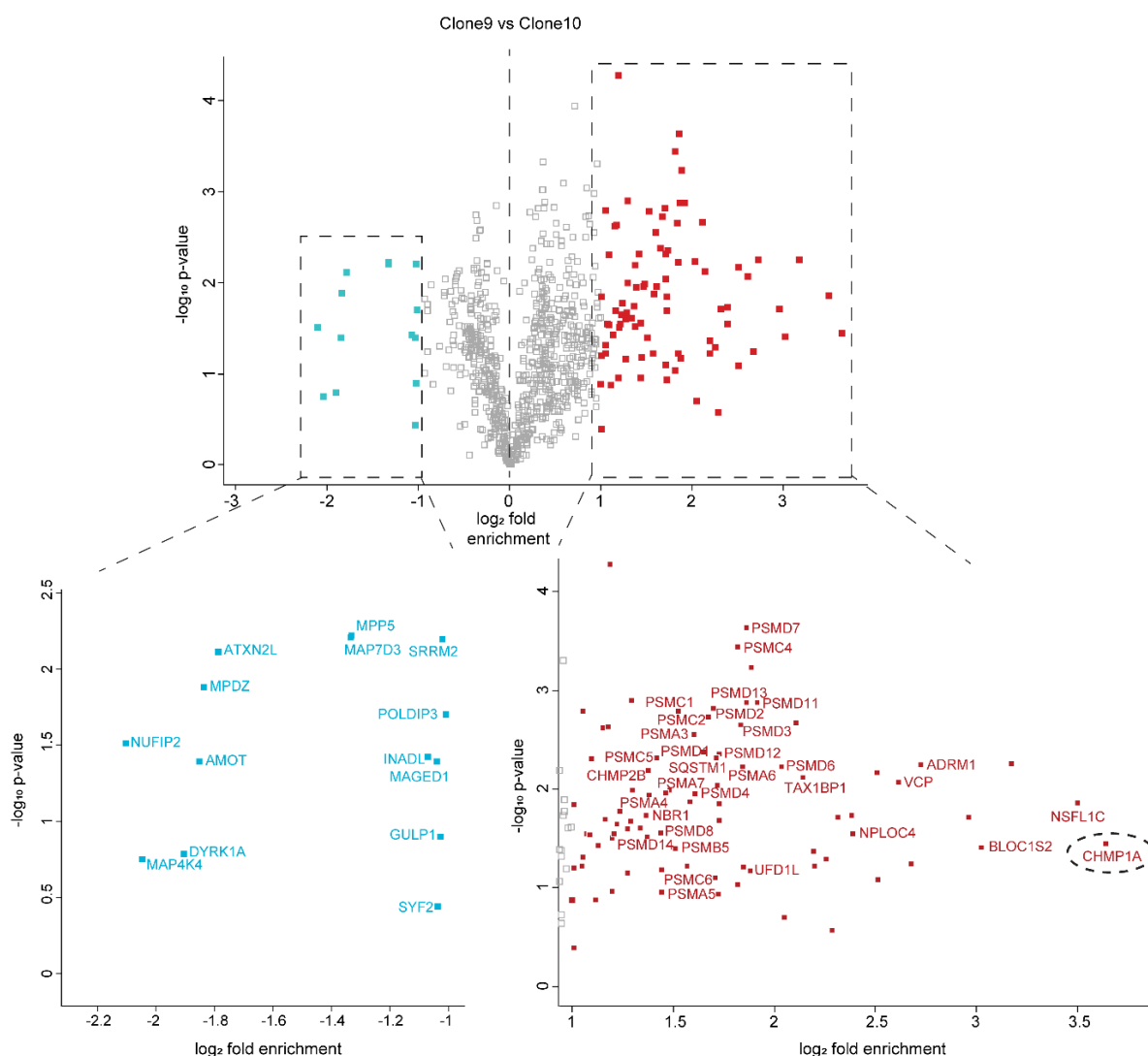


Figure 26. Comparison of Clone9 and Clone10 tau-YFP interactomes

Volcano plot comparing enriched proteins in Clone10 vs Clone9 (H/M). $-\log_{10}$ of p-value is plotted against \log_2 fold enrichment. At least 2-fold enriched proteins are highlighted and shown as zoom in bottom panel. Interactors enriched in Clone9 over Clone10 and Clone10 over Clone9 are displayed in blue and red respectively. CHMP1A shows the highest H/M fold change. Data analysis was performed in Perseus 1.6.2.3.

3.3 AUTOPHAGY PERTURBATION IN CLONE10

Autophagy is a crucial pathway for the maintenance of protein homeostasis and is implicated in the removal of protein aggregates and damaged organelles. Increasing evidence links neurodegeneration to perturbed autophagy (Fujikake et al., 2018). Analysis of brain samples from tauopathies like AD, corticobasal degeneration and progressive supranuclear palsy show increased accumulation of autophagic vesicles (Piras et al., 2016; Tan et al., 2014). However, it is often not clear if this accumulation results from defective or enhanced autophagy. Similar to protein aggregates in many neurodegenerative diseases, tau-YFP aggregates in our cellular model were found to interact with components of the autophagy-lysosomal pathway (Supplementary Table 3 highlighted hits). Therefore, we tested if our cellular model recapitulated autophagic defects observed in neurodegeneration.

3.3.1 Steady state levels of LC3-II and p62

To assess the state of autophagic degradation, we first compared the steady state levels of autophagy marker proteins p62 and LC3 in total cell lysates of Clones 1, 9, 10, and wild-type HEK293 cells. Interestingly, Clone10 showed elevated levels of LC3-II, the autophagosome resident lipidated form of LC3 (Figure 27, quantification in Figure 29). This indicates either increased autophagosome biogenesis or reduced turnover, because LC3-II is not only a functional component of the autophagy machinery but also a substrate degraded in the process with other cargo material. Elevated LC3-II levels in cells containing tau aggregates have been previously reported and were presumed to be due to increased LC3-II synthesis (Guo et al., 2016). In addition, Clone10 showed higher p62 levels than Clone 1, 9 and HEK293 cells (Figure 27), which in combination with increased LC3-II levels may point towards perturbed autophagic degradation (Klionsky et al. 2016).

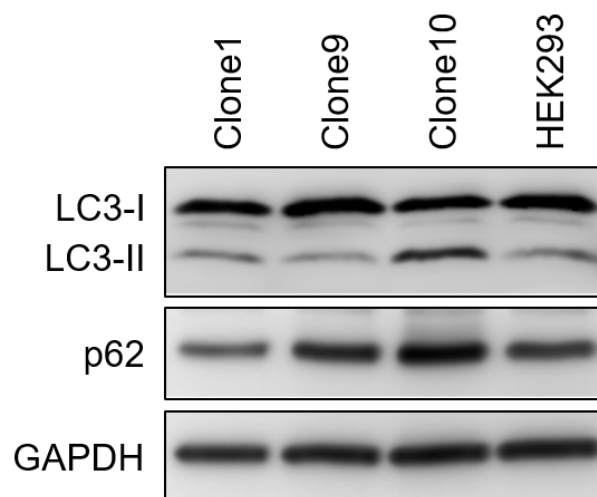


Figure 27. Steady state levels of LC3 and p62

Clone1, 9, 10 and HEK293 cell lysates from cells grown under steady state were analysed by western blotting. LC3 antibody recognises both lipidated (LC3-II) and non-lipidated forms (LC3-I). GAPDH was used as loading control.

To test if the increased LC3-II levels in Clone10 correspond to increased autophagosome load, we visualized autophagosomes in our cell lines by LC3 immunofluorescence. Consistent with western blotting results, Clone10 showed increased numbers of LC3 positive vesicles at steady state in comparison to Clone1, Clone9 and HEK293 cells. These vesicles did not directly co-localize with tau-YFP aggregates (Figure 28), in agreement with the fact that LC3 was not a tau-YFP interactor in these cell lines. Moreover, p62 which was identified as an interactor of tau-YFP in Clone9 and Clone10 was strongly enriched on tau-YFP aggregates in both Clone9 and Clone10 (Figure 28).

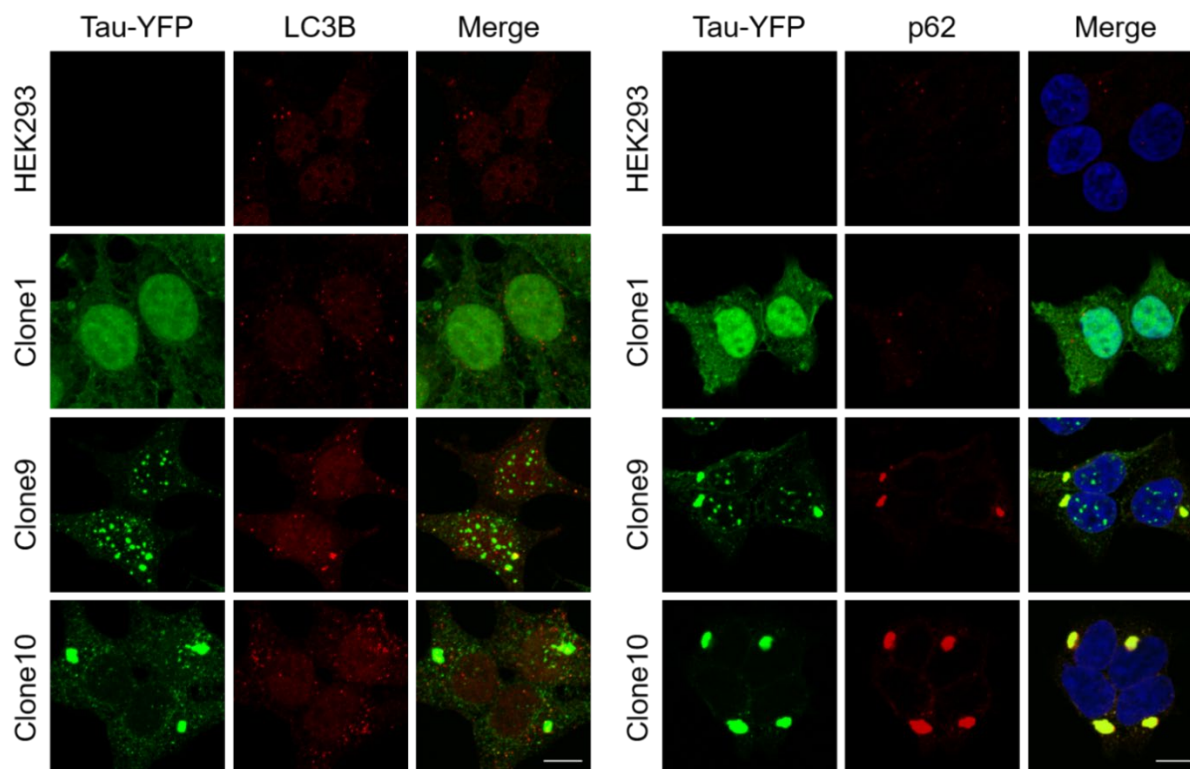


Figure 28. Association of tau-YFP aggregates with autophagy components

HEK293, Clone1, 9 and 10 cells were fixed and stained with anti-LC3B (left panel) and anti-p62 (right panel) primary and cy5 conjugated secondary antibodies. Merged images show tau-YFP (green), LC3B/p62 (red) and DAPI (blue). Scale bar: 10 μ m.

3.3.2 Assessment of autophagic flux

Autophagy is a dynamic and multi-step process. Accumulation of LC3-II and autophagosomes can indicate either autophagic activation or a disruption in the downstream steps of autophagy such as impaired fusion or degradation within lysosomes. To distinguish between these two possibilities, we measured autophagic flux. Autophagic flux is a measurement of autophagic degradation capacity. It is calculated as the ratio of LC3-II accumulation when autophagy is inhibited at the end stage by inhibitors like bafilomycinA1 (BafA1) to its steady state levels (Klionsky et al. 2016). BafA1 prevents lysosomal acidification by inhibiting the vacuolar type H⁺ ATPase, thereby impeding degradation of autophagic cargo (Yoshimori et al., 1991). Therefore, in a flux assessment assay, autophagic up-regulation would be reflected as increased amounts of LC3-II after BafA1 treatment in comparison to a condition with normal levels of autophagy. In contrast, if LC3-II levels were elevated because autophagy was inhibited, there is no further increase in LC3-II levels after BafA1 treatment.

Short term BafA1 treatment in Clone1, 9 and 10 resulted in additional LC3-II accumulation over the steady state levels indicating that LC3-II/autophagosome turnover was successfully inhibited by the treatment (Figure 29A). LC3-II accumulation after BafA1 treatment also confirms that all three cell lines were able to normally synthesize lipidated LC3-II/autophagosomes. However, when the LC3-II levels were compared in BafA1 treated and untreated samples, the autophagic flux in Clone10 was significantly lower than in Clone1 and Clone9, while autophagic flux in Clone9 did not significantly differ from Clone1 (Figure 29B). These results demonstrate that the Clone10 cells, containing aggresome-like tau-YFP aggregates, are impaired in late-stage autophagy.

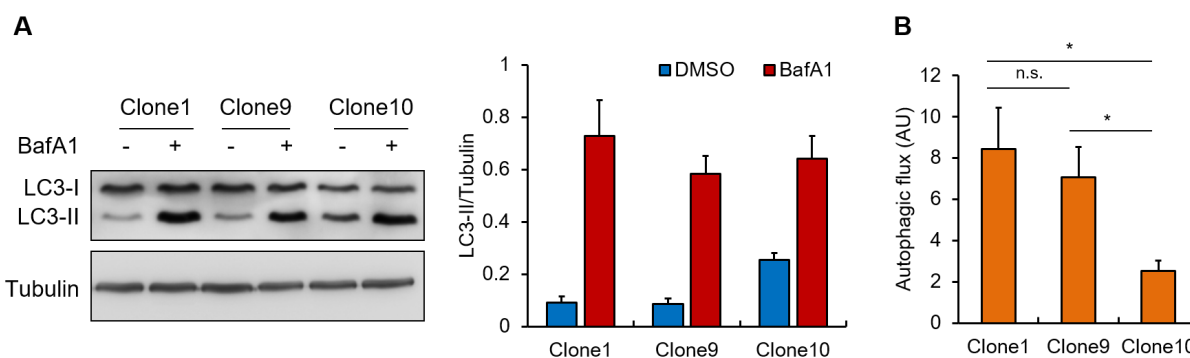


Figure 29. Assessment of autophagic flux

(A) Clone1, 9 and 10 cells were treated with DMSO or 200 nM BafA1 for 4h. Cell lysates were analysed by immune-blotting to quantify levels of LC3-II and the loading control tubulin (left panel). Normalized LC3-II/tubulin values from three independent repeats are shown (right panel). **(B)** Autophagic flux was calculated by comparing the ratio of LC3-II/tubulin values in BafA1 over DMSO treated cells. Error bars represent standard deviations. P-values were calculated from student's paired t-test; n.s. non-significant, * <0.05

3.4 AGGREGATE CLEARANCE IN CLONE10

Under conditions of amino acid deprivation, cells induce autophagic degradation in order to maintain amino acid supply for the synthesis of vital cellular proteins (Onodera and Ohsumi, 2005). Since we observed an autophagy impairment in Clone10, we speculated that these cells might be more vulnerable to an autophagy demanding state such as amino acid starvation. In order to understand the effect of starvation in tau-YFP clones, cells were shifted from full medium to Earle's balanced salt solution (EBSS) for 24 h, which contains glucose as an energy source but is lacking amino acids and serum. After growing Clone1, 9 and 10 in EBSS for 24 h, we observed a significant reduction in the number of visible aggregates in Clone10. Intriguingly, this effect was not seen in Clone9 (Figure 30A-B). Also, the average size of the aggregates was reduced by ~20% in Clone10, whereas the average inclusion size in Clone9 remained constant (Figure 30C). These results show that, in contrast to Clone9, the fibrillar tau-YFP aggregates in Clone10 were amenable to clearance in response to amino acid starvation, and further suggests that the inherent strain-like differences between these two aggregate types might uphold a different cellular response to each structure.

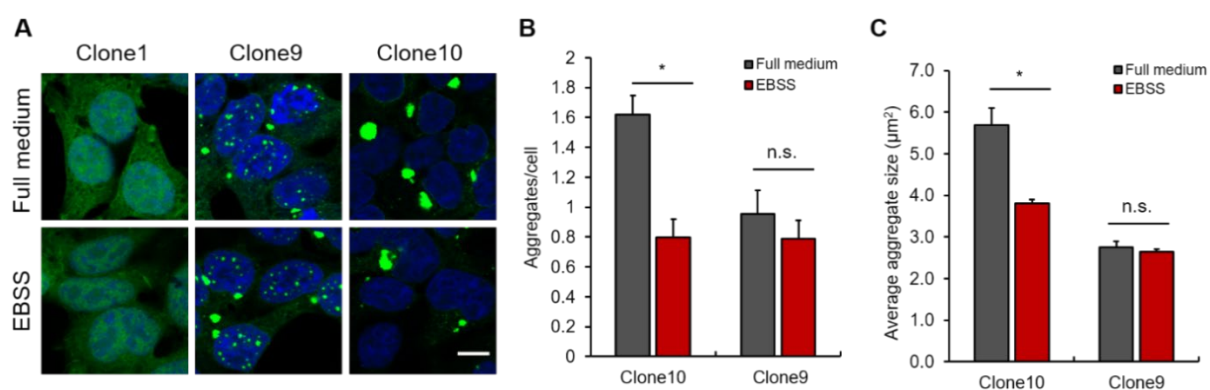


Figure 30. Effect of amino acid starvation on tau-YFP aggregation

(A) Clone1, 9 and 10 cells were grown on cover slips in DMEM, and switched to EBSS for 24 h or kept in full medium. Cells were fixed, counterstained with DAPI and imaged. (B-C) Cells were grown as in (A). Total number of aggregates in each condition was normalized to cell numbers to compute aggregates/cell. Values from three independent experiments with standard deviations are shown. P-values were calculated with student's paired t-test; n.s. non-significant, * <0.05 . Scale bar: 10μm.

3.4.1 Aggregate clearance by limiting tau synthesis with cycloheximide

Aggregates of full length GFP tagged tau carrying the P301L mutation are cleared in cultured cells by shutting off tau expression (Guo et al., 2016). We tested if this is also the case for tau-YFP in Clones 1, 9 and 10 by utilizing the protein translation inhibitor cycloheximide (CHX) to switch-off protein synthesis. While tau-YFP in Clone1 was efficiently degraded with a half-life of ~5 h (Figure 31A), there was almost no turnover of tau-YFP in Clone9 and only ~40% tau-YFP was degraded in Clone10 after 24 h of treatment. These observations indicated that the stability of tau-YFP was dictated by its physical status and suggests that aggregation interferes with efficient degradation.

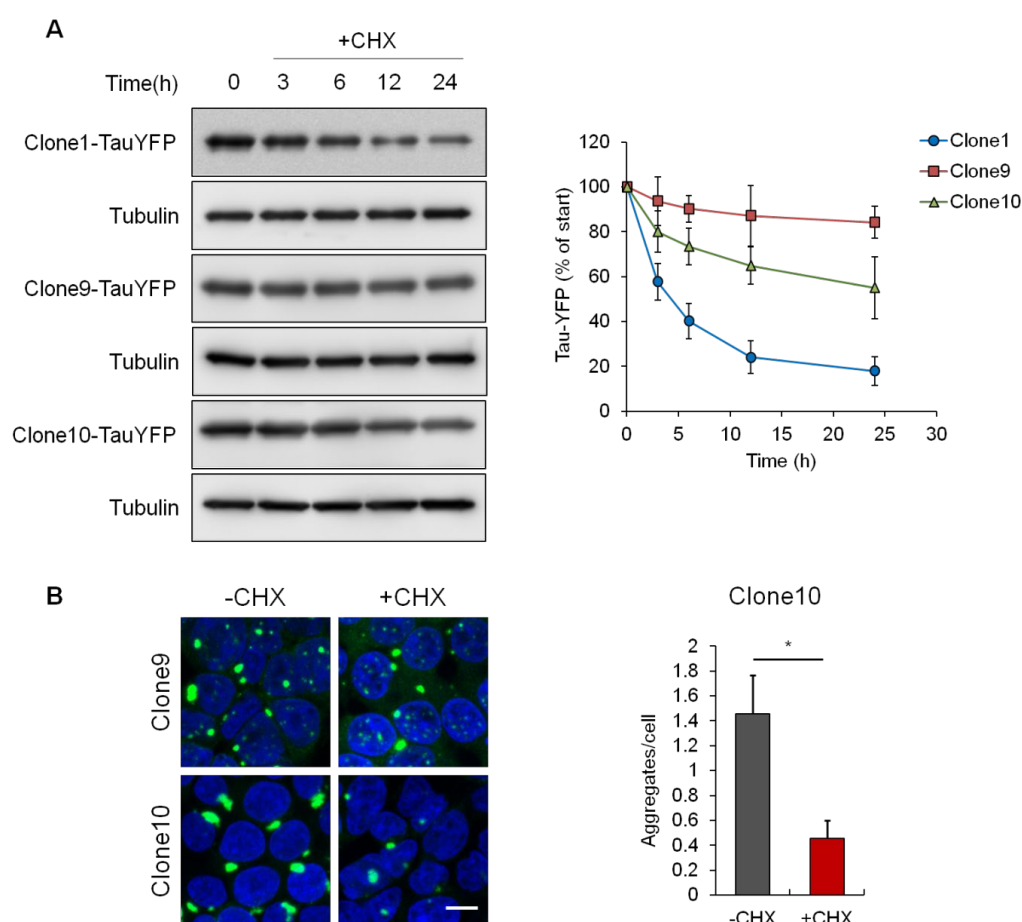


Figure 31. Effect of translation shut-off on tau-YFP turnover

(A) Clone1, 9 and 10 were treated with 50 $\mu\text{g}/\text{mL}$ CHX for the indicated times. Tau-YFP levels were assessed by western blotting against GFP and quantified by densitometry (right panel). (B) Clone9 and Clone10 with CHX where indicated and imaged by confocal microscopy. (Right panel) Aggregates/cell in Clone10 were quantified as stated in Figure 30. Scale bar: 10 μm . Error bars represent standard deviation from 3 independent experiments. P-value was calculated using student's paired t-test; * <0.05 .

Furthermore, we examined the state of tau-YFP aggregates by microscopy after inhibiting translation. Similar to starvation, Clone10 showed a reduced aggregate load compared to Clone9, wherein the aggregates remained unchanged after 24 h of CHX treatment (Figure 31B). This observation establishes that the amyloid-like tau-YFP aggregates in Clone10 are dynamic entities undergoing continuous turnover. In contrast, tau-YFP protein and aggregates in Clone9 are resistant to the cellular degradation machinery. Moreover, the kinetic delay in the turnover of tau-YFP in Clone10 compared to Clone1 upon the addition of CHX might either indicate limited synthesis of cellular factor/s required for the degradation of aggregated tau-YFP or the necessity of a pre-processing step such as disaggregation which would solubilise tau-YFP aggregates before degradation.

3.4.2 Proteasome dependent turnover of tau-YFP aggregates

The elimination of amyloid-like tau-YFP aggregates from Clone10 cells highlighted that these aggregates were substrates of an active clearance mechanism. We asked if this clearance mechanism was connected to any of the two major protein degradative pathways in cells: the ubiquitin proteasome system (UPS) and autophagy. To understand this connection and the fate of aggregated tau-YFP, we tested the effects of inhibition of these pathways on aggregate clearance. Specifically, Clone10 cells were treated with chemical inhibitors of the UPS (MG132) and autophagy (BafA1) under conditions of amino acid starvation. Strikingly, MG132 treatment effectively prevented aggregate clearance but not BafA1 (Figure 32A), even though BafA1 treated cells accumulated additional p62 positive puncta consistent with the inhibition of autophagic degradation by BafA1 treatment. Analysis of aggregated tau-YFP by filter trap assay confirmed that MG132 inhibited aggregate clearance (Figure 32B). In addition, total tau-YFP levels in both Clone1 and Clone10 were stabilized by proteasome inhibition demonstrating that tau-YFP was turned over by the proteasome in these cell lines.

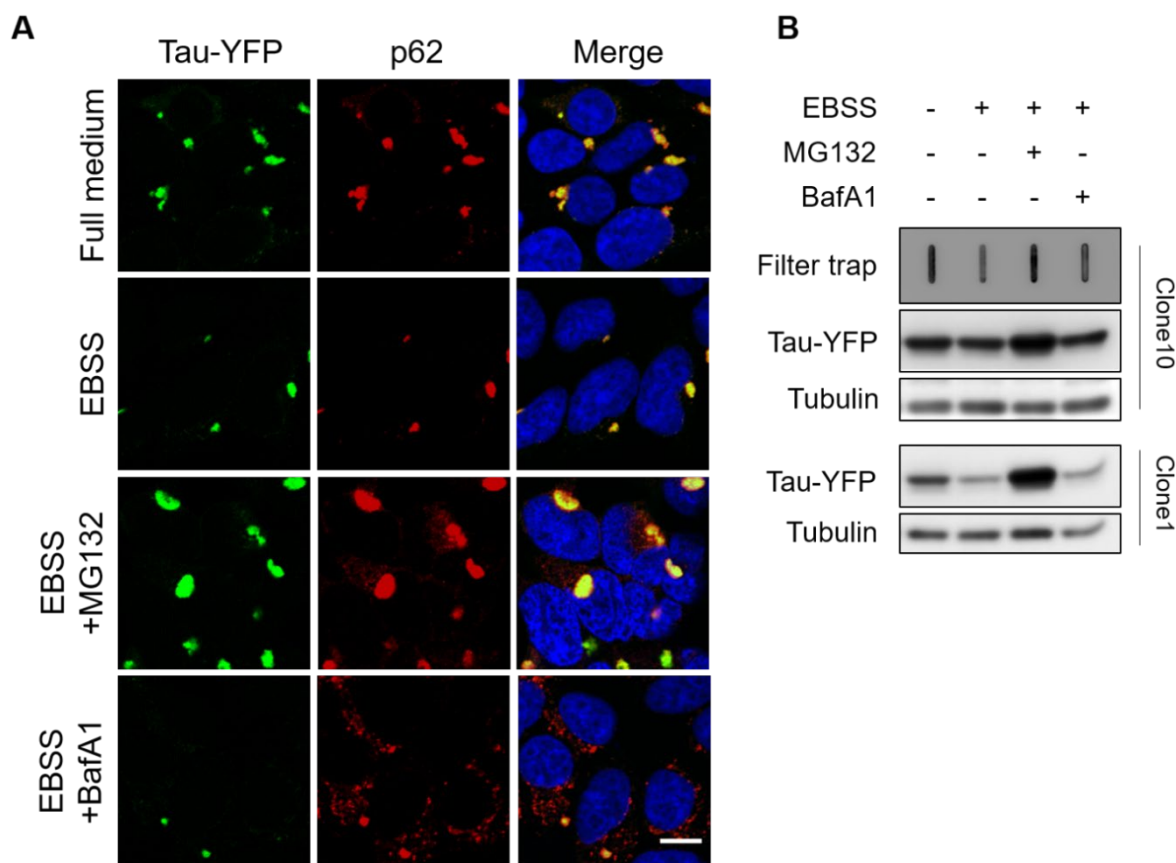


Figure 32. Effect of proteasome and autophagy inhibition on aggregate clearance

(A) Clone10 cells were starved in EBSS for 24 h in combination with 1 μ M proteasome inhibitor MG132 and 100 nM autophagy inhibitor BafA1. Cells were fixed and stained with an anti-p62 primary and cy5 conjugated secondary antibody. Merged images show tau-YFP (green), p62 (red) and DAPI (blue). Scale bar: 10 μ m. **(B)** Analysis of aggregated tau-YFP in Clone10 cells by filter trap and total tau-YFP levels in Clone10 and Clone1 cells starved in EBSS for 24 h in combination with 1 μ M proteasome inhibitor MG132 and 50 nM autophagy inhibitor BafA1.

MG132 has off-target effects and can also inhibit some lysosomal proteases and non-lysosomal cysteine proteases including calpains (Lee and Goldberg, 1998). To confirm the specificity of aggregate stabilization by MG132 in Clone10, we utilized two additional, more specific inhibitors of the proteasome: lactacystin and epoxomicin. Similar to MG132, both lactacystin and epoxomicin also resulted in stabilization of tau-YFP aggregates (Figure 33). Notably, the average size of the stabilized aggregates was \sim 2 times more than the average size in full medium. Aggregate enlargement was also observed when cells were treated with MG132 in full medium (See Figure 20).

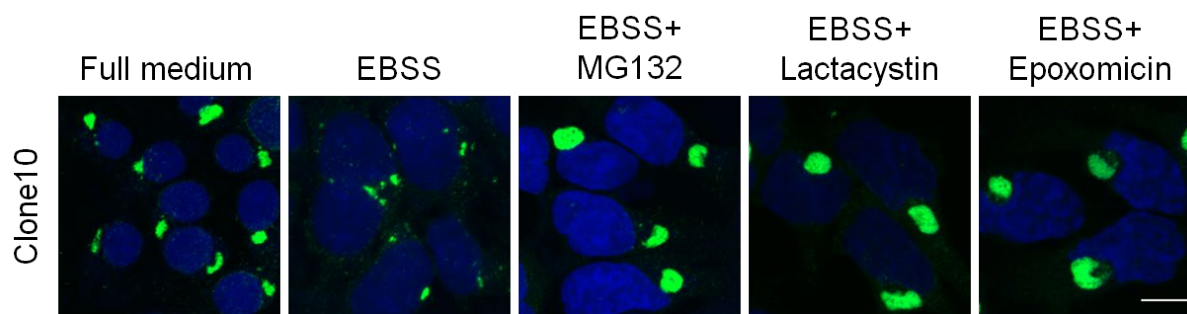


Figure 33. Effect of different proteasome inhibitors on aggregate clearance

Clone10 cells were starved in EBSS alone or in combination with 1 μ M MG132, 5 mM Lactacystin and 100 mM Epoxomicin for 24 h. Cells were fixed and counterstained with DAPI. Merged images with tau-YFP (green) and DAPI (blue) are shown. Scale bar: 10 μ m.

Aggregate enlargement upon proteasome inhibition suggested that the proteasome was involved in tau-YFP aggregate clearance. This is supported by the fact that we had identified interactions between multiple subunits of the 26S proteasome and aggregated tau-YFP by MS (Figure 25). Notably, subunits of the 19S regulatory particle were more enriched on the tau-YFP aggregates compared to 20S subunits. Enrichment of the 19S subunits has also been previously reported for insoluble Htt-polyQ aggregates (Kim et al., 2016). This observation could reflect either a 26S-independent chaperone-like interaction of the 19S particle with aggregated tau-YFP (Braun et al., 1999), or a dissociation of the 20S complex leaving behind the 19S particle (Nanduri et al., 2015). Interestingly under amino acid starvation, $\alpha\beta$ subunits of the 20S proteasome were robustly recruited to the tau-YFP aggregates while the appearance of 19S particles, as judged by PSMD4 immunofluorescence, remained unchanged (Figure 34A-B). This active recruitment of the 20S might result in the formation of an active 26S proteasome on the aggregates. In addition, both 19S and 20S subunits failed to co-localize with the inclusions under proteasome inhibition (Figure 34A-B), further indicating that proteasomes may not be terminally sequestered in tau-YFP aggregates, and instead actively interact and possibly process tau-YFP. Although the AAA+ ATPases of the 19S particle unfold substrates before they are translocated into the 20S chamber, it is not known if this unfolding activity *per se* is sufficient to extract polypeptides from aggregated material. Given that an unstructured region is a prerequisite for the proteasome to engage substrates and initiate unfolding (Tomita and Matouschek, 2019), it is likely that fibrillar aggregates are remodelled or disaggregated prior to

proteasomal processing. A similar model was presented by Hjerpe et al., where disaggregation by the Hsp70 system was required to clear heat-induced aggregates via the proteasome (Hjerpe et al., 2016).

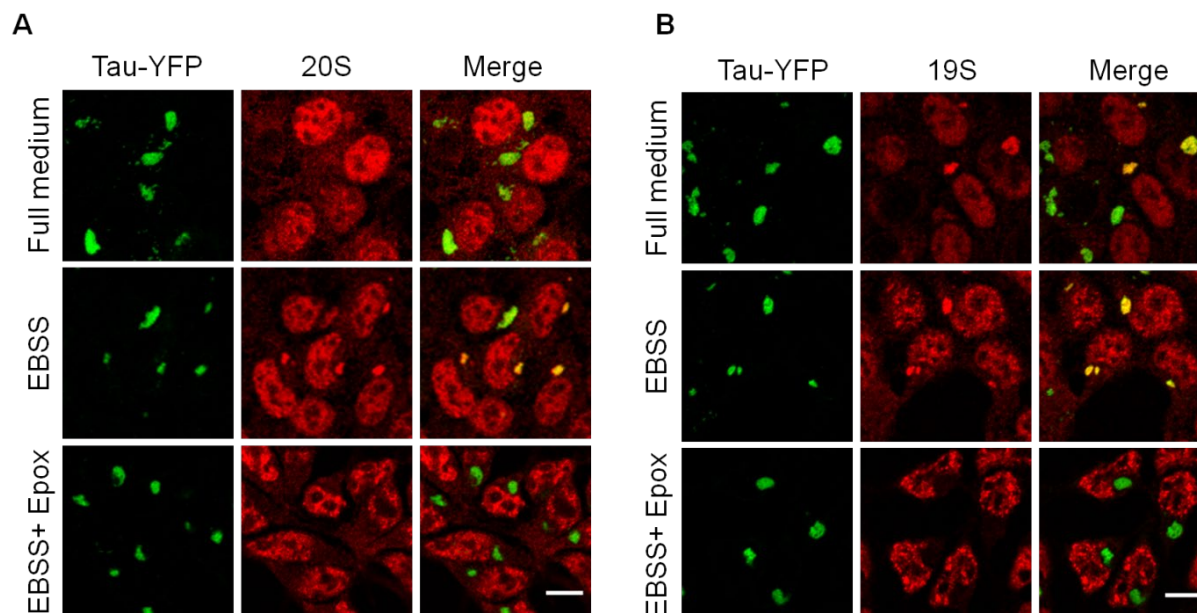


Figure 34. Proteasomal recruitment to tau-YFP aggregates

Clone10 cells were grown in full medium or starved in the absence or presence of 100 nM epoxomicin. Cells were fixed and stained with **(A)** anti-PSMD4/Rpn10 (19S) or **(B)** Anti- $\alpha\beta$ subunit (20S) antibody followed by cy5 conjugated secondary antibody. In the EBSS conditions, aggregate containing fields were deliberately chosen for imaging. Merge shows tau-YFP (green), 19S/20S (red) and co-localizing aggregates in yellow. Scale bar: 10 μ m.

3.5 UNDERSTANDING CELLULAR DISAGGREGATION IN A TET-REGULATED TAU-YFP EXPRESSION MODEL

So far, we observed that tau-YFP aggregates were cleared in Clone10 cells under amino acid starvation and cycloheximide treatment. Both conditions however cause global changes in the cellular physiology, making further investigation of disaggregation mechanisms complex. Since termination of new protein synthesis was sufficient for aggregate clearance, we utilized a tau-YFP aggregation model in HEK293 cells stably expressing tau-YFP under a Tet-off promoter (Gift from Marc Diamond, University of Texas Southwestern).

In this model, addition of a tetracycline homolog, doxycycline, in the concentration range 30-50 ng/mL exclusively shuts off tau-YFP production (Sanders et al., 2014), without causing any apparent perturbation in cellular health or proliferation (Ahler et al., 2013). As in the constitutive tau-YFP expressing Clone1, there was no aggregation detectable by microscopy and solubility assay in the Tet-regulated tau-YFP expressing cells (hereafter referred to as Tet-Clone1) (Figure 35A, C). The aggregate containing cells in this model (hereafter referred to as Tet-Clone10), were generated by treating Tet-Clone1 cells with lysates from Clone10 cells (performed in the Diamond lab). Tet-Clone10 cells, however, showed multiple smaller tau-YFP aggregates in the cytosol and nucleus distinct from the single juxtannuclear IB in the parental Clone10. The phenotypic difference between Clone10 and Tet-Clone10 may have been due to differences in the expression level of tau-YFP or the length of tau RD expressed in these cell lines (Supplementary Table 1 and 2). However, similar to Clone10, the cytosolic aggregates in Tet-Clone10 cells stained positive with AmyloGlo indicating their amyloid content and were detergent-insoluble (Figure 35B-C). The amount of detergent-insoluble tau-YFP in Tet-Clone10 was significantly lower than in the parental Clone10 where ~90% tau-YFP was found in the pellet fraction (see Figure 16D). After 24 h of halting tau-YFP expression by the addition of doxycycline, there was a substantial reduction in the number and size of tau-YFP aggregates in Tet-Clone10 and overall YFP fluorescence in Tet-Clone1 (Figure 35A). Western blot analysis of total cell lysates revealed that tau-YFP levels were reduced by ~80% in both Tet-Clone1 and Tet-Clone10 (Figure 35C) (quantified in Figure 37A). Doxycycline treatment also reduced

insoluble tau-YFP levels in Tet-Clone10 (Figure 35C), confirming the loss of tau-YFP aggregates upon termination of tau-YFP synthesis. In contrast to amino acid starvation or cycloheximide treatment, doxycycline did not stop cell division and thus dilution of existing proteins contributes to diminished tau-YFP levels. However, dilution by cell division would only result in a reduction of tau by about 50% (assuming that the doubling time of HEK293 cells is ~24 h) and would not explain changes in the size of the inclusions. This approximation indicated that a large fraction of tau-YFP was degraded by cellular protein degradation pathways (UPS or autophagy) during this time.

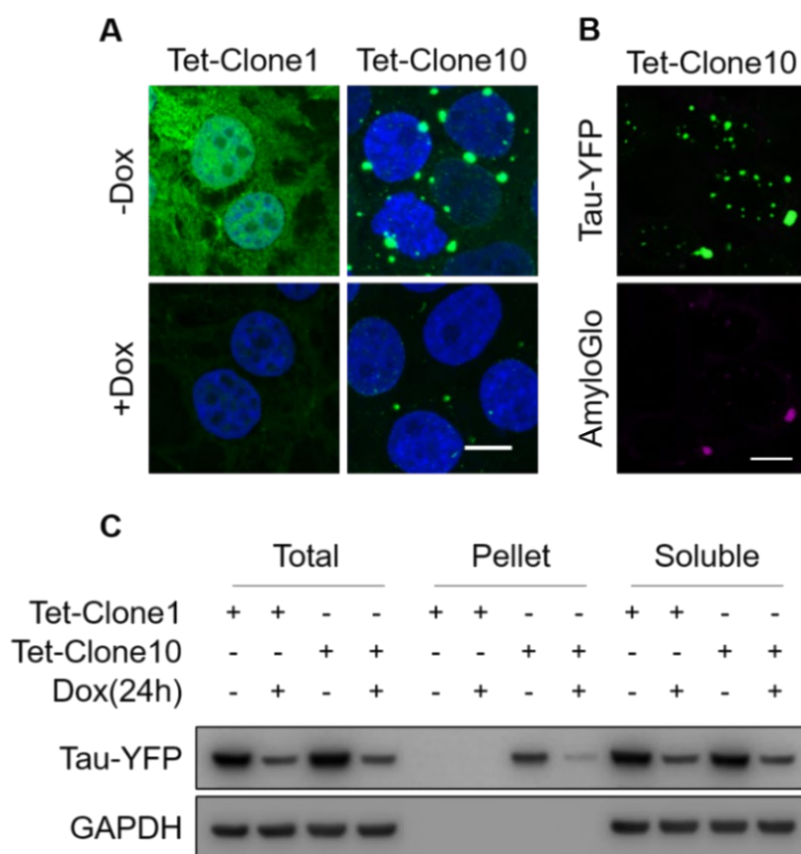


Figure 35. Aggregate clearance in a tet-regulated tau-YFP expression model

(A) Tet-tau-YFP clones were treated with doxycycline for 24 h and imaged by fluorescence microscopy. Images show merged tau-YFP (green) and DAPI (blue) signals. (B) Tet-Clone10 cells at steady state were labelled with amyloid-binding dye AmyloGlo (magenta). (C) Tet-tau-YFP clones were treated with doxycycline for 24 h where indicated. Cell lysates were centrifuged at 186,000xg for 1 h. Total (T), soluble (S) and pellet (P) fractions were analysed for tau-YFP by western blotting with an anti-GFP antibody. GAPDH was blotted as loading control. Scale bar: 10 μ m.

3.5.1 Tau-YFP mRNA and protein turnover kinetics

In order to determine the turnover kinetics of tau-YFP in the tet-clones, doxycycline chase experiments were performed. First, we analysed the efficiency of the promoter shut-off and the decay of tau-YFP mRNA post doxycycline treatment. Cells were treated with doxycycline for 3, 6, 12, 18 and 24 h and tau-YFP mRNA levels were compared to untreated cells by q-PCR. Tau-YFP mRNA level dropped to ~30% within 3 h in both Tet-Clone1 and Tet-Clone10 (Figure 36A). Between 6-12 h, the mRNA levels were at the baseline at ~5%, as a further drop with longer treatment times was not observed. The basal expression was likely a consequence of the inherent leakiness of the Tet system (Loew et al., 2010).

On the protein level, tau-YFP was degraded with a half-life of ~12 h in both Tet-Clone1 and Tet-Clone10 (Figure 36B). To detect differences in the fate of the soluble and insoluble tau-YFP, Tet-Clone10 lysate was fractionated by ultracentrifugation. The soluble tau-YFP in Tet-Clone10 had a half-life that was comparable to total tau-YFP in Tet-Clone1 and Tet-Clone10 (Figure 36B). However, the insoluble tau-YFP levels diminished faster than both total and soluble tau-YFP. This observation suggested that tau-YFP in the insoluble fraction was either degraded faster than soluble tau-YFP, or the aggregated material was re-solubilised over time. The first possibility is less plausible, since aggregated proteins are more resistant to degradation compared to their soluble state (Verhoef et al., 2002). To test whether the tau-YFP IBs were re-solubilised, Tet-Clone10 cells were treated with doxycycline for different time periods over 24 h and analysed by fluorescence microscopy. Post-doxycycline treatment, there was a gradual reduction in the size and number of tau-YFP IBs before they finally disappeared in the majority of cells after ~24 h (Figure 36C). This observation indicated that in the absence of tau-YFP synthesis, the IBs were constantly depleted of material which may have been released into the soluble fraction, thus creating a flux into this fraction. Moreover, aggregate clearance occurring at steady state suggests that aggregate disassembly is an ongoing process in equilibrium with aggregate formation. The solubilisation of aggregates predicts that a disaggregation process is in operation.

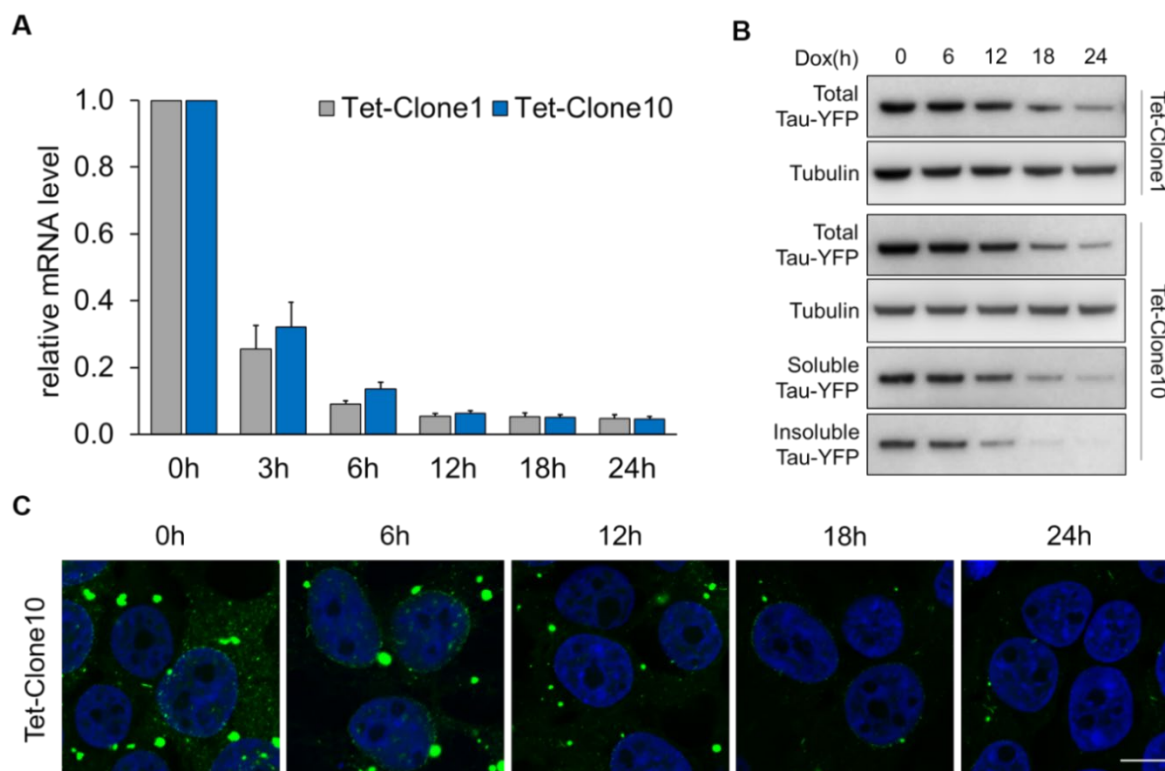


Figure 36. Tau-YFP protein and mRNA turnover in Tet-tau-YFP clones

(A) Tet-clones were treated with doxycycline for 0, 3, 6, 12, 18 and 24 h and mRNA was isolated. mRNA levels quantified by q-PCR were normalized to the reference gene RPS18 and are displayed as fraction of the untreated sample. Error bars represent standard deviation from three independent experiments. Q-PCR was performed in collaboration with Hauke Holthusen. (B) Tet-clones were treated with doxycycline for 0, 6, 12, 18 and 24 h and analysed for total tau-YFP levels by anti-GFP immunoblotting. Tubulin was blotted as loading control. Tet-Clone10 lysates were separated into a soluble and an insoluble fraction by centrifugation at 186,000xg for 1 h. Soluble and insoluble fractions were analysed by western blotting. (C) Tet-Clone10 was treated with doxycycline for 0, 6, 12, 18 and 24 h. After the indicated time cells were fixed and counterstained with DAPI. Merged tau-YFP (green) and DAPI (blue) single plane confocal images are shown. Scale bar: 10 μ m.

3.5.2 Proteasomal degradation of tau-YFP and aggregate stabilization

Full length tau is degraded by both UPS and autophagy (Chesser et al., 2013). In our model of constitutive expression, tau-YFP was degraded by the proteasome during amino acid starvation (see Figure 32). To examine if this was also true in the presence of amino acids in the tet-regulated tau-YFP expression system, Tet-Clone1 and Tet-Clone10 cells were treated with the proteasome inhibitor epoxomicin or late stage autophagy inhibitor BafA1 in the presence of doxycycline. As previously observed, doxycycline treatment alone resulted in the reduction of tau-YFP levels in both cell lines. Addition of epoxomicin, but not BafA1, in combination with doxycycline significantly stabilized tau-YFP in both cell lines similar to the constitutive

expression model (Figure 37A). Accumulation of LC3-II confirmed that autophagic degradation was efficiently blocked by BafA1 under these conditions. The filter trap assay and fluorescence microscopy analysis demonstrated that inhibition of the proteasome with epoxomicin resulted in stabilization of aggregates in Tet-Clone10 cells whereas as early stage inhibitor of autophagy, 3-methyladenine (3-MA), did not hinder aggregate clearance (Figure 37B-C).

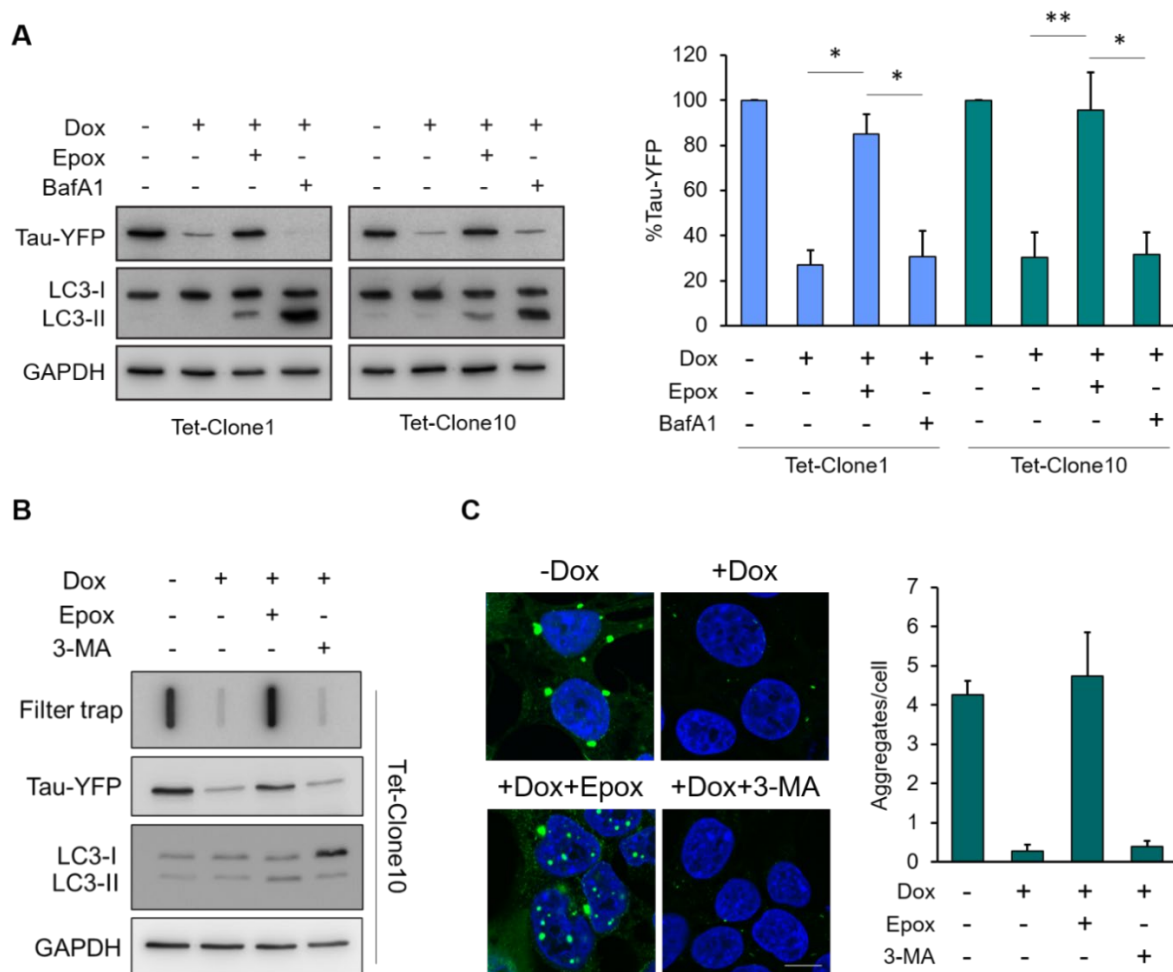


Figure 37. Effect of UPS and autophagy inhibition on tau-YFP levels and aggregate clearance

(A) Tet-clones were treated with 50 ng/ μ L doxycycline (Dox) alone or in combination with 50 nM epoxomicin (Epox) or 50 nM bafilomycin A1 (BafA1) for 24 h. Total protein levels were analysed by western blotting with GFP and LC3B antibodies. Right panel- Quantification of tau-YFP levels normalized to untreated control. Error bars represent SEM from four independent experiments. P-values were calculated using student's paired t-test. * <0.05 . ** <0.01 . **(B)** Tet-Clone10 was treated with 50 ng/ μ L dox alone or in combination with 50 nM epoxomicin or 5 mM 3-methyladenine (3-MA) for 24 h. Cell lysates were subjected to filter trap assay and the membrane was probed with anti-GFP antibody to detect tau-YFP. Total protein was analysed as described in (A). **(C)** Tet-Clone10 cells were grown on poly-lysine coated cover slips and treated with 50 ng/ μ L doxycycline alone or in combination with 50 nM epoxomicin or 5 mM 3-MA for 24 h. After the indicated treatments cells were fixed and counter stained with DAPI. Single plane confocal images show merged tau-YFP (green) and DAPI (blue) channels. Scale bar: 10 μ m. Right panel- Quantification of the number of visible tau-YFP aggregates/cell for the indicated treatments. Error bars represent standard deviation from three independent experiments.

To avoid non-specific effects of the pharmacological inhibitors, we performed siRNA mediated knockdown of a proteasome subunit, PSMD11/Rpn6 of the 19S regulatory particle, and of components of the autophagy pathway, Atg5 and Atg7. Atg5 and Atg7 are essential autophagy genes, the loss of which causes neurodegeneration in mice (Hara et al., 2006; Komatsu et al., 2006). Tet-Clone10 cells were first transfected with control or targeted siRNAs for 72 h followed by 24 h of doxycycline treatment. Consistent with our previous observation, downregulation of Atg5 or Atg7 did not interfere with aggregate clearance, whereas PSMD11 knockdown strongly impeded aggregate clearance (Figure 38A-B). Moreover, while the knockdown of Atg5 or Atg7 had no effect, downregulation of PSMD11 stabilized total tau-YFP levels indicating the degradation of tau-YFP by the proteasome in this cell line. Similar observations were made when the knockdowns were performed in the absence of doxycycline (Figure 38C). These results demonstrate that tau-YFP aggregates in this model are resolved in a proteasome dependent, but autophagy independent manner.

Proteins can only access the catalytic center of the 20S proteasome if they are unfolded. Thus, for aggregated proteins to be degraded by the proteasome, prior disaggregation would be necessary. We predict that disaggregation must be followed by proteasomal degradation to prevent re-aggregation, emphasizing the importance of a functional coupling between the two processes. Taken together, these results are in agreement with a model that suggests disaggregation of tau-YFP aggregates prior to proteasomal degradation. In the cellular context, disaggregation of amyloid-like fibrillar aggregates and the machinery required for this process has not yet been recognized.

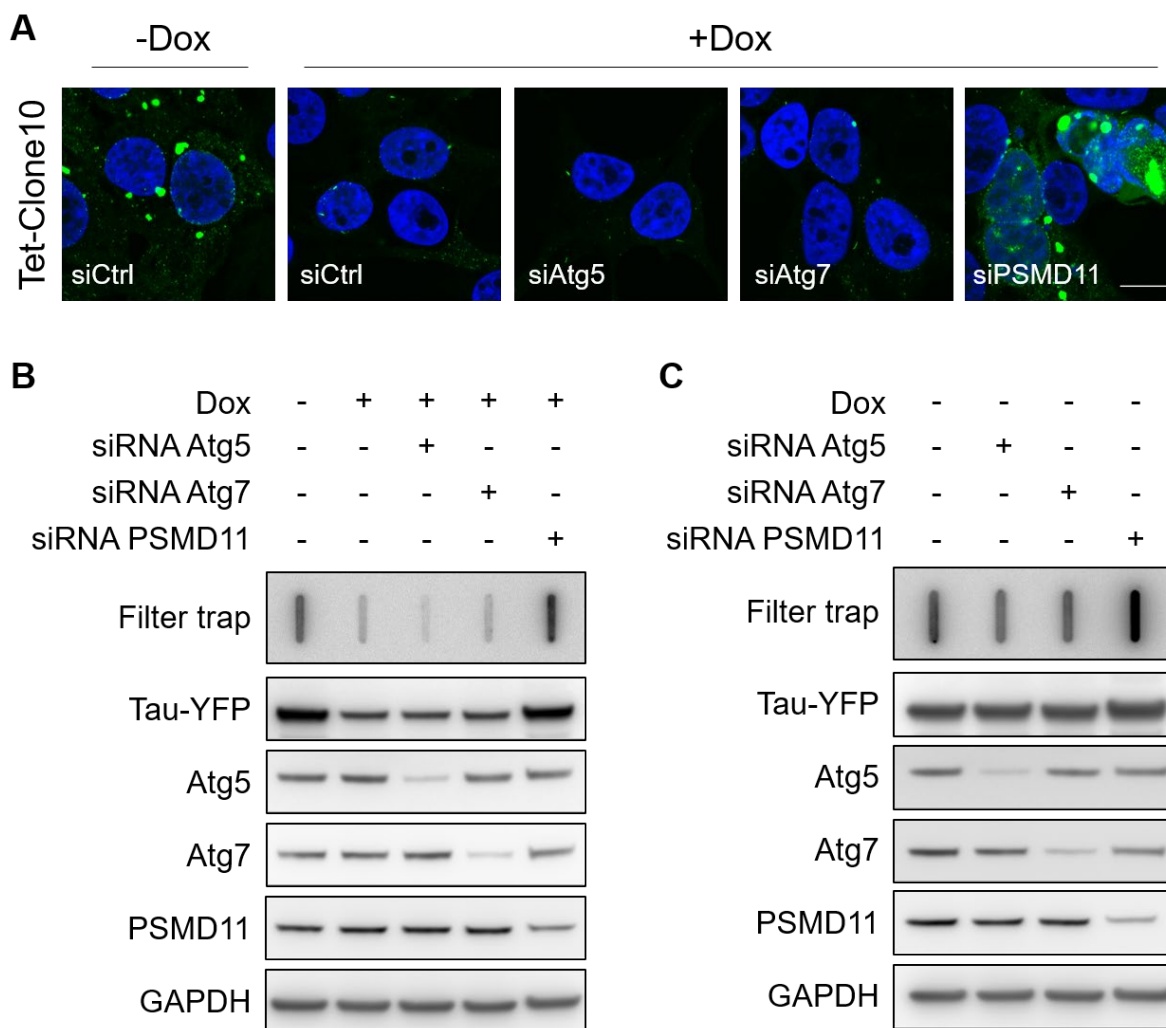


Figure 38. siRNA mediated downregulation of autophagy and proteasomal components

(A) Tet-Clone10 cells were transfected with 50 nM Atg5, Atg7 and 25 nM PSMD11 siRNA. 72 h after transfection, 50 ng/mL doxycycline was added for another 24 h where indicated. Cells were fixed, counterstained with DAPI and imaged. Merged images with tau-YFP (green) and DAPI (blue) are shown. Scale bar: 10 μ m. (B-C) Tet-Clone10 cells were transfected with indicated siRNAs and treated with doxycycline for 24 h (B) or not (C). Cell lysates were subjected to filter trap assay where tau-YFP aggregates were detected by blotting against GFP. Total levels of tau-YFP, Atg5, Atg7 and PSMD11 were analysed by western blotting. GAPDH was used as loading control.

3.6 IDENTIFICATION OF A CELLULAR DISAGGREGASE

In order to identify cellular factors involved in tau-YFP disaggregation, we speculated these factors to be among the specific interactors of tau-YFP aggregates. We further anticipated a stronger enrichment of these factors in the tau-YFP interactome of Clone10 relative to Clone9, since tau-YFP disaggregation was observed only in Clone10. By this rationale, gene ontology (GO) term analysis of candidate proteins showed that VCP and its cofactors were significantly enriched on tau-YFP aggregates in Clone10 (Supplementary Table 6).

VCP was a plausible contender for a disaggregase because, similar to bacterial and yeast disaggregases, it is a AAA+ chaperone that utilizes energy from ATP hydrolysis to structurally remodel and unfold proteins (van den Boom and Meyer, 2018). The VCP cofactors, NPLOC4 and UFD1L, that were enriched on tau-YFP aggregates in Clone10 form a complex with VCP and assist the disassembly of protein complexes on chromatin or extraction of misfolded proteins from ER and mitochondria for proteasomal degradation (Ye et al., 2017). However, it is yet to be established if VCP-mediated unfolding can result in disaggregation of amorphous or amyloidogenic protein aggregates in cells (van den Boom and Meyer, 2018).

3.6.1 VCP interacts with tau-YFP aggregates

To explore the role of VCP as a possible cellular disaggregase, we first biochemically verified the interaction of VCP with tau-YFP. Consistent with the MS results, endogenous VCP co-immunoprecipitated with tau-YFP in Clone10 (~ 3% of input or total cellular VCP) and to a lesser degree in Clone9 (<1%) (Figure 39A). VCP was not detected in the eluates from wild type HEK293 or Clone1 cells indicating the specificity of this interaction with aggregated tau-YFP.

To test if VCP co-localized with tau-YFP aggregates, immunofluorescence staining of endogenous VCP was performed. In HEK293 and Clone1 cells, VCP was diffusely distributed throughout the cell, whereas the protein co-localized with cytosolic tau-YFP inclusions in Clone9 and Clone10 (Figure 39B). Similarly, tau-YFP aggregates in Tet-Clone10 stained positive for VCP, further demonstrating the interaction between VCP and tau-YFP aggregates (Figure 39C). Notably, only a small fraction of the total cellular VCP co-immunoprecipitated with tau-YFP in

Clone10 (Figure 39A). This observation shows that VCP is not removed from other cellular processes by its association with aggregates. This idea is further supported by the fact that these cells do not show any overt toxicity, whereas VCP inhibition with the help of pharmacological inhibitors is toxic (Magnaghi et al., 2013). Therefore, VCP interacts with tau-YFP aggregates and this interaction may be functionally relevant.

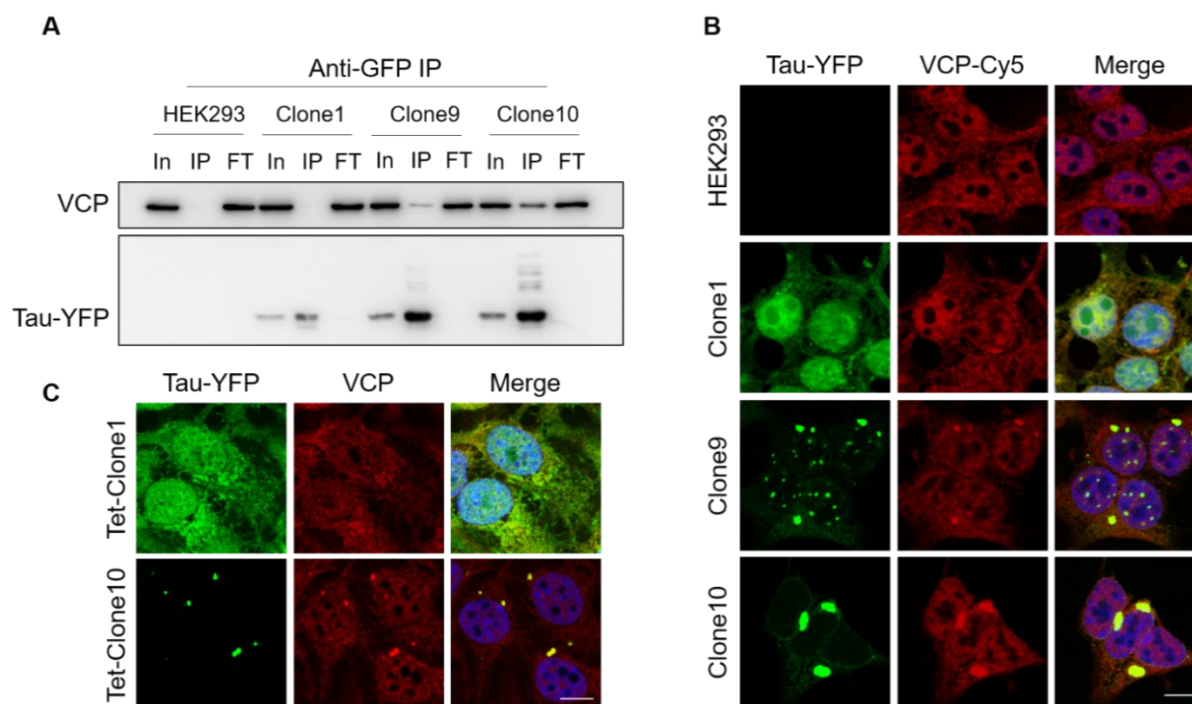


Figure 39. Interaction of tau-YFP aggregates with VCP

(A) Wild type HEK293, Clone1, 9 and 10 cells were subjected to an anti-GFP immunoprecipitation. Input (In), eluate (IP) and flow-through (FT) fractions were analysed by western blotting. Comparable amounts of In and FT were loaded. IP was ~10 times as concentrated as the In and FT. **(B-C)** Endogenous VCP was visualized in the indicated cell lines by staining with an anti-VCP primary antibody and cy5 conjugated secondary antibody. Merge shows tau-YFP (green), VCP (red) and DAPI (blue). Scale bar: 10 μ m.

3.6.2 VCP is required for tau-YFP aggregate clearance

To assess if VCP was involved in tau-YFP aggregate clearance, VCP activity was inhibited using the specific allosteric inhibitor NMS-873 (Magnaghi et al., 2013). Similar to proteasome inhibition, NMS-873 prevented aggregate clearance in Tet-Clone10 cells in the presence of doxycycline (Figure 40A). Filter trap analysis confirmed the stabilization of tau-YFP aggregates and total protein levels by NMS-873 treatment to a level comparable to proteasome inhibition (Figure 40B). To exclude off-target effects of NMS-873, we performed a partial knockdown of

endogenous VCP by siRNA and analysed the cells by microscopy after immuno-staining against VCP. The efficiency of downregulation by the siRNA treatment was ~50%. In cells treated with control siRNA, tau-YFP aggregates were efficiently cleared upon the addition of doxycycline. Downregulation of VCP levels resulted in the accumulation of enlarged aggregates which did not stain positive for VCP and persisted even after doxycycline treatment (Figure 40C).

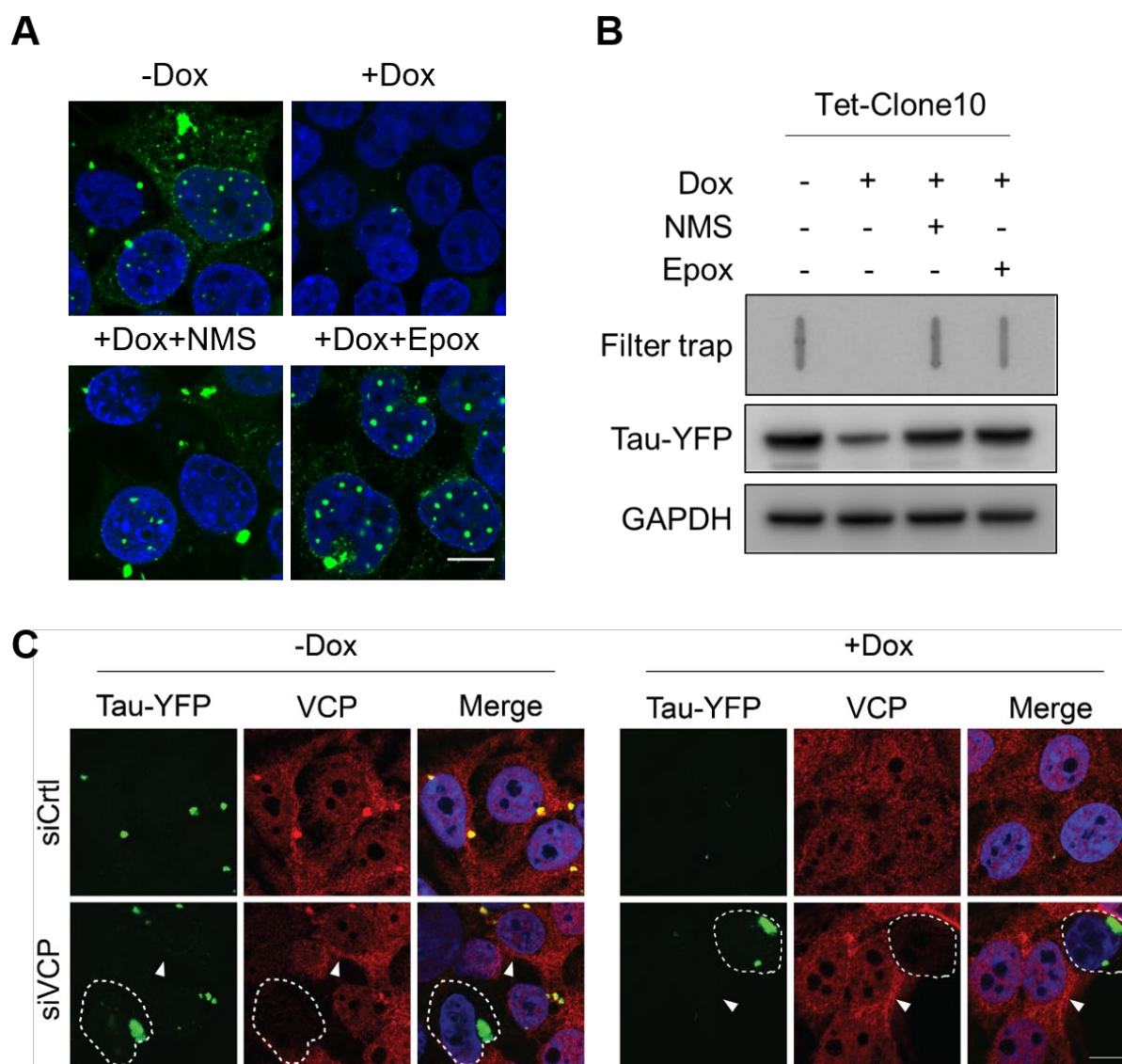


Figure 40. Effect of VCP inactivation on disaggregation in Tet-Clone10

(A) Tet-Clone10 cells were treated with 50 ng/ μ L doxycycline alone or in combination with 2.5 μ M NMS-873 or 50 nM epoxomicin for 24 h. Cells were fixed and counter stained with DAPI. Merged images with tau-YFP (green) and DAPI (blue) are shown. (B) Tet-Clone10 cells were treated as in (A). Cell lysates were subjected to filter trap assay and the membrane was probed with anti-GFP antibody to detect tau-YFP. Total tau-YFP protein was additionally analysed by western blotting. GAPDH was used as loading control. (C) Tet-Clone10 cells were transfected with siRNA against VCP. 72 h after transfection cells were left untreated or treated with 50 ng/ μ L doxycycline for another 24 h. Afterwards cells were fixed and stained with an anti-VCP primary antibody and cy5 conjugated secondary antibody. Merge shows tau-YFP (green), VCP (red) and DAPI (blue). Cells showing reduced VCP levels are encircled in dashed lines. White arrow heads indicate cells with normal levels of VCP. Scale bar: 10 μ m.

Furthermore, we tested whether VCP was also involved in starvation-induced aggregate clearance in Clone10. VCP knockdown resulted in stabilization of tau-YFP aggregates in EBSS and growth of inclusions in full medium (Figure 41A). This enlargement is reminiscent of the increase in size of Sup35 aggregates upon Hsp104 inactivation (Wegrzyn et al., 2001). Strikingly, tau-YFP aggregates in Clone9 which were not disaggregated upon starvation also developed into large tau-YFP agglomerates when VCP was knocked down in full medium and EBSS (Figure 41B). Therefore, in addition to disassembly of fibrillar aggregates, VCP might also participate in the disaggregation and degradation of tau-YFP oligomers that may not be present in the inclusions. In the absence of VCP, these oligomers may be recruited to the inclusions resulting in their enlargement. Taken together, these results demonstrate that VCP is required for the disaggregation and clearance of tau-YFP aggregates in mammalian cells.

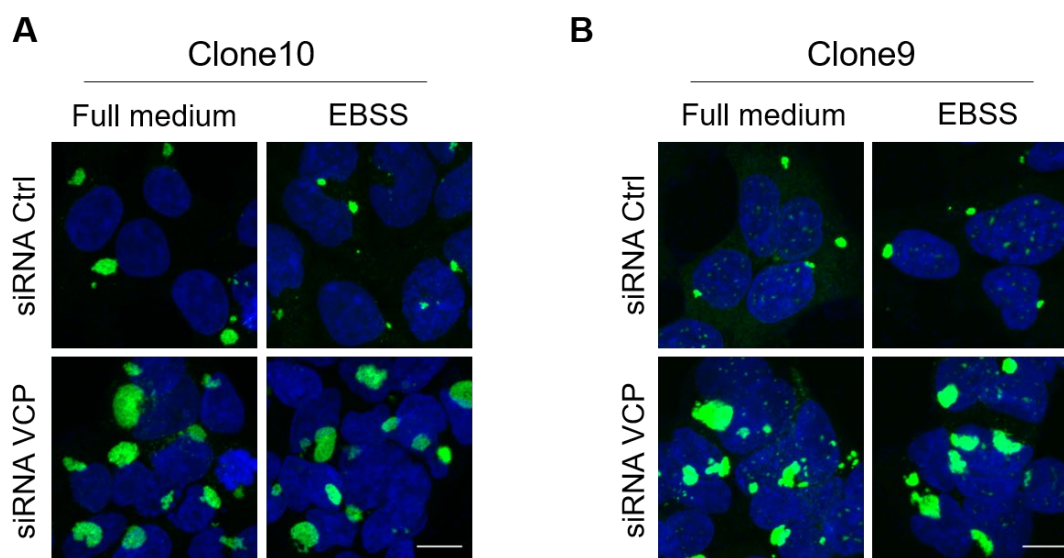


Figure 41. Effect of VCP downregulation on disaggregation in Clone10 & Clone9

(A) Clone10 and **(B)** Clone9 cells were transfected with siRNA against VCP. 72 h after transfection cells were either maintained in full medium or grown in EBSS for a further 24 h. Afterwards cells were fixed and counter stained with DAPI. Representative images with merged tau-YFP (green) and DAPI (blue) channels are shown. Scale bar: 10 μ m.

3.6.3 VCP minimally influences turnover or aggregation of non-aggregated tau-YFP

Next, we tested if VCP was also required for the turnover of non-aggregated tau-YFP. Towards this aim VCP was partially down-regulated in Tet-Clone1 cells that do not feature any detectable tau-YFP aggregates and total tau-YFP levels were compared to that in Tet-Clone10 cells. VCP knockdown in Tet-Clone1 cells caused a marginal but significant increase of steady state tau-YFP levels, but did not cause a significant stabilization after new synthesis of the protein was blocked (Figure 42B). However, Tet-Clone10 cells treated with VCP siRNA accumulated significantly higher amounts of tau-YFP both in the absence or presence of doxycycline (Figure 42A), consistent with the requirement of VCP in clearing aggregated tau-YFP. The altered steady state levels of tau-YFP in Tet-Clone1 could be due to an indirect effect of VCP depletion on cellular health. Overall these observations indicate that VCP did not play a major role in the turnover of non-aggregated tau-YFP.

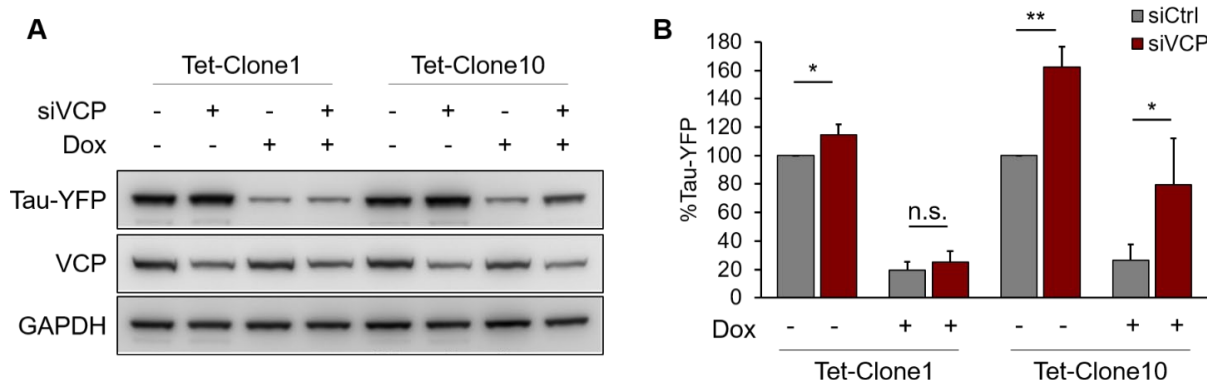


Figure 42. Effect of VCP downregulation on tau-YFP turnover

(A) Tet-Clone1 and Tet-Clone10 cells were transfected with siRNA against VCP where indicated. 72 h after transfection cells were left untreated or treated with 50 ng/ μ L doxycycline for another 24 h. Total cell lysates were analysed for tau-YFP and VCP levels. GAPDH was used as loading control. (B) Quantification of tau-YFP levels normalized to control siRNA –Dox treatment values for respective cell lines. Error bars represent standard deviation from at least 4 independent experiments. P-values were calculated using paired student's t-test. * <0.05 ** <0.01 .

Moreover, VCP downregulation did not result in tau-YFP aggregation in Tet-Clone1 as observed by microscopy (Figure 43A). Similarly, no tau-YFP aggregates could be detected biochemically in Tet-Clone1 cells treated with NMS-873 or epoxomicin (Figure 43B). Thus, VCP or proteasome inhibition *per se* did not cause detectable aggregation in Tet-Clone1 cells arguing against *de novo* aggregation of soluble tau-YFP. This observation further implies that enhanced tau-YFP

aggregation in Clone10 or Tet-Clone10 upon VCP downregulation was due to the accumulation of preformed tau-YFP aggregates, thereby supporting a key role of VCP in aggregate clearance. These results, together with the direct localization of endogenous VCP on tau-YFP aggregates, establish VCP as a disaggregase for tau-YFP aggregates in this cellular model.

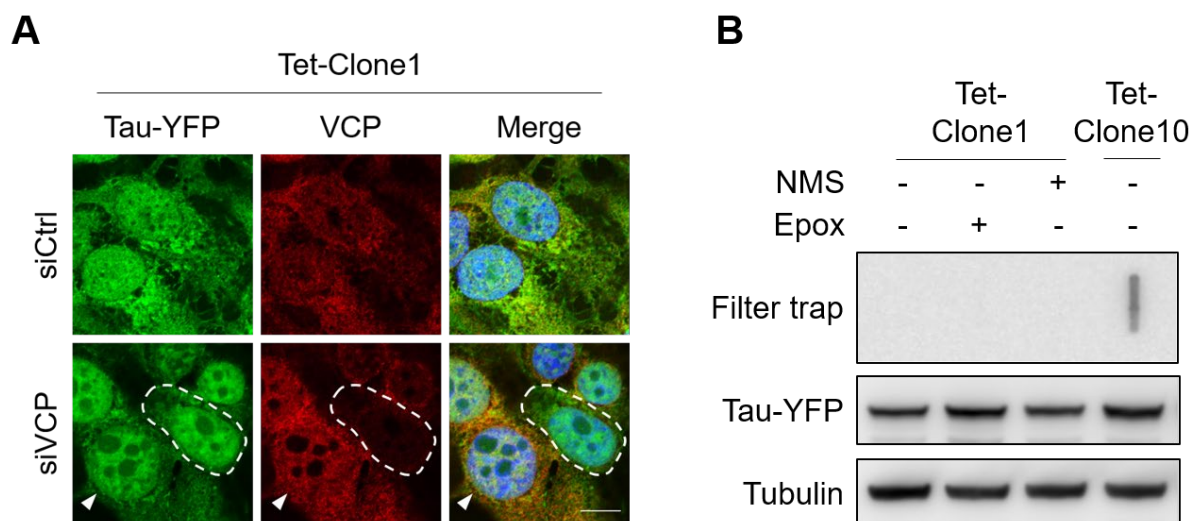


Figure 43. Analysis of aggregation in Tet-Clone1 by proteasome or VCP inhibition

(A) Tet-Clone1 cells were transfected with siRNA against VCP for 96 h. Afterwards cells were fixed and stained with an anti-VCP primary antibody and cy5 conjugated secondary antibody. Merge shows tau-YFP (green), VCP (red) and DAPI (blue). A cell showing reduced VCP levels is encircled in dashed lines. White arrow head indicates a cell with normal levels of VCP. Scale bar: 10 μ m. **(B)** Tet-Clone1 cells were treated with 50 nM epoxomicin or 2.5 μ M NMS-873 for 24 h where indicated. Cell lysates were subjected to filter trap and analysis of total tau-YFP by western blotting. Tet-Clone10 was used as control for filter trap.

3.7 ROLE OF UBIQUITINATION IN VCP DEPENDENT TAU-YFP DISAGGREGATION

Ubiquitination is crucial for both recruiting VCP and targeting substrates for proteasomal degradation (Blythe et al., 2017; van den Boom and Meyer, 2018). Although VCP has been long known to associate with ubiquitinated substrates, recently the involvement of VCP in a ubiquitin-independent segregation process was reported (Weith et al., 2018). Therefore, we examined if VCP mediated disaggregation required the ubiquitination of its substrate.

3.7.1 Ubiquitination status of tau-YFP

We assessed if tau-YFP in our cell lines was modified with ubiquitin. Immunofluorescence staining of Clone9 and Clone10 with an antibody specific for poly-ubiquitin revealed co-localization of ubiquitin-chains with tau-YFP aggregates (Figure 44A). The ubiquitin enrichment observed on tau-YFP aggregates can either result from the direct ubiquitin modification of tau-YFP or from the sequestration of other ubiquitin modified proteins in the inclusions. To distinguish between these possibilities, ubiquitinated proteins were isolated from cell lysates under denaturing conditions. To do this, cells transiently transfected with a 6x His-tagged Ubiquitin (His₆-Ub) construct were lysed in 6 M GuHCl and ubiquitinated proteins were pulled-down using Ni-NTA beads, followed by detection of tau-YFP by immuno-blotting. High molecular weight tau-YFP was detected in the eluates of Clone1, 9 and 10 transfected with His₆-Ub indicating covalent modification of tau-YFP with ubiquitin (Figure 44B). Unmodified tau-YFP was also detected in the eluates under all conditions which might be due to non-specific binding to Ni-NTA beads. The pattern and amount of ubiquitinated tau-YFP in the three cell lines showed both similarities and differences. Clone1 predominantly showed ubiquitin smear at the top of the blot, which is consistent with the formation of long polyubiquitin chains (LC Ub_n). Proteasome inhibition increased this signal in all three cell lines which supports tau-YFP ubiquitination and degradation by the 26S proteasome in this model. Clone9 and Clone10 additionally showed tau-YFP modified with shorter ubiquitin chains (SC Ub_n) (Figure 44B), indicating a specific ubiquitination pattern of aggregated tau-YFP. Clone10 in general showed higher levels of ubiquitinated tau-YFP compared to Clone9 which could be connected to the more efficient tau-YFP disaggregation and turnover in Clone10 as shown before (Figure 31). Furthermore, by

analysing the ubiquitin remnant K- ϵ -GG motifs in the MS data obtained during the interactome experiment, we identified a peptide from tau close to the C-terminus of the RD fragment, [IGSLDNITHVPGGGNKK], which confirmed that the tau moiety in the tau-YFP fusion protein was modified with ubiquitin. Taken together these experiments demonstrated that both soluble and aggregated tau-YFP was ubiquitinated in these cell lines.

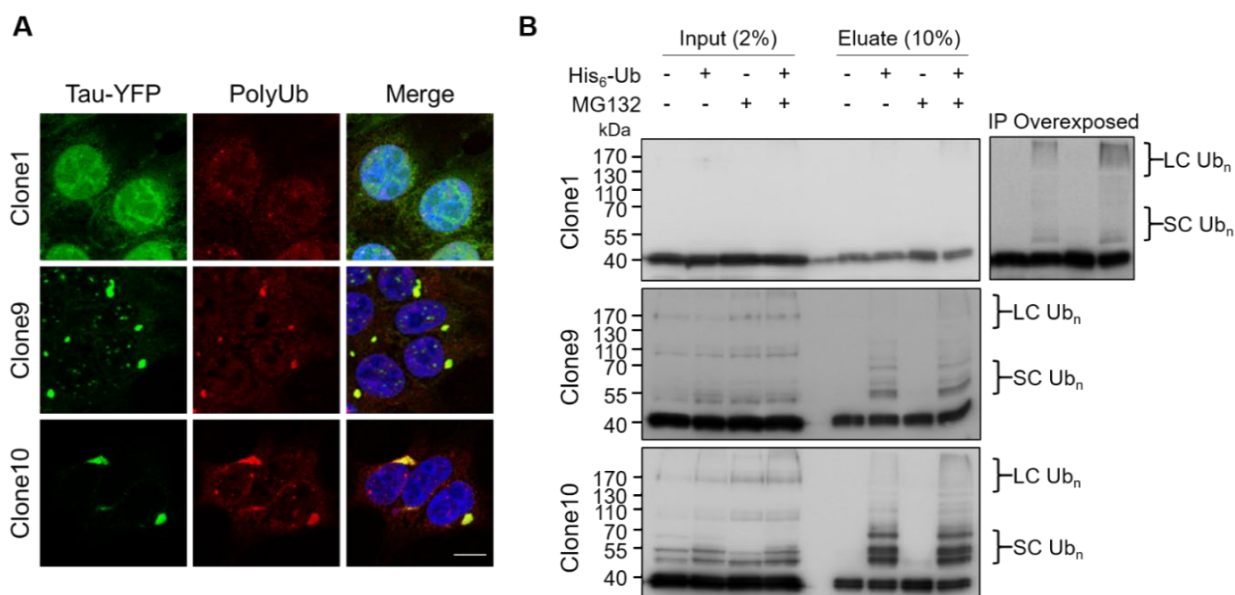


Figure 44. Ubiquitination of soluble and aggregated tau-YFP

(A) Clone1, 9 and 10 cells at steady state were stained with an antibody that recognizes polyubiquitin (clone FK2) followed by cy5 conjugated secondary antibody. Merge shows tau-YFP (green), polyUb (red) and DAPI (blue). Scale bar: 10 μ m. **(B)** Clone1, 9 and 10 cells were transfected with empty vector or His₆-Ub construct for 24 h. 5 μ M MG132 was added for another 24 h where indicated. Afterwards cell lysates were prepared in 6 M GuHCl and subjected to Ni-NTA pull-down. Input and eluates were resolved on 10% tris-glycine gels before western blotting. Blots were probed with an antibody against GFP to detect tau-YFP. Unmodified tau-YFP runs around 40 kDa. Long/short chain ubiquitination (LC/SC Ub_n) is indicated.

3.7.2 K48 ubiquitin chains on tau-YFP aggregates and clearance by VCP

Next, we analysed the nature of polyubiquitin chain linkage on tau-YFP aggregates since distinct chain linkages have different functions in determining protein fate. Tau-YFP aggregates were tested for the presence of specific ubiquitin chain types, K48 and K63, by using linkage specific antibodies. While tau-YFP aggregates in Clone9 and Clone10 stained positive for UbK48 chains, no co-localization was observed with UbK63 (Figure 45A-B).

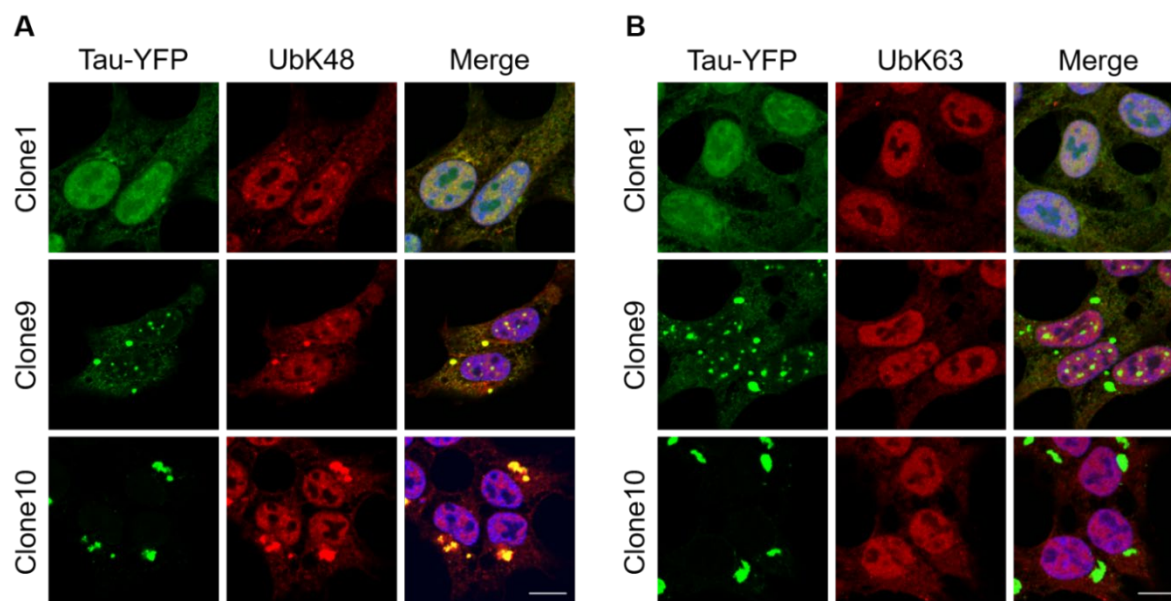


Figure 45. Analysis of ubiquitin chain linkage

Clone1, 9 and 10 cells at steady state were stained with an antibody that recognizes **(A)** K48 or **(B)** K63 ubiquitin chains followed by cy5 conjugated secondary antibody. Merge shows tau-YFP (green), Ub (red) and DAPI (blue). Scale bar: 10 μ m.

UbK48 modification of tau-YFP was biochemically confirmed by directly immunoprecipitating tau-YFP with anti-GFP beads under stringent non-denaturing buffer conditions to minimize co-purification of interacting proteins. The eluates were then resolved on a gradient SDS-PAGE gel prior to western blotting to obtain good separation of ubiquitinated bands. Upon probing against GFP, well resolved SC Ub_n tau-YFP bands were observed in Clone10 with molecular weights suggesting modification of tau-YFP with one to four ubiquitin molecules (Figure 46). The eluates when blotted on a different membrane and probed for UbK48 linkage showed the same tau-YFP bands with ≥ 2 ubiquitin moieties (Figure 46). This observation validated that our K48 antibody indeed recognizes ubiquitin linkages since it did not detect unmodified or monoubiquitinated tau-YFP. UbK48 chains were not detectable in Clone1 in this experiment possibly due to their low abundance and fast clearance. The presence of UbK48 linkages in Clone10 was consistent with tau-YFP aggregates being substrates of VCP and the proteasome.

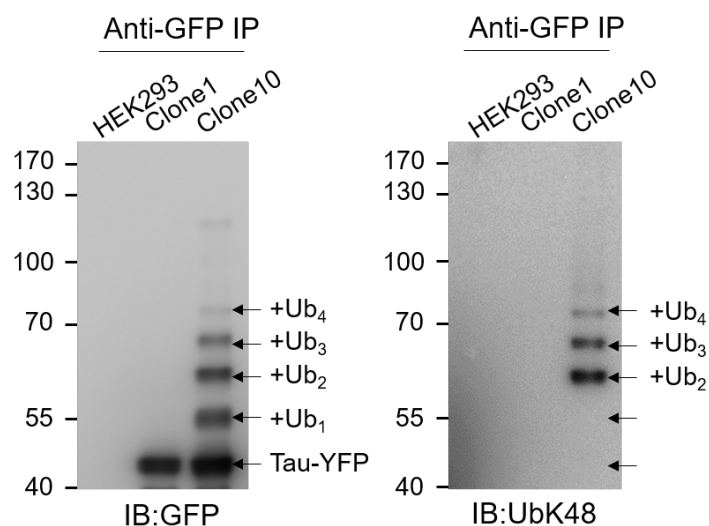


Figure 46. Biochemical analysis of ubiquitin K48 modified tau-YFP

Wild type HEK293, Clone1 and Clone10 cells were lysed in 0.1% SDS containing buffer and subjected to anti-GFP immunoprecipitation. Eluates were resolved on a commercial gradient gel prior to western blotting to obtain good separation of ubiquitinated bands. Two separate membranes were probed with antibodies against GFP and UbK48 chains.

Next, we tested if UbK48 modified tau-YFP was cleared by VCP. Towards this end, VCP was knocked-down by siRNA and accumulation of ubiquitinated tau-YFP was analysed in the total, soluble and insoluble fractions by immuno-blotting. After VCP down-regulation, the total levels of ubiquitinated tau-YFP increased in Tet-Clone10 while tau-YFP in Tet-Clone1 remained unchanged (Figure 47A). This ubiquitinated tau-YFP was almost entirely detergent-insoluble and suggested the accumulation of ubiquitin-positive tau-YFP aggregates in the absence of VCP. Furthermore, we immuno-stained endogenous UbK48 conjugates in Clone10 and Clone1 cells treated with a VCP siRNA and analysed them by microscopy. Cells with reduced VCP levels showed a strong increase in the UbK48 signal in both cell lines indicating the clearance of UbK48 modified substrates by VCP (Figure 47B). Furthermore, Clone10 cells contained enlarged UbK48 positive tau-YFP aggregates whereas tau-YFP appearance in Clone1 remained indistinguishable in cells with VCP knockdown compared to neighbouring cells with normal levels. Collectively, these results demonstrate that VCP is necessary for the clearance of UbK48 modified tau-YFP aggregates.

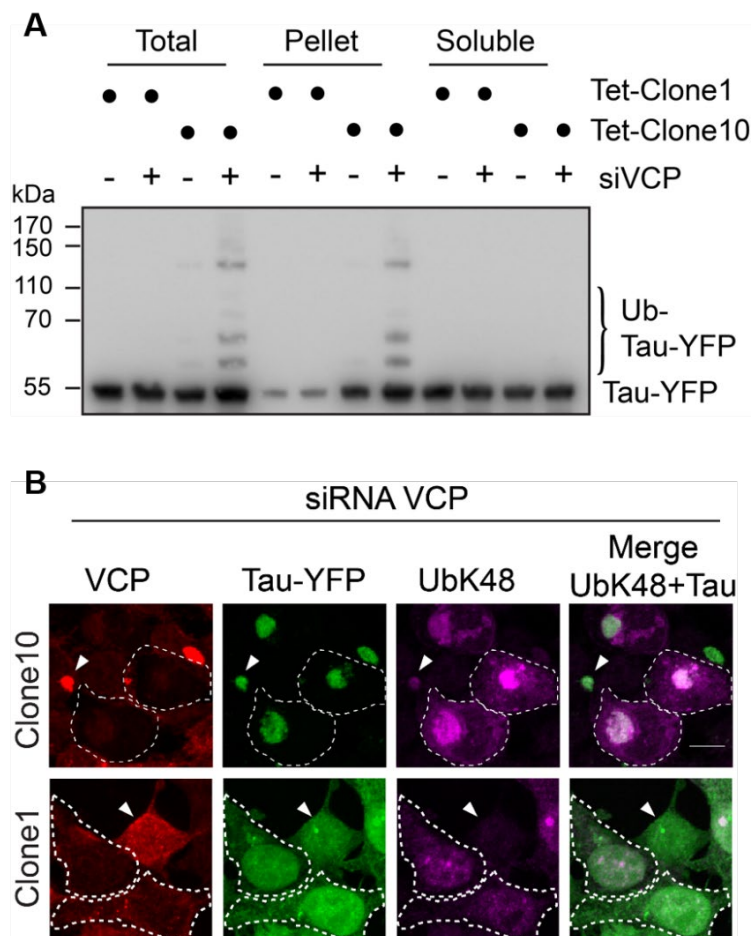


Figure 47. VCP mediated clearance of ubiquitinated tau-YFP aggregates

(A) Tet-Clone1 and Tet-Clone10 cells were transfected with control siRNA or siRNA against VCP for 96 h. Crude cell lysates were centrifuged at 186,000xg for 1 h. Total, pellet and soluble fractions were analysed by western blotting against GFP. **(B)** Clone1 and Clone10 cells were transfected with siRNA against VCP for 96 h. Afterwards cells were fixed and immuno-labelled for endogenous VCP and ubiquitin K48 linkages. Cy3 and cy5 conjugated secondary antibodies were used to detect VCP and UbK48 respectively. VCP is shown in red. Merge shows tau-YFP in green and UbK48 in magenta. Cells showing reduced VCP levels are encircled in dashed lines. White arrow heads indicate cells with normal levels of VCP. Scale bar: 10 μ m.

3.7.3 Ubiquitin dependent recruitment of VCP to tau-YFP aggregates

We tested if ubiquitination was necessary to recruit VCP to tau-YFP aggregates. To block the ubiquitin conjugation cascade in cells, the major cellular ubiquitin activating enzyme UAE1 was inhibited with the chemical inhibitor MLN7243. Biochemical analysis of cell lysates from MLN7243 treated cells, alone or in combination with the proteasome inhibitor MG132, revealed a dramatic reduction of ubiquitinated proteins, thereby confirming the inhibition of UAE1 and cellular ubiquitin conjugation (Figure 48).

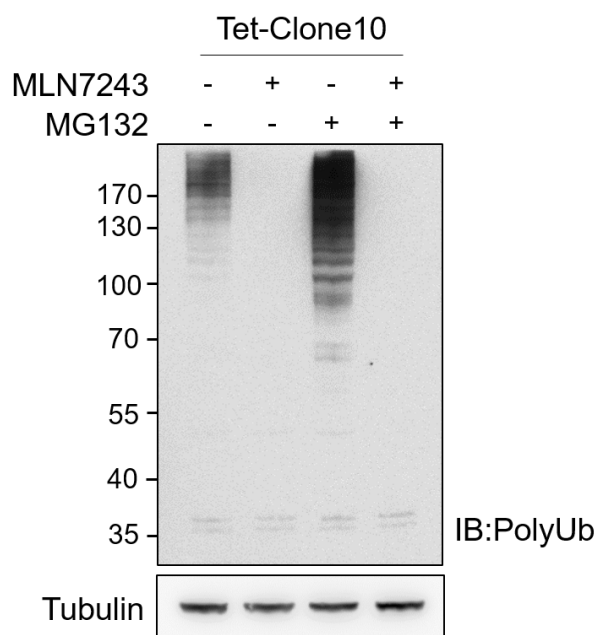


Figure 48. Effect of E1 inhibition on ubiquitinated proteins in cells

Tet-Clone10 cells were treated with 1 μ M MLN7243 or MG132 for 15 h. Cells were lysed in a buffer containing 5 mM N-ethylmaleimide to minimize deubiquitination activity and blotted against polyubiquitin. Tubulin was used as loading control.

Next, we analysed the ubiquitination status of tau-YFP aggregates in MLN7243 treated cells. After 6-12 h of treatment, tau-YFP aggregates in both Clone10 and Tet-Clone10 cells lost their UbK48 reactivity (Figure 49A-B), suggesting that tau-YFP aggregates may be constantly acted upon by deubiquitinating enzymes (DUBs) and the deubiquitinated state persists in the absence of E1 activity. In addition, these results imply that ubiquitination was not required for either the formation or the integrity of tau-YFP aggregates. Interestingly, the aggregates in MLN7243 treated cells also did not stain positive for VCP (Figure 49C-D), indicating that ubiquitin-chains recruit VCP to the inclusions. This observation also suggests that VCP was not merely sequestered in the aggregates but actively recruited. This is in contrast to what was seen for another ubiquitin binding protein, p62, which still co-localized to the ubiquitin negative aggregates (Supplementary Figure S2)

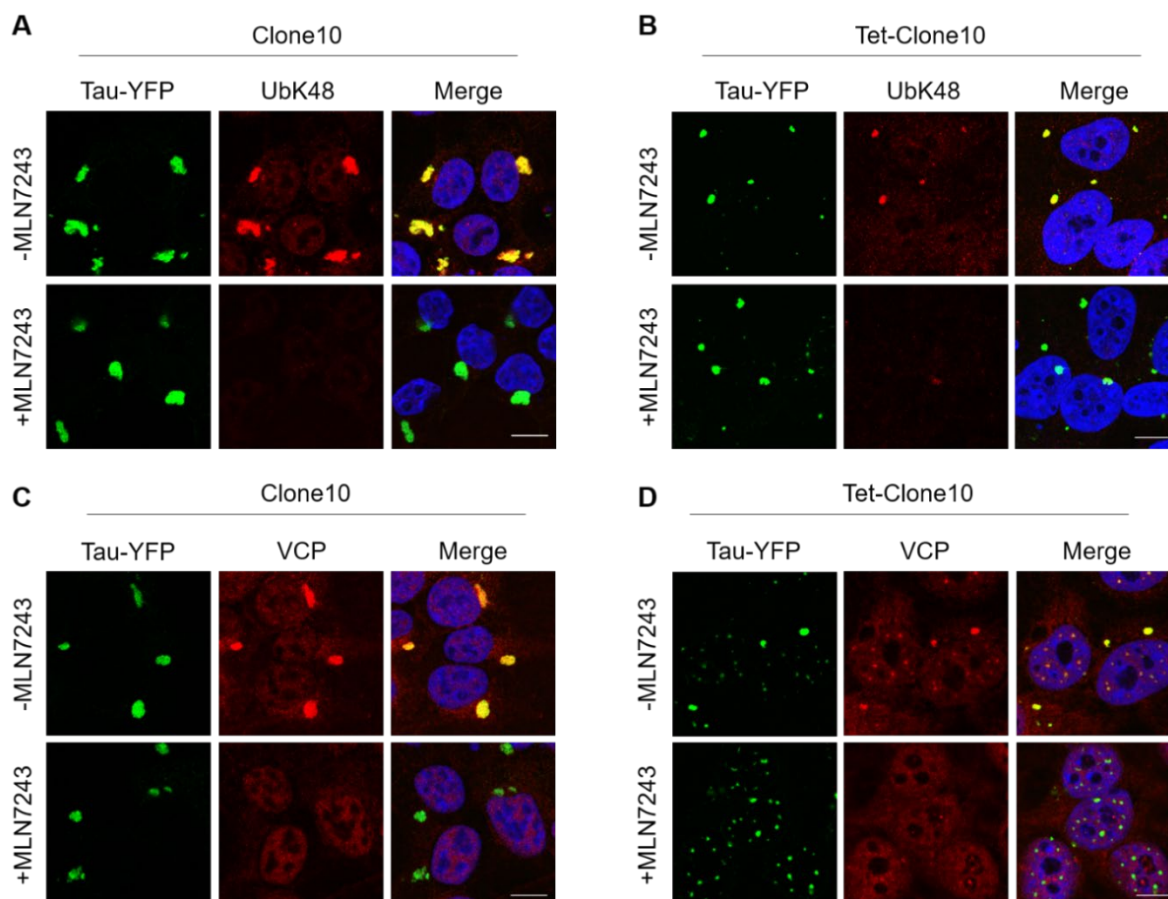


Figure 49. Ubiquitin dependent recruitment of VCP on tau-YFP aggregates

Clone10 and Tet-Clone10 cells were treated with 0.5 μM of the E1 inhibitor MLN7243 for 12 h and afterwards stained with antibodies against **(A-B)** K48 linked ubiquitin chains or **(C-D)** VCP. Cy5 conjugated secondary antibody was used for detection. Merged images show tau-YFP (green), UbK48/VCP (red) and DAPI (blue). Scale bar: 10 μm.

Since deubiquitinated tau-YFP aggregates did not recruit VCP, we reasoned that disaggregation might also be inhibited under such conditions. Indeed, MLN7243 treatment prevented disaggregation in Tet-Clone10 cells and stabilized tau-YFP levels (Figure 50A-B). Tau-YFP in Clone1 was also stabilized by MLN7243 treatment, to a degree comparable with proteasome inhibition (Figure 50B), therefore the inhibition of disaggregation under this treatment could result from both loss of VCP on the aggregates as well as stabilisation of soluble tau-YFP. Thus, it can be concluded that ubiquitination is either directly or indirectly essential for VCP recruitment and disaggregation of tau-YFP aggregates.

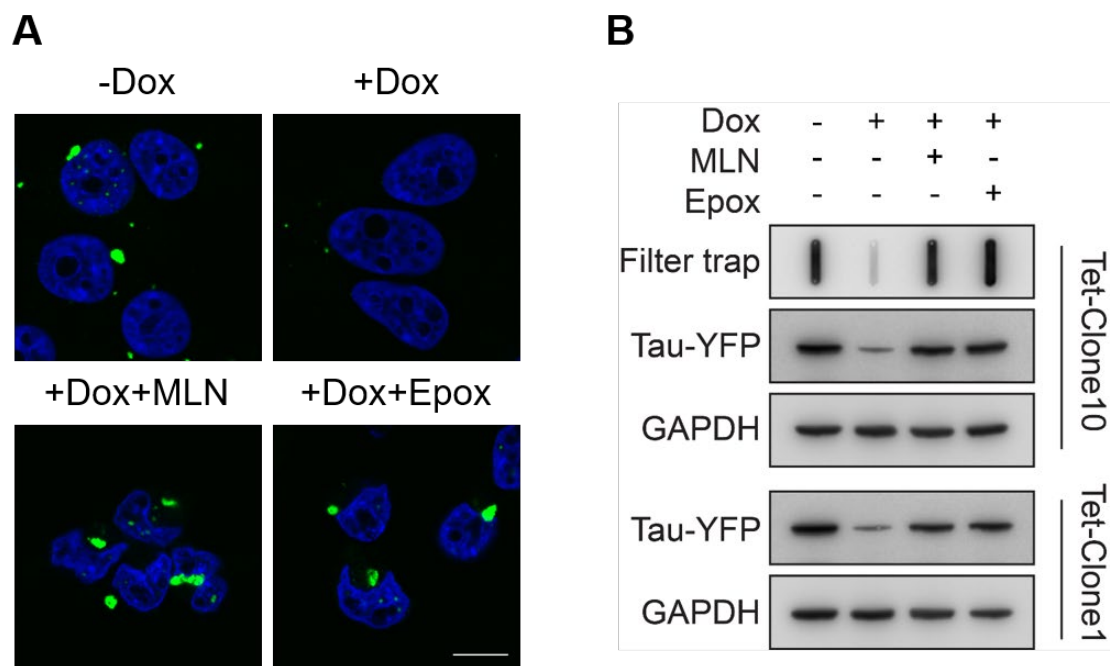


Figure 50. Ubiquitin dependent tau-YFP aggregate clearance

(A) Tet-Clone10 cells were treated with 50 ng/ μ L doxycycline alone or in combination with 0.5 μ M MLN7243 or 50 nM epoxomicin for 24 h. Cells were fixed and counter stained with DAPI. Merged images with tau-YFP (green) and DAPI (blue) are shown. Scale bar: 10 μ m. **(B)** Indicated cell lines were treated with 50 ng/ μ L doxycycline alone or in combination with 0.2 μ M MLN7243 or 50 nM epoxomicin for 24 h. Cell lysates were subjected to filter trap assay and the membrane was probed with anti-GFP antibody to detect tau-YFP. Total tau-YFP levels were analysed by western blotting. GAPDH was used as loading control.

3.8 CO-OPERATION OF HSP70 AND VCP IN PROTEIN DISAGGREGATION

Since higher eukaryotes do not possess homologs of ClpB/Hsp104 disaggregases, studies in recent years have highlighted the role of the metazoan Hsp70 system (Hsc70, Hsp40 and Hsp110) in protein disaggregation. The Hsp70 system can disaggregate amorphous firefly luciferase (Fluc) and more structured α -synuclein aggregates *in vitro* (Gao et al., 2015; Nillegoda et al., 2015). Disaggregation of Fluc aggregates generated in *C.elegans* by heat stress was also shown to require Hsc70, Hsp110 and different classes of DNAJ family of proteins (Kirstein et al., 2017; Rampelt et al., 2012). We therefore tested if the Hsp70 system acts in liaison with VCP to disaggregate the amyloid-like tau-YFP aggregates in our system.

3.8.1 Hsp70 in tau-YFP clearance

In order to investigate the involvement of the Hsp70 system in tau-YFP disaggregation, we first analysed the association of Hsp70, Hsp40 (DNAJB1) and Hsp110 (HSPH2), components of the previously described disaggregase machinery, with tau-YFP aggregates. While Hsp70 partially co-localized with tau-YFP aggregates in Clone10, we did not detect an enrichment of DNAJB1 and HSPH2 in tau-YFP inclusions (Figure 51A). Consistently, these proteins did not qualify as significant interactors of tau-YFP aggregates in the MS interactome analysis (Supplementary Table 3). Additionally, down-regulation of DNAJB1 with siRNA did not prevent tau-YFP disaggregation in Tet-Clone10, where under similar conditions VCP down-regulation abrogated aggregate clearance (Figure 51B). This result suggests that DNAJB1 is not necessary for the disaggregating of tau-YFP aggregates observed in this model. Due to the abundance of Hsp70 in HEK293 cells, it was not possible to sufficiently down-regulate Hsp70 protein levels by a siRNA approach. Instead, we used a small molecule, VER-155008, which acts as an ATP competitive inhibitor of the ATPase and chaperone activity of Hsp70.

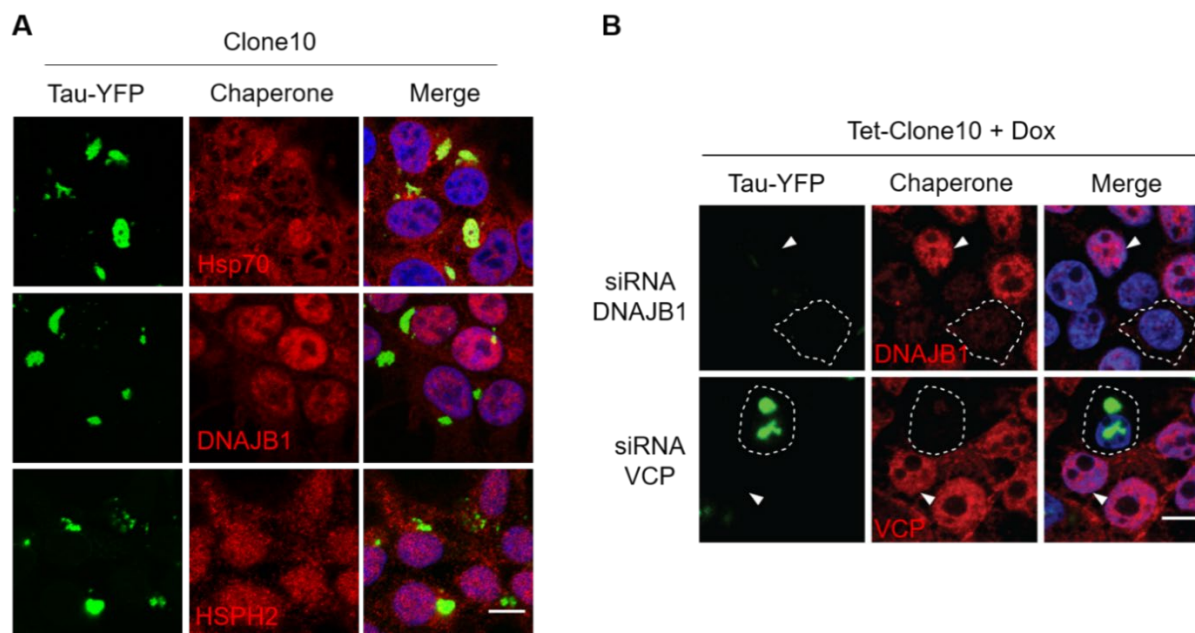


Figure 51. Hsp70 system in tau-YFP disaggregation

(A) Clone10 cells at steady state were stained with antibodies against the chaperones Hsp/Hsc70, DNAJB1 and HSPH2. Merged images show tau-YFP (green), chaperone (red) and DAPI (blue). **(B)** Tet-Clone10 cells were transfected with siRNA against DNAJB1 and VCP for 48 h and treated with doxycycline for additional 24 h. Afterwards cells were fixed and immuno-labelled for endogenous DNAJB1 and VCP. Merge shows tau-YFP (green), chaperone (red) and DAPI (blue). Cells showing reduced VCP/DNAJB1 levels are encircled in dashed lines. White arrow heads indicate cells with normal VCP/DNAJB1 levels. Scale bar: 10 μ m.

Tet-Clone10 cells were treated with VER-155008, and NMS-873 as a control, in parallel with doxycycline. Afterwards we analysed the aggregation status of tau-YFP by filter trap assay. As was observed for VCP inhibition, Hsp70 inhibition also impaired tau-YFP aggregate clearance (Figure 52A). This impairment was not due to de novo aggregation or stabilization of soluble tau-YFP, as Hsp70 inhibition in Tet-Clone1 did not show these effects (Figure 52B). Therefore, Hsp70 activity was also involved in the tau-YFP aggregate clearance. Noticeably, Hsp70 inhibited cells displayed additional smaller tau-YFP foci (<1.5 μ m) in the cytosol which were not observed with VCP inhibition (Figure 52C). However, compared to cells with VCP inhibition, the number of big inclusions (>1.5 μ m) were significantly reduced upon Hsp70 inhibition. Therefore, it appeared that the amyloid-like tau-YFP inclusions were still disaggregated, albeit less efficiently, in the absence of functional Hsp70 and re-aggregated into different structures.

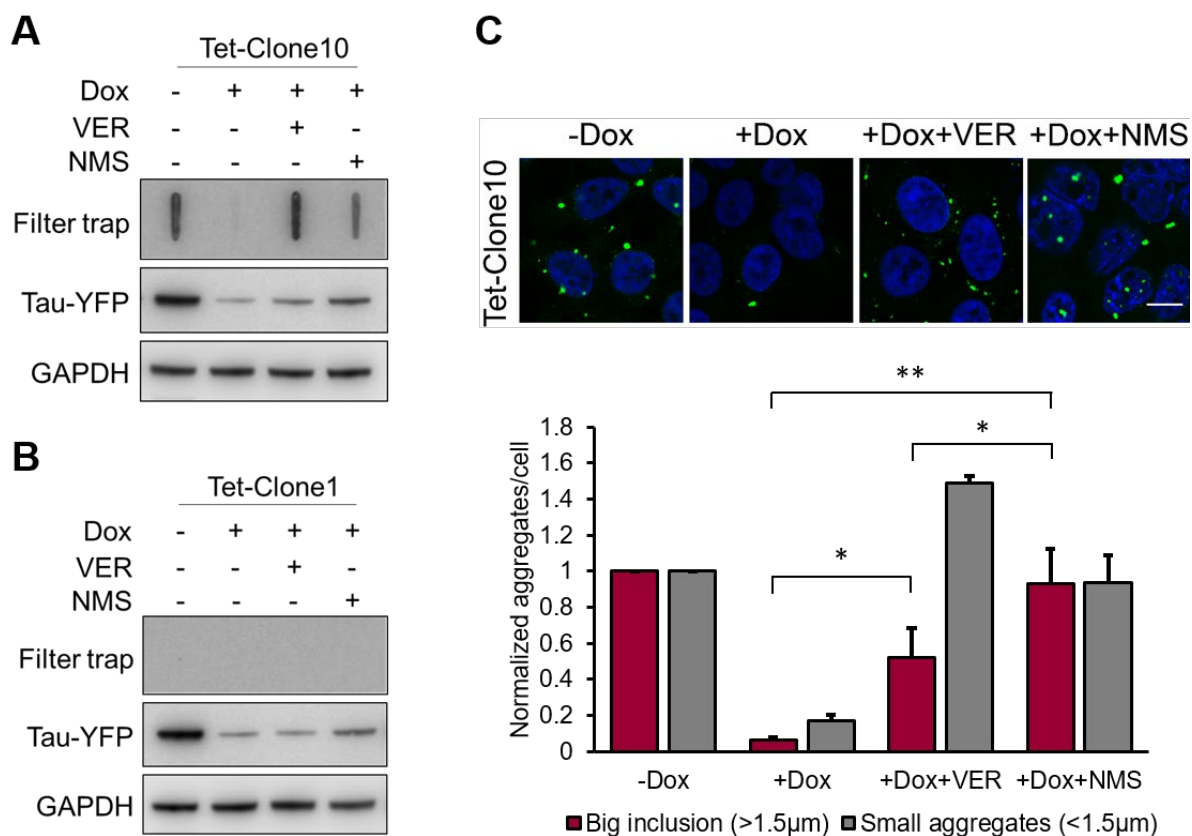


Figure 52. Involvement of Hsp70 in tau-YFP aggregate clearance

(A-B) Tet-Clone10 and Tet-Clone1 cells were treated with 50 ng/μL doxycycline alone or in combination with 10 μM VER-155008 or 2.5 μM NMS-873 for 24 h. Cell lysates were subjected to filter trap assay and the membrane was probed with anti-GFP antibody to detect tau-YFP. Total tau-YFP protein was analysed by western blotting. GAPDH was used as loading control. (C) Tet-Clone10 cells were treated as in (A). Cells were fixed and counter stained with DAPI. Merged images with tau-YFP (green) and DAPI (blue) are shown. Scale bar: 10 μm. Lower panel: Quantification of big (>1.5 μm) and small tau-YFP aggregates (<1.5 μm) in Tet-Clone10 cells. Aggregates/cell in the two size categories were normalized to their respective amounts in untreated cells. ~100-200 cells were analysed per condition/repeat. Error bars represent standard deviations from three independent experiments. P-values were calculated using student's paired t-test. *<0.05. **<0.01.

To understand the origin of the additional aggregates formed after Hsp70 inhibition, we speculated that newly formed tau-YFP monomers or oligomers *en route* to becoming amyloid fibrils might aggregate in the absence of functional Hsp70. Although the previous experiments with Hsp70 inhibition were performed in presence of doxycycline, quantification of tau-YFP mRNA showed that ~30% of the mRNA was still present 3 h post-treatment, which could contribute to new tau-YFP synthesis (Figure 36A). In order to minimize effects from the existing mRNA and to reach the basal mRNA levels, we added the inhibitors after 8 h of pre-treatment with doxycycline. Compared to untreated control, 8 h treatment with doxycycline did not alter the amount of aggregated tau-YFP but slightly reduced total tau-YFP levels probably due to the

degradation of soluble tau-YFP in this period (Figure 53A). Addition of Hsp70 and VCP inhibitors after the pre-treatment also prevented the clearance of tau aggregates (Figure 53A). This observation suggested that the additional small tau-YFP foci formed after Hsp70 inhibition originated from existing tau-YFP in the cells. Moreover, these small tau-YFP foci rarely co-localized with VCP, although the bigger and possibly pre-existing inclusions were still positive for VCP (Figure 53B). From these observations, it is plausible to speculate that Hsp70 stabilized a form of tau-YFP extracted from the large inclusions by VCP. Interestingly, these foci retained K48 ubiquitination (Figure 53C) indicating that disaggregation did not directly lead to deubiquitination and this ubiquitination might still serve as a signal for the delivery of this protein to the proteasome (Bodnar and Rapoport, 2017). Taken together, these results indicate that VCP is the primary disaggregase for amyloid-like tau-YFP aggregates in the cellular context, and is assisted by Hsp70 which either stabilizes the extracted tau-YFP species to prevent its rebinding to the inclusion or chaperones the extracted material to the proteasome for degradation. Alternatively, Hsp70 could handle an entirely different oligomeric species that exists in equilibrium with the amyloid-like aggregate and influences its dynamics.

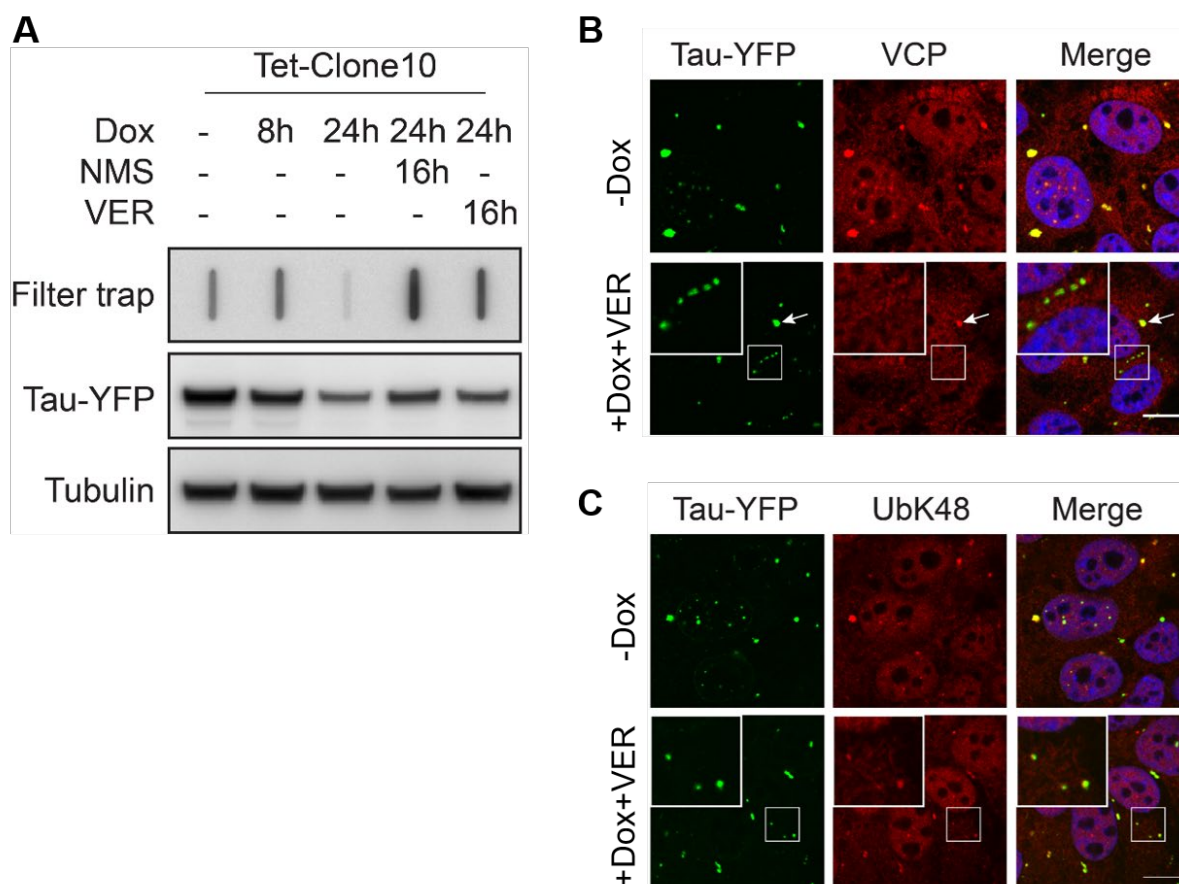


Figure 53. Nature of tau-YFP aggregates stabilized by Hsp70 inhibition

(A) Tet-Clone10 cells were pre-treated with 50 ng/mL doxycycline for 8 h and then additionally with 2.5 μ M NMS-873 or 10 μ M VER-155008 for the remaining 16 h. Cell lysates were subjected to filter trap assay and the membrane was probed with anti-GFP antibody to detect tau-YFP. Total tau-YFP protein was additionally analysed by western blotting. Tubulin was used as loading control. **(B)** Tet-Clone10 cells were left untreated or treated with doxycycline and VER-155008 together for 24 h. Tau-YFP aggregates were analysed for co-localization with VCP by immunostaining. White arrow points to an aggregate co-localizing with VCP. Zoomed inset shows small tau-YFP aggregates that do not co-localize with VCP. **(C)** Tet-Clone10 cells were treated as in (B) and stained for UbK48 linkages. Zoomed inset shows small tau-YFP aggregates positive for UbK48. Scale bar: 10 μ m.

3.8.2 Disaggregation of firefly luciferase aggregates

Next, we aimed to understand if VCP was a general disaggregase or if it was specific for tau-YFP aggregates. To address this question, we analysed the participation of VCP in the clearance of firefly luciferase (Fluc) aggregates in a stable HEK293 cell line expressing GFP tagged wild-type Fluc. Fluc-GFP was soluble in cells grown at 37°C. In order to induce Fluc-GFP aggregation, cells were exposed to heat stress at 43°C combined with MG132 treatment for 2 h. Unlike tau-YFP aggregates in Clone10, Fluc-GFP foci were not stained by AmyloGlo indicating that they were amorphous aggregates (Figure 54A). After 2 h, MG132 was washed

out and the cells were moved to 37°C for recovery. A recovery period of 8 h allowed complete resolution of Fluc-GFP foci, also in the presence of NMS-873 (Figure 54B). Consistent with previous reports, Hsp70 inhibition prevented Fluc-GFP aggregate dissolution (Figure 54B). These results indicate that amorphous Fluc-GFP aggregates in cells are disaggregated in an Hsp70 dependent manner, and VCP is not required for this process. This finding suggests that VCP is involved in the disaggregation of specific proteins, including tau-YFP.

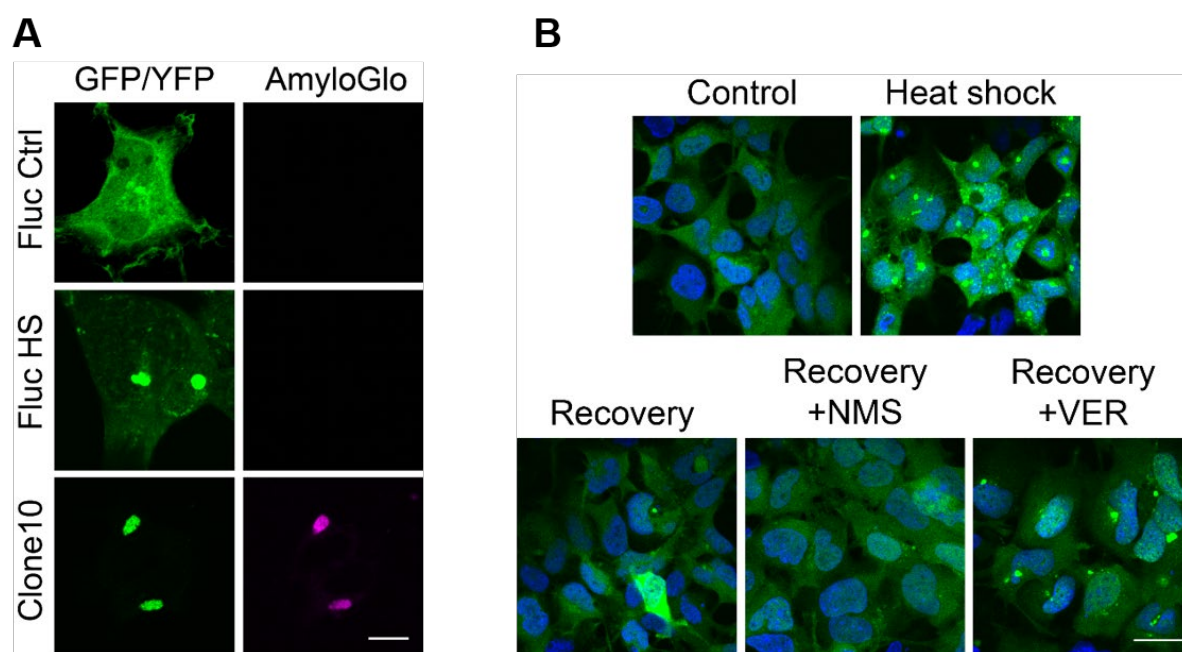


Figure 54. Effect of VCP inhibition on the disaggregation of amorphous Fluc aggregates

(A) Fluc-GFP cells were maintained at 37°C (Ctrl) or heat shocked at 43°C in presence of MG132 (HS) and fixed immediately after. Clone10 was fixed at steady state. Cells were then stained with the amyloid binding dye AmyloGlo (magenta). Scale bar: 10 μ m. **(B)** Fluc-GFP aggregation was induced as in (A). Cells were allowed to recover for 8 h without or with NMS-873 or VER-155008. Scale bar: 30 μ m.

3.9 VCP ACTIVITY AND TAU-YFP SEEDING

Tau-YFP aggregation in our model cell lines has been described as propagating in a prion-like manner (Sanders et al., 2014). Propagation of yeast prions requires the action of the disaggregase, Hsp104, which generates seeds for the spreading process (Shorter and Lindquist, 2004). However, a comparable mechanism in higher eukaryotes has not been described. We speculated that if tau-YFP aggregates were substrates of an unfoldase like VCP, then similar to Hsp104, VCP function should also contribute to seed formation and propagation of tau-YFP. In our model we were not able to directly access the role of VCP in cell-to-cell spreading, in a manner comparable to the experiments performed in yeast, because VCP itself is required for cell cycle progression (Mellman, 1995). Instead, we obtained lysates from cells where VCP activity was inhibited and tested the seeding competence in a FRET-based reporter cell line that allows quantitative measurement of seeding activity in the lysates. Our reporter cell line stably expresses the Tau-RD (LM) as YFP and mTurquoise2 (CFP) fusions in HEK293 cells. When cell lysates carrying seeding competent tau species are applied to these cells, the seed induced aggregation of the Tau-YFP and Tau-CFP results in FRET, which can be quantified by flow cytometry (Figure 55).

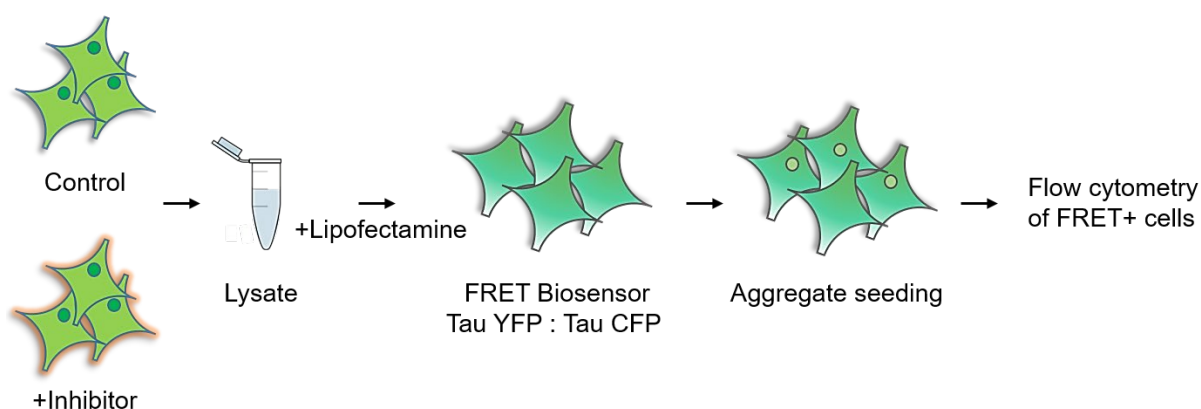


Figure 55. Experimental scheme for the analysis of tau-YFP seeding. See text above for explanation.

A similar cell line has been described to detect seeding competent tau species in brain material from tauopathy mouse models and AD patients (Holmes et al., 2014). Using this assay, in addition to VCP, we analysed the effects of inhibiting Hsp70, proteasome and the ubiquitination cascade on tau-YFP seeding activity. For this experiment, whole cell lysates were prepared to

rule out the loss of seeds in processing steps. Further, to control for effects of the used inhibitors on total tau-YFP levels, identical amounts of tau-YFP were added to the reporter cell line for each condition. Interestingly, treatment with the lysate from NMS-873 treated Clone10 cells resulted in > 50% drop in the number of FRET positive cells compared to DMSO treated cells (Figure 57A). This observation indicated that VCP inhibition significantly reduced tau-YFP seeding activity in Clone10 cells. Such an effect was not observed when the lysate of Clone10 cells treated with VER-155008 or epoxomicin were added to the reporter cell line (Figure 57A). MLN7243 treatment of Clone10, a condition that led to the loss of VCP on tau-YFP IBs (Figure 49), also caused around 50% reduction of FRET positive reporter cells compared to control. These results strongly suggest that VCP activity on tau-YFP inclusions is the primary source of seeding competent species in Clone10 cells. Comparing the effects of these different inhibitors allows us to discriminate between tau-YFP disaggregation and degradation mediated by VCP and proteasome, respectively.

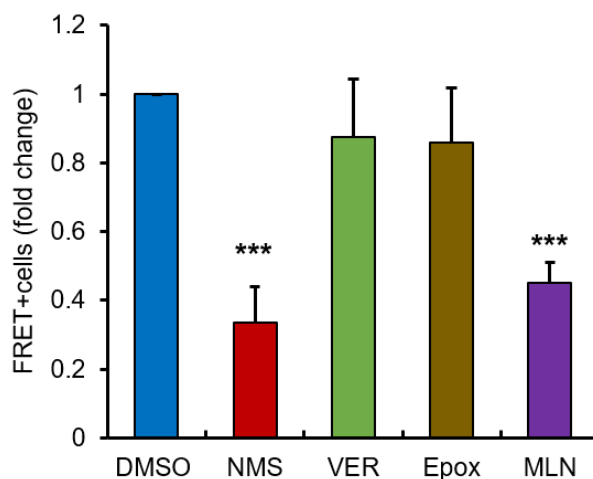


Figure 56. Analysis of tau-YFP seeding in Clone10

Clone10 cells were treated for 24 h with DMSO, 2 μ M NMS-873, 10 μ M VER-155008, 20 nM epoxomicin and 12 h with 0.5 μ M MLN7243. FRET positive cells were quantified as described in Figure 57. Fold changes with respect to DMSO treated cells are shown. Error bars represent standard deviation from three independent experiments. P-values were calculated using one-way ANOVA followed by a Tukey post hoc test. ***<0.001. Experiment performed by Dr.Patricia Yuste-Checa.

To validate that VCP inhibition reduced the amount of seeding competent tau-YFP species, we specifically isolated the seeding competent tau-YFP species from the lysate of control and NMS-873 treated Clone10 cells by size-exclusion chromatography (SEC) and compared their relative abundance. The lysates were pre-filtered with a 0.2 μm filter to remove large particles and debris which might obstruct the column. In the lysate of control Clone10 cells, the majority of tau-YFP appeared either in the void volume (VV) of the column (≥ 5000 kDa) or in a low molecular weight (LMW) fraction (52-220 kDa) (Figure 57B- blue trace). Quantitation of seeding activity from these fractions revealed that seeding competent tau-YFP was strongly enriched in the VV (Figure 57C- blue bars), which also indicates that these species were oligomeric. Treatment with NMS-873 resulted in the reduction of tau-YFP levels in both VV and LMW fractions, however the seed-enriched VV fraction was lost to a significantly higher amount than the LMW fraction (Figure 57B). The tau-YFP, which did not appear in the VV or LMW fraction after VCP inhibition, was perhaps present in the large IBs that have an average size of more than 5 μm in Clone10 (see Figure 30) and were likely to be removed from the lysates during the pre-filtration step. We further analysed the seeding activity of tau-YFP from the VV and the LMW fraction, and the total lysates after normalizing the amount of tau-YFP in all the samples. Interestingly, the VV fraction from control and NMS-873 treated cells seeded the reporter cells to similar efficiencies, suggesting that VCP inhibition only reduced the amount of seeds available for seeding without altering the seeding competence of these species (Figure 57C). These results demonstrate that VCP is involved in generating seeding-competent tau-YFP species in Clone10, which further strengthens the role of VCP as a disaggregase for amyloid-like tau-YFP aggregates in cells.

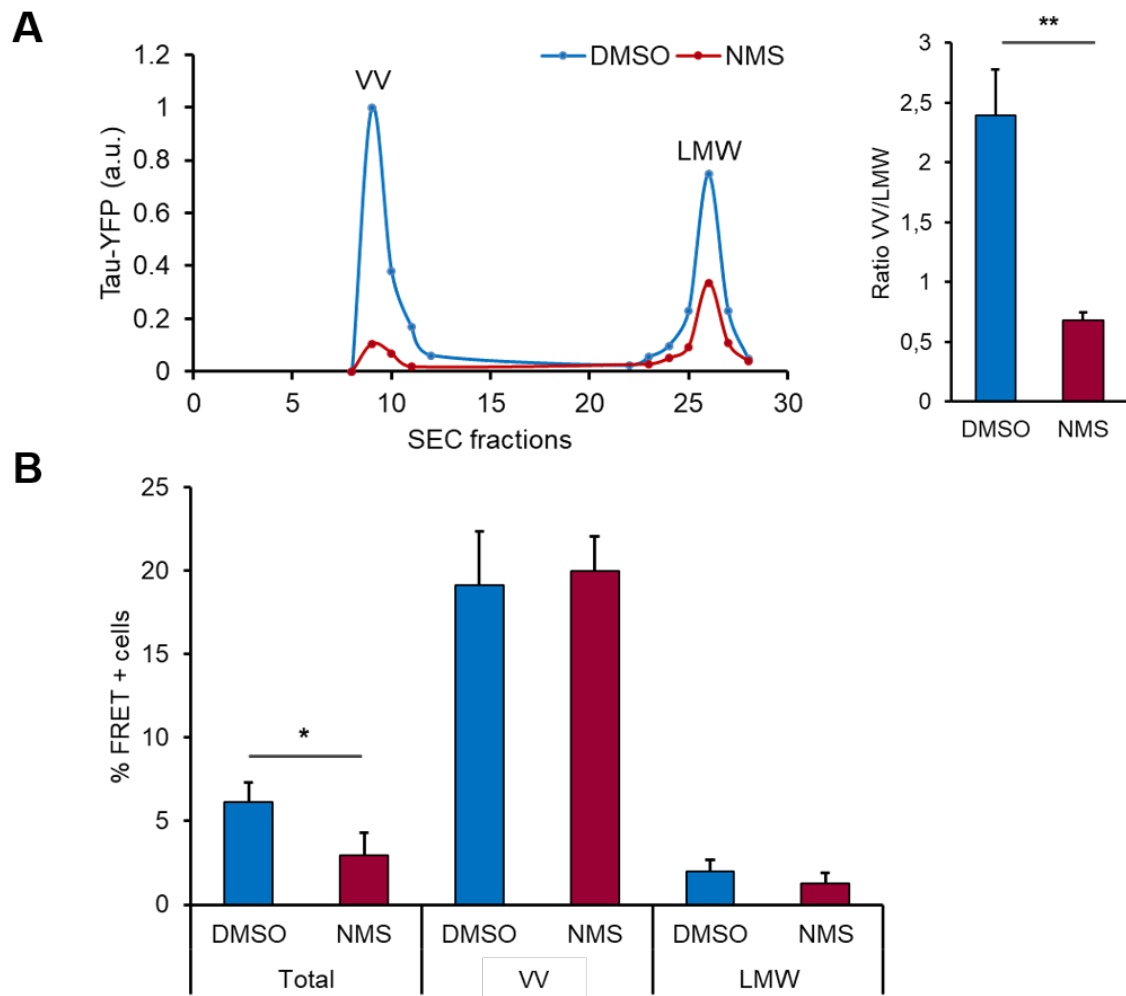


Figure 57. Analysis of tau-YFP seeding after VCP inhibition

(A) Left panel-Fractionation of tau-YFP from DMSO and NMS-873 treated Clone10 cell lysates by SEC. The y-axis represents the relative amount of tau-YFP in the void volume (VV) and the low molecular weight (LMW) fraction quantified by western blotting. Right panel- Ratio of tau-YFP in VV/LMW fractions from three independent experiments. **(B)** VV and LMW fractions from DMSO and NMS-873 treated cells were normalized by tau-YFP levels and analysed for seeding efficiency. Error bars represent standard deviations from three independent experiments. * <0.05 . ** <0.01 . Experiments performed by Dr. Patricia Yuste-Checa.

3.10 DISEASE ASSOCIATED VCP MUTATIONS IN TAU-YFP DISAGGREGATION

VCP is an important multifunctional cellular protein, mutations in which are associated with neurodegenerative conditions like ALS and IBMPFD (Tang and Xia, 2016). Consistent with the role of VCP in protein quality control, accumulation of polyubiquitinated inclusions can be observed in IBMPFD patient tissue (Weihl, 2011). We therefore investigated if the IBMPFD associated VCP mutations, A232E and R155H, disrupt the disaggregase activity of VCP.

Similar to wild type VCP, the mutant subunits assemble into hexamers (Weihl et al., 2006). When the mutant protein is exogenously expressed in cells, it can be incorporated into the wild type VCP hexamer, thus mediating its effect in a dominant negative fashion (Arhzaouy et al., 2012). We overexpressed C-terminal myc-tagged WT-VCP and variants containing the A232E and R155H mutations in addition to a mutant without ATPase activity (ATPase null E305Q/E578Q). 24 h after transfection, visual examination of cells expressing the A232E and R155H mutants did not show any signs of toxicity. However, cultures expressing the ATPase null mutant showed overt toxicity suggesting that the exogenous mutation carrying protomers had incorporated into the wild type VCP hexamer and impaired its function.

Overexpressed wild type and mutant VCP was diffusely distributed throughout the cells in Clone1 (Figure 43A). WT VCP, and the two disease associated mutants were recruited to the tau-YFP inclusions in Clone10 (Figure 58A-B). However, in case of the ATP null mutant, while there was an enrichment in the vicinity of the tau-YFP inclusions, there was no clear co-localization which might reflect an impairment of inactive VCP to appropriately interact with its substrates.

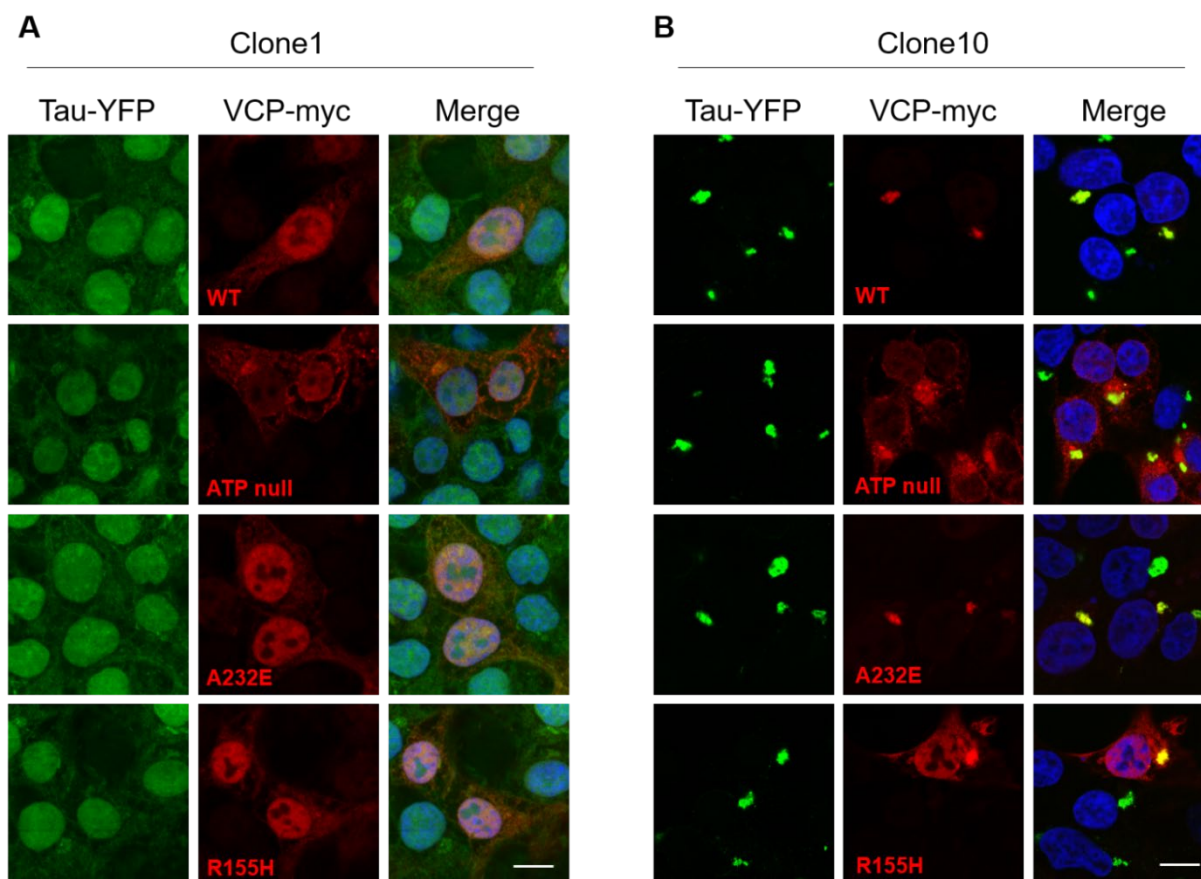


Figure 58. Cellular distribution overexpressed VCP variants

(A-B) Clone1 and Clone10 cells were transfected with constructs expressing wild type VCP and VCP mutants E305Q/E578Q (ATP null), A232E and R155H for 24 h. Cells were stained with an anti-myc primary and cy5 conjugated secondary antibody. Merged images show tau-YFP (green), VCP-myc (red) and DAPI (blue). Scale bar: 10 μ m.

Next, we tested if the VCP variants affected tau-YFP disaggregation in Tet-Clone10. A filter trap assay showed that empty vector and WT-VCP transfected cells cleared tau-YFP aggregates upon the addition of doxycycline (Figure 59A). Notably, WT-VCP overexpression did not further reduce the amount of filter trapped tau-YFP suggesting that VCP abundance was not limiting in the disaggregation process. Consistent with the role of VCP in disaggregation, the ATPase null mutant inhibited aggregate clearance even though it was expressed at lower levels than the other variants which did not perturb aggregate clearance (Figure 59A). These findings were confirmed by confocal imaging of cells expressing the different VCP variants, where expression of the two disease-associated mutants also did not result in aggregate stabilization (Figure 59B). Thus, the IBMPFD associated VCP mutations, A232E and R155H, did not disrupt the disaggregase activity of VCP in our model.

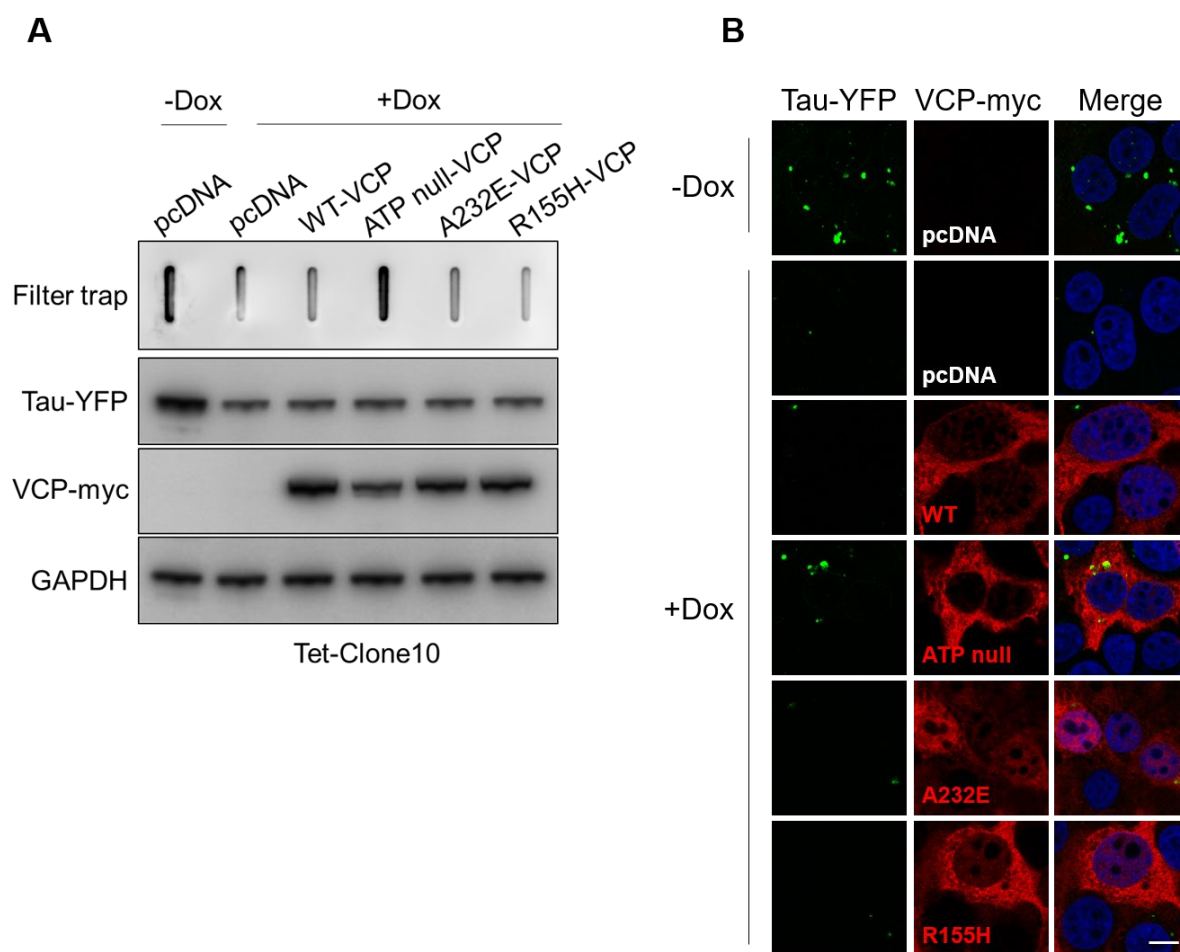


Figure 59. Effect of IBMPFD mutations on VCP mediated tau-YFP disaggregation

(A) Tet-Clone10 cells were transfected with empty vector (pcDNA) or constructs expressing myc-tagged wild type (WT), ATPase null E305Q/E578Q, A232E or R155H VCP mutants for 24 h. Doxycycline was added for another 24 h where indicated. Cell lysates were subjected to filter trap assay and the membrane was probed with anti-GFP antibody to detect tau-YFP. Total tau-YFP and overexpressed VCP-myc protein was analysed by western blotting. GAPDH was used as loading control. **(B)** Tet-Clone10 cells were transfected and treated with doxycycline as in (A). Cells were stained with an anti-myc primary and cy5 conjugated secondary antibody. Merge shows tau-YFP (green), VCP-myc (red) and DAPI (blue). Scale bar: 10 μ m.

4. DISCUSSION

In this work, we characterized morphologically distinct tau aggregates with regard to their localization, structure, cellular interactions and consequences. We further provide the first clear demonstration of disaggregation and degradation of amyloid-like tau aggregates in mammalian cells and identify VCP as a novel player involved in aggregate disassembly.

4.1 CELL CULTURE MODEL OF TAU STRAINS

The previously characterized tau-YFP strains, Clone9 and Clone10, are distinct from each other with respect to the visual morphology of tau aggregates, seeding efficiency and biochemical properties such as aggregate size, solubility and protease resistance (Sanders et al., 2014). In line with the observations of Sanders et al., we were able to induce aggregation of soluble tau-YFP in naïve Clone1 cells by adding lysates from aggregate containing Clone9 or Clone10 parental cells (Figure 16). Inducing aggregation by the exogenous addition of pre-formed aggregates was an effective strategy to enable the intracellular aggregation of tau which does not spontaneously aggregate in our model, even when cells are exposed to proteostasis stressors such as heat shock or proteasome inhibition (Figure 20) (Kopito, 2000; Wallace et al., 2015).

Transmission of the aggregated state occurs via the uptake of extracellular tau aggregates that act as seeds to initiate the aggregation of intracellular tau-YFP in a template-dependent manner (Frost et al., 2009). A structurally stable seed is able to transfer its conformation with high fidelity resulting in the formation of a similar aggregate in the recipient cells. We also observed that the resulting aggregate phenotypes in recipient cells were identical to those cells from which the lysates were derived, indicating that the strain behaviour is encoded in a stable conformation of aggregated tau-YFP present in the parental cell lines. This seeding competent conformation is able to propagate with cell division and induce an identical tau-YFP aggregation pattern in the entire cell population carrying the specific strains (Sanders et al., 2014). Such a phenomenon is also observed with yeast prions like Sup35/ [PSI⁺], which require the action of a disaggregating

chaperone, Hsp104, to fragment the prions and generate a transmission competent seed to maintain the prion state (Winkler et al., 2012a). It is plausible that tau aggregates in disease conditions are also fragmented by a disaggregase which generates seeds that enable the spread of tau pathology from the site of origin to adjoining brain regions.

Apart from seed-induced aggregation, we found that tau-YFP in Clone1 aggregated in response to the expression of aggregation-prone β -sheet proteins (Figure 21). These tau-YFP aggregates co-localized with β -sheet aggregates suggesting that the otherwise soluble tau-YFP was physically engaged by the aggregating β -sheet proteins. Tau-YFP may have formed β -sheet rich structures upon its aggregation with β 23 because mutations in tau-YFP that prevent the formation of cross β -structure (Sanders et al., 2014), also decreased its aggregation. Whether the β -sheet aggregates truly cross-seed tau-YFP aggregation remains to be verified in an *in vitro* setup. Moreover, while β 23 and tau both aggregate into amyloid-like fibrils independently (Goedert et al., 1996; Olzscha et al., 2011), it is not known whether the β 23-induced tau-YFP assemblies are also amyloid-like. Furthermore, it remains to be tested whether this tau-YFP conformation has prion-like properties and if it can persist in the absence of β 23 expression. Our results support the idea that tau aggregation *in vivo* may be triggered by the aggregation of another cellular protein (Giasson et al., 2003).

4.2 CELLULAR CHARACTERISTICS OF TAU-YFP STRAINS

Tau-YFP strains Clone9 and Clone10 propagate tau-YFP aggregates in distinct cellular localizations (Figure 17). While the occurrence of nuclear and cytosolic aggregates is toxic in different models of protein aggregation (Wen et al., 2014; Woerner et al., 2016), Clone9 and Clone10 cells do not exhibit any overt toxicity or growth defects. The fact that these cells were selected for their aggregate-containing phenotype suggests that there might be inherent adaptations or mechanisms that allow them to counteract the toxicity of protein aggregation. For instance, the formation of protective IBs may result in the spatial confinement of potentially toxic aggregates from the cellular milieu, thereby aiding cell survival (Arrasate et al., 2004; Escusa-Toret et al., 2013). Transcriptional profiling of these cells may provide additional information on cellular responses that are protective against aggregation and unique to each strain.

4.2.1 Compartmentalization and composition of IBs in tau-YFP strains

The cytosolic tau-YFP IBs in Clone9 and Clone10 represented distinct protein deposition sites in mammalian cells. The observed tau-YFP accumulation in juxtannuclear aggresome-like structures in Clone10 (Figure 18) was in agreement with published results (Sanders et al., 2014), and showed similarities with observations made in other cellular models of full-length tau aggregation (Guthrie and Kraemer, 2011; Piatnitskaia et al., 2019; Yu et al., 2018). Consistent with other features of aggresomes, tau-YFP IBs in Clone10 interacted with proteasomes (Figure 25C) (Kopito, 2000). We also observed that they were eliminated from cells more efficiently than the cytosolic IBs in Clone9 (Figure 30), which are not aggresomes, and so far remained uncharacterized in mammalian cells. Their peripheral cytoplasmic localization and resistance to clearance (Kaganovich et al., 2008) leads us to propose that the cytosolic IBs in Clone9 may be more similar to the yeast IPOD.

The spatially distinct IBs of Clone9 and Clone10 were composed of tau-YFP aggregates with different structural features. While the tau-YFP IBs in Clone10 contained fibrillar material, this morphology was less clear in Clone9 where only shorter assemblies could be observed (Figure 19C-D). While the resolution of our cryo-ET approach was not sufficient to detect cross- β structures, staining with amyloid-specific dyes suggested that the fibrillar aggregates in Clone10 are indeed amyloid-like structures, whereas the aggregates in Clone9 lack this property (Figure 19A-B). These observations fit to the idea of conformational variation between prion strains (Safar et al., 1998). Importantly, tau aggregates from AD and Pick's disease also show distinct atomic conformations of tau RD in the fibrillar core highlighting the physiological occurrence of tau polymorphs in human tauopathies (Zhang et al., 2019). How these polymorphic structures arise *in vivo* is not known, however the origin of the distinctive aggregate structures in Clone9 and Clone10 may trace back to the heparin-induced tau fibril preparation used to originally seed the aggregation of tau-YFP. It is known that structurally heterogeneous tau assemblies are formed in fibrillation reactions initiated by heparin (Fichou et al., 2018). Therefore, it is plausible that the seeds initially taken up by these cells had unique structures that were propagated to intracellular tau-YFP molecules generating the prion-like strains (Colby et al., 2009).

Alternatively, there could be cell-to-cell variations in the handling mechanisms of incoming seeds which may have given rise to unique aggregate structures. Notwithstanding, the structural variation of tau-YFP aggregates in this model is associated with the appearance of distinct protein quality control compartments hinting at different cellular consequences of these aggregates.

4.2.2 Consequences of polymorphic aggregation

The late-stage autophagy impairment observed in Clone10, but not in Clone9 cells (Figure 29), illustrates that strains can govern the biological consequences of protein aggregates. We propose that the molecular mechanism underlying this defect is based on the differences in the interaction of these aggregates with cellular proteins. It has been previously established that protein aggregates make aberrant interactions with essential proteins and sequester them from their normal cellular function (Kim et al., 2016; Olzscha et al., 2011). By analysing differential interactors of tau-YFP aggregates in the two strains, we found that an ESCRT pathway component, CHMP1A, was highly (~20-fold) enriched in the interactome of tau-YFP aggregates in Clone10 compared to Clone9 (Supplementary Table 5). Another protein of the same pathway, CHMP2B, was also ~2.5 fold more enriched in Clone10, suggesting that the sequestration of ESCRT components may be responsible for the observed defect in autophagy in Clone10. While the connection between autophagy and the ESCRT pathway is not fully established, there is increasing evidence for the involvement of ESCRT proteins in autophagy (Rusten and Stenmark, 2009; Schäfer et al., 2020; Takahashi et al., 2018), and it has been shown that the plant paralog of CHMP1A is required for autophagic turnover of plastid components (Spitzer et al., 2015). Furthermore, mutations in CHMP2B are associated with a rare form of Danish frontotemporal dementia (Skibinski et al., 2005), and produce phenotypes that suggest autophagic dysfunction (Lee et al., 2009). The specificity of this perturbation in Clone10 emphasizes the biological significance of aggregate polymorphism or strain behaviour and reflects its impact on cell physiology at the molecular level. Our results are in support of the idea that distinct tau strains may define different tauopathies (Sanders et al., 2014).

4.3 AGGREGATE CLEARANCE IN THE MAMMALIAN SYSTEM

Accumulation of protein aggregates is an aberrant proteostasis event. At the steady state in healthy cells, molecular chaperones prevent protein aggregation by assisting the folding of newly synthesized proteins, refolding misfolded proteins or handing them over for degradation (Kim et al., 2013). However, factors like external stress or destabilizing mutations in proteins overwhelm the chaperoning capacity of the cell, leading to aggregation. Despite being biophysically more stable than the native or misfolded state, research over the last decade has established that protein aggregates can be tractable (Lamark and Johansen, 2012). The cellular PQC machinery attempts to deal with aggregates in a manner that either involves disaggregation followed by refolding, or when disaggregation is not effective, targeting them for degradation by autophagy. In the following sections, we discuss new insights into the clearance of amyloid-like tau-YFP aggregates in mammalian cells induced by amino acid starvation, inhibiting global translation, or suppressing specifically tau-YFP expression. We further address the less appreciated role of proteasomes in the degradation of aggregated proteins.

4.3.1 Strain-specific clearance of tau-YFP aggregates

In this study, we observed the clearance of tau-YFP aggregates upon amino acid starvation or translation inhibition in the tau-YFP strain Clone10 (Figure 30, Figure 31B). While the clearance of aggregates formed from disease-associated exogenous or endogenous proteins has been previously reported, it is not clear if these aggregates contained amyloid-like structures (Guthrie and Kraemer, 2011; Hao et al., 2013; Wong et al., 2008). Clone10 contained amyloid-like fibrillar material, similar to tau PHFs isolated from patients suffering from tauopathies (Spillantini et al., 1997). Also, the tau-YFP IBs stained positive for ubiquitin and p62, both of which are hallmarks of tau lesions in a range of tauopathies (Kuusisto et al., 2001), suggesting that the aggregates in this cell line are similar to the ones observed in disease. The effective clearance of fibrillar tau-YFP aggregates from cells that we report here support the idea that also higher eukaryotes are endowed with mechanisms to eliminate pathogenic protein aggregates (Yamamoto et al., 2000; Zu et al., 2004). Notably, under conditions of amino acid starvation which resulted in aggregate clearance in Clone10, the IBs in Clone9 persisted (Figure 30), which is in line with

the suggested properties of the yeast IPOD compartment reported to contain rigid disease-related or prion protein aggregates (Kaganovich et al., 2008). In the context of strain behaviour, it is likely that the conformational differences between the tau-YFP aggregates influence their clearance from cells. This is reflected by the relatively inefficient ubiquitination (Figure 44), and the correspondingly slow turnover, of tau-YFP in Clone9 compared to Clone10 (Figure 31A). This observation suggests that the tau-YFP aggregate conformation in Clone10 harbours structural features which may facilitate the recruitment of PQC components such as the ubiquitination and the clearance machinery.

4.3.2 Aggregate clearance under amino acid starvation

Our observation of aggregate clearance upon amino acid starvation is supported by a previous study which showed the clearance of disease-associated Htt, tau and α -synuclein aggregates upon starvation by aggrephagy (Wong et al., 2008). However, the clearance of amyloid-like tau-YFP aggregates in starved Clone10 cells was not blocked by inhibition of autophagy, and was dependent on proteasomal activity (Figure 32). In agreement with this finding, we found that proteasomal subunits interacted with tau-YFP aggregates already in full medium (Figure 25C-D) and to an even greater extent under nutrient starvation (Figure 34). Although the interaction of proteasomes with aggregates is often observed in cultured cells, primary neurons, and patient brains, the functional relevance of this interaction is not well understood (Bennett et al., 2005; Deriziotis et al., 2011; Myeku et al., 2016; Rousseau et al., 2009; Waelter et al., 2001). Nutrient starvation-induced mTOR inhibition is shown to boost UPS capacity by increasing proteasome abundance and stimulating proteolysis by the proteasomes (Rousseau and Bertolotti, 2016; Zhao et al., 2015). Notably, stimulation of proteasome activity, via pharmacological agents that increase cellular cAMP levels, is associated with the loss of aggregated tau in a mouse model of tauopathy (Lokireddy et al., 2015; Myeku et al., 2016). Therefore, it is plausible that augmented proteasomal degradation upon amino acid starvation was conducive to tau-YFP aggregate clearance. Moreover, limited protein synthesis under starvation conditions (Onodera and Ohsumi, 2005) may have additionally contributed to limit aggregate load, since global translation inhibition by CHX in full medium resulted in a similar phenotype (Figure 31B). This

observation with CHX further established that the clearance mechanism of tau-YFP aggregates in Clone10 did not require new protein synthesis. The fact that CHX strongly inhibits autophagy (Watanabe-Asano et al., 2014), further excludes a role of autophagy in clearing tau-YFP aggregates in this model and supports the idea of autophagy-independent removal of protein aggregates by the proteasome (Hjerpe et al., 2016).

4.3.3 Role of proteasomes in handling protein aggregates

Our findings of proteasome-dependent aggregate clearance are in agreement with several other studies that collectively extend the role of the UPS beyond the degradation of soluble monomeric proteins (Gallardo et al., 2019; Hjerpe et al., 2016; Martín-Aparicio et al., 2001). The turnover of aggregated proteins via the proteasomal route suggests a model in which degradation is coupled to an upstream aggregate disassembly/disaggregation mechanism that generates degradation-compatible monomers. Protein aggregates range from being microscopically undetectable species to large IBs (several μm in size) and cannot be directly degraded by the proteasome, due to the spatial restriction posed for the incoming substrates through the axial pores (~ 2 nm diameter), and the limited size of the 20S proteolytic chamber. Additionally, while the AAA+ ATPases in the 19S particle unfold proteasomal substrates, there is no clear evidence that they can remodel either amorphous or amyloid-like protein aggregates and translocate them for degradation in the 20S chamber. Therefore, a disaggregation mechanism that is powerful enough to remodel structured amyloid-like aggregates is necessary to prepare the protein present in such aggregates for proteasomal degradation.

4.4 VCP-DEPENDENT DISAGGREGATION OF AGGREGATED TAU-YFP

We have shown that the clearance of amyloid-like tau-YFP aggregates upon amino acid starvation or termination of tau-YFP synthesis required, in addition to proteasomes, the activity of the AAA+ ATPase VCP (Figure 40). Contrary to what was observed for aggregated tau-YFP, degradation of tau-YFP in an aggregate-free cell line was largely independent of VCP, which indicated an aggregate-specific role of VCP (Figure 42). When tau-YFP expression was stopped by the addition of doxycycline, the loss of tau-YFP aggregates was accompanied by a reduction of tau-YFP levels suggesting that VCP-mediated disaggregation led to the proteasomal degradation of the solubilized protein (Figure 35). Consistent with the preference of VCP and proteasomes for UbK48 modified substrates (Blythe et al., 2017; Thrower et al., 2000), tau-YFP in the aggregated state was found to be conjugated with UbK48 chains (Figure 45). Inhibition of the cellular ubiquitin conjugation cascade resulted in the loss of ubiquitin signal on tau-YFP inclusions and reduced VCP recruitment to the inclusions (Figure 49). We further found that the observed stabilization of tau-YFP inclusions by VCP inhibition was accompanied by a reduction in the amount of seeding-competent material, which did not occur with proteasome or Hsp70 inhibition (Figure 56). While the mammalian Hsp70 system has been shown to disaggregate α -synuclein fibrils *in vitro* (Gao et al., 2015), in the cellular context of tau-YFP aggregates, Hsp70 may act downstream of VCP and assist aggregate clearance by preventing re-aggregation of the disaggregated material and maintaining its solubility prior to proteasomal degradation. Thus, we describe a novel clearance mechanism for amyloid-like tau-YFP aggregates in HEK293 cells and the role of VCP as a disaggregase (Figure 60).

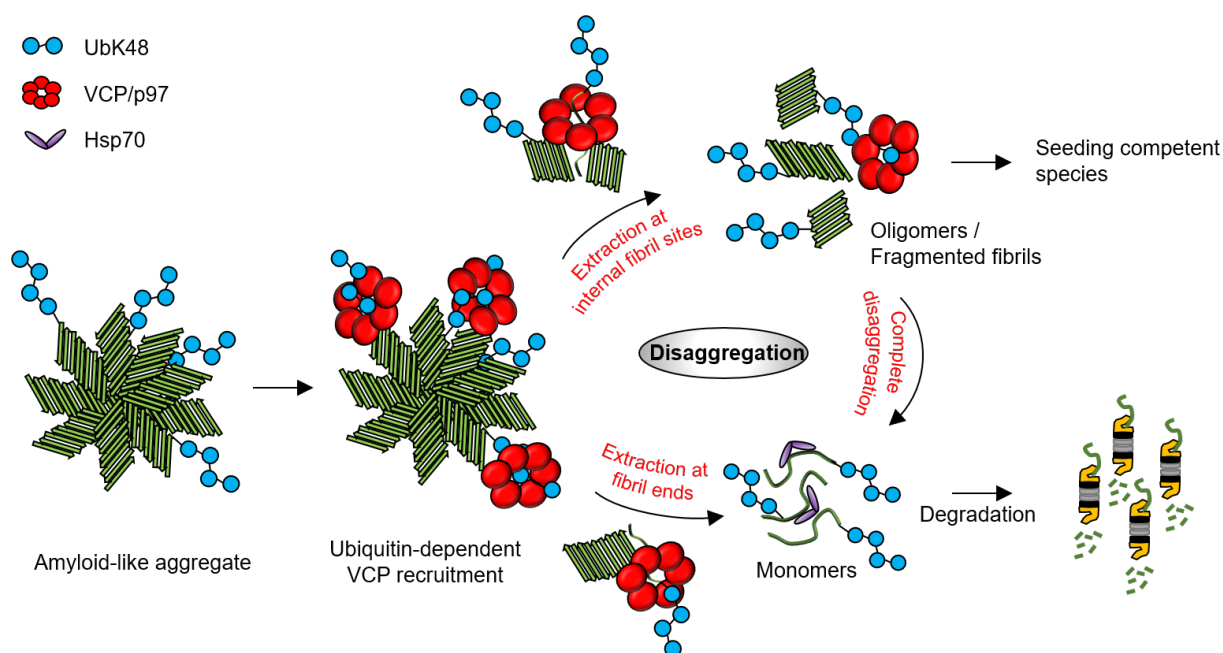


Figure 60. Model of VCP-mediated disaggregation and degradation of amyloid-like tau-YFP aggregates in cells. Protein aggregates are recognized as aberrant species by the PQC machinery and marked for degradation via attachment of K48 linked ubiquitin chains which recruit VCP to the aggregates. VCP may extract a ubiquitinated monomer from an internal site on the fibril resulting in fibril fragmentation and generation of smaller fibrils which can seed. These species may be further disaggregated by VCP to complete monomers which, by virtue of the attached polyubiquitin chain, are targeted to the proteasome for degradation. Alternatively, VCP activity on fibril ends can directly generate degradation competent monomers

4.4.1 Cellular dynamics of aggregate clearance

The occurrence of protein aggregates is closely tied to pathogenesis by a range of mechanisms (Ross and Poirier, 2004; Sweeney et al., 2017). While the exact mechanism of toxicity is still unclear, the association of aggregate loss with reversal of pathological symptoms in disease models (Polydoro et al., 2013; Yamamoto et al., 2000) suggests that aggregate clearance might be a potential therapeutic principle applicable to protein aggregation disorders with gain-of-function toxicity. Aggregate clearance relies on the inherent cellular PQC processes to recognise and eliminate aggregates, and understanding the underlying mechanisms of aggregate clearance is necessary to boost the capacity of cells to deal with toxic protein aggregation.

In cultured cells and mouse models of amyloid-associated neurodegenerative diseases such as HD and tauopathy, aggregate clearance is observed upon suppressing the expression of the precursor protein (Polydoro et al., 2013; Yamamoto et al., 2006; Yamamoto et al., 2000). Despite the extraordinary stability of amyloid-like aggregates, their clearance from cells points towards

the dynamic nature of this form of aggregates. In agreement with this idea and in line with previous findings of Sanders et al., we observed a gradual loss of amyloid-like tau-YFP aggregates from cells upon limiting tau-YFP expression (Figure 36C). Proteasome inhibition prevented this aggregate loss (Figure 37B-C) and under conditions of normal tau-YFP synthesis, resulted in the increase of aggregate size (Figure 20B). These observations led us to infer that these aggregates are subjected to continuous turnover at steady state and the aggregated state is maintained through a constant supply of newly synthesized protein that replenishes the depleted aggregated material. This is reminiscent of an *in vitro* amyloid aggregation reaction where the aggregated ensemble is thought to exist in a state of dynamic equilibrium with the soluble form (Chiti and Dobson, 2017). This equilibrium is illustrated by the cycling of protein molecules within the amyloid fibrils and suggests that parts of the fibrillar material are able to spontaneously dissociate and re-associate with the existing fibrils (Carulla et al., 2005). However, in the cellular context, this re-association may be prevented by the interaction with molecular chaperones which may act as holdases and facilitate further disaggregation of this material into monomers. Additionally, the fibrils may directly liberate monomers that are likely to be distinct from the naïve monomers owing to a specific ubiquitination pattern acquired in the aggregated state which directs them for proteasomal degradation. Owing to the multitude of aggregate species, parallel aggregate formation and disassembly reactions, and the different layers of PQC pathways and cellular factors that constantly remodel the aggregation landscape, the equilibrium between the aggregated and soluble forms in the cellular environment is far from simple. In broad terms, the persistent, yet dynamic, nature of aggregates in our tau-YFP aggregation model represent a balance between the formation and turnover of aggregates (Figure 61A), In the cellular context, terminating protein synthesis shifts this balance towards aggregate disassembly and degradation (Figure 61B), whereas inhibiting degradation increases the concentration of protein available for aggregation and favours aggregate formation (Figure 61C).

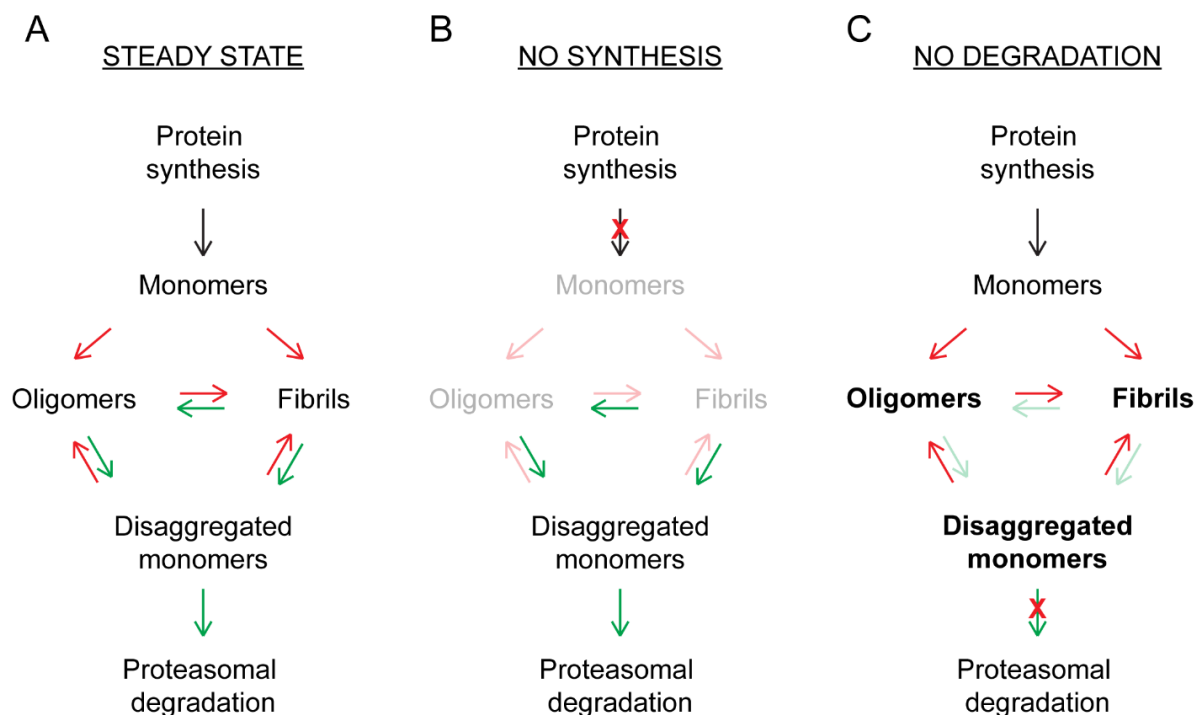


Figure 61. Dynamics of protein aggregation, disaggregation, and degradation by the proteasome.

(A) Protein aggregates exist in a state of dynamic equilibrium with the non-aggregated form of the protein. Ongoing protein synthesis generates monomers that contribute to aggregate formation. In cells, aggregates can be actively disaggregated to monomers which are then degraded by the proteasome. (B) Cessation of protein synthesis cuts off the monomer supply to aggregates thereby arresting aggregate formation and promoting disaggregation and degradation of aggregated material resulting in aggregate clearance. (C) Impaired protein degradation adds to the amount of protein available for aggregation thereby shifting the equilibrium towards aggregation and inhibiting aggregate clearance. Red and green arrows indicate aggregation and disaggregation respectively. Faded and bold texts indicate a decrease and increase in the amount of the stated species respectively.

4.4.2 Role of VCP in aggregate clearance

VCP is a critical component of the cellular PQC system. Human diseases caused by mutations in VCP such as IBMPFD and FTD exhibit an accumulation of ubiquitinated protein aggregates in the skeletal muscle and central nervous system of affected patients (Schroder et al., 2005; Watts et al., 2004). VCP itself co-localizes with ubiquitin-containing protein aggregates in patient material from HD, PD, dementia with Lewy bodies (DLB), and ALS (Hirabayashi et al., 2001; Ishigaki et al., 2004). It is not well understood whether the occurrence of VCP on protein aggregates represents a quality control measure to deal with the aggregates or a sequestration of this essential protein from the cellular milieu. Our findings support the idea of a functional interaction of VCP with protein aggregates. In agreement with other studies we have

demonstrated that VCP is required for the clearance of protein aggregates in cells (Ju et al., 2008; Kobayashi et al., 2007). It must be noted that VCP activity is involved in many processes such as promoting aggresome formation and regulating autophagy that are connected to maintaining proteostasis. In our model, aggresome formation was not significantly affected by VCP activity as we did not observe multiple dispersed aggregates, rather enlarged inclusions upon VCP down-regulation (Figure 41). Owing to the role of VCP in regulating autophagic degradation (Buchan et al., 2013; Kobayashi et al., 2019; Tresse et al., 2014), it is likely to participate in degradation of aggregates via autophagy. This idea supports the observation that aggregates, such as polyQ, which are degraded via the lysosomal route (Iwata et al., 2005a; Iwata et al., 2005b; Ravikumar et al., 2002; Yamamoto et al., 2006), also require VCP activity for clearance (Kobayashi et al., 2007). However, for aggregates cleared in an autophagy-independent manner via the UPS, it is plausible that VCP exercises its inherent protein unfolding activity directly on the aggregates which results in their solubilisation prior to proteasomal degradation (Gallagher et al., 2014). This idea is consistent with the role of VCP in UPS wherein it generates unstructured regions that are used by proteasomes to engage substrates and initiate degradation (Beskow et al., 2009; Olszewski et al., 2019).

4.4.3 VCP as a protein disaggregase

Our findings reveal a previously unidentified role of VCP in eliminating amyloid-like protein aggregates in cells, in concert with the UPS, which leads us to infer that VCP could be the long-sought AAA+ 'disaggregase' in higher eukaryotes. We note that this proposition has existed for more than a decade (Kobayashi et al., 2007), but missed definitive evidence (Nillegoda et al., 2018), plausibly due to the lack of appropriate experimental models. Notably, tau-YFP aggregates in our model were resolved in a time-frame of 24 h, which makes it feasible to observe effects of inhibiting the essential activity of VCP, in comparison to Htt IBs which require around 3-5 days for clearance (Iwata et al., 2005a; Ravikumar et al., 2002; Yamamoto et al., 2006). Additionally, such prolonged observation times, particularly with toxic aggregates like Htt, may complicate interpretations due to the death of aggregate-containing cells during the experiment. In this regard, the lack of toxicity from tau-YFP aggregation in our model is

advantageous. Furthermore, previous work on protein disaggregation has often focused on using non-ubiquitinated model substrates (Shorter, 2011), which may have obscured the disaggregation activity of VCP. Similar to the disaggregases of the Hsp100 family, VCP is a double ring homohexameric AAA+ ATPase and utilizes energy from ATP hydrolysis to structurally remodel and unfold its substrates. After a long standing debate, the molecular mechanism of VCP-mediated unfolding was demonstrated to be comparable to the Hsp100 chaperones, which involves entire substrate translocation through the central pore by a hand-over-hand mechanism resulting in strong pulling forces that unfold the substrate (Bodnar and Rapoport, 2017; Cooney et al., 2019; Puchades et al., 2020). The substrate unfolding principle can account for the disaggregase activity of VCP in mammalian cells since ATPase deficient VCP mutants which cannot unfold proteins *in vitro* (Blythe et al., 2017), also failed to resolve tau-YFP aggregates in cells (Figure 59). Notably, while amyloid-like tau-YFP aggregates were dependent on VCP for clearance, VCP was not required to resolve heat-induced amorphous luciferase aggregates in cells (Figure 54B), suggesting a more specific role of VCP in disaggregation. A possible explanation for this is that structurally robust aggregates such as amyloids rely on AAA+ proteins for disaggregation, coinciding with previous observations that ClpB/Hsp104 disaggregases are required, in addition to the Hsp70 system, to resolve more structured aggregates (Lewandowska et al., 2007). Therefore, biophysical properties of the aggregates may determine which disaggregation machinery is adept for clearance. Moreover, if VCP can disaggregate amyloid assemblies of full-length tau or other proteins still needs to be investigated. Such an investigation in cells, however, may be susceptible to ambiguities arising from aggregate clearance via autophagy and the role of VCP therein. In this regard, the *in vitro* reconstitution of VCP-mediated disaggregation would be beneficial to establish the generality of this process. Furthermore, if the disaggregation function of VCP is preserved in other organisms is also an open question. In yeast, although Hsp104 is the predominant disaggregase, solubilisation of certain substrates may require Cdc48 activity (Gallagher et al., 2014; Kama et al., 2018).

4.4.4 Fate of disaggregated material

VCP activity is coupled to proteasomal degradation in many of its proteostasis-related functions such as ERAD, MAD and RQC. This coupling has been proposed to differentiate the action of VCP from that of ClpB/Hsp104 disaggregases which mostly re-solubilise substrates for refolding (Nillegoda et al., 2018). Notably, the AAA+ modules of VCP in higher eukaryotes are not associated with a protease such as in Lon, ClpXP or ClpCP which directly degrade substrates after unfolding. While an archaeal homolog of VCP can substitute the 19S subunit to form a proteolysis-competent proteasome with the 20S core particle (Barthelme et al., 2014; Barthelme and Sauer, 2012), so far there is no evidence of such a complex in eukaryotes, despite several observations of VCP co-purifying with proteasomal preparations from different systems (Besche et al., 2009; Tai et al., 2010; Verma et al., 2000). These observations together with the fact that not all VCP substrates are degraded post-VCP processing (Radhakrishnan et al., 2014; Rape et al., 2001; Weith et al., 2018) suggest that the disaggregated material may persist in the cell awaiting its final turnover. Specialized shuttling factors or molecular chaperones may act downstream of VCP and assist the delivery of the disaggregated monomers to the proteasome (Hjerpe et al., 2016; Richly et al., 2005; Shiber and Ravid, 2014).

Disaggregation of Sup35 fibrils by Hsp104 generates seeding competent material (Winkler et al., 2012a), and implies that seeding capacity may serve as a proxy for disaggregation activity. Although the precise structural identity of the species generated after tau-YFP disaggregation in cells has not been determined, this material is present in the major seeding-competent fraction in cells and was lost when VCP was either inhibited by treatment with NMS-873 or prevented from being recruited to the aggregates by a block of ubiquitination through treatment with MLN7243 (Figure 56). This observation is akin to the disaggregation model of Sup35 fibrils by Hsp104 and suggests that VCP may extract internal tau-YFP molecules from a fibril leading to its breakage resulting in seed formation. Recently, tau monomers were also implicated in adopting seeding-competent conformations that could transmit specific aggregate phenotypes (Mirbaha et al., 2018; Sharma et al., 2018). The isolation of these monomeric conformers involved prolonged sonication induced physical breakage of pre-formed fibrils and aggregates

in cell lysates, which in principle may also occur within cells since VCP is expected to disaggregate fibrils via extraction of monomers from the internal region or at fibril ends (Figure 60). However, our SEC results indicated that the majority of the seeding-competent species were oligomeric. Notwithstanding, VCP-mediated disaggregation contributes to prion-like propagation in our model and supports the idea that disaggregation activity may enhance amyloid spreading in the disease context (Nillegoda et al., 2018). Generation of seeding competent species may therefore be a common risk and perhaps an inevitable consequence of amyloid clearance mechanisms via disaggregation.

4.4.5 Targeting VCP to protein aggregates

Recruitment of the disaggregation machinery to aggregates can be a crucial regulatory step in the aggregate clearance process. In the mechanism of disaggregation by the Hsp100 proteins, Hsp70 provides substrate specificity and plays a regulatory role upstream of the Hsp100 proteins (Doyle et al., 2013). Hsp70 first binds and then targets Hsp104/CipB disaggregases to aggregates in a manner that is dependent on the M-domain of the Hsp100 proteins (Seyffer et al., 2012; Winkler et al., 2012b). However, several observations argued against a role of Hsp70 in recruiting VCP to tau-YFP aggregates. Firstly, in our quantitative interactome analysis, Hsp70 (HSPA8) itself did not qualify as a specific interactor of tau-YFP aggregates (Supplementary Table 3), perhaps due to the binding of Hsp70 to soluble tau-YFP in Clone1. Alternatively, we considered the possibility that an unstable or transient interaction between Hsp70 and tau-YFP aggregates could have resulted in the loss of aggregate-bound Hsp70. However, immunofluorescent staining of Hsp70 in intact cells also showed only a small fraction of tau-YFP IBs co-localizing with Hsp70 (Figure 51A), in contrast to VCP which co-localized with almost all aggregates (Figure 39B-C). Additionally, VCP was observed to localize to tau-YFP IBs in cells where Hsp70 activity was inhibited using VER-155008 (Figure S3). This suggests that VCP was able to bind to tau-YFP aggregates independent of Hsp70 activity. Moreover, VCP also lacks the M-domain which mediates the binding of Hsp70 to Hsp100 proteins. From these observations, we conclude that Hsp70 may not be required to target VCP to aggregates.

The general mechanism of substrate recognition by VCP proceeds via the binding of different cofactors which regulate the targeting of VCP to diverse cellular processes. We identified two ubiquitin-binding VCP cofactors, NSFL1C (p47) and the heterodimeric cofactor complex UFD1L-NPLOC4 (UN), as interactors of tau-YFP aggregates in our model which may be involved in recruiting VCP to the aggregates. The UN cofactor is of particular importance in the UPS-related functions of VCP, which involve extracting ubiquitinated target proteins from the ER, mitochondria and ribosomes for degradation by the proteasome (Xia et al., 2016). In contrast to UN, p47 directs VCP to proteasome-independent pathways such as membrane fusion on the Golgi and endocytic sorting of proteins (Kondo et al., 1997; Rabouille et al., 1998; Ritz et al., 2011). While p47 is able to form a complex with ubiquitinated substrate and VCP, it does not induce substrate unfolding *in vitro*; which occurs only in the presence of the UN complex (Blythe et al., 2017). Therefore, we suggest that the UN complex may act as both the substrate-recruiting and substrate-processing VCP cofactor in the disaggregation process.

4.4.6 Regulation of VCP-mediated disaggregation by ubiquitination

Our results demonstrate that ubiquitin modification of the tau-YFP aggregates was necessary for VCP engagement followed by disaggregation and proteasomal degradation of the disaggregated material. It is known that both VCP recruitment and proteasomal degradation is favoured when the substrate ubiquitin modification involves K48 linkages (Blythe et al., 2017; Bodnar and Rapoport, 2017; Thrower et al., 2000). Consistently, tau-YFP aggregates in our model were modified with K48 polyubiquitin chains (Figure 45), which are relevant to disease-associated tau PHFs (Cripps et al., 2006). Besides K48 linkages, linear M1 and mixed K11/K48 ubiquitin chains have also been implicated in directing VCP to protein aggregates such as polyQ (van Well et al., 2019; Yau et al., 2017). However, the highly selective binding of the UN complex to K48 linkages (Tsuchiya et al., 2017), suggests that VCP recruitment to tau-YFP aggregates in this model may be mediated by K48 linkages. Polyubiquitin-dependent appearance of VCP on the aggregates correlated with ongoing disaggregation as judged by the seeding activity in the cell lysates (Figure 56). It has been recently shown that substrate poly-ubiquitination is not only critical for VCP binding but also for the initiation of unfolding as VCP unfolds ubiquitin

molecules attached to its substrate (Twomey et al., 2019). This observation, in the context of our findings, implies that VCP may initiate disaggregation by exerting pulling forces on the ubiquitin moiety conjugated to the protein within the fibrillar aggregates resulting in its dissociation from the rest of the fibril. This process may reiterate on disassembled aggregates or seeds until they are processed to monomers, a pre-requisite for their clearance via the proteasome (Figure 60). Thus, ubiquitination is a crucial regulator of VCP-mediated disaggregation.

4.4.7 VCP and Hsp70: Co-operators or competitors

The complex of eukaryotic Hsp70, Hsp40 and Hsp110 disaggregates a variety of substrates *in vitro* including amorphous and amyloid-like aggregates (Nillegoda et al., 2018). *In vivo*, while the Hsp70-40-110 complex effectively suppresses pathogenic protein aggregation (Scior et al., 2018), its bona fide disaggregation capacity is shown only for heat-induced aggregates (Kirstein et al., 2017). Thus, it is unknown whether this machinery can also reverse amyloid-like aggregation in cells and if there is an interplay with other disaggregation systems such as VCP. Our results suggest that the Hsp70 system is not sufficient to disaggregate amyloid-like aggregates in our tau-YFP aggregation model (Figure 52C). The fact that Hsp70 activity was partly dispensable for the clearance of amyloid-like tau-YFP aggregates, suggests that it is also not necessary (at least) for the initial steps of the disaggregation mechanism. This is in contrast to what we observed in cells with amorphous luciferase aggregates, which were resolved in an Hsp70-dependent manner (Figure 54). Contrary to VCP, we noted that Hsp70 was not a specific interactor of tau-YFP aggregates which further supports the idea that Hsp70 may not disaggregate the fibrillar material. Moreover, inhibition of Hsp70 did not decrease the seeding capacity of tau-YFP (Figure 56), suggesting that the seed generation (fibril fragmentation) step of disaggregation also occurred independent of Hsp70 activity. However, new tau-YFP foci appeared after Hsp70 inhibition, which did not form after VCP inhibition. This indicates that VCP and Hsp70 act on different stages of aggregate clearance. Since Hsp70 inhibition did not lead to *de novo* aggregation of tau-YFP in Clone1 (Figure 52B), the solubility of naïve/un-aggregated tau-YFP did not require the chaperoning of Hsp70 and excludes the aggregation of this form of

tau-YFP into the new foci. From this observation, we infer that Hsp70 maintains the solubility of an aggregation-prone conformation of tau-YFP that is not present in the IBs and succumbs to aggregation outside of the IBs when not chaperoned by Hsp70. The disaggregation activity of VCP on fibrillar aggregates in the IBs may be the source of such aggregation-prone material. Therefore, in the process of aggregate clearance, Hsp70 may act as a holdase that prevents re-aggregation of disaggregated material and facilitates its clearance via the proteasome (Shiber and Ravid, 2014). Substrate handover to the proteasome may be performed by Hsp70 directly or with the help of additional shuttling factors.

4.4.8 Degradation-coupled-disaggregation and protein aggregation disorders

VCP-mediated aggregate disassembly followed by proteasomal degradation may offer an alternative route to autophagy for the elimination of terminally aggregated proteins that have no possibility of entering the refolding cycle (Figure 62). Terminally aggregated proteins are marked with ubiquitin chains that may serve as the triage signal for their degradation (Itakura et al., 2016); however, a comprehensive understanding of factors that determine the preferred protein degradation pathway is still lacking. It is possible that the pathway choice is dictated by the ubiquitin chain topology on the aggregates, which further leads to the question of how specific ubiquitin ligases recognise aggregated substrates. The pathway choice, in the context of disease state, is particularly relevant because there can be perturbations in either pathway, in which case the role of the alternative pathway would become significant.

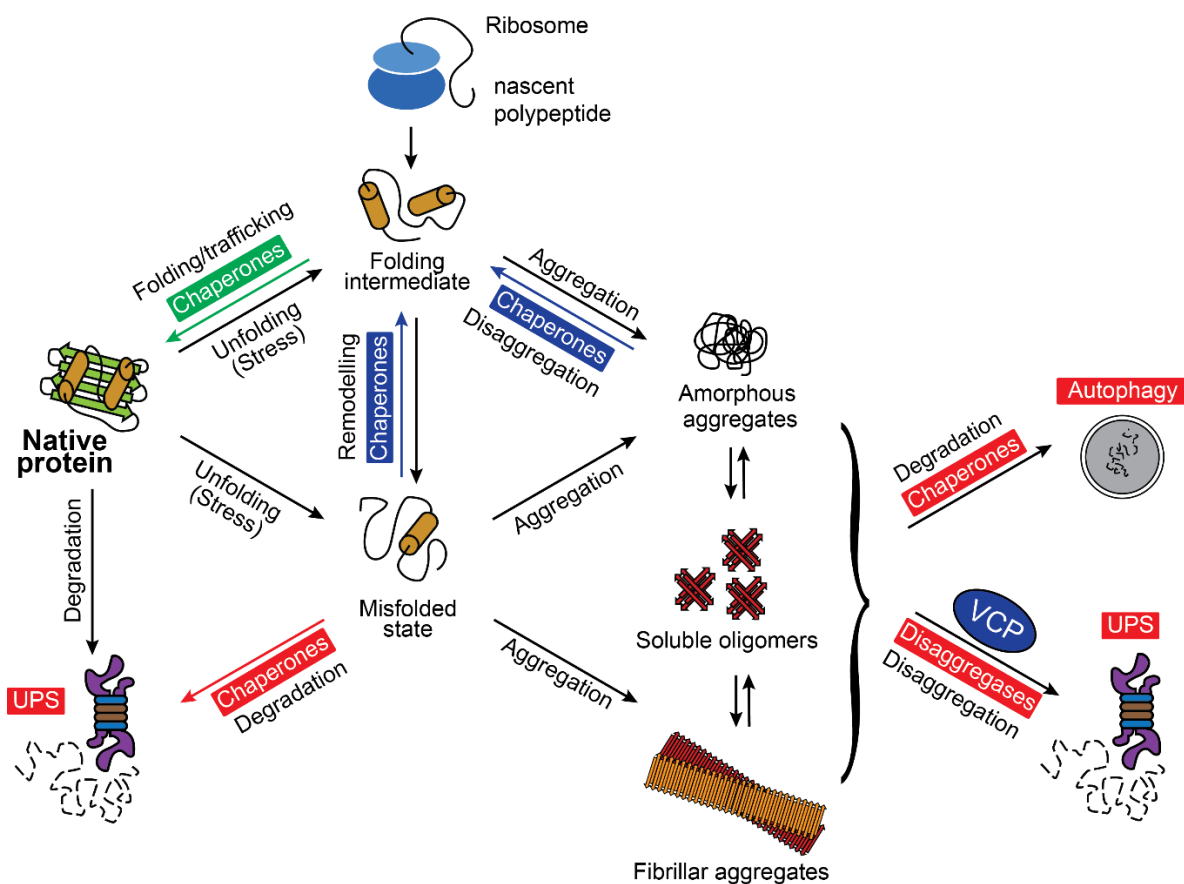


Figure 62. The stand of VCP-mediated disaggregation in the general scheme of PQC pathways

VCP may act on terminally aggregated proteins and solubilise them for proteasomal degradation. This pathway can complement autophagic removal of protein aggregates in cells. Pathway specificity for aggregate clearance may be conferred by specific ubiquitin topologies on substrates.

While autophagy modulation has been explored as a therapeutic target for protein aggregation disorders (Nixon, 2013), autophagy activating drugs act upstream of the substrate selection and may lead to non-specific degradation of soluble cellular proteins. In this regard, upregulating proteasome function may face similar bottlenecks, although substrate ubiquitination confers some degree of selectivity for proteasomal degradation. Therefore, boosting the cellular disaggregation capacity may be a more specific approach to deal with protein aggregates (Shorter, 2016). The absence of an Hsp100 homolog in metazoans has led to efforts in the last decade towards harnessing the potential of yeast and archaeal unfoldases to counteract protein aggregation (Brooks et al., 2018; Jackrel et al., 2014). Assuming that disaggregation is a general function of VCP in higher eukaryotes, then boosting the levels or activity of VCP may aid aggregate clearance. However, our results suggest otherwise. VCP is a highly abundant protein in eukaryotes (Zeiler et al., 2012) and further overexpressing wild-type VCP, or a mutant with

enhanced unfoldase activity, did not improve the efficiency of aggregate clearance (Figure 59A). Thus, neither VCP abundance nor activity is limiting for disaggregation. A major question for future research is to discover the rate-limiting step in this pathway, followed by its modulation to achieve aggregate clearance. Moreover, it should also be considered that therapeutic strategies targeting disaggregation might aid aggregate spreading, and could benefit from being combined with upregulated proteasomal activity to effectively eliminate all aggregate material downstream of disaggregation.

5. MATERIALS

5.1 CELL CULTURE REAGENTS

Description	Company	Catalog #
DMEM	Biochrom	F0435
EBSS	Gibco	24010-043
FBS	Gibco	10270-106
L-Glutamine	Gibco	25030-024
Pen/Strep	Gibco	15140-122
Trypsin	Gibco	12605-010
PBS	Gibco	20012-068
Non-essential amino acids	Gibco	11140-035
SILAC Deficient Medium	GE Healthcare	E15-086
Opti-MEM™ Reduced Serum Medium	Gibco	31985062
Lipofectamine® 2000	Thermo	11668027
FuGENE® 6 Transfection Reagent	Promega	E2692
DharmaFECT siRNA transfection reagent	Dharmacon	T-2001-02

5.2 INHIBITORS

Description	Company	Catalog #
3-Methyladenine	Invivogen	tlrl-3ma
Bafilomycin A1	Invivogen	tlrl-baf1
Epoxomicin	Cayman	10007806
MG132	Cayman	10012628
MLN-7243	Chemietek	CT-M7243
Lactacystin	Enzo	BML-PI104-0200
Torin	Cell Signalling	14379
NMS-873	Sigma	SML1128-5MG
VER-155008	Sigma	SML0271-5MG

5.3 ANTIBODIES

5.3.1 For western blotting

Description	Dilution	Company	Catalog #
GFP	1:1000	Roche	11814460001
Atg-5	1:1000	Cell Signalling	2630S
Atg-7	1:1000	Cell Signalling	8558
LC3B	1:2000	Sigma	L7543
p62/SQSTM1	1:2000	AbCam	ab56416
Ubiquitin FK2	1:2000	MerckMillipore	04-263
Ubiquitin Lys-48	1:1000	Millipore	05-1307
VCP	1:2000	AbCam	ab11433
Anti-Mouse HRP	1:10000	Sigma	A4416
Anti-Rabbit HRP	1:10000	Sigma	A9169

5.3.2 For immunofluorescence

Description	Dilution	Company	Catalog #
19S PSMD4	1:1000	AbCam	ab20239
20S α , β	1:1000	AbCam	ab22673
CHMP2B	1:1000	AbCam	ab33174
DNAJB1	1:500	AbCam	ab69402
Gamma-Tubulin	1:1000	Sigma	T5326
Hsp/Hsc70	1:500	Santa Cruz	sc-24
Hsp105	1:500	AbCam	ab109624
LC3B	1:1000	Sigma	L7543
NBR1	1:1000	Cell Signalling	9891
NPC	1:1000	Abcam	ab24609
NPLOC4	1:500	Sigma	HPA021560
NPM1	1:1000	Sigma	WH0004869M1
p47	1:1000	Santa Cruz	sc-376614
p62/SQSTM1	1:2000	AbCam	ab56416
Ubiquitin FK2	1:2000	MerckMillipore	04-263
Ubiquitin Lys-48	1:2000	Millipore	05-1307
Ubiquitin Lys-63	1:1000	AbCam	ab179434
UFD1L	1:500	AbCam	ab96648

VCP	1:2000	AbCam	ab11433
Vimentin	1:1000	Sigma	V6630
Anti-Mouse Cy5	1:5000	Life Technologies	A10524
Anti-Rabbit Cy5	1:5000	Life Technologies	A10523
Anti-Mouse Cy3	1:5000	Jackson ImmunoResearch	115-165-062
Anti-Rabbit Cy3	1:5000	Dianova	111-165-045

5.4 siRNAs

Description	Concentration	Company	Catalog #
Atg-7	100nM	Dharmacon	L-020112-00-0005
Atg-5	100nM	Dharmacon	M-004374-04-0005
DNAJB1	100nM	Dharmacon	L-012735-01-0005
VCP	50nM	Dharmacon	L-008727-00-0005

5.5 KITS & ACCESSORIES

Description	Company	Catalog #
μ -Columns	Miltenyi Biotech	130-042-701
μ MACS GFP Isolation kit	Miltenyi Biotech	130-091-125
μ MACS Separator	Miltenyi Biotech	130-042-602
Ni-NTA Dynabeads	Invitrogen	10103D
Plasmid Plus Midi Kit	Qiagen	12943
Q5 Site-Directed Mutagenesis Kit	New England Biolabs	E0554S
PureLink™ Genomic DNA Mini Kit	Thermo	K182001
QIAquick PCR Purification Kit	Qiagen	28104

5.6 CHEMICALS

Description	Company	Catalog #
16% Formaldehyde	Thermo	28908
3-(cyclohexylamino)-1-propanesulfonic acid (CAPS)	Sigma-Aldrich	C2632
Acrylamide/Bis Solution, 37.5:1	Serva	10688
Ammonium Persulphate	Sigma-Aldrich	A3678
AmyloGlo	Biosensis	TR-300-AG
AmyTracker	Ebba Biotech	Amytracker™680
Benzonase	MPI, Core Facility	

BSA	Serva	11924
Complete Tablets, Mini EDTA-free	Roche	04 693 159 001
Cycloheximide	Sigma-Aldrich	C7698-5G
DAPI	Thermo	D1306
DMSO	Sigma-Aldrich	D2650
Fluorescent Mounting medium	Dako	S3023
Glycerol	Merk	818709
Glycine	Roth	3187.4
GnHCl	Roth	35.3
HEPES	Roth	HN77.5
Imidazole	Roth	3899.3
Luminata Classico Western HRP Substrate	Millipore	WBLUC0500
MES PAGE Buffer	Thermo	NP0002
MOPS	Sigma-Aldrich	M3183
MOPS PAGE Buffer	Thermo	NP0001
NaCl	Roth	901318
N-Ethylmaleimide	Sigma-Aldrich	04260
NP40	United State Biochemical	19628
Ponceau	Sigma-Aldrich	P3504
Prestained protein ladder	Thermo	26616
Protein Assay Dye Reagent Concentrate	Biorad	5000006
Restore TM Western Blot Stripping Buffer	Thermo	21059
RIPA	Thermo	89900
SDS Pellets	Serva	20765
TEMED	Sigma-Aldrich	T7024
Tris	Sigma-Aldrich	A4416
Triton X-100	Sigma-Aldrich	T9284
Tween-20	Sigma-Aldrich	P9416-100ML
β-mercaptoethanol	Sigma-Aldrich	M6250

5.7 SOFTWARES

Description	Developer
AIDA Image analyser 4.27.039	Raytest, Straubenhardt, Germany
Adobe Illustrator CC 2018	Adobe Systems, San Jose, USA
Adobe Photoshop CC 2018	Adobe Systems, San Jose, USA
ImageJ	National Institutes of Health, MD, USA

Perseus 1.2.6.3	Max Planck Institute of Biochemistry, Martinsried, Germany
Snap Gene	GSL Biotech LLC, Chicago, USA

5.8 PLASMIDS

Name	Backbone	Antibiotic Resistance	Reference
Htt97Q-mCherry	pcDNA3.1	Amp	Gupta et al., 2011
Htt97Q-myc	pcDNA3.1	Amp	Woerner et al., 2016
VCP-myc	pcDNA3.1	Amp	This study, see methods
VCP-A232E-myc	pcDNA3.1	Amp	This study, see methods
VCP-E305Q/E578Q-myc	pcDNA3.1	Amp	This study, see methods
VCP-R115H-myc	pcDNA3.1	Amp	This study, see methods
α -S824	pcDNA3.1	Amp	Olzscha et al., 2011
β 4	pcDNA3.1	Amp	Olzscha et al., 2011
β 17	pcDNA3.1	Amp	Olzscha et al., 2011
β 23	pcDNA3.1	Amp	Olzscha et al., 2011
His ₆ -Ub	pcl	Amp	Addgene #31815

5.9 HUMAN CELL LINES

Name	Background	Description/ Reference	Source
Fluc- EGFP	HEK293	Wild-type luciferase fused to EGFP	From Dr. Gopal Jayaraj, Hartl lab, MPI Biochemistry
Clone1 (Tau RD (LM))	HEK293	Sanders et al., 2014	Gift from Prof. Marc Diamond, UT Southwestern, Texas
Clone9 (Parental)	HEK293	Sanders et al., 2014	Gift from Prof. Marc Diamond, UT Southwestern, Texas
Clone10 (Parental)	HEK293	Sanders et al., 2014	Gift from Prof. Marc Diamond, UT Southwestern, Texas
Tet-Clone1	HEK293	Sanders et al., 2014	Gift from Prof. Marc Diamond, UT Southwestern, Texas
Tet-Clone10	HEK293	Sanders et al., 2014	Gift from Prof. Marc Diamond, UT Southwestern, Texas
Tau RD (WT)	HEK293	Sanders et al., 2014	Gift from Prof. Marc Diamond, UT Southwestern, Texas

Tau RD (Δ K280/2P)	HEK293	Sanders et al., 2014	Gift from Prof. Marc Diamond, UT Southwestern, Texas
Tau FRET Biosensor	HEK293T	Tau RD(LM)-EYFP and Tau RD(LM)- mTurquoise2	From Dr. Patricia Yuste-Checa Hartl lab, MPI Biochemistry

5.10 MEDIA AND BUFFERS

Buffer	Recipe
LB media	10 g NaCl, 5 g Yeast extract, 10 g Tryptone in 1L water
SILAC Media	Deficient DMEM 4.5 g/l glucose, 10% Dialysed FCS, Pen/Strep, stable glutamine, Isotope labelled Heavy (R-HCl+10, K-2HCl+8), Medium (R-HCl+6, K-2HCl+4), Light (R-HCl, K-HCl) amino acids at 70% concentration of orthodox DMEM
CAPS transfer buffer	10 mM CAPS pH 11, 20% Methanol
Lamelli buffer (2x)	100 mM Tris pH6.8, 4% SDS, 0.2% Bromophenol Blue, 20% Glycerol, (freshly added), 5% β -mercaptoethanol
MOPS PAGE buffer (10x)	500 mM MOPS, 500 mM Tris, 10 mM EDTA, 1% SDS
Ni-NTA Elution Buffer	2x SDS loading buffer, β -mercaptoethanol, 300 mM Imidazole
Ni-NTA Lysis Buffer	6 M GnHCl, 0.1 M HEPES, 5 mM Imidazole pH 7.4
Ni-NTA Wash Buffer	300 mM NaCl, 50 mM Tris, 20 mM Imidazole, 1% NP40 pH 7.6
RIPA lysis buffer	50 mM Tris pH7.4, 0.1% SDS, 150 mM NaCl, 0.5% Sodium deoxycholate, 1% NP40
TBS	20 mM Tris, 137 mM NaCl pH 7.4
TBS-T	20 mM Tris, 137 mM NaCl pH 7.4, 0.01% Tween-20
Transformation buffer-I	30 mM Potassium Acetate, 50 mM Manganese Chloride, 100 mM Rubidium Chloride, 10 mM Calcium Chloride, 15% Glycerol, final pH 5.8 adjusted with Acetic Acid
Transformation buffer-II	10 mM MOPS, 75 mM Calcium Chloride, 10 mM Rubidium Chloride, 15% Glycerol, final pH 6.8 adjusted with 1 M NaOH
Tris-Glycine PAGE buffer	15 g/L Tris, 72 g/L Glycine, 5 g/L SDS
Tris-Glycine transfer buffer	50 mM Tris, 40 mM Glycine, 1 mM SDS, 20% Methanol

5.11 MISCELLANEOUS

Description	Company	Catalog #
Polycarbonate tubes (11x34mm)	Beckman Coulter	343778
Polycarbonate tubes (8x34mm)	Beckman Coulter	343776
12-well plates	Falcon	353043
6-well plates	Falcon	353046
10 cm dishes	Falcon	353003
Poly-L-Lysine coverslips	NeuVibro	GG-12-PLL
Uncoated glass coverslips	NeuVibro	GG-12-pre
Cuvettes, Acrylic 10x4x45mm	Sarstedt	67.74
Nitrocellulose membrane	GE Healthcare	10600002
PVDF membrane	Roche	3010040001
Cellulose acetate membrane	GE Healthcare	10404131

6. METHODS

6.1 REGENERATION OF CLONE9 AND CLONE10 CELL LINES

The regeneration protocol was adapted from Sanders et al. with minor modifications.

6.1.1 Preparation of cell lysates

Parental Clone9 and Clone10 cells were harvested, washed with PBS and pelleted. Cell pellets were re-suspended by gentle pipetting in 0.05% Triton X-100 in PBS supplemented with protease inhibitor cocktail and kept on ice for 20 min. Lysates were centrifuged at 1000xg for 5 min to sediment cell debris. Supernatant was collected and protein concentration was determined using a standard Bradford assay. In order to minimize the amount of detergent later added to cells with the lysates, the lysates should roughly have a protein concentration of up to ~10 µg/µL. Lysates were used immediately after preparation.

6.1.2 Seeding Clone1 with aggregate containing lysates

24 h before treatment 100,000 Clone1 cells were plated in 12 well plates. 30 µg of freshly prepared lysate was diluted in 100 µL reduced serum medium optimum. In a separate tube 4 µL Lipofectamine 2000 was diluted in 100 µL optimum and incubated at room temperature (RT) for 5 min. Contents of the tubes were gently mixed together and incubated again at RT for 20 min. The lysate-lipofectamine mixture was added to cells drop-wise and incubated.

6.1.3 Propagation and selection of aggregate containing cells

24 h later cells were trypsinized and re-plated in a 6-well plate. 3 days later cells were re-split and sparsely plated in 10 cm dishes (<200 cells/dish) to allow the formation of well separated colonies. The cells were allowed to grow for 8 days until clear colonies were observed. 48 colonies were randomly picked and each transferred to a well in 48 well plate. Colonies were allowed to attach and were then screened for the presence of aggregates under a fluorescent microscope. Clones displaying aggregate morphologies similar to parental Clone9 and Clone10

were confirmed by confocal imaging. Selected clones were amplified and frozen in fetal bovine serum (FBS) containing 10% DMSO as single use aliquots and stored at -80°C for future use.

6.2 CELL CULTURE AND MAINTENANCE

Tau-YFP clones and parental HEK293 cells used to generate these clones (provided by Marc Diamond lab) were cultured in Dulbecco's MEM supplemented with 10% FBS, 2 mM L-Glutamine, 100 Units/mL Penicillin, 100 µg/mL Streptomycin and non-essential amino acids cocktail and grown at 37°C in a 5% CO₂ incubator. No selection antibiotics were added in the media for tau clones. HEK293 cells expressing WT firefly luciferase fused EGFP (WT-Fluc-EGFP: Generated in the Hartl lab by Dr. Gopal Jayaraj) were maintained in 50 µg/mL hygromycin containing media.

6.3 CHEMICAL TREATMENTS

Cells were plated 24 h (Tet-Clones1 &10) to 48 h (Clones 1, 9, 10) before treatment. Treatments were performed at the following concentrations for 24 h in DMEM or EBSS as indicated.

Inhibitor	Working concentration	Target
Doxycycline	50ng/mL	Tau shut-off in Tet-Clones
3-Methyladenine	5mM	Autophagy inhibitor (Early stage)
Bafilomycin A1	50nM	Autophagy inhibitor (Late stage)
Epoxomicin	50-100nM	Proteasome Inhibitor
MG132	1-5µM	Proteasome Inhibitor
Lactacystin	10µM	Proteasome Inhibitor
NMS-873	2.5µM	VCP inhibitor
VER-155008	10µM	Hsp70 inhibitor
MLN-7243	0.1-0.5µM	UAE E1 inhibitor

6.4 GENOMIC SEQUENCING OF TAU-YFP CONSTRUCT IN CELL LINES

Genomic DNA was isolated from $\sim 5 \times 10^6$ Clone1 and Tet-Clone1 cells. PCR primers were designed using the online primer design tool Primer3. To sequence the tau segment in Clone1, 3 primer pairs were tested. The forward primers were selected from the UbC promoter region and reverse primers from YFP as follows:

Primer Description	Sequence	Tm
UbCFwd_1	CTGAAGCTCCGGTTTTGAACTAT	66°C
YFPRev_1	GCTGAACTTGTGGCCGTTTAC	
UbCFwd_2	GGTCGGTTTTATGTACCTATCTTCTTA	64°C
YFPRev_2	AGATGAACTTCAGGGTCAGCTTG	
UbCFwd_3	ATAAGTGAGGCGTCAGTTTCTTTG	66°C
YFPRev_3	AGATGAACTTCAGGGTCAGCTTG	

The Tet-Clone1 construct was sequenced in two steps. To sequence the tau segment in Tet-Clone1, forward primer was placed in the TRE tight promoter and the reverse primer in YFP. To sequence downstream of YFP, a second primer pair with a UbC forward and tTA reverse primer was used.

Primer Description	Sequence	Tm
TRE_Fwd	GTATGTCGAGGTAGGCGTGT	67°C
YFPRev_1	GCTGAACTTGTGGCCGTTTAC	
UbCFwd_1	CTGAAGCTCCGGTTTTGAACTAT	66°C
tTA_Rev	CTGTTTTTCTGTAGGCGTGT	

The PCR was performed in a 25 μ L reaction with the following components:

Reagent	1X
Q5 reaction buffer	5 μ L
10mM dNTPs	0.5 μ L
10 μ M Fwd Primer	1.25 μ L
10 μ M Rev Primer	1.25 μ L
gDNA template	50ng (1 μ L)
Q5 polymerase	0.25 μ L
dH ₂ O	Upto 25 μ L (16.75 μ L)

PCR reaction was run for 35 cycles according to the following parameters:

Reaction step	Temperature	Duration
Denaturation	98°C	30s
<i>Cycle denaturation</i>	98°C	10s
<i>Annealing (as per primer T_m)</i>	66/64°C	30s
<i>Extension</i>	72°C	30s
Final extension	72°C	2min
Hold	4°C	∞

The PCR products were purified with a PCR purification kit, eluted in 30 μ L dH₂O and sequenced.

6.5 siRNA TRANSFECTIONS

Cells were plated at 85,000 (Tet-Clones) or 150,000 (Non-Tet-Clones) cells per well in a 24-well plate in 500 μ L of antibiotic free media. 2 μ L of Dharmafect transfection reagent or 50-100 nM of non-targeted or targeted siRNA was diluted in 50 μ L optimum in separate tubes and incubated at RT for 5 min. Contents of the tubes were mixed gently by pipetting and incubated further at RT for 15 min. the transfection mixture was added to the cells drop-wise. 24 h later cells were split and plated in 12- or 6-well plates and allowed to grow additionally for 48-72 h before protein was analysed. Doxycycline treatments were done 72 h post siRNA transfection.

6.6 WESTERN BLOTTING

6.6.1 Sample preparation & electrophoresis

Cells were harvested by trypsinization, washed once with PBS, pelleted and stored at -20°C or lysed directly in RIPA buffer supplemented with protease inhibitors and benzonase. 20 mM N-ethylmaleimide was included in the buffer whenever cells were lysed for the detection of ubiquitinated proteins. Cells were kept on ice for 30 min with intermittent vortexing. Protein concentration in total cell lysates was determined using Bradford reagent against a BSA standard curve and normalized in all samples before adding 2x Laemmli buffer. Samples were denatured by boiling at 95°C for 5 min.

To resolve tau, 10-20 µg total protein was resolved on self-made 10% Tris-Glycine gels or on commercial NuPAGE 4-12% gradient gels with MES or MOPS running buffer at 200 V for 45 min. For LC3 detection, electrophoresis was carried out on self-made 15% Tris-Glycine gels. 40 µg total protein was loaded to detect Atg5 and Atg7.

6.6.2 Transfer and imaging

Proteins were transferred to nitrocellulose or PVDF membrane in tris-glycine buffer on 110 V for 1 h. LC3 was blotted on PVDF membrane and transferred in 3-(Cyclohexylamino)-1-propanesulfonic acid (CAPS) buffer. Membranes were washed 1x in TBS-T and blocked in 5% low-fat dry milk dissolved in TBS-T for 1 h at RT. Primary antibodies were diluted in blocking solution at concentrations listed in section 5.3.1 and incubated overnight at 4°C. Subsequently, blots were washed 3 times with TBS-T and probed with HRP conjugated anti-mouse (1:10000 in TBS-T) or anti-rabbit (1:20000 in blocking solution) secondary antibodies for at least 1 h at RT. Thereafter, blots were washed 3 times with TBS-T and chemiluminiscence was developed using an HRP substrate and detected on a Fuji LAS 4000 imager. AIDA image software was used to quantify intensity of protein bands. Microsoft Excel was used for plotting graphs and computing statistical parameters.

6.7 FLUORESCENT STAINING

6.7.1 Antibody staining

Cells were grown on poly-L-lysine coated glass coverslips for 24 h (Tet-Clones) or 48 h (Non-Tet-Clones) in 12-well plates before any treatment. At the end of the experiment, media was aspirated and cells were directly fixed in 4% formaldehyde for 10 min at RT. Cells were washed once with PBS and permeabilized in 0.1% TritonX-100 in PBS for 5 min. For staining LC3, coverslips were additionally treated with 1:1 mixture of ice-cold methanol-acetone for 5 min and subsequently washed once with PBS. Cells were then blocked with 5% low-fat dry milk dissolved in PBS supplemented with 0.1% TritonX-100 for 1 h at RT. Primary antibodies at dilutions listed in section 5.3.2 were applied to cells in blocking solution overnight. Afterwards cells were

washed 3 times with PBS and incubated with fluorescently labelled secondary antibodies at dilutions 1:5000 in PBS for at least 1 h. Finally, cells were counterstained with DAPI and coverslips were mounted in fluorescent mounting medium on glass slides and stored at 4°C until imaging. Images were acquired with a Zeiss LSM 780 confocal scanning microscope and analysed using ImageJ software.

6.7.2 Amyloid dye staining

Cells were fixed and permeabilized as described in section 6.7.1 followed by a PBS wash. AmyloGlo was applied at a dilution of 1:200 in PBS for 10 min and AmyTracker at 1:1000 in PBS for 30 min with gentle shaking. Thereafter cells were washed 2 times with PBS for 5 min. AmyloGlo absorption-emission spectra overlaps with DAPI, therefore only AmyTracker stained cells were counterstained with DAPI. Cells were mounted and imaged as described earlier.

6.8 QUANTIFICATION OF AGGREGATES/CELL AND AVERAGE SIZE

The images were acquired with a Zeiss LSM 780 scanning confocal microscope. In order to analyse the entirety of cell volume for aggregates, z-stacks were acquired. The z-stacks were used to create a maximum intensity projection (MIP) using the image acquisition software ZEN. MIPs were further analysed using ImageJ software. Image type was converted to 8-bit and a threshold of 0-30 or 0-40 was set. Thresholded images were processed into binary images and aggregate number and size were computed by the Analyse Particle feature. Number of cells were determined by manually counting the DAPI stained nuclei with the help of Cell Counter plugin. At least 100 cells per condition were analysed. Experiments were performed minimum 3 times in biologically independent repeats.

6.9 BIOCHEMICAL DETECTION OF AGGREGATED TAU

Cells were subjected to treatments as indicated, and harvested. Lysis was performed in 1% TritonX-100 followed by sonication for 10 s (5 s pulse, 30 s pause) at 10% power or without sonication in RIPA buffer for 30 min on ice. Lysates were pre-cleared at 2000xg for 5 min.

Supernatant was carefully removed and protein concentration was normalized across all samples. Lysates were then subjected to the following assays:

6.9.1 Ultracentrifugation based solubility assay

50-100 μ L lysate was centrifuged at 186,000xg for 1 h at 4°C. Supernatant was removed and the pellet was washed with 200 μ L PBS and centrifuged again for 30 min. Pellet was re-suspended by vigorous pipetting in the same volume of PBS as the supernatant to have them directly comparable.

6.9.2 Filter trap assay

Upto 100 μ g (for Clone9, Clone10) and 200 μ g (for Tet-Clone10) total protein from the lysates was diluted in 200 μ L lysis buffer. Cellulose acetate membrane was pre-equilibrated in 0.1% SDS and affixed to the filter trap apparatus. Samples were loaded and allowed to be completely drawn through. Wells were then washed 3 times with 200 μ L 0.1% SDS followed by standard immuno-blotting of the membrane.

6.10 AMINO ACID STARVATION

Cells were first grown in full medium on cover slips or directly on plates for 48 h. Afterwards, media was aspirated and directly replaced with either full medium or EBSS.

6.11 DETECTION OF TAU UBIQUITINATION BY BIOCHEMICAL ASSAYS

6.11.1 Denaturing ubiquitin pulldown

Equal numbers of cells were plated in 10 cm dishes and transfected next day with a His₆-Ub plasmid (Addgene Plasmid#31815) using Fugene. 24 h after transfection cells were treated with 5 μ M MG132 and harvested another 24 h later. 1/10th of the cells were lysed directly in Laemmli buffer to be used as the input fraction. Rest of the cells were lysed in 800 μ L lysis buffer (6 M GnHCl, 0.1 M HEPES, 5 mM Imidazole pH 7.4) with end over end rotation for 30 min at 4°C. All the samples were sonicated with a tip sonicator for 10 s at 10% power to shear the DNA. Sonicated lysates were centrifuged at 16,000xg for 10 min and clarified supernatant was

collected. 50 μ L Ni-NTA Dynabeads (Invitrogen Cat#10103D) were equilibrated in 500 μ L lysis buffer shortly before adding the clarified lysate. The lysate was incubated with the beads end over end for 15 min at RT. Thereafter beads were washed 2 times with 500 μ L lysis buffer and 4 times with wash buffer (300 mM NaCl, 50 mM Tris, 20 mM Imidazole, 1% NP40 pH 7.6). Bound proteins were eluted in 100 μ L elution buffer (2x SDS loading buffer, β -mercaptoethanol, 300 mM Imidazole). Input and eluate fractions were resolved on self-made 10% Tris-Glycine gels, transferred to nitrocellulose membranes and probed with antibodies against GFP or ubiquitin.

6.11.2 Non-denaturing Tau-YFP pulldown

Cells were plated in 10 cm dishes (\sim 3- 3.5x10⁶) and allowed to settle for 48 hr. Cells were harvested by trypsinization, washed in cold PBS and pelleted. The cell pellets were resuspended by vortexing in 400 μ L ice cold RIPA buffer supplemented with protease inhibitor cocktail and 20 mM NEM. Lysates were sonicated with a tip sonicator for 10 s at 10% power and centrifuged at 2000xg for 5 min. Protein concentration was determined using Bradford reagent against a BSA standard curve. 50 μ L anti-GFP beads were added to 1000 μ g total protein diluted in a total volume of 600 μ L RIPA buffer. Lysates were incubated for 1 h at 4°C with end over end rotation. μ -Columns were placed in the magnetic field of μ MACS Separator and equilibrated with 250 μ L lysis buffer. Cell lysates were applied onto the column and allowed to run through. Columns were washed 4 times with 1 mL 0.1% SDS in PBS. Bound proteins were eluted by applying 50 μ L pre-heated (95°C) 1x Laemmli buffer. Input and eluates were resolved on commercial NuPAGE 4-12% gradient gels in MOPS running buffer and transferred to nitrocellulose membranes. Membranes were probed with antibodies against GFP or ubiquitin K48 chains.

6.12 INTERACTOME ANALYSIS

6.12.1 SILAC labelling of cells and tau-YFP immunoprecipitation

Frozen aliquots of Clone1, 9 and 10 cells were thawed directly into SILAC media containing light (L), medium (M) and heavy (H) amino acid isotopes respectively. Cells were passaged for a minimum of two weeks to allow efficient incorporation of amino acid isotopes into the cellular proteome. For tau-YFP immunoprecipitation (IP), cells were plated in 10 cm dishes (\sim 3- 3.5x10⁶)

in respective SILAC media and allowed to settle for 48 hr. Afterwards, cells were harvested by trypsinization, washed in cold PBS and used for IP the same day. The cell pellets were lysed by gentle pipetting in 400 μ L ice cold lysis buffer, 1% TritonX-100 in PBS supplemented with protease inhibitor cocktail. Lysates were sonicated with a tip sonicator for 10 s at 10% power (5 s pulse- 30 s pause- 5 s pulse) and centrifuged at 2000xg for 5 min at 4°C. 300 μ L of the supernatant was removed and protein concentration was determined using Bradford reagent against a BSA standard curve. 50 μ L anti-GFP beads were added to 500 μ g total protein diluted in a total volume of 800 μ L lysis buffer. Lysates were incubated for 1 h at 4°C with end over end rotation at 10 rpm. μ -Columns were placed in the magnetic field of μ MACS Separator and equilibrated with 250 μ L lysis buffer. Cell lysates were applied onto the column and allowed to run through. Columns were washed 4 times with 1 mL cold wash buffer (0.05% TritonX-100 in PBS) and 2 times with 1mL PBS. 1x Laemmli buffer without bromophenol blue was used as elution buffer. 20 μ L of pre-heated elution buffer was applied to the column and incubated for 5 min at room temperature. 50 μ L of additional elution buffer was applied to the column and collected eluate was used for further processing.

6.12.2 MS Sample processing

20 μ L sample from each of the H, M and L eluates was mixed and processed by the filter-aided sample preparation (FASP) method as previously described (Wisniewski et al., 2011). The sample was loaded in a 30 kDa centrifugation device and washed 3 times with 200 μ L freshly prepared urea buffer (UB) (8 M urea, 0.1 M Tris pH 8.5). Reduction and alkylation was performed sequentially using 10 mM DTT and 50 mM Acetamide in UB respectively. Samples were washed 2 times with 200 μ L 50 mM ammonium bicarbonate (NH_4HCO_3) to remove urea before an overnight trypsin treatment. Peptides were recovered in 40 μ L NH_4HCO_3 , diluted with 25% TFA and dried in a vacuum concentrator. The peptides were further fractionated using home-made SAX columns in 200 μ L microtips by stacking 2 punch-outs of Empore High Performance Extraction Disk (Anion-SR) material. Peptides were sequentially eluted with 6 different Britton & Robinson buffers (BURB) of decreasing pH (pH 11, 8, 6, 5, 4, 3) and acidified with 20% TFA solution. The fractionated peptides were desalted with home-made micro-columns containing C18 Empore

disk and eluted with 70% ACN 1% formic acid followed by drying in a vacuum concentrator. The samples were stored at -20°C until analysis.

6.12.3 LC-MS

The desalted peptides were dissolved in 5 μ L of 5% formic acid, sonicated in an ultrasonic bath, centrifuged and transferred to MS autosampler vials. Samples were analyzed on an Easy nLC-1000 nanoHPLC system (Thermo) coupled to a Q-Exactive Orbitrap mass spectrometer (Thermo). Peptides were separated on home-made spray-columns (ID 75 μ m, 20 cm long, 8 μ m tip opening, NewObjective) packed with 1.9 μ m C18 particles (Reprosil-Pur C18-AQ, Dr Maisch GmbH) using a stepwise 115 min gradient between buffer A (0.2% formic acid in water) and buffer B (0.2% formic acid in acetonitrile). Samples were loaded on the column by the nanoHPLC autosampler at a flow rate of 0.5 μ l per min. No trap column was used. The HPLC flow rate was set to 0.25 μ l per min during analysis. MS/MS analysis was performed with standard settings using cycles of 1 high resolution (70000 FWHM setting) MS scan followed by MS/MS scans (resolution 17500 FWHM setting) of the 10 most intense ions with charge states of 2 or higher.

6.12.4 MS data analysis

Protein identification and SILAC based quantitation was performed using MaxQuant (version 1.5.4.1) using default settings. For identifying ubiquitination, Gly-Gly modification of lysine was included as variable modification. The human sequences of UNIPROT (version 2019-03-12) were used as database for protein identification. MaxQuant used a decoy version of the specified UNIPROT database to adjust the false discovery rates for proteins and peptides below 1%. Enrichment or depletion of an identified protein in at least two repeat experiments indicated alteration of abundance of the protein during the experiment.

6.13 FIREFLY LUCIFERASE AGGREGATION AND DISAGGREGATION ANALYSIS

100,000 WT-Fluc-EGFP expressing cells were plated on uncoated glass coverslips in 12-well plates. Next day, cells were treated with 5 μ M MG132 and heat shocked at 43°C for 2 h. One set of cells was fixed immediately after heat shock. For the other sets, fresh media was provided which did not contain any inhibitors or contained 1 μ M MG132, 2.5 μ M NMS-873 or 10 μ M VER-

155008 and cells were allowed to recover at 37°C for 8 h. As a control cells not exposed to heat shock were also treated with the inhibitors for 8 h. At the end of 8 h, cells were fixed and visualized.

6.14 HEK293T FRET BIOSENSOR CELL LINE GENERATION

A stable HEK293T cell line expressing the tau RD (aa 244-372) including the mutations P301L and V337M (tau RD-LM) fused to EYFP and tau RD-LM fused to mTurquoise2 was generated. HEK293T cells were transfected with both constructs cloned into the N1 backbone plasmid with lipofectamine 3000 (Thermo Fisher Scientific) following the manufacturer's instructions. Monoclonal cell lines expressing both tau fusion proteins were then sorted in a 96-well plate with a BD FACS Aria III following amplification. The most sensitive monoclonal cell line to study tau aggregation by flow cytometry (FRET signal detection) was selected.

6.15 TAU-YFP SEEDING ASSAY

Clone 10 cells were plated in 6- or 12-well plates. After attachment, cells were treated with 2 µM NMS-873, 10 µM VER-155008 or 50 nM Epoxomicin for 24 h or 0.5 µM MLN7243 for 12 h. The corresponding controls were performed adding the same amount of DMSO. Cells were lysed with 0.05% Triton-X, protease inhibitor and benzonase for 20 min on ice. Total protein concentration of the lysates was determined using Bio-Rad protein assay following manufacturer's instructions. In order to normalize the seeding material by the amount of tau, western blot was performed using anti-GFP antibody and anti-GAPDH antibody as loading control.

HEK293T FRET Biosensor cells were plated in 6- or 12-well plates. For 6-well plate experiment, 400 ng of total lysate of the control sample (DMSO treatment) and the corresponding amount of lysate containing the same amount of tau protein (normalized by WB) of the treated samples was combined with 120 µl of OptiMEM. 117 µl of OptiMEM mixed with 6 µl of lipofectamine 3000 were then added to the lysate-OptiMEM mix. The mixture was incubated for 20 min at RT and then added to the cells with 1 ml of fresh media. For 6-well plate experiment, 20 ng of total lysate of the control sample (DMSO treatment) and the corresponding amount of lysate containing the

same amount of tau protein (normalized by WB) of the treated samples was combined with a mixture of 1.6 μ l of lipofectamine 3000 and 50 μ l OptiMEM. The mixture was incubated for 20 min at RT and then added to the cells with 0.5 ml of fresh media. After 24 h cells were harvested with trypsin, washed with PBS and analysed on an Attune NxT flow cytometer. To measure mTurquoise2 and FRET fluorescence signal, cells were excited by 405 nm laser and fluorescence was collected with 440/50 nm and 530/30 nm filters, respectively. To measure YFP fluorescence signal, cells were excited with 488 nm laser and emission was collected by 530/30 nm filter. For each sample 50,000 single cells were evaluated. The data was processed using FlowJo V9 software (FlowJo LLC). After gating single cells, an additional gate was introduced to exclude cells that exert false-positive signal in the FRET channel due to single YFP positive cells being excited at 405 nm. FRET positive gate was drawn by plotting FRET fluorescence signal vs mTurquoise2 fluorescence signal using not seeded cells as reference.

6.16 SIZE EXCLUSION CHROMATOGRAPHY

Clone10 cells were plated in a T175 flask. After attachment, cells were treated with 2 μ M NMS-873. The corresponding control was performed adding the same amount of DMSO. After 24 h, cells were harvested and lysed with 0.05% Triton-X, protease inhibitor and benzonase for 20 min on ice. The lysate was clarified by centrifugation at 1000xg 5 min at 4 °C and filtered with a PVDF 0.22 μ m filter. The total protein amount of the lysates was determined by Bio-Rad protein assay. The same amount of total protein (3 mg) was loaded on a Superose 6 HR10/30 (GE Healthcare) column equilibrated with PBS. The individual fractions separated by SEC were analysed and quantified by WB using anti-GFP antibody. The intensity of the bands were quantified by Aida v4.27.039 software (Elysia Raytest). Tau-YFP species were detected in the void volume (VV) and low molecular weight (LMW) fraction. Corresponding fractions were pooled and analysed by western blotting using anti-GFP antibody and quantified measuring the YFP fluorescence on a CLARIOstar (BMG Labtech) using purified tau-YFP as reference (excitation 497-15 nm; emission 540-20 nm). Seeding experiment was performed as described before in a 6-well plate using 400 ng of total lysate of the control sample (DMSO treatment) and the corresponding amount of lysate containing the same amount of tau protein (normalized by

western blotting) of the treated sample or 0.5 ng of tau-YFP in the case of the VV and LMW fractions.

6.17 GENERATION OF VCP-MYC CONSTRUCTS

VCP-EGFP constructs (WT, R155H, A232E, and E305Q/E578Q) were obtained from Addgene (#23971, #23972, #23973, #23974). VCP fragments were excised from the plasmids using HindIII & BamHI and inserted in mAppleN1 vectors (Addgene #54567) to generate VCP-mApple fusion constructs. These plasmids were not used in this study. Myc-tags and stop codons were introduced at the C-terminus of VCP in the VCP-mApple plasmids via site-directed mutagenesis. The resulting VCP-myc-stop fragment was cut out using HindIII & BamHI and inserted in pcDNA3.1 vector.

6.18 GENERATION OF TRANSFORMATION COMPETENT *E. coli*

DH5 α cells from a single colony were grown in 5 mL LB media overnight with shaking at 37°C. Next day the overnight culture was used to inoculate 500 mL of fresh LB media and grown until OD₆₀₀ 0.5 was reached. Cells were then pelleted by centrifugation at 5,000xg for 10 min at 4°C. The cell pellet was re-suspended in 125 mL of ice-cold transformation buffer-I and incubated on ice for 20 min. The cells were again pelleted by centrifugation and gently suspended in 20 mL ice-cold transformation buffer-II. The suspension was made into 50 μ L aliquots in pre-chilled Eppendorf tubes, snap frozen in liquid nitrogen and stored at -80°C.


6.19 PLASMID PREPARATION

50 μ L competent DH5 α cells were thawed on ice, incubated with 100 ng plasmid DNA for 15 min, heat shocked for 90 s at 42°C and replaced on ice for 5 min. 1 mL of LB media was added to the cells and incubated at 37°C for 1 h with shaking. The cells were spread on LB plates containing Ampicillin or Kanamycin and allowed to grow overnight at 37°C. Next day single colonies were picked and inoculated in 50 mL liquid LB media containing 50 μ g/ml Ampicillin or 10 μ g/mL Kanamycin. Plasmid purification for mammalian cell transfections was performed

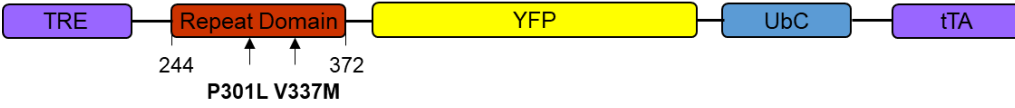
using a Qiagen Plasmid Plus Midi Kit after manufacturer's instructions. Plasmids aliquots were stored at -20°C until further use.

7. APPENDIX

Supplementary Table 1: Genomic DNA and corresponding amino acid sequence of tau-RD from Clone1

DNA sequence	ATGCTGCAGACAGCCCCCGTGCCCATGCCAGACCTGAAGAATGTCAAG TCCAAGATCGGCTCCACTGAGAACCTGAAGCACCAGCCGGGAGGCGG GAAGGTGCAGATAATTAATAAGAAGCTGGATCTTAGCAACGTCCAGTCC AAGTGTGGCTCAAAGGATAATATCAAACACGTCTGAGGAGGCGGCAGT GTGCAAATAGTCTACAAACCAGTTGACCTGAGCAAGGTGACCTCCAAG TGTGGCTCATTAGGCAACATCCATCATAAACCAGGAGGTGGCCAGATG GAAGTAAAATCTGAGAAGCTTGACTTCAAGGACAGAGTCCAGTCGAAG ATTGGGTCCCTGGACAATATCACCCACGTCCCTGGCGGAGGAAATAAA AAGATTGAAACCCACAAG
Amino acid sequence	MLQTAPVPMPDLKNVKSIGSTENLKHQPGGGKVQIINKKLDLSNVQSKC GSKDNIKHVLLGGGSVQIVYKPVLDLSKVTSKCGSLGNIHHKPGGGQMEVKS EKLDFKDRVQSKIGSLDNITHVPGGGNKKIETHK
Construct architecture	 <p>Tau-RD sequence corresponds to aa243-aa375 of full-length human tau.</p>

Supplementary Table 2: Genomic DNA and corresponding amino acid sequence of tau-RD from Tet-Clone1

DNA sequence	ATGCAGACAGCCCCCGTGCCCATGCCAGACCTGAAGAATGTCAAGTCC AAGATCGGCTCCACTGAGAACCTGAAGCACCAGCCGGGAGGCGGGAA GGTGCAGATAATTAATAAGAAGCTGGATCTTAGCAACGTCCAGTCCAAG TGTGGCTCAAAGGATAATATCAAACACGTCTGAGGAGGCGGCAGTGTG CAAATAGTCTACAAACCAGTTGACCTGAGCAAGGTGACCTCCAAGTGT GGCTCATTAGGCAACATCCATCATAAACCAGGAGGTGGCCAGATGGAA GTAAAATCTGAGAAGCTTGACTTCAAGGACAGAGTCCAGTCGAAGATTG GGTCCCTGGACAATATCACCCACGTCCCTGGCGGAGGAAATAAAAAGA TTGAA
Amino acid sequence	MQTAPVPMPDLKNVKSIGSTENLKHQPGGGKVQIINKKLDLSNVQSKCG SKDNIKHVLLGGGSVQIVYKPVLDLSKVTSKCGSLGNIHHKPGGGQMEVKSE KLDLDFKDRVQSKIGSLDNITHVPGGGNKKIE
Construct architecture	 <p>Tau-RD sequence corresponds to aa244-aa372 of full-length human tau.</p>

Supplementary Table 3: List of tau-YFP interactors in Clone10/Clone1 [H/L]

Protein IDs	Protein names	Gene names	Median Ratio H/L IP
Q9UNZ2	NSFL1 cofactor p47	NSFL1C	42.7
Q9UQN3	Charged multivesicular body protein 2b	CHMP2B	18.2
P55072	Transitional endoplasmic reticulum ATPase	VCP	17.0
Q9UNM6	26S proteasome non-ATPase regulatory subunit 13	PSMD13	16.1
Q6PEV8	Protein FAM199X	FAM199X	15.2
F8VUA2	Charged multivesicular body protein 1a	CHMP1A	14.6
Q15773	Myeloid leukemia factor 2	MLF2	13.8
O43242	26S proteasome non-ATPase regulatory subunit 3	PSMD3	13.4
O00231	26S proteasome non-ATPase regulatory subunit 11	PSMD11	13.1
P62191	26S protease regulatory subunit 4	PSMC1	12.7
P17480	Nucleolar transcription factor 1	UBTF	11.6
O14545	TRAF-type zinc finger domain-containing protein 1	TRAFD1	11.5
Q13501	Sequestosome-1	SQSTM1	11.4
Q13200	26S proteasome non-ATPase regulatory subunit 2	PSMD2	11.3
H0Y6K2	Bromodomain-containing protein 2	BRD2	11.0
H0YFD6	Trifunctional enzyme subunit alpha, mitochondrial	HADHA	10.9
P55036	26S proteasome non-ATPase regulatory subunit 4	PSMD4	10.9
Q6QNY1	Biogenesis of lysosome-related organelles complex 1 subunit 2	BLOC1S2	10.8
P55084	Trifunctional enzyme subunit beta, mitochondrial	HADHB	10.0
P25788	Proteasome subunit alpha type-3	PSMA3	10.0
A8MUA9	Small ubiquitin-related modifier 4; Small ubiquitin-related modifier 2; Small ubiquitin-related modifier 3	SUMO	9.8
Q8TAT6	Nuclear protein localization protein 4 homolog	NPLOC4	9.7
P25789	Proteasome subunit alpha type-4	PSMA4	9.5
Q9UHD9	Ubiquilin-2	UBQLN2	9.2
O14818	Proteasome subunit alpha type-7	PSMA7	9.2
Q9UID3	Vacuolar protein sorting-associated protein 51 homolog	VPS51	9.0
Q14596	Next to BRCA1 gene 1 protein	NBR1	8.8
Q92890	Ubiquitin fusion degradation protein 1 homolog	UFD1L	8.8
Q15008	26S proteasome non-ATPase regulatory subunit 6	PSMD6	8.6
Q96DX7	Tripartite motif-containing protein 44	TRIM44	8.5
Q16643	Drebrin	DBN1	8.3
A0A087X2I1	26S protease regulatory subunit 10B	PSMC6	8.3

P51665	26S proteasome non-ATPase regulatory subunit 7	PSMD7	8.2
P35998	26S protease regulatory subunit 7	PSMC2	8.1
B3KVL5	Zinc finger CCHC domain-containing protein 10	ZCCHC10	7.8
Q8IXW5	Putative RNA polymerase II subunit B1 CTD phosphatase RPAP2	RPAP2	7.8
P62979	Ubiquitin	UBC	7.7
Q99460	26S proteasome non-ATPase regulatory subunit 1	PSMD1	7.4
P43686	26S protease regulatory subunit 6B	PSMC4	6.8
R4GMR5	26S proteasome non-ATPase regulatory subunit 8	PSMD8	6.6
P0CAP2	DNA-directed RNA polymerase II subunit GRINL1A	POLR2M	6.6
P49721	Proteasome subunit beta type-2	PSMB2	6.3
Q9UQ35	Serine/arginine repetitive matrix protein 2	SRRM2	6.3
O75487	Glypican-4;Secreted glypican-4	GPC4	6.1
Q9H307	Pinin	PNN	6.0
Q99615	DnaJ homolog subfamily C member 7	DNAJC7	5.9
O95816	BAG family molecular chaperone regulator 2	BAG2	5.7
Q9BYN8	28S ribosomal protein S26, mitochondrial	MRPS26	5.7
P10644	cAMP-dependent protein kinase type I-alpha regulatory subunit	PRKAR1A	5.7
A0A0C4DG62	ADP-ribosylation factor-like protein 6-interacting protein 4	ARL6IP4	5.7
Q15545	Transcription initiation factor TFIID subunit 7	TAF7	5.6
F5H442	Tumor susceptibility gene 101 protein	TSG101	5.2
Q14677	Clathrin interactor 1	CLINT1	4.8
Q16531	DNA damage-binding protein 1	DDB1	4.8
O14646	Chromodomain-helicase-DNA-binding protein 1	CHD1	4.7
G3V5Z7	Proteasome subunit alpha type-6	PSMA6	4.6
P17980	26S protease regulatory subunit 6A	PSMC3	4.6
O00232	26S proteasome non-ATPase regulatory subunit 12	PSMD12	4.5
P61964	WD repeat-containing protein 5	WDR5	4.1
O00487	26S proteasome non-ATPase regulatory subunit 14	PSMD14	4.0
P62195	26S protease regulatory subunit 8	PSMC5	4.0
P24928	DNA-directed RNA polymerase II subunit RPB1	POLR2A	4.0
O14974	Protein phosphatase 1 regulatory subunit 12A	PPP1R12A	3.9
Q5VIR6	Vacuolar protein sorting-associated protein 53 homolog	VPS53	3.8
Q8WV44	E3 ubiquitin-protein ligase TRIM41	TRIM41	3.8
F8W118	Nucleosome assembly protein 1-like 1	NAP1L1	3.6
E9PNW4	CD59 glycoprotein	CD59	3.4
Q96BQ5	Coiled-coil domain-containing protein 127	CCDC127	3.4
O43164	E3 ubiquitin-protein ligase Praja-2	PJA2	3.3
B8ZZD4	Tax1-binding protein 1	TAX1BP1	3.3

P62857	40S ribosomal protein S28	RPS28	3.3
P62873	Guanine nucleotide-binding protein G(I)/G(S)/G(T) subunit beta-1	GNB1	3.2
Q7L7X3	Serine/threonine-protein kinase TAO1	TAOK1	3.1
O75955	Flotillin-1	FLOT1	3.1
Q12899	Tripartite motif-containing protein 26	TRIM26	3.1
Q99986	Serine/threonine-protein kinase VRK1	VRK1	3.1
C9J2Y9	DNA-directed RNA polymerase II subunit RPB2	POLR2B	3.1
H3BV80	RNA-binding protein with serine-rich domain 1	RNPS1	3.0
Q9UBI6	Guanine nucleotide-binding protein G(I)/G(S)/G(O) subunit gamma-12	GNG12	3.0
I1E4Y6	PERQ amino acid-rich with GYF domain-containing protein 2	GIGYF2	3.0
P16403	Histone H1.2;Histone H1.4	HIST1H1C	3.0
P19387	DNA-directed RNA polymerase II subunit RPB3	POLR2C	3.0
Q5HYB6	Epididymis luminal protein 189	DKFZp686J1372	3.0
P06748	Nucleophosmin	NPM1	2.9
J3QLD9	Flotillin-2	FLOT2	2.9
P62879	Guanine nucleotide-binding protein G(I)/G(S)/G(T) subunit beta-2	GNB2	2.9
Q53H12	Acylglycerol kinase, mitochondrial	AGK	2.9
Q13112	Chromatin assembly factor 1 subunit B	CHAF1B	2.9
A0A087WVZ9	DNA-directed RNA polymerases I, II, and III subunit RPABC1	POLR2E	2.8
Q92820	Gamma-glutamyl hydrolase	GGH	2.8
Q96GA3	Protein LTV1 homolog	LTV1	2.8
P60709	Actin, cytoplasmic 1	ACTB	2.8
Q99613	Eukaryotic translation initiation factor 3 subunit C	EIF3C	2.7
P28066	Proteasome subunit alpha type-5	PSMA5	2.7
Q9HCM4	Band 4.1-like protein 5	EPB41L5	2.6
A0A087WYV5	Slit homolog 2 protein	SLIT2	2.6
A0A1W2PQ90	DNA repair protein RAD50	RAD50	2.5
Q9H0U4	Ras-related protein Rab-1B;Putative Ras-related protein Rab-1C	RAB1B	2.5
Q13823	Nucleolar GTP-binding protein 2	GNL2	2.4
Q07021	Complement component 1 Q subcomponent-binding protein, mitochondrial	C1QBP	2.4
Q7Z417	Nuclear fragile X mental retardation-interacting protein 2	NUFIP2	2.4
P08670	Vimentin	VIM	2.4
P19525	Interferon-induced, double-stranded RNA-activated protein kinase	EIF2AK2	2.4
Q01082	Spectrin beta chain, non-erythrocytic 1	SPTBN1	2.4
A0A0D9SF54	Spectrin alpha chain, non-erythrocytic 1	SPTAN1	2.4
P07948	Tyrosine-protein kinase Lyn	LYN	2.3

Q9UN86	Ras GTPase-activating protein-binding protein 2	G3BP2	2.3
P07900	Heat shock protein HSP 90-alpha	HSP90AA1	2.3
P46013	Antigen KI-67	MKI67	2.2
P60228	Eukaryotic translation initiation factor 3 subunit E	EIF3E	2.2
P49916	DNA ligase 3	LIG3	2.2
Q5RKV6	Exosome complex component MTR3	EXOSC6	2.2
P12931	Proto-oncogene tyrosine-protein kinase Src	SRC	2.2
P63092	Guanine nucleotide-binding protein G(s) subunit alpha isoforms short	GNAS	2.2
O75531	Barrier-to-autointegration factor	BANF1	2.2
Q9Y265	RuvB-like 1	RUVBL1	2.2
O14578	Citron Rho-interacting kinase	CIT	2.1
P27986	Phosphatidylinositol 3-kinase regulatory subunit alpha	PIK3R1	2.1
Q6WCQ1	Myosin phosphatase Rho-interacting protein	MPRIP	2.1
P08754	Guanine nucleotide-binding protein G(k) subunit alpha	GNAI3	2.1
O15234	Protein CASC3	CASC3	2.1
P17987	T-complex protein 1 subunit alpha	TCP1	2.1
Q5SRQ6	Casein kinase II subunit beta	CSNK2B	2.0
P08238	Heat shock protein HSP 90-beta	HSP90AB1	2.0
O95425	Supervillin	SVIL	2.0
Q14676	Mediator of DNA damage checkpoint protein 1	MDC1	2.0
Q14008	Cytoskeleton-associated protein 5	CKAP5	2.0

Supplementary Table 4: List of tau-YFP interactors in Clone9/Clone1 [M/L]

Protein ID	Protein Name	Gene Name	Median Ratio M/L IP
Q9UQ35	Serine/arginine repetitive matrix protein 2	SRRM2	14.1
H0YFD6	Trifunctional enzyme subunit alpha, mitochondrial	HADHA	13.5
Q6PEV8	Protein FAM199X	FAM199X	12.8
Q7Z417	Nuclear fragile X mental retardation-interacting protein 2	NUFIP2	12.4
Q99615	DnaJ homolog subfamily C member 7	DNAJC7	11.7
B3KVL5	Zinc finger CCHC domain-containing protein 10	ZCCHC10	11.0
P55084	Trifunctional enzyme subunit beta, mitochondrial	HADHB	10.9
Q15773	Myeloid leukemia factor 2	MLF2	10.4
P17480	Nucleolar transcription factor 1	UBTF	9.1
A0A0C4DG62	ADP-ribosylation factor-like protein 6-interacting protein 4	ARL6IP4	8.4
O95816	BAG family molecular chaperone regulator 2	BAG2	8.3
O75487	Glypican-4;Secreted glypican-4	GPC4	7.6
Q9UQN3	Charged multivesicular body protein 2b	CHMP2B	7.3

E7EN19	Mitogen-activated protein kinase kinase kinase kinase 4	MAP4K4	7.3
Q14677	Clathrin interactor 1	CLINT1	7.2
A8MUA9	Small ubiquitin-related modifier 4;Small ubiquitin-related modifier 2;Small ubiquitin-related modifier 3	SUMO	6.8
A0A2R8Y6L5	Dual specificity tyrosine-phosphorylation-regulated kinase 1A	DYRK1A	6.6
H0Y6K2	Bromodomain-containing protein 2	BRD2	6.3
A0A0A0MRP0	MAP7 domain-containing protein 3	MAP7D3	5.7
Q9H307	Pinin	PNN	5.5
Q8WWM7	Ataxin-2-like protein	ATXN2L	5.4
Q9UNM6	26S proteasome non-ATPase regulatory subunit 13	PSMD13	4.7
Q15545	Transcription initiation factor TFIIID subunit 7	TAF7	4.4
Q96BQ5	Coiled-coil domain-containing protein 127	CCDC127	4.3
P62191	26S protease regulatory subunit 4	PSMC1	4.3
Q13501	Sequestosome-1	SQSTM1	4.3
P51665	26S proteasome non-ATPase regulatory subunit 7	PSMD7	4.1
O14646	Chromodomain-helicase-DNA-binding protein 1	CHD1	4.0
Q13200	26S proteasome non-ATPase regulatory subunit 2	PSMD2	4.0
Q92820	Gamma-glutamyl hydrolase	GGH	3.7
O43242	26S proteasome non-ATPase regulatory subunit 3	PSMD3	3.7
Q96DX7	Tripartite motif-containing protein 44	TRIM44	3.7
Q16531	DNA damage-binding protein 1	DDB1	3.6
P55036	26S proteasome non-ATPase regulatory subunit 4	PSMD4	3.5
O00231	26S proteasome non-ATPase regulatory subunit 11	PSMD11	3.5
E9PNW4	CD59 glycoprotein	CD59	3.5
P25788	Proteasome subunit alpha type-3	PSMA3	3.5
G3V1C3	Apoptosis inhibitor 5	API5	3.4
Q99460	26S proteasome non-ATPase regulatory subunit 1	PSMD1	3.3
P35998	26S protease regulatory subunit 7	PSMC2	3.3
Q9BYN8	28S ribosomal protein S26, mitochondrial	MRPS26	3.2
P63092	Guanine nucleotide-binding protein G(s) subunit alpha isoforms short	GNAS	3.2
Q9HCG8	Pre-mRNA-splicing factor CWC22 homolog	CWC22	3.1
O14818	Proteasome subunit alpha type-7	PSMA7	3.1
Q0ZGT2	Nexilin	NEXN	3.0
H3BV80	RNA-binding protein with serine-rich domain 1	RNPS1	3.0
O15234	Protein CASC3	CASC3	3.0
P62979	Ubiquitin	UBC	3.0
Q9UNZ2	NSFL1 cofactor p47	NSFL1C	2.9
P55072	Transitional endoplasmic reticulum ATPase	VCP	2.8
D3DTX6	Neurabin-2	PPP1R9B	2.7
P10644	cAMP-dependent protein kinase type I-alpha regulatory subunit	PRKAR1A	2.6
P62873	Guanine nucleotide-binding protein G(I)/G(S)/G(T) subunit beta-1	GNB1	2.6
P50750	Cyclin-dependent kinase 9	CDK9	2.6
P28074	Proteasome subunit beta type-5	PSMB5	2.5

O14974	Protein phosphatase 1 regulatory subunit 12A	PPP1R12 A	2.5
R4GMR5	26S proteasome non-ATPase regulatory subunit 8	PSMD8	2.5
O43707	Alpha-actinin-4	ACTN4	2.4
P27986	Phosphatidylinositol 3-kinase regulatory subunit alpha	PIK3R1	2.4
Q8N9M1	Uncharacterized protein C19orf47	C19orf47	2.4
O00232	26S proteasome non-ATPase regulatory subunit 12	PSMD12	2.4
P08754	Guanine nucleotide-binding protein G(k) subunit alpha	GNAI3	2.4
Q14126	Desmoglein-2	DSG2	2.3
Q53H12	Acylglycerol kinase, mitochondrial	AGK	2.3
Q15008	26S proteasome non-ATPase regulatory subunit 6	PSMD6	2.3
O95425	Supervillin	SVIL	2.3
Q9UBI6	Guanine nucleotide-binding protein G(I)/G(S)/G(O) subunit gamma-12	GNG12	2.3
O75190	DnaJ homolog subfamily B member 6	DNAJB6	2.3
P12931	Proto-oncogene tyrosine-protein kinase Src	SRC	2.2
P62879	Guanine nucleotide-binding protein G(I)/G(S)/G(T) subunit beta-2	GNB2	2.2
A0A0D9SEI3	Cyclin-dependent kinase 11B;Cyclin-dependent kinase 11A	CDK11A	2.2
Q5VZR0	Golgi-associated plant pathogenesis-related protein 1	GLIPR2	2.2
Q6WCQ1	Myosin phosphatase Rho-interacting protein	MPRIIP	2.2
P63096	Guanine nucleotide-binding protein G(i) subunit alpha-1	GNAI1	2.2
Q9Y3X0	Coiled-coil domain-containing protein 9	CCDC9	2.2
O00161	Synaptosomal-associated protein 23;Synaptosomal-associated protein	SNAP23	2.2
Q9UN86	Ras GTPase-activating protein-binding protein 2	G3BP2	2.1
J3QLD9	Flotillin-2	FLOT2	2.1
O75955	Flotillin-1	FLOT1	2.1
P43686	26S protease regulatory subunit 6B	PSMC4	2.1
O43166	Signal-induced proliferation-associated 1-like protein 1	SIPA1L1	2.1
A0A087WWS1	THO complex subunit 1	THOC1	2.1
Q13838	Spliceosome RNA helicase DDX39B	DDX39B	2.1
Q13769	THO complex subunit 5 homolog	THOC5	2.1
O75165	DnaJ homolog subfamily C member 13	DNAJC13	2.0
Q53F19	Uncharacterized protein C17orf85	C17orf85	2.0
A0A087X295	WD repeat-containing protein 6	WDR6	2.0
Q9BY77	Polymerase delta-interacting protein 3	POLDIP3	2.0

Supplementary Table 5: List of tau-YFP interactors in Clone10/Clone9 [H/M]

Protein IDs	Protein names	Gene names	Median Ratio H/M IP
F8VUA2	Charged multivesicular body protein 1a	CHMP1A	19.8
Q9UNZ2	NSFL1 cofactor p47	NSFL1C	14.2
Q6QNY1	Biogenesis of lysosome-related organelles complex 1 subunit 2	BLOC1S2	10.2
O14545	TRAF-type zinc finger domain-containing protein 1	TRAFD1	9.3
Q16186	Proteasomal ubiquitin receptor ADRM1	ADRM1	6.6
P55072	Transitional endoplasmic reticulum ATPase	VCP	6.5
Q9UID3	Vacuolar protein sorting-associated protein 51 homolog	VPS51	6.5
F5H442	Tumor susceptibility gene 101 protein	TSG101	6.1
O43164	E3 ubiquitin-protein ligase Praja-2	PJA2	5.9
A0A0C4DFV9	Protein SET	SET	5.9
P0CAP2	DNA-directed RNA polymerase II subunit GRINL1A	POLR2M	5.7
Q8TAT6	Nuclear protein localization protein 4 homolog	NPLOC4	5.2
B8ZZD4	Tax1-binding protein 1	TAX1BP1	5.0
Q9UHD9	Ubiquilin-2	UBQLN2	4.8
Q96CS2	HAUS augmin-like complex subunit 1	HAUS1	4.6
Q9NQA3	WAS protein family homolog 6;WAS protein family homolog 1	WASH6P	4.6
Q12899	Tripartite motif-containing protein 26	TRIM26	4.6
Q8N3C0	Activating signal cointegrator 1 complex subunit 3	ASCC3	4.6
Q8IXW5	Putative RNA polymerase II subunit B1 CTD phosphatase RPAP2	RPAP2	4.6
P24928	DNA-directed RNA polymerase II subunit RPB1	POLR2A	4.3
O00231	26S proteasome non-ATPase regulatory subunit 11	PSMD11	3.7
Q15008	26S proteasome non-ATPase regulatory subunit 6	PSMD6	3.7
Q92890	Ubiquitin fusion degradation protein 1 homolog	UFD1L	3.7
C9J2Y9	DNA-directed RNA polymerase II subunit RPB2	POLR2B	3.7
Q9UNM6	26S proteasome non-ATPase regulatory subunit 13	PSMD13	3.7
P51665	26S proteasome non-ATPase regulatory subunit 7	PSMD7	3.6
Q5VIR6	Vacuolar protein sorting-associated protein 53 homolog	VPS53	3.6
P19387	DNA-directed RNA polymerase II subunit RPB3	POLR2C	3.6
O76094	Signal recognition particle subunit SRP72	SRP72	3.6
G3V5Z7	Proteasome subunit alpha type-6	PSMA6	3.6
P43686	26S protease regulatory subunit 6B	PSMC4	3.6
O43242	26S proteasome non-ATPase regulatory subunit 3	PSMD3	3.6
O00232	26S proteasome non-ATPase regulatory subunit 12	PSMD12	3.4
Q6P5Z2	Serine/threonine-protein kinase N3	PKN3	3.4

Q99460	26S proteasome non-ATPase regulatory subunit 1	PSMD1	3.3
A0A087X2I1	26S protease regulatory subunit 10B	PSMC6	3.3
P35998	26S protease regulatory subunit 7	PSMC2	3.3
Q16643	Drebrin	DBN1	3.3
Q13200	26S proteasome non-ATPase regulatory subunit 2	PSMD2	3.2
P25788	Proteasome subunit alpha type-3	PSMA3	3.1
Q13501	Sequestosome-1	SQSTM1	3.0
A0A087WVZ9	DNA-directed RNA polymerases I, II, and III subunit RPABC1	POLR2E	3.0
R4GMR5	26S proteasome non-ATPase regulatory subunit 8	PSMD8	3.0
C9JLU1	DNA-directed RNA polymerases I, II, and III subunit RPABC3	POLR2H	3.0
P62191	26S protease regulatory subunit 4	PSMC1	3.0
Q5RKV6	Exosome complex component MTR3	EXOSC6	2.9
Q8IU6	Histone H2A type 2-B	HIST2H2AB	2.9
O14818	Proteasome subunit alpha type-7	PSMA7	2.9
P28074	Proteasome subunit beta type-5	PSMB5	2.9
P55036	26S proteasome non-ATPase regulatory subunit 4	PSMD4	2.8
P28066	Proteasome subunit alpha type-5	PSMA5	2.8
P49721	Proteasome subunit beta type-2	PSMB2	2.7
F8W118	Nucleosome assembly protein 1-like 1	NAP1L1	2.7
P62195	26S protease regulatory subunit 8	PSMC5	2.7
H0Y6K2	Bromodomain-containing protein 2	BRD2	2.6
Q9UQN3	Charged multivesicular body protein 2b	CHMP2B	2.6
P25789	Proteasome subunit alpha type-4;Proteasome subunit alpha type;Proteasome subunit beta type	PSMA4	2.6
P17980	26S protease regulatory subunit 6A	PSMC3	2.6
O00487	26S proteasome non-ATPase regulatory subunit 14	PSMD14	2.6
Q14596	Next to BRCA1 gene 1 protein	NBR1	2.6
A0A087WUT6	Eukaryotic translation initiation factor 5B	EIF5B	2.5
O15371	Eukaryotic translation initiation factor 3 subunit D	EIF3D	2.4
Q9Y3B9	RRP15-like protein	RRP15	2.4
Q99613	Eukaryotic translation initiation factor 3 subunit C	EIF3C	2.3
B7Z6D5	Probable ATP-dependent RNA helicase DDX27	DDX27	2.3
P10644	cAMP-dependent protein kinase type I-alpha regulatory subunit	PRKAR1A	2.3
Q96DX7	Tripartite motif-containing protein 44	TRIM44	2.3
P02545	Prelamin-A/C;Lamin-A/C	LMNA	2.3
Q9BYN8	28S ribosomal protein S26, mitochondrial	MRPS26	2.3
Q96SB4	SRSF protein kinase 1	SRPK1	2.2
P06748	Nucleophosmin	NPM1	2.2
P56182	Ribosomal RNA processing protein 1 homolog A	RRP1	2.2
P07199	Major centromere autoantigen B	CENPB	2.2
A0A0B4J2E5	Periodic tryptophan protein 2 homolog	PWP2	2.2

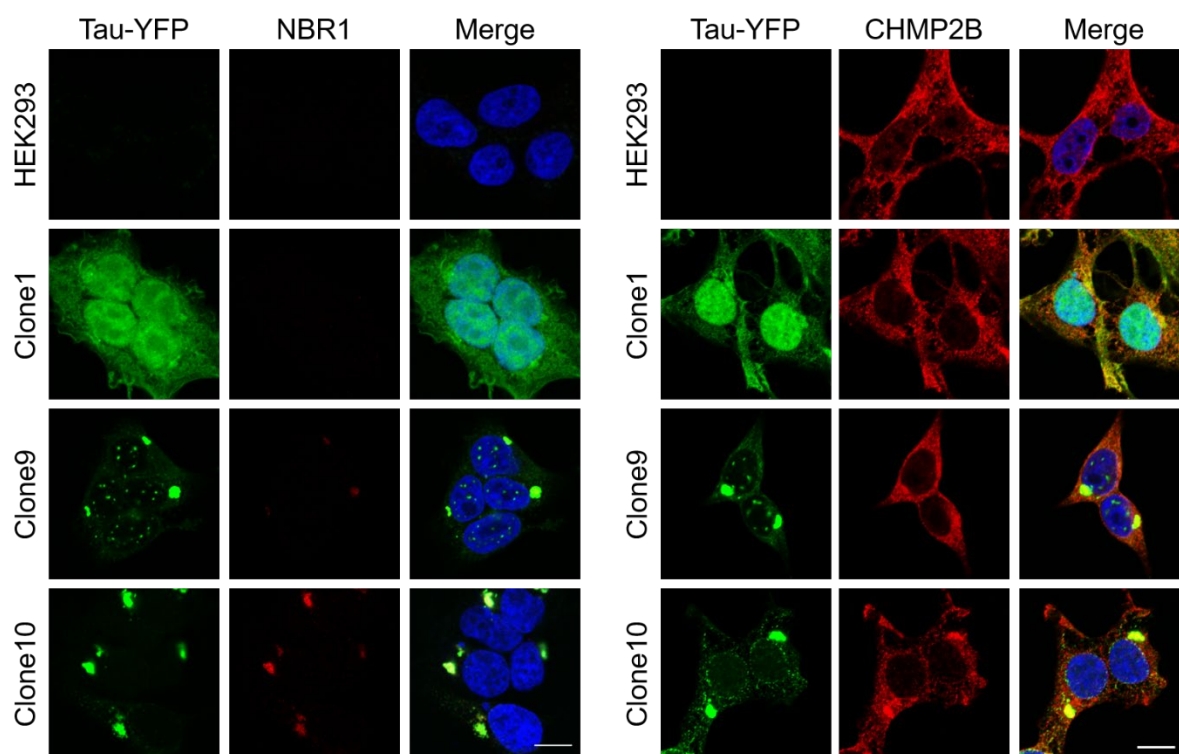
Q9NY93	Probable ATP-dependent RNA helicase DDX56	DDX56	2.2
Q8WV44	E3 ubiquitin-protein ligase TRIM41	TRIM41	2.2
D6RIC3	Nucleolar protein 16	NOP16	2.2
P62979	Ubiquitin	UBC	2.2
Q8TDD1	ATP-dependent RNA helicase DDX54	DDX54	2.2
Q14137	Ribosome biogenesis protein BOP1	BOP1	2.1
Q8WXF1	Paraspeckle component 1	PSPC1	2.1
P19525	Interferon-induced, double-stranded RNA-activated protein kinase	EIF2AK2	2.1
A0A2R8YD50	Peroxisomal multifunctional enzyme type 2	HSD17B4	2.1
Q12788	Transducin beta-like protein 3	TBL3	2.1
Q9UNX4	WD repeat-containing protein 3	WDR3	2.1
A0A0A0MTB8	WD repeat-containing protein 36	WDR36	2.0
Q8NC51	Plasminogen activator inhibitor 1 RNA-binding protein	SERBP1	2.0
Q7L7X3	Serine/threonine-protein kinase TAO1	TAOK1	2.0
Q9NYH9	U3 small nucleolar RNA-associated protein 6 homolog	UTP6	2.0

Supplementary Table 6: GO term enrichment of tau-YFP interactors in Clone10/ Clone9 (Top 20 terms)

GO cellular component	Fold enrichment	P-value
proteasome regulatory particle, lid subcomplex (GO:0008541)	> 100	1.70E-10
proteasome regulatory particle (GO:0005838)	> 100	4.42E-30
proteasome regulatory particle, base subcomplex (GO:0008540)	> 100	1.15E-13
proteasome accessory complex (GO:0022624)	> 100	2.35E-29
cytosolic proteasome complex (GO:0031597)	> 100	3.35E-08
Pwp2p-containing subcomplex of 90S preribosome (GO:0034388)	> 100	2.17E-06
proteasome core complex, alpha-subunit complex (GO:0019773)	> 100	3.37E-06
proteasome complex (GO:0000502)	92.93	2.17E-38
endopeptidase complex (GO:1905369)	91.55	3.00E-38
VCP-NPL4-UFD1 AAA ATPase complex (GO:0034098)	88.47	1.70E-02
RNA polymerase II, core complex (GO:0005665)	78.64	2.56E-05
proteasome core complex (GO:0005839)	75.06	3.94E-08
peptidase complex (GO:1905368)	65.25	5.38E-35
90S preribosome (GO:0030686)	44.23	1.71E-05
small-subunit processome (GO:0032040)	31.04	1.47E-03
preribosome (GO:0030684)	25.89	2.41E-07
ficolin-1-rich granule (GO:0101002)	22.83	7.14E-10
ficolin-1-rich granule lumen (GO:1904813)	22.83	7.14E-10
RNA polymerase II, holoenzyme (GO:0016591)	17.76	3.17E-04
nuclear DNA-directed RNA polymerase complex (GO:0055029)	13.99	1.45E-03

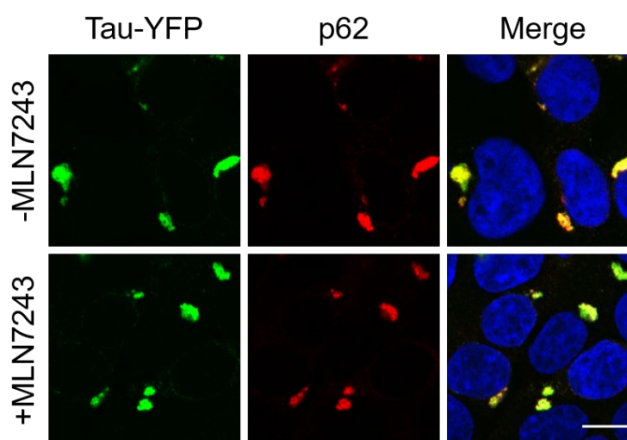
Supplementary figures

Figure S1, related to Figure 10- Interactome analysis of tau-YFP in Clone1, 9 and 10.



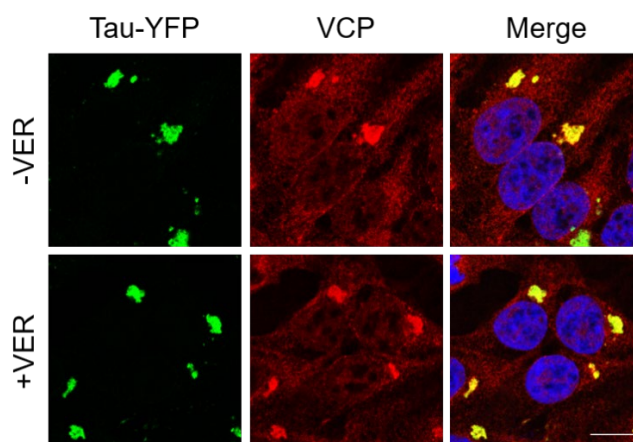
HEK293, Clone1, 9 and 10 cells at steady state were fixed and stained with anti-NBR1 (left panel) and anti-CHMP2B (right panel) primary and cy5 conjugated secondary antibodies. Merged images show tau-YFP (green), NBR1/CHMP2B (red) and DAPI (blue). Scale bar: 10 μ m.

Figure S2, related to Figure 34 – Ubiquitin independent recruitment of p62 on tau-YFP aggregates



Clone10 cells were treated with 0.5 μ M MLN7243 for 6 h and afterwards stained for endogenous VCP. Cy5 conjugated secondary antibody was used for detection. Merged images show tau-YFP (green), VCP (red) and DAPI (blue). Scale bar: 10 μ m.

Figure S3, related to Discussion – VCP recruitment on tau-YFP aggregates upon Hsp70 inhibition



Clone10 cells were treated with 10 μ M VER-155008 for 24 h and afterwards stained for endogenous VCP. Cy5 conjugated secondary antibody was used for detection. Merged images show tau-YFP (green), VCP (red) and DAPI (blue). Scale bar: 10 μ m.

Abbreviations

aa	Amino acid
AD	Alzheimer's Disease
ADP	Adenosine diphosphate
ALS	Amyotrophic Lateral Sclerosis
APS	Ammonium persulphate
ATP	Adenosine triphosphate
A β	Amyloid β protein
BSA	Bovine Serum Albumin
ACN	Acetonitrile
CAPS	3-(Cyclohexylamino)-1-propanesulfonic acid
CHX	Cycloheximide
CTD	Carboxyl terminal Domain
DAPI	4',6-diamidino-2-phenylindole
DMEM	Dulbecco's Modified Eagle Medium
DMSO	Dimethyl sulfoxide
DTT	Dithiothreitol
DUBs	Deubiquitylating Enzymes
EDTA	Ethylenediaminetetraacetic acid
ER	Endoplasmic reticulum
ERAD	ER-associated degradation
FBS	Fetal Bovine Serum
Fluc	Firefly luciferase
FTDP-17	Frontotemporal dementia and parkinsonism linked to chromosome 17
g	Acceleration of gravity, 9.81m/sec ²
GnHCl	Guanidinium Chloride
h	Hour
HD	Huntington's Disease
HRP	Horseradish peroxidase
Hsp	Heat Shock Protein
Htt	Huntingtin
IBMPFD	Inclusion body myopathy with early-onset Paget disease and frontotemporal dementia
IBs	Inclusion Bodies
IPOD	Insoluble Protein Deposit
JUNQ	Juxtannuclear Quality Control
KO	Knockout

LB	Luria-Bertani
MAD	Mitochondria-associated degradation
MAPT	Microtubule associated protein tau
MD	Middle Domain
MES	2-(N-morpholino)ethanesulfonic acid
MOPS	3-(N-morpholino)propanesulfonic acid
MTOC	Microtubule Organizing Centre
NBD	Nucleotide binding domain
NEF	Nucleotide Exchange Factor
NEM	N-ethylmaleimide
NFTs	Neurofibrillary tangles
O.D.	Optical Density
PAGE	Polyacrylamide gel electrophoresis
PBS	Phosphate Buffered Saline
PCR	Polymerase Chain Reaction
PD	Parkinson's Disease
PHFs	Paired helical filaments
PN	Proteostasis Network
PQC	Protein Quality control
PVDF	Polyvinylidene fluoride
RD	Repeat domain
RIPA	Radioimmunoprecipitation assay buffer
RQC	Ribosomal quality control
RT	Room temperature
Rubisco	Ribulose-1,5-bisphosphate carboxylase/oxygenase
SBD	Substrate binding domain
SDS	Sodium-dodecyl sulphate
SF	Straight filament
TBST	Tris-buffered saline with Triton
TFA	Trifluoroacetic acid
UPS	Ubiquitin Proteasome System
VCP	Valosin-containing protein
WT	Wild type

8. REFERENCES

- Acebron, S.P., Fernandez-Saiz, V., Taneva, S.G., Moro, F., and Muga, A. (2008). DnaJ recruits DnaK to protein aggregates. *J Biol Chem* 283, 1381-1390.
- Acebron, S.P., Martin, I., del Castillo, U., Moro, F., and Muga, A. (2009). DnaK-mediated association of ClpB to protein aggregates. A bichaperone network at the aggregate surface. *FEBS Lett* 583, 2991-2996.
- Aguzzi, A., Heikenwalder, M., and Polymenidou, M. (2007). Insights into prion strains and neurotoxicity. *Nat Rev Mol Cell Biol* 8, 552-561.
- Ahler, E., Sullivan, W.J., Cass, A., Braas, D., York, A.G., Bensinger, S.J., Graeber, T.G., and Christofk, H.R. (2013). Doxycycline alters metabolism and proliferation of human cell lines. *PLoS One* 8, e64561.
- Alonso Adel, C., Mederlyova, A., Novak, M., Grundke-Iqbal, I., and Iqbal, K. (2004). Promotion of hyperphosphorylation by frontotemporal dementia tau mutations. *J Biol Chem* 279, 34873-34881.
- Anding, A.L., and Baehrecke, E.H. (2017). Cleaning House: Selective Autophagy of Organelles. *Dev Cell* 41, 10-22.
- Anfinsen, C.B. (1973). Principles that govern the folding of protein chains. *Science* 181, 223-230.
- Arendt, T., Stieler, J., Strijkstra, A.M., Hut, R.A., Rudiger, J., Van der Zee, E.A., Harkany, T., Holzer, M., and Hartig, W. (2003). Reversible paired helical filament-like phosphorylation of tau is an adaptive process associated with neuronal plasticity in hibernating animals. *J Neurosci* 23, 6972-6981.
- Arhzaouy, K., Strucksberg, K.H., Tung, S.M., Tangavelou, K., Stumpf, M., Faix, J., Schroder, R., Clemen, C.S., and Eichinger, L. (2012). Heteromeric p97/p97R155C complexes induce dominant negative changes in wild-type and autophagy 9-deficient Dictyostelium strains. *PLoS One* 7, e46879.
- Arrasate, M., Mitra, S., Schweitzer, E.S., Segal, M.R., and Finkbeiner, S. (2004). Inclusion body formation reduces levels of mutant huntingtin and the risk of neuronal death. *Nature* 431, 805-810.
- Ashburner, M., and Bonner, J.J. (1979). The induction of gene activity in drosophila by heat shock. *Cell* 17, 241-254.
- Balchin, D., Hayer-Hartl, M., and Hartl, F.U. (2016). In vivo aspects of protein folding and quality control. *Science* 353, aac4354.
- Bancher, C., Brunner, C., Lassmann, H., Budka, H., Jellinger, K., Wiche, G., Seitelberger, F., Grundke-Iqbal, I., Iqbal, K., and Wisniewski, H.M. (1989). Accumulation of abnormally phosphorylated tau precedes the formation of neurofibrillary tangles in Alzheimer's disease. *Brain Res* 477, 90-99.
- Banerjee, S., Bartesaghi, A., Merk, A., Rao, P., Bulfer, S.L., Yan, Y., Green, N., Mroczkowski, B., Neitz, R.J., Wipf, P., *et al.* (2016). 2.3 A resolution cryo-EM structure of human p97 and mechanism of allosteric inhibition. *Science* 351, 871-875.
- Barghorn, S., Davies, P., and Mandelkow, E. (2004). Tau paired helical filaments from Alzheimer's disease brain and assembled in vitro are based on beta-structure in the core domain. *Biochemistry* 43, 1694-1703.
- Barnhart, M.M., and Chapman, M.R. (2006). Curli biogenesis and function. *Annu Rev Microbiol* 60, 131-147.
- Barthelme, D., Chen, J.Z., Grabenstatter, J., Baker, T.A., and Sauer, R.T. (2014). Architecture and assembly of the archaeal Cdc48*20S proteasome. *Proc Natl Acad Sci U S A* 111, E1687-1694.
- Barthelme, D., and Sauer, R.T. (2012). Identification of the Cdc48*20S proteasome as an ancient AAA+ proteolytic machine. *Science* 337, 843-846.
- Bates, G. (2003). Huntingtin aggregation and toxicity in Huntington's disease. *Lancet* 361, 1642-1644.

- Bauerlein, F.J.B., Saha, I., Mishra, A., Kalemanov, M., Martinez-Sanchez, A., Klein, R., Dudanova, I., Hipp, M.S., Hartl, F.U., Baumeister, W., *et al.* (2017). In Situ Architecture and Cellular Interactions of PolyQ Inclusions. *Cell* *171*, 179-187 e110.
- Benaki, D.C., Aggeli, A., Chryssikos, G.D., Yiannopoulos, Y.D., Kamitsos, E.I., Brumley, E., Case, S.T., Boden, N., and Hamodrakas, S.J. (1998). Laser-Raman and FT-IR spectroscopic studies of peptide-analogues of silkworm chorion protein segments. *Int J Biol Macromol* *23*, 49-59.
- Bennett, E.J., Bence, N.F., Jayakumar, R., and Kopito, R.R. (2005). Global Impairment of the Ubiquitin-Proteasome System by Nuclear or Cytoplasmic Protein Aggregates Precedes Inclusion Body Formation. *Molecular Cell* *17*, 351-365.
- Besche, H.C., Haas, W., Gygi, S.P., and Goldberg, A.L. (2009). Isolation of mammalian 26S proteasomes and p97/VCP complexes using the ubiquitin-like domain from HHR23B reveals novel proteasome-associated proteins. *Biochemistry* *48*, 2538-2549.
- Beskow, A., Grimberg, K.B., Bott, L.C., Salomons, F.A., Dantuma, N.P., and Young, P. (2009). A conserved unfoldase activity for the p97 AAA-ATPase in proteasomal degradation. *J Mol Biol* *394*, 732-746.
- Bhattacharyya, A.M., Thakur, A.K., and Wetzel, R. (2005). polyglutamine aggregation nucleation: thermodynamics of a highly unfavorable protein folding reaction. *Proc Natl Acad Sci U S A* *102*, 15400-15405.
- Blythe, E.E., Olson, K.C., Chau, V., and Deshaies, R.J. (2017). Ubiquitin- and ATP-dependent unfoldase activity of P97/VCP*NPLOC4*UFD1L is enhanced by a mutation that causes multisystem proteinopathy. *Proc Natl Acad Sci U S A* *114*, E4380-E4388.
- Bodnar, N.O., and Rapoport, T.A. (2017). Molecular Mechanism of Substrate Processing by the Cdc48 ATPase Complex. *Cell* *169*, 722-735 e729.
- Boluda, S., Iba, M., Zhang, B., Raible, K.M., Lee, V.M., and Trojanowski, J.Q. (2015). Differential induction and spread of tau pathology in young PS19 tau transgenic mice following intracerebral injections of pathological tau from Alzheimer's disease or corticobasal degeneration brains. *Acta Neuropathol* *129*, 221-237.
- Bosl, B., Grimminger, V., and Walter, S. (2005). Substrate binding to the molecular chaperone Hsp104 and its regulation by nucleotides. *J Biol Chem* *280*, 38170-38176.
- Brandman, O., and Hegde, R.S. (2016). Ribosome-associated protein quality control. *Nature structural & molecular biology* *23*, 7-15.
- Braun, B.C., Glickman, M., Kraft, R., Dahlmann, B., Kloetzel, P.-M., Finley, D., and Schmidt, M. (1999). The base of the proteasome regulatory particle exhibits chaperone-like activity. *Nature Cell Biology* *1*, 221-226.
- Braun, R.J., and Zischka, H. (2008). Mechanisms of Cdc48/VCP-mediated cell death — from yeast apoptosis to human disease. *Biochimica et Biophysica Acta (BBA) - Molecular Cell Research* *1783*, 1418-1435.
- Brockwell, D.J., and Radford, S.E. (2007). Intermediates: ubiquitous species on folding energy landscapes? *Curr Opin Struct Biol* *17*, 30-37.
- Brooks, C., Snoberger, A., Belcastro, M., Murphy, J., Kisselev, O.G., Smith, D.M., and Sokolov, M. (2018). Archaeal Unfoldase Counteracts Protein Misfolding Retinopathy in Mice. *The Journal of neuroscience : the official journal of the Society for Neuroscience* *38*, 7248-7254.
- Bryan, J.B., Nagle, B.W., and Doenges, K.H. (1975). Inhibition of tubulin assembly by RNA and other polyanions: evidence for a required protein. *Proc Natl Acad Sci U S A* *72*, 3570-3574.
- Buchan, J.R., Kolaitis, R.M., Taylor, J.P., and Parker, R. (2013). Eukaryotic stress granules are cleared by autophagy and Cdc48/VCP function. *Cell* *153*, 1461-1474.
- Bulfer, S.L., Chou, T.F., and Arkin, M.R. (2016). p97 Disease Mutations Modulate Nucleotide-Induced Conformation to Alter Protein-Protein Interactions. *ACS chemical biology* *11*, 2112-2116.
- Caceres, A., and Kosik, K.S. (1990). Inhibition of neurite polarity by tau antisense oligonucleotides in primary cerebellar neurons. *Nature* *343*, 461-463.
- Cappadocia, L., and Lima, C.D. (2018). Ubiquitin-like Protein Conjugation: Structures, Chemistry, and Mechanism. *Chem Rev* *118*, 889-918.

- Carroni, M., Kummer, E., Oguchi, Y., Wendler, P., Clare, D.K., Sinning, I., Kopp, J., Mogk, A., Bukau, B., and Saibil, H.R. (2014). Head-to-tail interactions of the coiled-coil domains regulate ClpB activity and cooperation with Hsp70 in protein disaggregation. *Elife* 3, e02481.
- Carulla, N., Caddy, G.L., Hall, D.R., Zurdo, J., Gairi, M., Feliz, M., Giral, E., Robinson, C.V., and Dobson, C.M. (2005). Molecular recycling within amyloid fibrils. *Nature* 436, 554-558.
- Chamera, T., Klosowska, A., Janta, A., Wyszowski, H., Obuchowski, I., Gumowski, K., and Liberek, K. (2019). Selective Hsp70-Dependent Docking of Hsp104 to Protein Aggregates Protects the Cell from the Toxicity of the Disaggregase. *J Mol Biol* 431, 2180-2196.
- Chau, V., Tobias, J.W., Bachmair, A., Marriott, D., Ecker, D.J., Gonda, D.K., and Varshavsky, A. (1989). A multiubiquitin chain is confined to specific lysine in a targeted short-lived protein. *Science* 243, 1576-1583.
- Chen, S., Ferrone, F.A., and Wetzel, R. (2002). Huntington's disease age-of-onset linked to polyglutamine aggregation nucleation. *Proc Natl Acad Sci U S A* 99, 11884-11889.
- Cheng, M.Y., Hartl, F.U., Martin, J., Pollock, R.A., Kalousek, F., Neupert, W., Hallberg, E.M., Hallberg, R.L., and Horwich, A.L. (1989). Mitochondrial heat-shock protein hsp60 is essential for assembly of proteins imported into yeast mitochondria. *Nature* 337, 620-625.
- Chernoff, Y.O., Derkach, I.L., and Inge-Vechtsov, S.G. (1993). Multicopy SUP35 gene induces de-novo appearance of psi-like factors in the yeast *Saccharomyces cerevisiae*. *Curr Genet* 24, 268-270.
- Chernoff, Y.O., Lindquist, S.L., Ono, B., Inge-Vechtsov, S.G., and Liebman, S.W. (1995). Role of the chaperone protein Hsp104 in propagation of the yeast prion-like factor [psi+]. *Science* 268, 880-884.
- Chesser, A.S., Pritchard, S.M., and Johnson, G.V. (2013). Tau clearance mechanisms and their possible role in the pathogenesis of Alzheimer disease. *Front Neurol* 4, 122.
- Chiti, F., and Dobson, C.M. (2017). Protein Misfolding, Amyloid Formation, and Human Disease: A Summary of Progress Over the Last Decade. *Annu Rev Biochem* 86, 27-68.
- Choe, Y.J., Park, S.H., Hassemmer, T., Korner, R., Vincenz-Donnelly, L., Hayer-Hartl, M., and Hartl, F.U. (2016). Failure of RQC machinery causes protein aggregation and proteotoxic stress. *Nature* 531, 191-195.
- Ciechanover, A., Heller, H., Elias, S., Haas, A.L., and Hershko, A. (1980). ATP-dependent conjugation of reticulocyte proteins with the polypeptide required for protein degradation. *Proc Natl Acad Sci U S A* 77, 1365-1368.
- Ciryam, P., Kundra, R., Morimoto, R.I., Dobson, C.M., and Vendruscolo, M. (2015). Supersaturation is a major driving force for protein aggregation in neurodegenerative diseases. *Trends in pharmacological sciences* 36, 72-77.
- Clavaguera, F., Bolmont, T., Crowther, R.A., Abramowski, D., Frank, S., Probst, A., Fraser, G., Stalder, A.K., Beibel, M., Staufenbiel, M., *et al.* (2009). Transmission and spreading of tauopathy in transgenic mouse brain. *Nat Cell Biol* 11, 909-913.
- Cleveland, D.W., Hwo, S.Y., and Kirschner, M.W. (1977). Physical and chemical properties of purified tau factor and the role of tau in microtubule assembly. *J Mol Biol* 116, 227-247.
- Cohen, E., Bieschke, J., Perciavalle, R.M., Kelly, J.W., and Dillin, A. (2006). Opposing activities protect against age-onset proteotoxicity. *Science* 313, 1604-1610.
- Colby, D.W., Giles, K., Legname, G., Wille, H., Baskakov, I.V., DeArmond, S.J., and Prusiner, S.B. (2009). Design and construction of diverse mammalian prion strains. *Proceedings of the National Academy of Sciences* 106, 20417.
- Collins, G.A., and Goldberg, A.L. (2017). The Logic of the 26S Proteasome. *Cell* 169, 792-806.
- Cooney, I., Han, H., Stewart, M.G., Carson, R.H., Hansen, D.T., Iwasa, J.H., Price, J.C., Hill, C.P., and Shen, P.S. (2019). Structure of the Cdc48 segregase in the act of unfolding an authentic substrate. *Science*.
- Cox, B.S., Tuite, M.F., and McLaughlin, C.S. (1988). The psi factor of yeast: a problem in inheritance. *Yeast* 4, 159-178.
- Cripps, D., Thomas, S.N., Jeng, Y., Yang, F., Davies, P., and Yang, A.J. (2006). Alzheimer disease-specific conformation of hyperphosphorylated paired helical filament-Tau is

- polyubiquitinated through Lys-48, Lys-11, and Lys-6 ubiquitin conjugation. *J Biol Chem* **281**, 10825-10838.
- Crowther, R.A. (1991). Straight and paired helical filaments in Alzheimer disease have a common structural unit. *Proc Natl Acad Sci U S A* **88**, 2288-2292.
- Crowther, R.A., Olesen, O.F., Jakes, R., and Goedert, M. (1992). The microtubule binding repeats of tau protein assemble into filaments like those found in Alzheimer's disease. *FEBS Lett* **309**, 199-202.
- Crowther, R.A., Olesen, O.F., Smith, M.J., Jakes, R., and Goedert, M. (1994). Assembly of Alzheimer-like filaments from full-length tau protein. *FEBS Lett* **337**, 135-138.
- Crowther, T., Goedert, M., and Wischik, C.M. (1989). The repeat region of microtubule-associated protein tau forms part of the core of the paired helical filament of Alzheimer's disease. *Ann Med* **21**, 127-132.
- Culp, E., and Wright, G.D. (2017). Bacterial proteases, untapped antimicrobial drug targets. *J Antibiot (Tokyo)* **70**, 366-377.
- D'Agostino, C., Nogalska, A., Cacciottolo, M., Engel, W.K., and Askanas, V. (2011). Abnormalities of NBR1, a novel autophagy-associated protein, in muscle fibers of sporadic inclusion-body myositis. *Acta Neuropathol* **122**, 627-636.
- Daugaard, M., Rohde, M., and Jäättelä, M. (2007). The heat shock protein 70 family: Highly homologous proteins with overlapping and distinct functions. *FEBS Letters* **581**, 3702-3710.
- Davies, J.M., Brunger, A.T., and Weis, W.I. (2008). Improved structures of full-length p97, an AAA ATPase: implications for mechanisms of nucleotide-dependent conformational change. *Structure (London, England : 1993)* **16**, 715-726.
- Dawson, H.N., Ferreira, A., Eyster, M.V., Ghoshal, N., Binder, L.I., and Vitek, M.P. (2001). Inhibition of neuronal maturation in primary hippocampal neurons from tau deficient mice. *J Cell Sci* **114**, 1179-1187.
- de Calignon, A., Polydoro, M., Suarez-Calvet, M., William, C., Adamowicz, D.H., Kopeikina, K.J., Pitstick, R., Sahara, N., Ashe, K.H., Carlson, G.A., *et al.* (2012). Propagation of tau pathology in a model of early Alzheimer's disease. *Neuron* **73**, 685-697.
- de Waal, G.M., Engelbrecht, L., Davis, T., de Villiers, W.J.S., Kell, D.B., and Pretorius, E. (2018). Correlative Light-Electron Microscopy detects lipopolysaccharide and its association with fibrin fibres in Parkinson's Disease, Alzheimer's Disease and Type 2 Diabetes Mellitus. *Scientific Reports* **8**, 16798.
- Defenouillere, Q., Yao, Y., Mouaikel, J., Namane, A., Galopier, A., Decourty, L., Doyen, A., Malabat, C., Saveanu, C., Jacquier, A., *et al.* (2013). Cdc48-associated complex bound to 60S particles is required for the clearance of aberrant translation products. *Proc Natl Acad Sci U S A* **110**, 5046-5051.
- Deichsel, A., Mouysset, J., and Hoppe, T. (2009). The ubiquitin-selective chaperone CDC-48/p97, a new player in DNA replication. *Cell Cycle* **8**, 185-190.
- Deng, Z., Purtell, K., Lachance, V., Wold, M.S., Chen, S., and Yue, Z. (2017). Autophagy Receptors and Neurodegenerative Diseases. *Trends Cell Biol* **27**, 491-504.
- Denk, F., and Wade-Martins, R. (2009). Knock-out and transgenic mouse models of tauopathies. *Neurobiol Aging* **30**, 1-13.
- Deriziotis, P., André, R., Smith, D.M., Goold, R., Kinghorn, K.J., Kristiansen, M., Nathan, J.A., Rosenzweig, R., Krutauz, D., Glickman, M.H., *et al.* (2011). Misfolded PrP impairs the UPS by interaction with the 20S proteasome and inhibition of substrate entry. *The EMBO Journal* **30**, 3065-3077.
- Diamant, S., Ben-Zvi, A.P., Bukau, B., and Goloubinoff, P. (2000). Size-dependent disaggregation of stable protein aggregates by the DnaK chaperone machinery. *J Biol Chem* **275**, 21107-21113.
- Dikic, I., and Elazar, Z. (2018). Mechanism and medical implications of mammalian autophagy. *Nat Rev Mol Cell Biol* **19**, 349-364.
- Dill, K.A. (1990). Dominant forces in protein folding. *Biochemistry* **29**, 7133-7155.
- Dinner, A.R., Sali, A., Smith, L.J., Dobson, C.M., and Karplus, M. (2000). Understanding protein folding via free-energy surfaces from theory and experiment. *Trends Biochem Sci* **25**, 331-339.

- Doyle, S.M., Genest, O., and Wickner, S. (2013). Protein rescue from aggregates by powerful molecular chaperone machines. *Nat Rev Mol Cell Biol* *14*, 617-629.
- Doyle, S.M., and Wickner, S. (2009). Hsp104 and ClpB: protein disaggregating machines. *Trends Biochem Sci* *34*, 40-48.
- Drubin, D.G., and Kirschner, M.W. (1986). Tau protein function in living cells. *J Cell Biol* *103*, 2739-2746.
- Dumanchin, C., Camuzat, A., Campion, D., Verpillat, P., Hannequin, D., Dubois, B., Saugier-Verber, P., Martin, C., Penet, C., Charbonnier, F., *et al.* (1998). Segregation of a missense mutation in the microtubule-associated protein tau gene with familial frontotemporal dementia and parkinsonism. *Hum Mol Genet* *7*, 1825-1829.
- Eftekharzadeh, B., Daigle, J.G., Kapinos, L.E., Coyne, A., Schiantarelli, J., Carlomagno, Y., Cook, C., Miller, S.J., Dujardin, S., Amaral, A.S., *et al.* (2018). Tau Protein Disrupts Nucleocytoplasmic Transport in Alzheimer's Disease. *Neuron* *99*, 925-940 e927.
- Eisenberg, D., and Jucker, M. (2012). The amyloid state of proteins in human diseases. *Cell* *148*, 1188-1203.
- Elbaum-Garfinkle, S., and Rhoades, E. (2012). Identification of an aggregation-prone structure of tau. *J Am Chem Soc* *134*, 16607-16613.
- Ellis, J. (1987). Proteins as molecular chaperones. *Nature* *328*, 378-379.
- Erales, J., and Coffino, P. (2014). Ubiquitin-independent proteasomal degradation. *Biochim Biophys Acta* *1843*, 216-221.
- Escusa-Toret, S., Vonk, W.I., and Frydman, J. (2013). Spatial sequestration of misfolded proteins by a dynamic chaperone pathway enhances cellular fitness during stress. *Nat Cell Biol* *15*, 1231-1243.
- Evans, L.D., Wassmer, T., Fraser, G., Smith, J., Perkinson, M., Billinton, A., and Livesey, F.J. (2018). Extracellular Monomeric and Aggregated Tau Efficiently Enter Human Neurons through Overlapping but Distinct Pathways. *Cell Rep* *22*, 3612-3624.
- Faber, P.W., Alter, J.R., MacDonald, M.E., and Hart, A.C. (1999). Polyglutamine-mediated dysfunction and apoptotic death of a *Caenorhabditis elegans* sensory neuron. *Proc Natl Acad Sci U S A* *96*, 179-184.
- Falcon, B., Zhang, W., Murzin, A.G., Murshudov, G., Garringer, H.J., Vidal, R., Crowther, R.A., Ghetti, B., Scheres, S.H.W., and Goedert, M. (2018). Structures of filaments from Pick's disease reveal a novel tau protein fold. *Nature* *561*, 137-140.
- Falcon, B., Zivanov, J., Zhang, W., Murzin, A.G., Garringer, H.J., Vidal, R., Crowther, R.A., Newell, K.L., Ghetti, B., Goedert, M., *et al.* (2019). Novel tau filament fold in chronic traumatic encephalopathy encloses hydrophobic molecules. *Nature*.
- Feijo Delgado, F., Cermak, N., Hecht, V.C., Son, S., Li, Y., Knudsen, S.M., Olcum, S., Higgins, J.M., Chen, J., Grover, W.H., *et al.* (2013). Intracellular water exchange for measuring the dry mass, water mass and changes in chemical composition of living cells. *PLoS One* *8*, e67590.
- Ferdous, A., Gonzalez, F., Sun, L., Kodadek, T., and Johnston, S.A. (2001). The 19S regulatory particle of the proteasome is required for efficient transcription elongation by RNA polymerase II. *Mol Cell* *7*, 981-991.
- Ferdous, A., Kodadek, T., and Johnston, S.A. (2002). A nonproteolytic function of the 19S regulatory subunit of the 26S proteasome is required for efficient activated transcription by human RNA polymerase II. *Biochemistry* *41*, 12798-12805.
- Fernandez-Nogales, M., Cabrera, J.R., Santos-Galindo, M., Hoozemans, J.J., Ferrer, I., Rozemuller, A.J., Hernandez, F., Avila, J., and Lucas, J.J. (2014). Huntington's disease is a four-repeat tauopathy with tau nuclear rods. *Nat Med* *20*, 881-885.
- Ferreira, J.V., Soares, A.R., Ramalho, J.S., Pereira, P., and Girao, H. (2015). K63 linked ubiquitin chain formation is a signal for HIF1A degradation by Chaperone-Mediated Autophagy. *Sci Rep* *5*, 10210.
- Fichou, Y., Vigers, M., Goring, A.K., Eschmann, N.A., and Han, S. (2018). Heparin-induced tau filaments are structurally heterogeneous and differ from Alzheimer's disease filaments. *Chem Commun (Camb)* *54*, 4573-4576.
- Finley, D. (2009). Recognition and processing of ubiquitin-protein conjugates by the proteasome. *Annu Rev Biochem* *78*, 477-513.

- Finley, D., Sadis, S., Monia, B.P., Boucher, P., Ecker, D.J., Crooke, S.T., and Chau, V. (1994). Inhibition of proteolysis and cell cycle progression in a multiubiquitination-deficient yeast mutant. *Mol Cell Biol* *14*, 5501-5509.
- Fitzpatrick, A.W.P., Falcon, B., He, S., Murzin, A.G., Murshudov, G., Garringer, H.J., Crowther, R.A., Ghetti, B., Goedert, M., and Scheres, S.H.W. (2017). Cryo-EM structures of tau filaments from Alzheimer's disease. *Nature* *547*, 185-190.
- Fowler, D.M., Koulov, A.V., Alory-Jost, C., Marks, M.S., Balch, W.E., and Kelly, J.W. (2006). Functional amyloid formation within mammalian tissue. *PLoS Biol* *4*, e6.
- Frost, B., Jacks, R.L., and Diamond, M.I. (2009). Propagation of tau misfolding from the outside to the inside of a cell. *J Biol Chem* *284*, 12845-12852.
- Fujikake, N., Shin, M., and Shimizu, S. (2018). Association Between Autophagy and Neurodegenerative Diseases. *Front Neurosci* *12*, 255-255.
- Fujita, N., Hayashi-Nishino, M., Fukumoto, H., Omori, H., Yamamoto, A., Noda, T., and Yoshimori, T. (2008). An Atg4B mutant hampers the lipidation of LC3 paralogues and causes defects in autophagosome closure. *Mol Biol Cell* *19*, 4651-4659.
- Gallagher, P.S., Clowes Candadai, S.V., and Gardner, R.G. (2014). The requirement for Cdc48/p97 in nuclear protein quality control degradation depends on the substrate and correlates with substrate insolubility. *J Cell Sci* *127*, 1980-1991.
- Gallardo, G., Wong, C.H., Ricardez, S.M., Mann, C.N., Lin, K.H., Leyns, C.E.G., Jiang, H., and Holtzman, D.M. (2019). Targeting tauopathy with engineered tau-degrading intrabodies. *Mol Neurodegener* *14*, 38.
- Gao, X., Carroni, M., Nussbaum-Krammer, C., Mogk, A., Nillegoda, N.B., Szlachcic, A., Guilbride, D.L., Saibil, H.R., Mayer, M.P., and Bukau, B. (2015). Human Hsp70 Disaggregase Reverses Parkinson's-Linked alpha-Synuclein Amyloid Fibrils. *Mol Cell* *59*, 781-793.
- Gerlach, B., Cordier, S.M., Schmukle, A.C., Emmerich, C.H., Rieser, E., Haas, T.L., Webb, A.I., Rickard, J.A., Anderton, H., Wong, W.W., *et al.* (2011). Linear ubiquitination prevents inflammation and regulates immune signalling. *Nature* *471*, 591-596.
- Giasson, B.I., Forman, M.S., Higuchi, M., Golbe, L.I., Graves, C.L., Kotzbauer, P.T., Trojanowski, J.Q., and Lee, V.M.Y. (2003). Initiation and Synergistic Fibrillization of Tau and Alpha-Synuclein. *Science* *300*, 636.
- Glover, J.R., Kowal, A.S., Schirmer, E.C., Patino, M.M., Liu, J.J., and Lindquist, S. (1997). Self-seeded fibers formed by Sup35, the protein determinant of [PSI⁺], a heritable prion-like factor of *S. cerevisiae*. *Cell* *89*, 811-819.
- Glover, J.R., and Lindquist, S. (1998). Hsp104, Hsp70, and Hsp40: a novel chaperone system that rescues previously aggregated proteins. *Cell* *94*, 73-82.
- Goedert, M., Eisenberg, D.S., and Crowther, R.A. (2017a). Propagation of Tau Aggregates and Neurodegeneration. *Annu Rev Neurosci* *40*, 189-210.
- Goedert, M., Jakes, R., Spillantini, M.G., Hasegawa, M., Smith, M.J., and Crowther, R.A. (1996). Assembly of microtubule-associated protein tau into Alzheimer-like filaments induced by sulphated glycosaminoglycans. *Nature* *383*, 550-553.
- Goedert, M., Masuda-Suzukake, M., and Falcon, B. (2017b). Like prions: the propagation of aggregated tau and alpha-synuclein in neurodegeneration. *Brain* *140*, 266-278.
- Goedert, M., and Spillantini, M.G. (2000). Tau mutations in frontotemporal dementia FTDP-17 and their relevance for Alzheimer's disease. *Biochim Biophys Acta* *1502*, 110-121.
- Goedert, M., Spillantini, M.G., Jakes, R., Rutherford, D., and Crowther, R.A. (1989). Multiple isoforms of human microtubule-associated protein tau: sequences and localization in neurofibrillary tangles of Alzheimer's disease. *Neuron* *3*, 519-526.
- Goldknopf, I.L., French, M.F., Musso, R., and Busch, H. (1977). Presence of protein A24 in rat liver nucleosomes. *Proc Natl Acad Sci U S A* *74*, 5492-5495.
- Goldstein, G., Scheid, M., Hammerling, U., Schlesinger, D.H., Niall, H.D., and Boyse, E.A. (1975). Isolation of a polypeptide that has lymphocyte-differentiating properties and is probably represented universally in living cells. *Proc Natl Acad Sci U S A* *72*, 11-15.
- Groll, M., Bajorek, M., Kohler, A., Moroder, L., Rubin, D.M., Huber, R., Glickman, M.H., and Finley, D. (2000). A gated channel into the proteasome core particle. *Nat Struct Biol* *7*, 1062-1067.

- Grundke-Iqbal, I., Iqbal, K., Tung, Y.C., Quinlan, M., Wisniewski, H.M., and Binder, L.I. (1986). Abnormal phosphorylation of the microtubule-associated protein tau (tau) in Alzheimer cytoskeletal pathology. *Proc Natl Acad Sci U S A* **83**, 4913-4917.
- Guo, J.L., Buist, A., Soares, A., Callaerts, K., Calafate, S., Stevenaert, F., Daniels, J.P., Zoll, B.E., Crowe, A., Brunden, K.R., *et al.* (2016). The Dynamics and Turnover of Tau Aggregates in Cultured Cells: INSIGHTS INTO THERAPIES FOR TAUOPATHIES. *J Biol Chem* **291**, 13175-13193.
- Guo, Q., Lehmer, C., Martinez-Sanchez, A., Rudack, T., Beck, F., Hartmann, H., Perez-Berlanga, M., Frottin, F., Hipp, M.S., Hartl, F.U., *et al.* (2018). In Situ Structure of Neuronal C9orf72 Poly-GA Aggregates Reveals Proteasome Recruitment. *Cell* **172**, 696-705 e612.
- Guo, T., Noble, W., and Hanger, D.P. (2017). Roles of tau protein in health and disease. *Acta Neuropathol* **133**, 665-704.
- Gupta, R., Kasturi, P., Bracher, A., Loew, C., Zheng, M., Vilella, A., Garza, D., Hartl, F.U., and Raychaudhuri, S. (2011). Firefly luciferase mutants as sensors of proteome stress. *Nat Methods* **8**, 879-884.
- Guthrie, C.R., and Kraemer, B.C. (2011). Proteasome inhibition drives HDAC6-dependent recruitment of tau to aggresomes. *Journal of molecular neuroscience : MN* **45**, 32-41.
- Hao, R., Nanduri, P., Rao, Y., Panichelli, R.S., Ito, A., Yoshida, M., and Yao, T.P. (2013). Proteasomes activate aggresome disassembly and clearance by producing unanchored ubiquitin chains. *Mol Cell* **51**, 819-828.
- Hara, T., Nakamura, K., Matsui, M., Yamamoto, A., Nakahara, Y., Suzuki-Migishima, R., Yokoyama, M., Mishima, K., Saito, I., Okano, H., *et al.* (2006). Suppression of basal autophagy in neural cells causes neurodegenerative disease in mice. *Nature* **441**, 885-889.
- Harada, A., Oguchi, K., Okabe, S., Kuno, J., Terada, S., Ohshima, T., Sato-Yoshitake, R., Takei, Y., Noda, T., and Hirokawa, N. (1994). Altered microtubule organization in small-calibre axons of mice lacking tau protein. *Nature* **369**, 488-491.
- Hardy, J., and Selkoe, D.J. (2002). The amyloid hypothesis of Alzheimer's disease: progress and problems on the road to therapeutics. *Science* **297**, 353-356.
- Hartl, F.U. (1996). Molecular chaperones in cellular protein folding. *Nature* **381**, 571-579.
- Hartl, F.U., Bracher, A., and Hayer-Hartl, M. (2011). Molecular chaperones in protein folding and proteostasis. *Nature* **475**, 324-332.
- Hartl, F.U., Hlodan, R., and Langer, T. (1994). Molecular chaperones in protein folding: the art of avoiding sticky situations. *Trends Biochem Sci* **19**, 20-25.
- Haslberger, T., Zdanowicz, A., Brand, I., Kirstein, J., Turgay, K., Mogk, A., and Bukau, B. (2008). Protein disaggregation by the AAA+ chaperone ClpB involves partial threading of looped polypeptide segments. *Nat Struct Mol Biol* **15**, 641-650.
- Hattendorf, D.A., and Lindquist, S.L. (2002). Cooperative kinetics of both Hsp104 ATPase domains and interdomain communication revealed by AAA sensor-1 mutants. *EMBO J* **21**, 12-21.
- Heinemeyer, W., Fischer, M., Krimmer, T., Stachon, U., and Wolf, D.H. (1997). The active sites of the eukaryotic 20 S proteasome and their involvement in subunit precursor processing. *J Biol Chem* **272**, 25200-25209.
- Heink, S., Ludwig, D., Kloetzel, P.M., and Kruger, E. (2005). IFN-gamma-induced immune adaptation of the proteasome system is an accelerated and transient response. *Proc Natl Acad Sci U S A* **102**, 9241-9246.
- Heo, J.M., Livnat-Levanon, N., Taylor, E.B., Jones, K.T., Dephore, N., Ring, J., Xie, J., Brodsky, J.L., Madeo, F., Gygi, S.P., *et al.* (2010). A stress-responsive system for mitochondrial protein degradation. *Mol Cell* **40**, 465-480.
- Hershko, A., Ciechanover, A., Heller, H., Haas, A.L., and Rose, I.A. (1980). Proposed role of ATP in protein breakdown: conjugation of protein with multiple chains of the polypeptide of ATP-dependent proteolysis. *Proc Natl Acad Sci U S A* **77**, 1783-1786.
- Hershko, A., Ciechanover, A., and Rose, I.A. (1981). Identification of the active amino acid residue of the polypeptide of ATP-dependent protein breakdown. *J Biol Chem* **256**, 1525-1528.

- Heuck, A., Schitter-Sollner, S., Suskiewicz, M.J., Kurzbauer, R., Kley, J., Schleiffer, A., Rombaut, P., Herzog, F., and Clausen, T. (2016). Structural basis for the disaggregase activity and regulation of Hsp104. *Elife* 5.
- Hipp, M.S., Kalveram, B., Raasi, S., Groettrup, M., and Schmidtke, G. (2005). FAT10, a ubiquitin-independent signal for proteasomal degradation. *Mol Cell Biol* 25, 3483-3491.
- Hipp, M.S., Kasturi, P., and Hartl, F.U. (2019). The proteostasis network and its decline in ageing. *Nat Rev Mol Cell Biol*.
- Hipp, M.S., Park, S.H., and Hartl, F.U. (2014). Proteostasis impairment in protein-misfolding and -aggregation diseases. *Trends Cell Biol* 24, 506-514.
- Hirabayashi, M., Inoue, K., Tanaka, K., Nakadate, K., Ohsawa, Y., Kamei, Y., Popiel, A.H., Sinohara, A., Iwamatsu, A., Kimura, Y., *et al.* (2001). VCP/p97 in abnormal protein aggregates, cytoplasmic vacuoles, and cell death, phenotypes relevant to neurodegeneration. *Cell Death Differ* 8, 977-984.
- Hjerpe, R., Bett, J.S., Keuss, M.J., Solovyova, A., McWilliams, T.G., Johnson, C., Sahu, I., Varghese, J., Wood, N., Wightman, M., *et al.* (2016). UBQLN2 Mediates Autophagy-Independent Protein Aggregate Clearance by the Proteasome. *Cell* 166, 935-949.
- Hochstrasser, M. (1996). Ubiquitin-dependent protein degradation. *Annu Rev Genet* 30, 405-439.
- Holmes, B.B., Furman, J.L., Mahan, T.E., Yamasaki, T.R., Mirbaha, H., Eades, W.C., Belaygorod, L., Cairns, N.J., Holtzman, D.M., and Diamond, M.I. (2014). Proteopathic tau seeding predicts tauopathy in vivo. *Proceedings of the National Academy of Sciences of the United States of America* 111, E4376-E4385.
- Howie, A.J., and Brewer, D.B. (2009). Optical properties of amyloid stained by Congo red: history and mechanisms. *Micron* 40, 285-301.
- Hsiao, K.K., Groth, D., Scott, M., Yang, S.L., Serban, H., Rapp, D., Foster, D., Torchia, M., Dearmond, S.J., and Prusiner, S.B. (1994). Serial transmission in rodents of neurodegeneration from transgenic mice expressing mutant prion protein. *Proc Natl Acad Sci U S A* 91, 9126-9130.
- Hutton, M., Lendon, C.L., Rizzu, P., Baker, M., Froelich, S., Houlden, H., Pickering-Brown, S., Chakraverty, S., Isaacs, A., Grover, A., *et al.* (1998). Association of missense and 5'-splice-site mutations in tau with the inherited dementia FTDP-17. *Nature* 393, 702-705.
- Hyer, M.L., Milhollen, M.A., Ciavarrri, J., Fleming, P., Traore, T., Sappal, D., Huck, J., Shi, J., Gavin, J., Brownell, J., *et al.* (2018). A small-molecule inhibitor of the ubiquitin activating enzyme for cancer treatment. *Nat Med* 24, 186-193.
- Iadanza, M.G., Jackson, M.P., Hewitt, E.W., Ranson, N.A., and Radford, S.E. (2018). A new era for understanding amyloid structures and disease. *Nat Rev Mol Cell Biol* 19, 755-773.
- Iba, M., Guo, J.L., McBride, J.D., Zhang, B., Trojanowski, J.Q., and Lee, V.M. (2013). Synthetic tau fibrils mediate transmission of neurofibrillary tangles in a transgenic mouse model of Alzheimer's-like tauopathy. *J Neurosci* 33, 1024-1037.
- Iconomidou, V.A., Vriend, G., and Hamodrakas, S.J. (2000). Amyloids protect the silkworm oocyte and embryo. *FEBS Lett* 479, 141-145.
- Iqbal, K., Grundke-Iqbal, I., Zaidi, T., Merz, P.A., Wen, G.Y., Shaikh, S.S., Wisniewski, H.M., Alafuzoff, I., and Winblad, B. (1986). Defective brain microtubule assembly in Alzheimer's disease. *Lancet* 2, 421-426.
- Ishigaki, S., Hishikawa, N., Niwa, J., Iemura, S., Natsume, T., Hori, S., Kakizuka, A., Tanaka, K., and Sobue, G. (2004). Physical and functional interaction between Dorfin and Valosin-containing protein that are colocalized in ubiquitylated inclusions in neurodegenerative disorders. *J Biol Chem* 279, 51376-51385.
- Itakura, E., Zavodszky, E., Shao, S., Wohlever, Matthew L., Keenan, Robert J., and Hegde, Ramanujan S. (2016). Ubiquilins Chaperone and Triage Mitochondrial Membrane Proteins for Degradation. *Molecular Cell* 63, 21-33.
- Iwata, A., Christianson, J.C., Bucci, M., Ellerby, L.M., Nukina, N., Forno, L.S., and Kopito, R.R. (2005a). Increased susceptibility of cytoplasmic over nuclear polyglutamine aggregates to autophagic degradation. *Proceedings of the National Academy of Sciences of the United States of America* 102, 13135.

- Iwata, A., Riley, B.E., Johnston, J.A., and Kopito, R.R. (2005b). HDAC6 and microtubules are required for autophagic degradation of aggregated huntingtin. *J Biol Chem* 280, 40282-40292.
- Jackrel, M.E., DeSantis, M.E., Martinez, B.A., Castellano, L.M., Stewart, R.M., Caldwell, K.A., Caldwell, G.A., and Shorter, J. (2014). Potentiated Hsp104 variants antagonize diverse proteotoxic misfolding events. *Cell* 156, 170-182.
- Jackson, G.R., Salecker, I., Dong, X., Yao, X., Arnheim, N., Faber, P.W., MacDonald, M.E., and Zipursky, S.L. (1998). Polyglutamine-expanded human huntingtin transgenes induce degeneration of *Drosophila* photoreceptor neurons. *Neuron* 21, 633-642.
- Jacobson, A.D., Zhang, N.Y., Xu, P., Han, K.J., Noone, S., Peng, J., and Liu, C.W. (2009). The lysine 48 and lysine 63 ubiquitin conjugates are processed differently by the 26 S proteasome. *J Biol Chem* 284, 35485-35494.
- Jahn, T.R., and Radford, S.E. (2005). The Yin and Yang of protein folding. *Febs j* 272, 5962-5970.
- Jayaraj, G.G., Hipp, M.S., and Hartl, F.U. (2019). Functional Modules of the Proteostasis Network. *Cold Spring Harb Perspect Biol*.
- Johnston, J.A., Ward, C.L., and Kopito, R.R. (1998). Aggresomes: a cellular response to misfolded proteins. *J Cell Biol* 143, 1883-1898.
- Ju, J.S., Miller, S.E., Hanson, P.I., and Weihl, C.C. (2008). Impaired protein aggregate handling and clearance underlie the pathogenesis of p97/VCP-associated disease. *J Biol Chem* 283, 30289-30299.
- Jucker, M., and Walker, L.C. (2018). Propagation and spread of pathogenic protein assemblies in neurodegenerative diseases. *Nat Neurosci* 21, 1341-1349.
- Kaganovich, D., Kopito, R., and Frydman, J. (2008). Misfolded proteins partition between two distinct quality control compartments. *Nature* 454, 1088-1095.
- Kama, R., Gabriely, G., Kanneganti, V., and Gerst, J.E. (2018). Cdc48 and ubiquilins confer selective anterograde protein sorting and entry into the multivesicular body in yeast. *Mol Biol Cell* 29, 948-963.
- Kampinga, H.H., and Craig, E.A. (2010). The HSP70 chaperone machinery: J proteins as drivers of functional specificity. *Nat Rev Mol Cell Biol* 11, 579-592.
- Kar, K., Jayaraman, M., Sahoo, B., Kodali, R., and Wetzel, R. (2011). Critical nucleus size for disease-related polyglutamine aggregation is repeat-length dependent. *Nat Struct Mol Biol* 18, 328-336.
- Karbowski, M., and Youle, R.J. (2011). Regulating mitochondrial outer membrane proteins by ubiquitination and proteasomal degradation. *Curr Opin Cell Biol* 23, 476-482.
- Kaufman, S.K., Sanders, D.W., Thomas, T.L., Ruchinskas, A.J., Vaquer-Alicea, J., Sharma, A.M., Miller, T.M., and Diamond, M.I. (2016). Tau Prion Strains Dictate Patterns of Cell Pathology, Progression Rate, and Regional Vulnerability In Vivo. *Neuron* 92, 796-812.
- Kaushik, S., and Cuervo, A.M. (2018). The coming of age of chaperone-mediated autophagy. *Nat Rev Mol Cell Biol* 19, 365-381.
- Keates, R.A., and Hall, R.H. (1975). Tubulin requires an accessory protein for self assembly in microtubules. *Nature* 257, 418-421.
- Kellogg, E.H., Hejab, N.M.A., Poepsel, S., Downing, K.H., DiMaio, F., and Nogales, E. (2018). Near-atomic model of microtubule-tau interactions. *Science* 360, 1242-1246.
- Kenessey, A., and Yen, S.H. (1993). The extent of phosphorylation of fetal tau is comparable to that of PHF-tau from Alzheimer paired helical filaments. *Brain Res* 629, 40-46.
- Kfoury, N., Holmes, B.B., Jiang, H., Holtzman, D.M., and Diamond, M.I. (2012). Trans-cellular propagation of Tau aggregation by fibrillar species. *J Biol Chem* 287, 19440-19451.
- Khaminets, A., Behl, C., and Dikic, I. (2016). Ubiquitin-Dependent And Independent Signals In Selective Autophagy. *Trends Cell Biol* 26, 6-16.
- Khlistunova, I., Biernat, J., Wang, Y., Pickhardt, M., von Bergen, M., Gazova, Z., Mandelkow, E., and Mandelkow, E.M. (2006). Inducible expression of Tau repeat domain in cell models of tauopathy: aggregation is toxic to cells but can be reversed by inhibitor drugs. *J Biol Chem* 281, 1205-1214.
- Kim, Y.E., Hipp, M.S., Bracher, A., Hayer-Hartl, M., and Hartl, F.U. (2013). Molecular chaperone functions in protein folding and proteostasis. *Annu Rev Biochem* 82, 323-355.

- Kim, Y.E., Hosp, F., Frottin, F., Ge, H., Mann, M., Hayer-Hartl, M., and Hartl, F.U. (2016). Soluble Oligomers of PolyQ-Expanded Huntingtin Target a Multiplicity of Key Cellular Factors. *Mol Cell* 63, 951-964.
- Kirstein, J., Arnsburg, K., Scior, A., Szlachcic, A., Guilbride, D.L., Morimoto, R.I., Bukau, B., and Nillegoda, N.B. (2017). In vivo properties of the disaggregase function of J-proteins and Hsc70 in *Caenorhabditis elegans* stress and aging. *Aging Cell*.
- Kisselev, A.F., Akopian, T.N., Woo, K.M., and Goldberg, A.L. (1999). The sizes of peptides generated from protein by mammalian 26 and 20 S proteasomes. Implications for understanding the degradative mechanism and antigen presentation. *J Biol Chem* 274, 3363-3371.
- Klaips, C.L., Jayaraj, G.G., and Hartl, F.U. (2018). Pathways of cellular proteostasis in aging and disease. *J Cell Biol* 217, 51-63.
- Knowles, T.P., Fitzpatrick, A.W., Meehan, S., Mott, H.R., Vendruscolo, M., Dobson, C.M., and Welland, M.E. (2007). Role of intermolecular forces in defining material properties of protein nanofibrils. *Science* 318, 1900-1903.
- Knowles, T.P., Vendruscolo, M., and Dobson, C.M. (2014). The amyloid state and its association with protein misfolding diseases. *Nat Rev Mol Cell Biol* 15, 384-396.
- Kobayashi, H., Shoji, K., Kiyokawa, K., Negishi, L., and Tomari, Y. (2019). VCP Machinery Mediates Autophagic Degradation of Empty Argonaute. *Cell Rep* 28, 1144-1153.e1144.
- Kobayashi, T., Manno, A., and Kakizuka, A. (2007). Involvement of valosin-containing protein (VCP)/p97 in the formation and clearance of abnormal protein aggregates. *Genes Cells* 12, 889-901.
- Kolarova, M., Garcia-Sierra, F., Bartos, A., Ricny, J., and Ripova, D. (2012). Structure and pathology of tau protein in Alzheimer disease. *Int J Alzheimers Dis* 2012, 731526.
- Komander, D. (2009). The emerging complexity of protein ubiquitination. *Biochem Soc Trans* 37, 937-953.
- Komander, D., and Rape, M. (2012). The ubiquitin code. *Annu Rev Biochem* 81, 203-229.
- Komatsu, M., Waguri, S., Chiba, T., Murata, S., Iwata, J., Tanida, I., Ueno, T., Koike, M., Uchiyama, Y., Kominami, E., *et al.* (2006). Loss of autophagy in the central nervous system causes neurodegeneration in mice. *Nature* 441, 880-884.
- Kondo, H., Rabouille, C., Newman, R., Levine, T.P., Pappin, D., Freemont, P., and Warren, G. (1997). p47 is a cofactor for p97-mediated membrane fusion. *Nature* 388, 75-78.
- Kopito, R.R. (2000). Aggresomes, inclusion bodies and protein aggregation. *Trends Cell Biol* 10, 524-530.
- Kopke, E., Tung, Y.C., Shaikh, S., Alonso, A.C., Iqbal, K., and Grundke-Iqbal, I. (1993). Microtubule-associated protein tau. Abnormal phosphorylation of a non-paired helical filament pool in Alzheimer disease. *J Biol Chem* 268, 24374-24384.
- Kosik, K.S., Orecchio, L.D., Bakalis, S., and Neve, R.L. (1989). Developmentally regulated expression of specific tau sequences. *Neuron* 2, 1389-1397.
- Koss, D.J., Robinson, L., Drever, B.D., Plucinska, K., Stoppelkamp, S., Veselcic, P., Riedel, G., and Platt, B. (2016). Mutant Tau knock-in mice display frontotemporal dementia relevant behaviour and histopathology. *Neurobiol Dis* 91, 105-123.
- Kraft, C., Peter, M., and Hofmann, K. (2010). Selective autophagy: ubiquitin-mediated recognition and beyond. *Nat Cell Biol* 12, 836-841.
- Ksiezak-Reding, H., Liu, W.K., and Yen, S.H. (1992). Phosphate analysis and dephosphorylation of modified tau associated with paired helical filaments. *Brain Res* 597, 209-219.
- Kundel, F., Hong, L., Falcon, B., McEwan, W.A., Michaels, T.C.T., Meisl, G., Esteras, N., Abramov, A.Y., Knowles, T.J.P., Goedert, M., *et al.* (2018). Measurement of Tau Filament Fragmentation Provides Insights into Prion-like Spreading. *ACS Chem Neurosci* 9, 1276-1282.
- Kuusisto, E., Salminen, A., and Alafuzoff, I. (2001). Ubiquitin-binding protein p62 is present in neuronal and glial inclusions in human tauopathies and synucleinopathies. *Neuroreport* 12, 2085-2090.
- Lamark, T., and Johansen, T. (2012). Aggrephagy: selective disposal of protein aggregates by macroautophagy. *Int J Cell Biol* 2012, 736905.

- Laskey, R.A., Honda, B.M., Mills, A.D., and Finch, J.T. (1978). Nucleosomes are assembled by an acidic protein which binds histones and transfers them to DNA. *Nature* 275, 416-420.
- Lee, D.H., and Goldberg, A.L. (1998). Proteasome inhibitors: valuable new tools for cell biologists. *Trends Cell Biol* 8, 397-403.
- Lee, J.A., Liu, L., and Gao, F.B. (2009). Autophagy defects contribute to neurodegeneration induced by dysfunctional ESCRT-III. *Autophagy* 5, 1070-1072.
- LeVine, H., 3rd (1993). Thioflavine T interaction with synthetic Alzheimer's disease beta-amyloid peptides: detection of amyloid aggregation in solution. *Protein Sci* 2, 404-410.
- Lewandowska, A., Matuszewska, M., and Liberek, K. (2007). Conformational properties of aggregated polypeptides determine ClpB-dependence in the disaggregation process. *J Mol Biol* 371, 800-811.
- Li, S.H., and Li, X.J. (1998). Aggregation of N-terminal huntingtin is dependent on the length of its glutamine repeats. *Hum Mol Genet* 7, 777-782.
- Lindwall, G., and Cole, R.D. (1984). Phosphorylation affects the ability of tau protein to promote microtubule assembly. *J Biol Chem* 259, 5301-5305.
- Lipinska, N., Zietkiewicz, S., Sobczak, A., Jurczyk, A., Potocki, W., Morawiec, E., Wawrzycka, A., Gumowski, K., Slusarz, M., Rodziewicz-Motowidlo, S., *et al.* (2013). Disruption of ionic interactions between the nucleotide binding domain 1 (NBD1) and middle (M) domain in Hsp100 disaggregase unleashes toxic hyperactivity and partial independence from Hsp70. *J Biol Chem* 288, 2857-2869.
- Loew, R., Heinz, N., Hampf, M., Bujard, H., and Gossen, M. (2010). Improved Tet-responsive promoters with minimized background expression. *BMC Biotechnology* 10, 81.
- Lokireddy, S., Kukushkin, N.V., and Goldberg, A.L. (2015). cAMP-induced phosphorylation of 26S proteasomes on Rpn6/PSMD11 enhances their activity and the degradation of misfolded proteins. *Proc Natl Acad Sci U S A* 112, E7176-7185.
- Lomakin, A., Chung, D.S., Benedek, G.B., Kirschner, D.A., and Teplow, D.B. (1996). On the nucleation and growth of amyloid beta-protein fibrils: detection of nuclei and quantitation of rate constants. *Proc Natl Acad Sci U S A* 93, 1125-1129.
- Magnaghi, P., D'Alessio, R., Valsasina, B., Avanzi, N., Rizzi, S., Asa, D., Gasparri, F., Cozzi, L., Cucchi, U., Orrenius, C., *et al.* (2013). Covalent and allosteric inhibitors of the ATPase VCP/p97 induce cancer cell death. *Nat Chem Biol* 9, 548-556.
- Maji, S.K., Perrin, M.H., Sawaya, M.R., Jessberger, S., Vadodaria, K., Rissman, R.A., Singru, P.S., Nilsson, K.P., Simon, R., Schubert, D., *et al.* (2009). Functional amyloids as natural storage of peptide hormones in pituitary secretory granules. *Science* 325, 328-332.
- Malcolm, J.C., Breuillaud, L., Do Carmo, S., Hall, H., Welikovitsh, L.A., Macdonald, J.A., Goedert, M., and Cuelllo, A.C. (2019). Neuropathological changes and cognitive deficits in rats transgenic for human mutant tau recapitulate human tauopathy. *Neurobiol Dis* 127, 323-338.
- Martín-Aparicio, E., Yamamoto, A., Hernández, F., Hen, R., Avila, J., and Lucas, J.J. (2001). Proteasomal-Dependent Aggregate Reversal and Absence of Cell Death in a Conditional Mouse Model of Huntington's Disease. *The Journal of Neuroscience* 21, 8772.
- Mayer, M.P. (2010). Gymnastics of molecular chaperones. *Mol Cell* 39, 321-331.
- Mellman, I. (1995). Enigma variations: protein mediators of membrane fusion. *Cell* 82, 869-872.
- Metzger, M.B., Hristova, V.A., and Weissman, A.M. (2012). HECT and RING finger families of E3 ubiquitin ligases at a glance. *J Cell Sci* 125, 531-537.
- Meusser, B., Hirsch, C., Jarosch, E., and Sommer, T. (2005). ERAD: the long road to destruction. *Nat Cell Biol* 7, 766-772.
- Meyer, H., Bug, M., and Bremer, S. (2012). Emerging functions of the VCP/p97 AAA-ATPase in the ubiquitin system. *Nat Cell Biol* 14, 117-123.
- Meyer, H.H. (2005). Golgi reassembly after mitosis: the AAA family meets the ubiquitin family. *Biochim Biophys Acta* 1744, 481-492.
- Meyer, R.K., McKinley, M.P., Bowman, K.A., Braunfeld, M.B., Barry, R.A., and Prusiner, S.B. (1986). Separation and properties of cellular and scrapie prion proteins. *Proc Natl Acad Sci U S A* 83, 2310-2314.
- Milanesi, L., Sheynis, T., Xue, W.-F., Orlova, E.V., Hellewell, A.L., Jelinek, R., Hewitt, E.W., Radford, S.E., and Saibil, H.R. (2012). Direct three-dimensional visualization of

- membrane disruption by amyloid fibrils. *Proceedings of the National Academy of Sciences* *109*, 20455.
- Mirbaha, H., Chen, D., Morazova, O.A., Ruff, K.M., Sharma, A.M., Liu, X., Goodarzi, M., Pappu, R.V., Colby, D.W., Mirzaei, H., *et al.* (2018). Inert and seed-competent tau monomers suggest structural origins of aggregation. *eLife* *7*, e36584.
- Mizuno, Y., Hori, S., Kakizuka, A., and Okamoto, K. (2003). Vacuole-creating protein in neurodegenerative diseases in humans. *Neurosci Lett* *343*, 77-80.
- Mogk, A., Bukau, B., and Kampinga, H.H. (2018). Cellular Handling of Protein Aggregates by Disaggregation Machines. *Mol Cell* *69*, 214-226.
- Mogk, A., Kummer, E., and Bukau, B. (2015). Cooperation of Hsp70 and Hsp100 chaperone machines in protein disaggregation. *Frontiers in molecular biosciences* *2*, 22-22.
- Mogk, A., Tomoyasu, T., Goloubinoff, P., Rudiger, S., Roder, D., Langen, H., and Bukau, B. (1999). Identification of thermolabile *Escherichia coli* proteins: prevention and reversion of aggregation by DnaK and ClpB. *EMBO J* *18*, 6934-6949.
- Moir, D., Stewart, S.E., Osmond, B.C., and Botstein, D. (1982). Cold-sensitive cell-division-cycle mutants of yeast: isolation, properties, and pseudoreversion studies. *Genetics* *100*, 547-563.
- Morris, M., Maeda, S., Vossel, K., and Mucke, L. (2011). The many faces of tau. *Neuron* *70*, 410-426.
- Muller, A.U., and Weber-Ban, E. (2019). The Bacterial Proteasome at the Core of Diverse Degradation Pathways. *Front Mol Biosci* *6*, 23.
- Murakami, Y., Matsufuji, S., Kameji, T., Hayashi, S., Igarashi, K., Tamura, T., Tanaka, K., and Ichihara, A. (1992). Ornithine decarboxylase is degraded by the 26S proteasome without ubiquitination. *Nature* *360*, 597-599.
- Murata, S., Sasaki, K., Kishimoto, T., Niwa, S., Hayashi, H., Takahama, Y., and Tanaka, K. (2007). Regulation of CD8+ T cell development by thymus-specific proteasomes. *Science* *316*, 1349-1353.
- Murata, S., Takahama, Y., Kasahara, M., and Tanaka, K. (2018). The immunoproteasome and thymoproteasome: functions, evolution and human disease. *Nat Immunol* *19*, 923-931.
- Myeku, N., Clelland, C.L., Emrani, S., Kukushkin, N.V., Yu, W.H., Goldberg, A.L., and Duff, K.E. (2016). Tau-driven 26S proteasome impairment and cognitive dysfunction can be prevented early in disease by activating cAMP-PKA signaling. *Nature Medicine* *22*, 46-53.
- Nakatogawa, H., Suzuki, K., Kamada, Y., and Ohsumi, Y. (2009). Dynamics and diversity in autophagy mechanisms: lessons from yeast. *Nat Rev Mol Cell Biol* *10*, 458-467.
- Nanduri, P., Hao, R., Fitzpatrick, T., and Yao, T.P. (2015). Chaperone-mediated 26S proteasome remodeling facilitates free K63 ubiquitin chain production and aggresome clearance. *J Biol Chem* *290*, 9455-9464.
- Nillegoda, N.B., Kirstein, J., Szlachcic, A., Berynsky, M., Stank, A., Stengel, F., Arnsburg, K., Gao, X., Scior, A., Aebersold, R., *et al.* (2015). Crucial HSP70 co-chaperone complex unlocks metazoan protein disaggregation. *Nature* *524*, 247-251.
- Nillegoda, N.B., Stank, A., Malinverni, D., Alberts, N., Szlachcic, A., Barducci, A., De Los Rios, P., Wade, R.C., and Bukau, B. (2017). Evolution of an intricate J-protein network driving protein disaggregation in eukaryotes. *Elife* *6*.
- Nillegoda, N.B., Wentink, A.S., and Bukau, B. (2018). Protein Disaggregation in Multicellular Organisms. *Trends Biochem Sci* *43*, 285-300.
- Nisbet, R.M., Polanco, J.C., Ittner, L.M., and Gotz, J. (2015). Tau aggregation and its interplay with amyloid-beta. *Acta Neuropathol* *129*, 207-220.
- Niwa, H., Ewens, C.A., Tsang, C., Yeung, H.O., Zhang, X., and Freemont, P.S. (2012). The Role of the N-Domain in the ATPase Activity of the Mammalian AAA ATPase p97/VCP. *Journal of Biological Chemistry* *287*, 8561-8570.
- Nixon, R.A. (2013). The role of autophagy in neurodegenerative disease. *Nat Med* *19*, 983-997.
- Oguchi, Y., Kummer, E., Seyffer, F., Berynsky, M., Anstett, B., Zahn, R., Wade, R.C., Mogk, A., and Bukau, B. (2012). A tightly regulated molecular toggle controls AAA+ disaggregase. *Nat Struct Mol Biol* *19*, 1338-1346.
- Olivares, A.O., Baker, T.A., and Sauer, R.T. (2016). Mechanistic insights into bacterial AAA+ proteases and protein-remodelling machines. *Nat Rev Microbiol* *14*, 33-44.

- Olszewski, M.M., Williams, C., Dong, K.C., and Martin, A. (2019). The Cdc48 unfoldase prepares well-folded protein substrates for degradation by the 26S proteasome. *Communications Biology* 2, 29.
- Olzmann, J.A., Li, L., and Chin, L.S. (2008). Aggresome formation and neurodegenerative diseases: therapeutic implications. *Curr Med Chem* 15, 47-60.
- Olzscha, H., Schermann, S.M., Woerner, A.C., Pinkert, S., Hecht, M.H., Tartaglia, G.G., Vendruscolo, M., Hayer-Hartl, M., Hartl, F.U., and Vabulas, R.M. (2011). Amyloid-like aggregates sequester numerous metastable proteins with essential cellular functions. *Cell* 144, 67-78.
- Ong, S.E., Blagoev, B., Kratchmarova, I., Kristensen, D.B., Steen, H., Pandey, A., and Mann, M. (2002). Stable isotope labeling by amino acids in cell culture, SILAC, as a simple and accurate approach to expression proteomics. *Mol Cell Proteomics* 1, 376-386.
- Onodera, J., and Ohsumi, Y. (2005). Autophagy is required for maintenance of amino acid levels and protein synthesis under nitrogen starvation. *J Biol Chem* 280, 31582-31586.
- Ostermann, J., Horwich, A.L., Neupert, W., and Hartl, F.U. (1989). Protein folding in mitochondria requires complex formation with hsp60 and ATP hydrolysis. *Nature* 341, 125-130.
- Parsell, D.A., Kowal, A.S., and Lindquist, S. (1994a). *Saccharomyces cerevisiae* Hsp104 protein. Purification and characterization of ATP-induced structural changes. *J Biol Chem* 269, 4480-4487.
- Parsell, D.A., Kowal, A.S., Singer, M.A., and Lindquist, S. (1994b). Protein disaggregation mediated by heat-shock protein Hsp104. *Nature* 372, 475-478.
- Parsell, D.A., Sanchez, Y., Stitzel, J.D., and Lindquist, S. (1991). Hsp104 is a highly conserved protein with two essential nucleotide-binding sites. *Nature* 353, 270-273.
- Patino, M.M., Liu, J.J., Glover, J.R., and Lindquist, S. (1996). Support for the prion hypothesis for inheritance of a phenotypic trait in yeast. *Science* 273, 622-626.
- Paushkin, S.V., Kushnirov, V.V., Smirnov, V.N., and Ter-Avanesyan, M.D. (1996). Propagation of the yeast prion-like [psi⁺] determinant is mediated by oligomerization of the SUP35-encoded polypeptide chain release factor. *EMBO J* 15, 3127-3134.
- Perez, M., Valpuesta, J.M., Medina, M., Montejo de Garcini, E., and Avila, J. (1996). Polymerization of tau into filaments in the presence of heparin: the minimal sequence required for tau-tau interaction. *J Neurochem* 67, 1183-1190.
- Piatnitskaia, S., Takahashi, M., Kitaura, H., Katsuragi, Y., Kakihana, T., Zhang, L., Kakita, A., Iwakura, Y., Nawa, H., Miura, T., *et al.* (2019). USP10 is a critical factor for Tau-positive stress granule formation in neuronal cells. *Scientific Reports* 9, 10591.
- Pickart, C.M. (2001). Mechanisms underlying ubiquitination. *Annu Rev Biochem* 70, 503-533.
- Pieri, L., Madiona, K., Bousset, L., and Melki, R. (2012). Fibrillar α -Synuclein and Huntingtin Exon 1 Assemblies Are Toxic to the Cells. *Biophysical Journal* 102, 2894-2905.
- Pinto, M., Morange, M., and Bensaude, O. (1991). Denaturation of proteins during heat shock. In vivo recovery of solubility and activity of reporter enzymes. *J Biol Chem* 266, 13941-13946.
- Piras, A., Collin, L., Gruninger, F., Graff, C., and Ronnback, A. (2016). Autophagic and lysosomal defects in human tauopathies: analysis of post-mortem brain from patients with familial Alzheimer disease, corticobasal degeneration and progressive supranuclear palsy. *Acta Neuropathol Commun* 4, 22.
- Poepsel, S., Sprengel, A., Sacca, B., Kaschani, F., Kaiser, M., Gatsogiannis, C., Raunser, S., Clausen, T., and Ehrmann, M. (2015). Determinants of amyloid fibril degradation by the PDZ protease HTRA1. *Nat Chem Biol* 11, 862-869.
- Poirier, M.A., Li, H., Macosko, J., Cai, S., Amzel, M., and Ross, C.A. (2002). Huntingtin spheroids and protofibrils as precursors in polyglutamine fibrilization. *J Biol Chem* 277, 41032-41037.
- Polydoro, M., de Calignon, A., Suarez-Calvet, M., Sanchez, L., Kay, K.R., Nicholls, S.B., Roe, A.D., Pitsstick, R., Carlson, G.A., Gomez-Isla, T., *et al.* (2013). Reversal of neurofibrillary tangles and tau-associated phenotype in the rTgTauEC model of early Alzheimer's disease. *J Neurosci* 33, 13300-13311.

- Poorkaj, P., Bird, T.D., Wijsman, E., Nemens, E., Garruto, R.M., Anderson, L., Andreadis, A., Wiederholt, W.C., Raskind, M., and Schellenberg, G.D. (1998). Tau is a candidate gene for chromosome 17 frontotemporal dementia. *Ann Neurol* **43**, 815-825.
- Prusiner, S.B. (2013). Biology and genetics of prions causing neurodegeneration. *Annu Rev Genet* **47**, 601-623.
- Prusiner, S.B., McKinley, M.P., Bowman, K.A., Bolton, D.C., Bendheim, P.E., Groth, D.F., and Glenner, G.G. (1983). Scrapie prions aggregate to form amyloid-like birefringent rods. *Cell* **35**, 349-358.
- Puchades, C., Sandate, C.R., and Lander, G.C. (2020). The molecular principles governing the activity and functional diversity of AAA+ proteins. *Nature Reviews Molecular Cell Biology* **21**, 43-58.
- Qiu, X.B., Lin, Y.L., Thome, K.C., Pian, P., Schlegel, B.P., Weremowicz, S., Parvin, J.D., and Dutta, A. (1998). An eukaryotic RuvB-like protein (RUVBL1) essential for growth. *J Biol Chem* **273**, 27786-27793.
- Rabouille, C., Kondo, H., Newman, R., Hui, N., Freemont, P., and Warren, G. (1998). Syntaxin 5 Is a Common Component of the NSF- and p97-Mediated Reassembly Pathways of Golgi Cisternae from Mitotic Golgi Fragments In Vitro. *Cell* **92**, 603-610.
- Radhakrishnan, S.K., den Besten, W., and Deshaies, R.J. (2014). p97-dependent retrotranslocation and proteolytic processing govern formation of active Nrf1 upon proteasome inhibition. *Elife* **3**, e01856.
- Ramadan, K., Bruderer, R., Spiga, F.M., Popp, O., Baur, T., Gotta, M., and Meyer, H.H. (2007). Cdc48/p97 promotes reformation of the nucleus by extracting the kinase Aurora B from chromatin. *Nature* **450**, 1258.
- Rampelt, H., Kirstein-Miles, J., Nillegoda, N.B., Chi, K., Scholz, S.R., Morimoto, R.I., and Bukau, B. (2012). Metazoan Hsp70 machines use Hsp110 to power protein disaggregation. *EMBO J* **31**, 4221-4235.
- Rape, M., Hoppe, T., Gorr, I., Kalocay, M., Richly, H., and Jentsch, S. (2001). Mobilization of processed, membrane-tethered SPT23 transcription factor by CDC48(UFD1/NPL4), a ubiquitin-selective chaperone. *Cell* **107**, 667-677.
- Ravikumar, B., Duden, R., and Rubinsztein, D.C. (2002). Aggregate-prone proteins with polyglutamine and polyalanine expansions are degraded by autophagy. *Hum Mol Genet* **11**, 1107-1117.
- Richly, H., Rape, M., Braun, S., Rumpf, S., Hoegel, C., and Jentsch, S. (2005). A series of ubiquitin binding factors connects CDC48/p97 to substrate multiubiquitylation and proteasomal targeting. *Cell* **120**, 73-84.
- Richter, K., Haslbeck, M., and Buchner, J. (2010). The heat shock response: life on the verge of death. *Mol Cell* **40**, 253-266.
- Rittinger, K., and Ikeda, F. (2017). Linear ubiquitin chains: enzymes, mechanisms and biology. *Open Biol* **7**, 170026.
- Ritz, D., Vuk, M., Kirchner, P., Bug, M., Schütz, S., Hayer, A., Bremer, S., Lusk, C., Baloh, R.H., Lee, H., *et al.* (2011). Endolysosomal sorting of ubiquitylated caveolin-1 is regulated by VCP and UBXD1 and impaired by VCP disease mutations. *Nature Cell Biology* **13**, 1116-1123.
- Roberson, E.D., Scarce-Levie, K., Palop, J.J., Yan, F., Cheng, I.H., Wu, T., Gerstein, H., Yu, G.Q., and Mucke, L. (2007). Reducing endogenous tau ameliorates amyloid beta-induced deficits in an Alzheimer's disease mouse model. *Science* **316**, 750-754.
- Rochet, J.C., Conway, K.A., and Lansbury, P.T., Jr. (2000). Inhibition of fibrillization and accumulation of prefibrillar oligomers in mixtures of human and mouse alpha-synuclein. *Biochemistry* **39**, 10619-10626.
- Rosenzweig, R., Moradi, S., Zarrine-Afsar, A., Glover, J.R., and Kay, L.E. (2013). Unraveling the mechanism of protein disaggregation through a ClpB-DnaK interaction. *Science* **339**, 1080-1083.
- Rosenzweig, R., Nillegoda, N.B., Mayer, M.P., and Bukau, B. (2019). The Hsp70 chaperone network. *Nat Rev Mol Cell Biol*.
- Rosenzweig, R., Osmulski, P.A., Gaczynska, M., and Glickman, M.H. (2008). The central unit within the 19S regulatory particle of the proteasome. *Nat Struct Mol Biol* **15**, 573-580.

- Ross, C.A., and Poirier, M.A. (2004). Protein aggregation and neurodegenerative disease. *Nat Med* 10 *Suppl*, S10-17.
- Rouiller, I., Butel, V.M., Latterich, M., Milligan, R.A., and Wilson-Kubalek, E.M. (2000). A Major Conformational Change in p97 AAA ATPase upon ATP Binding. *Molecular Cell* 6, 1485-1490.
- Rousseau, A., and Bertolotti, A. (2016). An evolutionarily conserved pathway controls proteasome homeostasis. *Nature* 536, 184-189.
- Rousseau, E., Kojima, R., Hoffner, G., Djian, P., and Bertolotti, A. (2009). Misfolding of proteins with a polyglutamine expansion is facilitated by proteasomal chaperones. *J Biol Chem* 284, 1917-1929.
- Rubin, D.M., Glickman, M.H., Larsen, C.N., Dhruvakumar, S., and Finley, D. (1998). Active site mutants in the six regulatory particle ATPases reveal multiple roles for ATP in the proteasome. *EMBO J* 17, 4909-4919.
- Rubinsztein, D.C. (2002). Lessons from animal models of Huntington's disease. *Trends Genet* 18, 202-209.
- Rudiger, S., Buchberger, A., and Bukau, B. (1997). Interaction of Hsp70 chaperones with substrates. *Nat Struct Biol* 4, 342-349.
- Rumpf, S., and Jentsch, S. (2006). Functional Division of Substrate Processing Cofactors of the Ubiquitin-Selective Cdc48 Chaperone. *Molecular Cell* 21, 261-269.
- Rusten, T.E., and Stenmark, H. (2009). How do ESCRT proteins control autophagy? *J Cell Sci* 122, 2179-2183.
- Ryan, J.J., Sprunger, M.L., Holthaus, K., Shorter, J., and Jackrel, M.E. (2019). Engineered protein disaggregases mitigate toxicity of aberrant prion-like fusion proteins underlying sarcoma. *J Biol Chem* 294, 11286-11296.
- Sadowski, M., Suryadinata, R., Tan, A.R., Roesley, S.N., and Sarcevic, B. (2012). Protein monoubiquitination and polyubiquitination generate structural diversity to control distinct biological processes. *IUBMB Life* 64, 136-142.
- Safar, J., Wille, H., Itri, V., Groth, D., Serban, H., Torchia, M., Cohen, F.E., and Prusiner, S.B. (1998). Eight prion strains have PrP(Sc) molecules with different conformations. *Nat Med* 4, 1157-1165.
- Salminen, A., Kaarniranta, K., Haapasalo, A., Hiltunen, M., Soininen, H., and Alafuzoff, I. (2012). Emerging role of p62/sequestosome-1 in the pathogenesis of Alzheimer's disease. *Prog Neurobiol* 96, 87-95.
- Sanchez, Y., and Lindquist, S.L. (1990). HSP104 required for induced thermotolerance. *Science* 248, 1112-1115.
- Sanders, D.W., Kaufman, S.K., DeVos, S.L., Sharma, A.M., Mirbaha, H., Li, A., Barker, S.J., Foley, A.C., Thorpe, J.R., Serpell, L.C., *et al.* (2014). Distinct tau prion strains propagate in cells and mice and define different tauopathies. *Neuron* 82, 1271-1288.
- Sanders, D.W., Kaufman, S.K., Holmes, B.B., and Diamond, M.I. (2016). Prions and Protein Assemblies that Convey Biological Information in Health and Disease. *Neuron* 89, 433-448.
- Schäfer, J.A., Schessner, J.P., Bircham, P.W., Tsuji, T., Funaya, C., Pajonk, O., Schaeff, K., Ruffini, G., Papagiannidis, D., Knop, M., *et al.* (2020). ESCRT machinery mediates selective microautophagy of endoplasmic reticulum in yeast. 39, e102586.
- Schmued, L., Raymick, J., Tolleson, W., Sarkar, S., Zhang, Y.-H., and Bell-Cohn, A. (2012). Introducing Amylo-Glo, a novel fluorescent amyloid specific histochemical tracer especially suited for multiple labeling and large scale quantification studies. *Journal of Neuroscience Methods* 209, 120-126.
- Schroder, R., Watts, G.D., Mehta, S.G., Evert, B.O., Broich, P., Fließbach, K., Pauls, K., Hans, V.H., Kimonis, V., and Thal, D.R. (2005). Mutant valosin-containing protein causes a novel type of frontotemporal dementia. *Ann Neurol* 57, 457-461.
- Schulman, B.A., and Harper, J.W. (2009). Ubiquitin-like protein activation by E1 enzymes: the apex for downstream signalling pathways. *Nat Rev Mol Cell Biol* 10, 319-331.
- Schwarz, K., Eggers, M., Soza, A., Koszinowski, U.H., Kloetzel, P.M., and Groettrup, M. (2000). The proteasome regulator PA28alpha/beta can enhance antigen presentation without affecting 20S proteasome subunit composition. *Eur J Immunol* 30, 3672-3679.

- Scior, A., Buntru, A., Arnsburg, K., Ast, A., Iburg, M., Juenemann, K., Pigazzini, M.L., Mlody, B., Puchkov, D., Priller, J., *et al.* (2018). Complete suppression of Htt fibrilization and disaggregation of Htt fibrils by a trimeric chaperone complex. *EMBO J* 37, 282-299.
- Sengupta, U., Guerrero-Munoz, M.J., Castillo-Carranza, D.L., Lasagna-Reeves, C.A., Gerson, J.E., Paulucci-Holthauzen, A.A., Krishnamurthy, S., Farhed, M., Jackson, G.R., and Kaye, R. (2015). Pathological interface between oligomeric alpha-synuclein and tau in synucleinopathies. *Biol Psychiatry* 78, 672-683.
- Seyffer, F., Kummer, E., Oguchi, Y., Winkler, J., Kumar, M., Zahn, R., Sourjik, V., Bukau, B., and Mogk, A. (2012). Hsp70 proteins bind Hsp100 regulatory M domains to activate AAA+ disaggregase at aggregate surfaces. *Nat Struct Mol Biol* 19, 1347-1355.
- Sharma, A.M., Thomas, T.L., Woodard, D.R., Kashmer, O.M., and Diamond, M.I. (2018). Tau monomer encodes strains. *eLife* 7, e37813.
- Sharma, S.K., De Los Rios, P., Christen, P., Lustig, A., and Goloubinoff, P. (2010). The kinetic parameters and energy cost of the Hsp70 chaperone as a polypeptide unfoldase. *Nature Chemical Biology* 6, 914-920.
- Shiber, A., and Ravid, T. (2014). Chaperoning proteins for destruction: diverse roles of Hsp70 chaperones and their co-chaperones in targeting misfolded proteins to the proteasome. *Biomolecules* 4, 704-724.
- Shorter, J. (2011). The mammalian disaggregase machinery: Hsp110 synergizes with Hsp70 and Hsp40 to catalyze protein disaggregation and reactivation in a cell-free system. *PLoS One* 6, e26319.
- Shorter, J. (2016). Engineering therapeutic protein disaggregases. *Mol Biol Cell* 27, 1556-1560.
- Shorter, J., and Lindquist, S. (2004). Hsp104 catalyzes formation and elimination of self-replicating Sup35 prion conformers. *Science* 304, 1793-1797.
- Sibille, N., Sillen, A., Leroy, A., Wieruszeski, J.M., Mulloy, B., Landrieu, I., and Lippens, G. (2006). Structural impact of heparin binding to full-length Tau as studied by NMR spectroscopy. *Biochemistry* 45, 12560-12572.
- Simic, G., Babic Leko, M., Wray, S., Harrington, C., Delalle, I., Jovanov-Milosevic, N., Bazadona, D., Buee, L., de Silva, R., Di Giovanni, G., *et al.* (2016). Tau Protein Hyperphosphorylation and Aggregation in Alzheimer's Disease and Other Tauopathies, and Possible Neuroprotective Strategies. *Biomolecules* 6, 6.
- Sipe, J.D., and Cohen, A.S. (2000). Review: history of the amyloid fibril. *J Struct Biol* 130, 88-98.
- Skibinski, G., Parkinson, N.J., Brown, J.M., Chakrabarti, L., Lloyd, S.L., Hummerich, H., Nielsen, J.E., Hodges, J.R., Spillantini, M.G., Thusgaard, T., *et al.* (2005). Mutations in the endosomal ESCRTIII-complex subunit CHMP2B in frontotemporal dementia. *Nat Genet* 37, 806-808.
- Skowrya, D., Georgopoulos, C., and Zylicz, M. (1990). The E. coli dnaK gene product, the hsp70 homolog, can reactivate heat-inactivated RNA polymerase in an ATP hydrolysis-dependent manner. *Cell* 62, 939-944.
- Sontag, E.M., Samant, R.S., and Frydman, J. (2017). Mechanisms and Functions of Spatial Protein Quality Control. *Annu Rev Biochem* 86, 97-122.
- Soto, C., and Pritzkow, S. (2018). Protein misfolding, aggregation, and conformational strains in neurodegenerative diseases. *Nat Neurosci* 21, 1332-1340.
- Spillantini, M.G., Goedert, M., Crowther, R.A., Murrell, J.R., Farlow, M.R., and Ghetti, B. (1997). Familial multiple system tauopathy with presenile dementia: a disease with abundant neuronal and glial tau filaments. *Proc Natl Acad Sci U S A* 94, 4113-4118.
- Spitzer, C., Li, F., Buono, R., Roschztardt, H., Chung, T., Zhang, M., Osteryoung, K.W., Vierstra, R.D., and Otegui, M.S. (2015). The endosomal protein CHARGED MULTIVESICULAR BODY PROTEIN1 regulates the autophagic turnover of plastids in Arabidopsis. *Plant Cell* 27, 391-402.
- Squires, C.L., Pedersen, S., Ross, B.M., and Squires, C. (1991). ClpB is the Escherichia coli heat shock protein F84.1. *J Bacteriol* 173, 4254-4262.
- Stolz, A., Hilt, W., Buchberger, A., and Wolf, D.H. (2011). Cdc48: a power machine in protein degradation. *Trends in Biochemical Sciences* 36, 515-523.
- Sweeney, P., Park, H., Baumann, M., Dunlop, J., Frydman, J., Kopito, R., McCampbell, A., Leblanc, G., Venkateswaran, A., Nurmi, A., *et al.* (2017). Protein misfolding in

- neurodegenerative diseases: implications and strategies. *Translational Neurodegeneration* 6, 6.
- Tai, H.-C., Besche, H., Goldberg, A.L., and Schuman, E.M. (2010). Characterization of the Brain 26S Proteasome and its Interacting Proteins. *Front Mol Neurosci* 3, 12.
- Takahashi, Y., He, H., Tang, Z., Hattori, T., Liu, Y., Young, M.M., Serfass, J.M., Chen, L., Gebru, M., Chen, C., *et al.* (2018). An autophagy assay reveals the ESCRT-III component CHMP2A as a regulator of phagophore closure. *Nat Commun* 9, 2855.
- Takei, Y., Teng, J., Harada, A., and Hirokawa, N. (2000). Defects in axonal elongation and neuronal migration in mice with disrupted tau and map1b genes. *J Cell Biol* 150, 989-1000.
- Tan, C.-C., Yu, J.-T., Tan, M.-S., Jiang, T., Zhu, X.-C., and Tan, L. (2014). Autophagy in aging and neurodegenerative diseases: implications for pathogenesis and therapy. *Neurobiology of Aging* 35, 941-957.
- Tan, J.M., Wong, E.S., Kirkpatrick, D.S., Pletnikova, O., Ko, H.S., Tay, S.P., Ho, M.W., Troncoso, J., Gygi, S.P., Lee, M.K., *et al.* (2008). Lysine 63-linked ubiquitination promotes the formation and autophagic clearance of protein inclusions associated with neurodegenerative diseases. *Hum Mol Genet* 17, 431-439.
- Tanaka, A., Cleland, M.M., Xu, S., Narendra, D.P., Suen, D.F., Karbowski, M., and Youle, R.J. (2010). Proteasome and p97 mediate mitophagy and degradation of mitofusins induced by Parkin. *J Cell Biol* 191, 1367-1380.
- Tanaka, K. (2009). The proteasome: overview of structure and functions. *Proc Jpn Acad Ser B Phys Biol Sci* 85, 12-36.
- Tang, W.K., Li, D., Li, C.-c., Esser, L., Dai, R., Guo, L., and Xia, D. (2010a). A novel ATP-dependent conformation in p97 N-D1 fragment revealed by crystal structures of disease-related mutants. *The EMBO Journal* 29, 2217-2229.
- Tang, W.K., Li, D., Li, C.C., Esser, L., Dai, R., Guo, L., and Xia, D. (2010b). A novel ATP-dependent conformation in p97 N-D1 fragment revealed by crystal structures of disease-related mutants. *Embo j* 29, 2217-2229.
- Tang, W.K., and Xia, D. (2013). Altered intersubunit communication is the molecular basis for functional defects of pathogenic p97 mutants. *J Biol Chem* 288, 36624-36635.
- Tang, W.K., and Xia, D. (2016). Mutations in the Human AAA(+) Chaperone p97 and Related Diseases. *Front Mol Biosci* 3, 79.
- Taylor, E.B., and Rutter, J. (2011). Mitochondrial quality control by the ubiquitin-proteasome system. *Biochem Soc Trans* 39, 1509-1513.
- Tennstaedt, A., Popsel, S., Truebestein, L., Hauske, P., Brockmann, A., Schmidt, N., Irlle, I., Sacca, B., Niemeyer, C.M., Brandt, R., *et al.* (2012). Human high temperature requirement serine protease A1 (HTRA1) degrades tau protein aggregates. *J Biol Chem* 287, 20931-20941.
- Tessarz, P., Mogk, A., and Bukau, B. (2008). Substrate threading through the central pore of the Hsp104 chaperone as a common mechanism for protein disaggregation and prion propagation. *Mol Microbiol* 68, 87-97.
- Thrower, J.S., Hoffman, L., Rechsteiner, M., and Pickart, C.M. (2000). Recognition of the polyubiquitin proteolytic signal. *EMBO J*.
- Tomita, T., and Matouschek, A. (2019). Substrate selection by the proteasome through initiation regions. *Protein Sci*.
- Tremblay, P., Ball, H.L., Kaneko, K., Groth, D., Hegde, R.S., Cohen, F.E., DeArmond, S.J., Prusiner, S.B., and Safar, J.G. (2004). Mutant PrPSc conformers induced by a synthetic peptide and several prion strains. *J Virol* 78, 2088-2099.
- Tresse, E., Salomons, F.A., Vesa, J., Bott, L.C., Kimonis, V., Yao, T.-P., Dantuma, N.P., and Taylor, J.P. (2014). VCP/p97 is essential for maturation of ubiquitin-containing autophagosomes and this function is impaired by mutations that cause IBMPFD. *Autophagy* 6, 217-227.
- Tsuchiya, H., Ohtake, F., Arai, N., Kaiho, A., Yasuda, S., Tanaka, K., and Saeki, Y. (2017). In Vivo Ubiquitin Linkage-type Analysis Reveals that the Cdc48-Rad23/Dsk2 Axis Contributes to K48-Linked Chain Specificity of the Proteasome. *Mol Cell* 66, 488-502 e487.

- Tucker, K.L., Meyer, M., and Barde, Y.A. (2001). Neurotrophins are required for nerve growth during development. *Nat Neurosci* *4*, 29-37.
- Tutar, Y., Song, Y., and Masison, D.C. (2006). Primate chaperones Hsc70 (constitutive) and Hsp70 (induced) differ functionally in supporting growth and prion propagation in *Saccharomyces cerevisiae*. *Genetics* *172*, 851-861.
- Twomey, E.C., Ji, Z., Wales, T.E., Bodnar, N.O., Ficarro, S.B., Marto, J.A., Engen, J.R., and Rapoport, T.A. (2019). Substrate processing by the Cdc48 ATPase complex is initiated by ubiquitin unfolding. *Science*.
- Tycko, R. (2015). Amyloid polymorphism: structural basis and neurobiological relevance. *Neuron* *86*, 632-645.
- Tyedmers, J., Mogk, A., and Bukau, B. (2010). Cellular strategies for controlling protein aggregation. *Nat Rev Mol Cell Biol* *11*, 777-788.
- Ulrich, J. (1985). Alzheimer changes in nondemented patients younger than sixty-five: possible early stages of Alzheimer's disease and senile dementia of Alzheimer type. *Ann Neurol* *17*, 273-277.
- Uptain, S.M., and Lindquist, S. (2002). Prions as protein-based genetic elements. *Annu Rev Microbiol* *56*, 703-741.
- van den Boom, J., and Meyer, H. (2018). VCP/p97-Mediated Unfolding as a Principle in Protein Homeostasis and Signaling. *Mol Cell* *69*, 182-194.
- van der Veen, A.G., and Ploegh, H.L. (2012). Ubiquitin-like proteins. *Annu Rev Biochem* *81*, 323-357.
- van Well, E.M., Bader, V., Patra, M., Sanchez-Vicente, A., Meschede, J., Furthmann, N., Schnack, C., Blusch, A., Longworth, J., Petrasch-Parwez, E., *et al.* (2019). A protein quality control pathway regulated by linear ubiquitination. *EMBO J* *38*.
- Vaz-Silva, J., Gomes, P., Jin, Q., Zhu, M., Zhuravleva, V., Quintremil, S., Meira, T., Silva, J., Dioli, C., Soares-Cunha, C., *et al.* (2018). Endolysosomal degradation of Tau and its role in glucocorticoid-driven hippocampal malfunction. *EMBO J* *37*.
- Vembar, S.S., and Brodsky, J.L. (2008). One step at a time: endoplasmic reticulum-associated degradation. *Nat Rev Mol Cell Biol* *9*, 944-957.
- Venteicher, A.S., Meng, Z., Mason, P.J., Veenstra, T.D., and Artandi, S.E. (2008). Identification of ATPases pontin and reptin as telomerase components essential for holoenzyme assembly. *Cell* *132*, 945-957.
- Verhoef, L.G., Lindsten, K., Masucci, M.G., and Dantuma, N.P. (2002). Aggregate formation inhibits proteasomal degradation of polyglutamine proteins. *Hum Mol Genet* *11*, 2689-2700.
- Verma, R., Aravind, L., Oania, R., McDonald, W.H., Yates, J.R., 3rd, Koonin, E.V., and Deshaies, R.J. (2002). Role of Rpn11 metalloprotease in deubiquitination and degradation by the 26S proteasome. *Science* *298*, 611-615.
- Verma, R., Chen, S., Feldman, R., Schieltz, D., Yates, J., Dohmen, J., and Deshaies, R.J. (2000). Proteasomal proteomics: identification of nucleotide-sensitive proteasome-interacting proteins by mass spectrometric analysis of affinity-purified proteasomes. *Molecular biology of the cell* *11*, 3425-3439.
- Verma, R., Oania, R., Fang, R., Smith, G.T., and Deshaies, R.J. (2011). Cdc48/p97 Mediates UV-Dependent Turnover of RNA Pol II. *Molecular Cell* *41*, 82-92.
- Verma, R., Oania, R.S., Kolawa, N.J., and Deshaies, R.J. (2013). Cdc48/p97 promotes degradation of aberrant nascent polypeptides bound to the ribosome. *Elife* *2*, e00308.
- von Bergen, M., Barghorn, S., Biernat, J., Mandelkow, E.M., and Mandelkow, E. (2005). Tau aggregation is driven by a transition from random coil to beta sheet structure. *Biochim Biophys Acta* *1739*, 158-166.
- von Bergen, M., Barghorn, S., Jeganathan, S., Mandelkow, E.M., and Mandelkow, E. (2006). Spectroscopic approaches to the conformation of tau protein in solution and in paired helical filaments. *Neurodegener Dis* *3*, 197-206.
- von Bergen, M., Barghorn, S., Li, L., Marx, A., Biernat, J., Mandelkow, E.M., and Mandelkow, E. (2001). Mutations of tau protein in frontotemporal dementia promote aggregation of paired helical filaments by enhancing local beta-structure. *J Biol Chem* *276*, 48165-48174.

- von Bergen, M., Friedhoff, P., Biernat, J., Heberle, J., Mandelkow, E.M., and Mandelkow, E. (2000). Assembly of tau protein into Alzheimer paired helical filaments depends on a local sequence motif ((306)VQIVYK(311)) forming beta structure. *Proc Natl Acad Sci U S A* *97*, 5129-5134.
- Waelter, S., Boeddrich, A., Lurz, R., Scherzinger, E., Lueder, G., Lehrach, H., and Wanker, E.E. (2001). Accumulation of mutant huntingtin fragments in aggresome-like inclusion bodies as a result of insufficient protein degradation. *Molecular biology of the cell* *12*, 1393-1407.
- Wallace, E.W.J., Kear-Scott, J.L., Pilipenko, E.V., Schwartz, M.H., Laskowski, P.R., Rojek, A.E., Katanski, C.D., Riback, J.A., Dion, M.F., Franks, A.M., *et al.* (2015). Reversible, Specific, Active Aggregates of Endogenous Proteins Assemble upon Heat Stress. *Cell* *162*, 1286-1298.
- Wang, Q., Song, C., and Li, C.C. (2003). Hexamerization of p97-VCP is promoted by ATP binding to the D1 domain and required for ATPase and biological activities. *Biochem Biophys Res Commun* *300*, 253-260.
- Wang, Y., and Mandelkow, E. (2016). Tau in physiology and pathology. *Nat Rev Neurosci* *17*, 5-21.
- Watanabe-Asano, T., Kuma, A., and Mizushima, N. (2014). Cycloheximide inhibits starvation-induced autophagy through mTORC1 activation. *Biochemical and Biophysical Research Communications* *445*, 334-339.
- Watanabe, A., Hasegawa, M., Suzuki, M., Takio, K., Morishima-Kawashima, M., Titani, K., Arai, T., Kosik, K.S., and Ihara, Y. (1993). In vivo phosphorylation sites in fetal and adult rat tau. *J Biol Chem* *268*, 25712-25717.
- Watts, G.D., Wymer, J., Kovach, M.J., Mehta, S.G., Mumm, S., Darvish, D., Pestronk, A., Whyte, M.P., and Kimonis, V.E. (2004). Inclusion body myopathy associated with Paget disease of bone and frontotemporal dementia is caused by mutant valosin-containing protein. *Nat Genet* *36*, 377-381.
- Wegrzyn, R.D., Bapat, K., Newnam, G.P., Zink, A.D., and Chernoff, Y.O. (2001). Mechanism of prion loss after Hsp104 inactivation in yeast. *Mol Cell Biol* *21*, 4656-4669.
- Weibezahn, J., Schlieker, C., Bukau, B., and Mogk, A. (2003). Characterization of a trap mutant of the AAA+ chaperone ClpB. *J Biol Chem* *278*, 32608-32617.
- Weibezahn, J., Tessarz, P., Schlieker, C., Zahn, R., Maglica, Z., Lee, S., Zentgraf, H., Weber-Ban, E.U., Dougan, D.A., Tsai, F.T., *et al.* (2004). Thermotolerance requires refolding of aggregated proteins by substrate translocation through the central pore of ClpB. *Cell* *119*, 653-665.
- Weihl, C.C. (2011). Valosin containing protein associated fronto-temporal lobar degeneration: clinical presentation, pathologic features and pathogenesis. *Curr Alzheimer Res* *8*, 252-260.
- Weihl, C.C., Dalal, S., Pestronk, A., and Hanson, P.I. (2006). Inclusion body myopathy-associated mutations in p97/VCP impair endoplasmic reticulum-associated degradation. *Hum Mol Genet* *15*, 189-199.
- Weingarten, M.D., Lockwood, A.H., Hwo, S.Y., and Kirschner, M.W. (1975). A protein factor essential for microtubule assembly. *Proc Natl Acad Sci U S A* *72*, 1858-1862.
- Weith, M., Seiler, J., van den Boom, J., Kracht, M., Hulsmann, J., Primorac, I., Del Pino Garcia, J., Kaschani, F., Kaiser, M., Musacchio, A., *et al.* (2018). Ubiquitin-Independent Disassembly by a p97 AAA-ATPase Complex Drives PP1 Holoenzyme Formation. *Mol Cell* *72*, 766-777 e766.
- Wen, X., Tan, W., Westergard, T., Krishnamurthy, K., Markandaiah, S.S., Shi, Y., Lin, S., Shneider, N.A., Monaghan, J., Pandey, U.B., *et al.* (2014). Antisense proline-arginine RAN dipeptides linked to C9ORF72-ALS/FTD form toxic nuclear aggregates that initiate in vitro and in vivo neuronal death. *Neuron* *84*, 1213-1225.
- Wendler, P., Ciniawsky, S., Kock, M., and Kube, S. (2012). Structure and function of the AAA+ nucleotide binding pocket. *Biochim Biophys Acta* *1823*, 2-14.
- West, M.W., Wang, W., Patterson, J., Mancias, J.D., Beasley, J.R., and Hecht, M.H. (1999). De novo amyloid proteins from designed combinatorial libraries. *Proc Natl Acad Sci U S A* *96*, 11211-11216.

- Wickner, R.B. (1994). [URE3] as an altered URE2 protein: evidence for a prion analog in *Saccharomyces cerevisiae*. *Science* *264*, 566-569.
- Wigley, W.C., Fabunmi, R.P., Lee, M.G., Marino, C.R., Muallem, S., DeMartino, G.N., and Thomas, P.J. (1999). Dynamic association of proteasomal machinery with the centrosome. *J Cell Biol* *145*, 481-490.
- Wilcox, A.J., and Laney, J.D. (2009). A ubiquitin-selective AAA-ATPase mediates transcriptional switching by remodelling a repressor-promoter DNA complex. *Nat Cell Biol* *11*, 1481-1486.
- Wilkinson, K.D., Urban, M.K., and Haas, A.L. (1980). Ubiquitin is the ATP-dependent proteolysis factor I of rabbit reticulocytes. *J Biol Chem* *255*, 7529-7532.
- Wille, H., Drewes, G., Biernat, J., Mandelkow, E.M., and Mandelkow, E. (1992). Alzheimer-like paired helical filaments and antiparallel dimers formed from microtubule-associated protein tau in vitro. *J Cell Biol* *118*, 573-584.
- Winkler, J., Tyedmers, J., Bukau, B., and Mogk, A. (2012a). Chaperone networks in protein disaggregation and prion propagation. *J Struct Biol* *179*, 152-160.
- Winkler, J., Tyedmers, J., Bukau, B., and Mogk, A. (2012b). Hsp70 targets Hsp100 chaperones to substrates for protein disaggregation and prion fragmentation. *J Cell Biol* *198*, 387-404.
- Wischik, C.M., Novak, M., Thogersen, H.C., Edwards, P.C., Runswick, M.J., Jakes, R., Walker, J.E., Milstein, C., Roth, M., and Klug, A. (1988). Isolation of a fragment of tau derived from the core of the paired helical filament of Alzheimer disease. *Proc Natl Acad Sci U S A* *85*, 4506-4510.
- Wisniewski, J.R., Zielinska, D.F., and Mann, M. (2011). Comparison of ultrafiltration units for proteomic and N-glycoproteomic analysis by the filter-aided sample preparation method. *Analytical biochemistry* *410*, 307-309.
- Woerner, A.C., Frottin, F., Hornburg, D., Feng, L.R., Meissner, F., Patra, M., Tatzelt, J., Mann, M., Winklhofer, K.F., Hartl, F.U., *et al.* (2016). Cytoplasmic protein aggregates interfere with nucleocytoplasmic transport of protein and RNA. *Science* *351*, 173-176.
- Wong, E.S.P., Tan, J.M.M., Soong, W.-E., Hussein, K., Nukina, N., Dawson, V.L., Dawson, T.M., Cuervo, A.M., and Lim, K.-L. (2008). Autophagy-mediated clearance of aggregates is not a universal phenomenon. *Human Molecular Genetics* *17*, 2570-2582.
- Wood, S.J., Wypych, J., Steavenson, S., Louis, J.C., Citron, M., and Biere, A.L. (1999). alpha-synuclein fibrillogenesis is nucleation-dependent. Implications for the pathogenesis of Parkinson's disease. *J Biol Chem* *274*, 19509-19512.
- Xia, D., Tang, W.K., and Ye, Y. (2016). Structure and function of the AAA+ ATPase p97/Cdc48p. *Gene* *583*, 64-77.
- Xu, P., Duong, D.M., Seyfried, N.T., Cheng, D., Xie, Y., Robert, J., Rush, J., Hochstrasser, M., Finley, D., and Peng, J. (2009). Quantitative proteomics reveals the function of unconventional ubiquitin chains in proteasomal degradation. *Cell* *137*, 133-145.
- Xu, Y., Anderson, D.E., and Ye, Y. (2016). The HECT domain ubiquitin ligase HUWE1 targets unassembled soluble proteins for degradation. *Cell Discov* *2*, 16040-16040.
- Yamamoto, A., Cremona, M.L., and Rothman, J.E. (2006). Autophagy-mediated clearance of huntingtin aggregates triggered by the insulin-signaling pathway. *J Cell Biol* *172*, 719-731.
- Yamamoto, A., Lucas, J.J., and Hen, R. (2000). Reversal of neuropathology and motor dysfunction in a conditional model of Huntington's disease. *Cell* *101*, 57-66.
- Yang, Z., and Klionsky, D.J. (2010). Mammalian autophagy: core molecular machinery and signaling regulation. *Curr Opin Cell Biol* *22*, 124-131.
- Yau, R., and Rape, M. (2016). The increasing complexity of the ubiquitin code. *Nat Cell Biol* *18*, 579-586.
- Yau, R.G., Doerner, K., Castellanos, E.R., Haakonsen, D.L., Werner, A., Wang, N., Yang, X.W., Martinez-Martin, N., Matsumoto, M.L., Dixit, V.M., *et al.* (2017). Assembly and Function of Heterotypic Ubiquitin Chains in Cell-Cycle and Protein Quality Control. *Cell* *171*, 918-933.e920.
- Ye, Y., Tang, W.K., Zhang, T., and Xia, D. (2017). A Mighty "Protein Extractor" of the Cell: Structure and Function of the p97/CDC48 ATPase. *Front Mol Biosci* *4*, 39.

- Yin, Z., Pascual, C., and Klionsky, D.J. (2016). Autophagy: machinery and regulation. *Microb Cell* 3, 588-596.
- Yoshimori, T., Yamamoto, A., Moriyama, Y., Futai, M., and Tashiro, Y. (1991). Bafilomycin A1, a specific inhibitor of vacuolar-type H(+)-ATPase, inhibits acidification and protein degradation in lysosomes of cultured cells. *J Biol Chem* 266, 17707-17712.
- Yu, Q., Zhang, H., Li, Y., Liu, C., Wang, S., and Liao, X. (2018). UCH-L1 Inhibition Suppresses tau Aggresome Formation during Proteasomal Impairment. *Molecular Neurobiology* 55, 3812-3821.
- Zaarur, N., Xu, X., Lestienne, P., Meriin, A.B., McComb, M., Costello, C.E., Newnam, G.P., Ganti, R., Romanova, N.V., Shanmugasundaram, M., *et al.* (2015). RuvbL1 and RuvbL2 enhance aggresome formation and disaggregate amyloid fibrils. *EMBO J* 34, 2363-2382.
- Zeiler, M., Straube, W.L., Lundberg, E., Uhlen, M., and Mann, M. (2012). A Protein Epitope Signature Tag (PrEST) library allows SILAC-based absolute quantification and multiplexed determination of protein copy numbers in cell lines. *Mol Cell Proteomics* 11, O111.009613.
- Zhang, W., Falcon, B., Murzin, A.G., Fan, J., Crowther, R.A., Goedert, M., and Scheres, S.H. (2019). Heparin-induced tau filaments are polymorphic and differ from those in Alzheimer's and Pick's diseases. *Elife* 8.
- Zhang, W., Tarutani, A., Newell, K.L., Murzin, A.G., Matsubara, T., Falcon, B., Vidal, R., Garringer, H.J., Shi, Y., Ikeuchi, T., *et al.* (2020). Novel tau filament fold in corticobasal degeneration. *Nature*.
- Zhang, X., Gui, L., Zhang, X., Bulfer, S.L., Sanghez, V., Wong, D.E., Lee, Y., Lehmann, L., Lee, J.S., Shih, P.Y., *et al.* (2015). Altered cofactor regulation with disease-associated p97/VCP mutations. *Proc Natl Acad Sci U S A* 112, E1705-1714.
- Zhang, X., Shaw, A., Bates, P.A., Newman, R.H., Gowen, B., Orlova, E., Gorman, M.A., Kondo, H., Dokurno, P., Lally, J., *et al.* (2000). Structure of the AAA ATPase p97. *Molecular Cell* 6, 1473-1484.
- Zhang, Y. (2003). Transcriptional regulation by histone ubiquitination and deubiquitination. *Genes Dev* 17, 2733-2740.
- Zhao, Y., Tseng, I.C., Heyser, C.J., Rockenstein, E., Mante, M., Adame, A., Zheng, Q., Huang, T., Wang, X., Arslan, P.E., *et al.* (2015). Apoptosis-Mediated Caspase Cleavage of Tau Contributes to Progressive Supranuclear Palsy Pathogenesis. *Neuron* 87, 963-975.
- Zietkiewicz, S., Krzewska, J., and Liberek, K. (2004). Successive and synergistic action of the Hsp70 and Hsp100 chaperones in protein disaggregation. *J Biol Chem* 279, 44376-44383.
- Zietkiewicz, S., Lewandowska, A., Stocki, P., and Liberek, K. (2006). Hsp70 chaperone machine remodels protein aggregates at the initial step of Hsp70-Hsp100-dependent disaggregation. *J Biol Chem* 281, 7022-7029.
- Zolkowski, M., Kessel, M., Ginsburg, A., and Maurizi, M.R. (1999). Nucleotide-dependent oligomerization of ClpB from *Escherichia coli*. *Protein Sci* 8, 1899-1903.
- Zu, T., Duvick, L.A., Kaytor, M.D., Berlinger, M.S., Zoghbi, H.Y., Clark, H.B., and Orr, H.T. (2004). Recovery from polyglutamine-induced neurodegeneration in conditional SCA1 transgenic mice. *J Neurosci* 24, 8853-8861.